A study on the CO_2 fixation pathway of *Ignicoccus hospitalis*

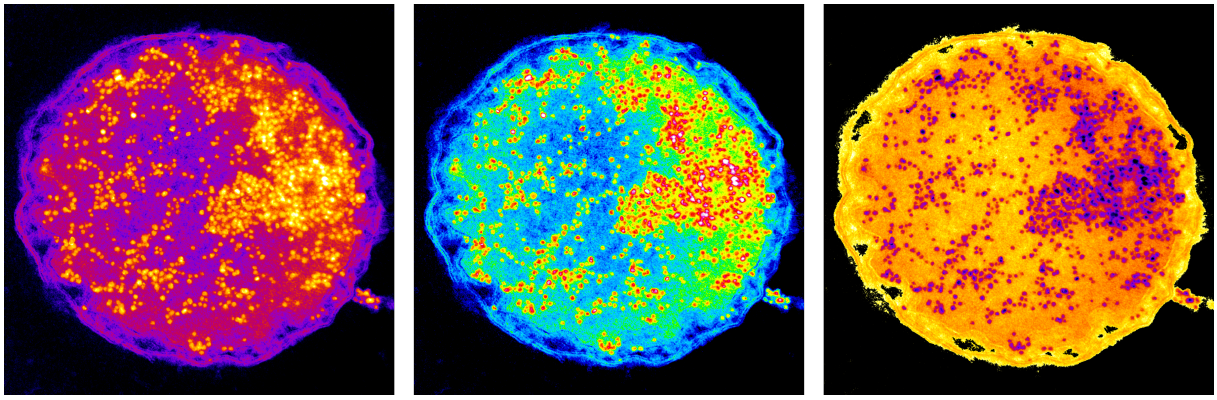

Dissertation zur Erlangung des
Doktorgrades der Naturwissenschaften (Dr. rer. nat.)
der Fakultät für Biologie und Vorklinische Medizin
der Universität Regensburg

vorgelegt von

Jennifer Flechsler

aus Dinkelsbühl

Juli 2015

Transmission electron micrograph on the cover visualizes an *Ignicoccus hospitalis* cell immuno labeled with an antibody directed against DNA. (Color edits: ImageJ)

Das Promotionsgesuch wurde eingereicht am: 03.07.2015

Die Arbeit wurde angeleitet von: Prof. Dr. Reinhard Rachel

Unterschrift:

Contents

I. Introduction

1. Autotrophic carbon fixation

The term 'autotrophy' describes the ability of an organism to grow without the assimilation of organic carbon. Instead, organic carbon for synthesis of biomolecules is derived from inorganic carbon sources such as CO_2 (Schuchmann and Müller, 2014). As all forms of life are directly or indirectly reliant on autotrophic carbon fixation, these pathways are considered "the most important biosynthetic processes on earth" (Hügler, 2003, Berg, 2011, Hügler and Sievert, 2011).

In autotrophic Eukaryotes, CO_2 is fixed via the Calvin Benson Bassham cycle (Calvin cycle); autotrophic Prokaryotes however, have developed at least five alternative ways of CO_2 fixation: The reductive acetyl-CoA pathway (Ljungdahl, 1986, Wood, 1991), the reductive citric acid cycle (Evans *et al.*, 1966), the 3-hyroxypropionate bicycle (3-HP bicycle, Strauss and Fuchs, 1993), the 3-hyroxypropionate/4-hydroxybutyrate cycle (3-HP/4-HB cycle, Berg *et al.*, 2007) and the dicarboxylate/4-hydroxybutyrate cycle (DC/4-HB cycle, Huber *et al.*, 2008). The existence of further carbon fixation pathways seems likely, considering the increasing availability of genomic data and the fact that most of these pathways were unraveled in the last decade (Berg *et al.*, 2010a, Berg, 2011, Fuchs, 2011).

To date, the reductive citric acid cycle and the 3-HP bicycle were shown to solely operate in Bacteria, while the the 3-HP/4-HB- and the DC/4-HB cycle were exclusively found in Archaea. The only carbon fixation pathway occurring in both, Archaea and Bacteria is the reductive acetyl-CoA pathway (Hügler and Sievert, 2011). Based on proteomic and enzymatic studies, even the co-existence of two autotrophic pathways in one organism was described. Depending on the energy situation, an uncultured endosymbiont of a deep-sea tube worm belonging to the Gammaproteobacteria uses the Calvin cycle or the reductive citric acid cycle (Berg, 2011, Hügler and Sievert, 2011, Markert *et al.*, 2007). Except for the Calvin cycle, all pathways start from acetyl-CoA (Berg, 2011, Fuchs and Berg, 2014). This is in line with the fact that biosynthe-

sis of precursors is mainly derived from acetyl-CoA (29 %) and pyruvate (21 %) in Prokaryotes (Fuchs, 2011). Being well-adapted to distinct environments, the routes of CO_2 fixation differ from each other in oxygen tolerance, energy demand, utilization of inorganic carbon species and type of reduction equivalents (Berg, 2011, Bar-Even *et al.*, 2012). Notably, anaerobic pathways appear to require less ATP than aerobic versions and carboxylating enzymes show different preferences for inorganic carbon species (McCollom and Amend, 2005, Berg, 2011). Since the concentration of HCO_3^- in slightly alkaline seawater is much higher than the concentration of CO_2, fixation of HCO_3^- might be an asset (Berg, 2011, Hügler and Sievert, 2011). The enzymes 2-ketoglutarate synthase, pyruvate synthase and 4-hydroxybutyryl-CoA dehydratase are considered oxygen sensitive, since they contain iron-sulfur clusters and/or a free radical intermediate (Bar-Even *et al.*, 2012). Nevertheless, the oxygen tolerance of these enzymes was shown to range between different organisms (Bar-Even *et al.*, 2012). This affects for example the enhanced oxygen tolerance of 4-hydroxybutyryl-CoA hydratase in organisms fixing CO_2 according to the 3-HP/4-HB cycle and the notable oxygen tolerance of pyruvate synthase in *Desulfovibrio africanus* (Pieulle *et al.*, 1997, Bar-Even *et al.*, 2012).

An overview on the different ways of autotrophic CO_2 fixation regarding key enzymes, energy consumption and special features of the respective pathway is given below. The DC/4-HB cycle is discussed in detail, mainly highlighting the version of the *I. hospitalis* CO_2 fixation pathway.

Tab. I.1.: *Pathways of autotrophic carbon fixation; from Berg* et al.*, 2010a*

Pathway	ATP equivalents for synthesis of one pyruvate	Reductants for synthesis of one pyruvate (10 [H])	CO_2-fixing enzymes	Active CO_2 species	Intermediates that can be used for biosynthesis	Key enzymes
Calvin-Benson-Bassham cycle	Seven	Five NADH or NADPH	RuBisCO	CO_2	3-Phospho-glycerate, triose phosphates and sugar phosphates	RuBisCO and phosphoribulokinase
Reductive citric acid cycle	Two	Two NADH or NADPH, one unknown donor and two ferredoxin	2-Oxoglutarate synthase, Isocitrate dehydrogenase, Pyruvate synthase and PEP carboxylase	CO_2, CO_2, CO_2, HCO_3^-	Acetyl-CoA, pyruvate, PEP, oxaloacetate, succinyl-CoA and 2-oxoglutarate	2-Oxoglutarate synthase and ATP-citrate lyase
Reductive acetyl-CoA pathway	Approx. one	Three ferredoxin and two $F_{420}H_2$ (in methanogens)	Acetyl-CoA synthetase/ CO dehydrogenase, Formylmethanofuran dehydrogenase (in methanogens), Pyruvate synthase	CO_2, CO_2, HCO_2	Acetyl-CoA and pyruvate	Acetyl-CoA synthase-CO dehydrogenase and enzymes reducing CO_2 to methyltetrahydropterin
3-Hydroxypropionate bicycle	Seven	Six NADH or NADPH, but one FAD is reduced	Acetyl-CoA and propionyl-CoA carboxylase	HCO_3^-	Acetyl-CoA, pyruvate and succinyl-CoA	Malonyl-CoA reductase, propionyl-CoA synthase and malyl-CoA lyase
3-Hydroxypropionate/ 4-hydroxybutyrate cycle	Nine	Six NADH or NADPH, but one FAD is reduced	Acetyl-CoA and propionyl-CoA carboxylase	HCO_3^-	Acetyl-CoA and succinyl-CoA	Acetyl-CoA/propionyl-CoA carboxylase, enzymes reducing malonyl-CoA to propionyl-CoA, methylmalonyl-CoA mutase and 4-hydroxybutyryl-CoA dehydratase
Dicarboxylate/ 4-hydroxybutyrate cycle	Five	Two or three ferredoxin, one or two NADH or NADPH, and one unknown donor	Pyruvate synthase, PEP carboxylase	CO_2, HCO_3^-	Acetyl-CoA, pyruvate, PEP, oxaloacetate and succinyl-CoA	4-hydroxybutyryl-CoA dehydratase

The Calvin Benson Bassham cycle or the reductive pentose phosphate cycle is probably the best-known and also for a long time the solely accepted way of autotrophic CO_2 fixation (Fuchs, 2011). This cycle was unraveled in the 1940's and 1950's and is considered the "most significant carbon fixation pathway on today's Earth" (Hügler and Sievert, 2011). The cycle operates in plants, algae, cyanobacteria and in many aerobic proteobacteria. Taking into account the wide distribution of the cycle and the low affinity of RuBisCO for CO_2, it is not surprising that RuBisCO is the most abundant enzyme in the world (Berg, 2011). So far, three different forms of RuBisCO and one structural homologue involved in sulfur metabolism, referred to as RuBisCO-like protein, have been identified (Berg *et al.*, 2010a). Form III RuBisCO was exclusively found in Archaea, however since the Calvin cycle was not shown to operate in Archaea, its function here remains enigmatic (Berg *et al.*, 2010a).

In a simplified overview the Calvin cycle consists of three elements, starting with the fixation of CO_2 by RuBisCO to a five carbon sugar (ribulose 1,5-biphosphate). This results in hydrolysis of an unstable 6-carbon molecule into two molecules of triose phosphate, which are further processed into hexoses. One step of the acceptor regeneration is performed by the phoshoribulokinase, which is considered a key enzyme of the cycle together with RuBisCO (Stryer *et al.*, 2003). Intermediates such as triose- or sugar phosphates are used as precursors for cellulose, amino acids or can be integrated into glycolysis and gluconeogenesis (Berg *et al.*, 2010a). Regarding energy and reductant consumption for synthesis of one molecule pyruvate, the cycle spends seven ATP and five NAD(P)H equivalents (Berg *et al.*, 2010a).

The reductive acetyl-CoA pathway or the Wood-Ljungdahl pathway is a non-cyclic version of CO_2 fixation (Fig. I.1 c). It fundamentally differs from all other cycles in its added benefit of generating one ATP when fixing CO_2 (Fuchs, 2011). This process is assumed to be the most ancient autotrophic CO_2 fixation pathway (Martin *et al.*, 2008, Fuchs, 2011, Berg *et al.*, 2010a) and it is mainly found in acetogenic bacteria, sulfate-reducing Bacteria and Archaea, Methanogenic Archaea and Planctomycetes (Fuchs, 1986, Hügler and Sievert, 2011, Ljungdahl, 1986, Wood, 1991). Two molecules of CO_2 are fixed for the assimilation of carbon, resulting in the formation of acetyl CoA (Hügler and Sievert, 2011).

The pathway consists of a methyl- and a carbonyl branch, with acetyl-CoA synthase/CO dehydrogenase representing the key enzyme: In the methyl branch, one molecule of CO_2 is reduced to the level of a methyl group, which is bound to a tetra-

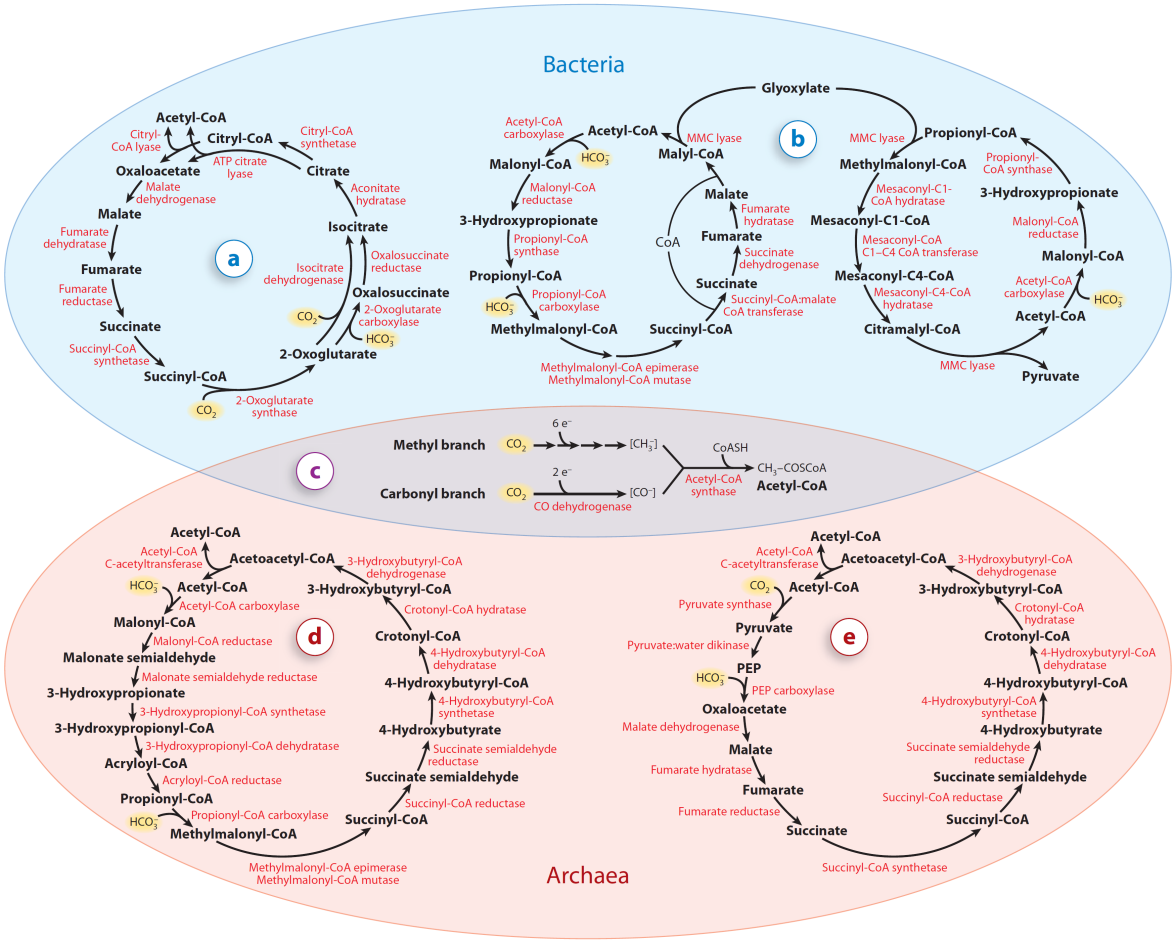

Fig. I.1.: ***Carbon fixation pathways in Archaea and Bacteria.*** *a: Reductive citric acid cycle, b: 3-hydroxypropionate bicycle, c: reductive acetyl-CoA pathway, d: 3-hydroxypropionate/4-hydroxybutyrate cycle, e: dicarboxylate/4-hydroxybutyrate cycle, from Hügler and Sievert, 2011*

hydropterin coenzmye. In the carbonyl branch, a second molecule of CO_2 is reduced to a carbonyl residue attached to the metal center of acetyl-CoA synthase/CO dehydrogenase. Acetyl-CoA is synthesized from the methyl and the carbonyl residues catalyzed by a bifunctional key enzyme (Pezacka and Wood, 1984, Hügler and Sievert, 2011, Berg, 2011).

Different versions of the pathway have been identified, which is in line with the diversity of organisms using this way of CO_2 fixation. Consuming less than one ATP equivalent for the formation of one molecule of pyruvate, the pathway is energetically favorable and it therefore seems reasonable that it is employed by organisms living close to the thermodynamic limit (Berg, 2011). However, the process requires an enormous

amount of metals and coenzymes, giving a whole new dimension to that consideration (Berg, 2011). Moreover, the reductive acetyl-CoA pathway works only under strictly anaerobic conditions which is due to oxygen sensitivity of the key enzyme and the use of ferredoxin (Berg, 2011).

The reductive citric acid cycle. In 1966, the reductive citric acid cycle or the reductive tricarboxylic acid cycle was the second pathway of autotrophic CO_2 fixation to be discovered (Fig. I.1 a). It is mainly distributed among mesophiles but can also be found in thermophiles. So far, the cycle was not shown to operate in Archaea and it seems to be restricted to anaerobic and microaerobic organisms. Inverting the direction of the citric acid cycle, the pathway needs to exhibit a slightly different set of enzymes. Regarding the three irreversible steps of the citric acid cycle, which are catalyzed by a succinate dehydrogenase, a NAD^+-dependent 2-oxoglutarate dehydrogenase and a citrate synthase, the reductive version of the cycle replaced these enzymes by a fumarate reductase, a ferredoxin dependent 2-oxoglutarate synthase and an ATP citrate lyase (Hügler and Sievert, 2011). Furthermore, the pathway involves two CO_2 fixation steps, which includes the carboxylation of succinyl-CoA to 2-oxoglutarate by 2-oxoglutarate synthase. The second carboxylation of 2-oxoglutarate to isocitrate is implemented by a isocitrate dehydrogenase (*C. limicola*) or by a the combination of two enzymes, namely 2-oxoglutarate carboxylase and oxalocacetate reductase (*H. thermophilus*, Aoshima, 2007, Hügler and Sievert, 2011).

The key reaction of the reductive citric acid cycle is the ATP-depending cleavage of citrate to acetyl-CoA and oxaloacetate. Depending on the organisms, the reaction is performed either by an ATP citrate lyase or it proceeds in a two step reaction catalyzed by a citryl-CoA synthetase and a citryl-CoA lyase (Hügler and Sievert, 2011). The formation of pyruvate requires two ATP equivalents and involves an additional carboxylation via a pyruvate synthase (Evans *et al.*, 1966, Hügler and Sievert, 2011).

The 3-hyroxypropionate bicycle also known as Fuchs-Holo cycle, is utilized by the phototrophic green nonsulfur bacterium *Chloroflexus auranticus* (Fig. I.1 b). Despite featuring highly efficient carboxylases and being compatible with aerobic conditions, this way of CO_2 fixation was only shown to operate in members of the Chloroflexaceae (Berg, 2011). Comprising 19 steps catalyzed by 13 different enzymes only, the cycle employs various multifunctional enzymes (Hügler and Sievert, 2011). As the name suggests, the 3-hyroxypropionate cycle consists of two cycles. In the first part,

glyoxylate is synthesized by the carboxylation of acetyl-CoA via the formation of 3-hydroxypropionate, which is the eponymous intermediate for the bicycle. Carboxylation is catalyzed by an acetyl-CoA- and propionyl-CoA carboxylase, each fixing HCO_3^-. The second cycle starts with the addition of glyoxylate to propionyl-CoA, yielding in the formation of pyruvate and acetyl-CoA. Malonyl-CoA reductase, propionyl-CoA synthase and malyl-CoA lyase is regarded as key enzymes of the bicycle (Berg, 2011). Consuming seven ATP equivalents for synthesis of one pyruvate, the cycle can be regarded as expensive (Berg, 2011).

The 3-hyroxypropionate/4-hydroxybutyrate cycle and the dicarboxylate/ 4-hydroxybutyrate cycle are routes for autotrophic carbon fixation mainly used by Crenarchaeotes (Fig. I.1 d and e).

The 3-HP/4-HB cycle occurs in aerobic autotrophic *Sulfolobales* and in the strictly anaerobe *Stygiolobus azoricus* (Berg *et al.*, 2010b). Very recently, a slightly modified version of the cycle was described for the Thaumarchaeum *Nitrosopumilus maritimus*, which presently appears to be the most energy-efficient aerobic carbon fixation pathway (Könneke *et al.*, 2014). In accordance with the aerobic lifestyle of some *Sulfolobales* and of *Nitrosopumilus*, the pathway operates under microoxic and oxic conditions and exhibits an oxygen tolerant 4-hydroxybutyryl-CoA dehydratase enzyme representing the key enzyme of the cycle (Berg *et al.*, 2010b). Similar as the bicyle, the 3-HP/4-HB pathway starts with the carboxylation of acetyl-CoA to succiniyl-CoA via 3-hydroxypropionate. This involves a further carboxylation step of propionyl-CoA to methylmalonyl-CoA. Although resulting in the same reaction products as the bicycle, the first half of this pathway differs in the enzyme set used for catalysis of individual steps. While *M. sedula* (representative of the 3-HP/4-HB cycle) employs five different enzymes for the conversion of malonyl-CoA to propionyl-CoA, *C. auranticus* (representative of the bicycle) uses two multifunctional enzymes to catalyze the same reaction sequence (Berg *et al.*, 2010b). Fixation of HCO_3^- is accomplished by a bifunctional biotin-dependent acetyl-CoA/propionyl-CoA carboxylase (Hügler and Sievert, 2011, Berg *et al.*, 2010a). In the second part of the cycle, succinyl CoA is regenerated to acetyl-CoA via 4-hydroxybutyrate, representing the second characteristic intermediate of the cycle. Synthesis of pyruvate, which requires nine ATP and another half turn of the cycle, starts from succinyl-CoA (Fuchs, 2011, Berg *et al.*, 2010a).

In the hyperthermophilic Crenarchaeum *Ignicoccus hospitalis*, CO_2 fixation proceeds via the DC/4-HB cycle (Huber *et al.*, 2008). This metabolic pathway includes 14 steps

and seems to be limited to only few representatives belonging to the *Thermoproteales* and *Desulfurococcales* (*Thermoproteus neutrophilus*, *Pyrolobus fumarii*) (Huber *et al.*, 2008, Ramos-Vera *et al.*, 2009, Berg *et al.*, 2010a). As shown for the 3-HP/4-HB cycle, the DC/4-HB cycle is based on the formation of succinyl-CoA from acetyl-CoA followed by the regeneration of succinyl-CoA to acetyl-CoA. However, the pathway starts by the fixation of one molecule of CO_2 to acetyl-CoA by a pyruvate synthase resulting in pyruvate. Depending on ATP, pyruvate is further converted to PEP by a pyruvate:water dikinase. This is followed by a second carboxylation step catalyzed by a PEP carboxylase, which fixes one molecule HCO_3^-. The resulting oxaloacetate is further processed to malate, fumarate, succinate and succinyl-CoA via MDH, fumarate hydratase, fumarate reductase and an ATP-depending succinyl-CoA synthetase. The reaction sequence from oxaloacetate to succinyl-CoA corresponds with the equivalent part in the reductive citric acid cyle (Fuchs, 2011). Yet, regeneration of acetyl-CoA is identical with the 4-HB part of the 3-HP/4-HB cycle from *M. sedula*. It starts with succinyl-CoA being converted to 4-hydroxybutyrate via succinyl-CoA- and succinic semialdehyde reductase (Fuchs, 2011). In an ATP-dependent reaction, 4-hydroxybutyrate is ligated with CoA by a 4-hydroxybutyryl-CoA synthetase resulting in 4-hydroxybutyryl-CoA. This is followed by the key reaction of the cycle, which includes the elimination of water from 4-hydroxybutyryl-CoA by a ketyl radical mechanism leading to the formation of crotonyl-CoA (Fuchs, 2011). Similar as in the 3-HP/4-HB cycle this reaction is performed by a 4-hydroxybutyryl-CoA dehydratase, containing an [4Fe-4S] cluster and FAD. For the conversion of crotonyl-CoA into acetoacetyl-CoA, a fusion protein is employed (crotonyl-CoA hydratase/3-hydroxybutyryl-CoA DHG). In a final step, acetoacetyl-CoA is cleaved into two molecules acetyl-CoA by an acetoacetyl-CoA β-ketothiolase. One molecule of acetyl-CoA is needed to maintain the operation of the cycle, while the other molecule can be branched off for biosynthesis (Ramos-Vera *et al.*, 2011, Fuchs, 2011). The formation of pyruvate requires five ATP equivalents (Fuchs, 2011, Fuchs and Berg, 2014). In Tab. I.2 enzyme activities measured in cell extracts of *I. hospitalis* and the gene numbers putatively encoding for the respective genes in *I. hospitalis* are summarized (Huber *et al.*, 2008). As indicated, no candidates for a succinyl-CoA reductase and a succinic semialdehyde reductase could be identified within the genome of *I. hospitalis*, so far. In context of this pathway, it turned out that the genes *Igni_0256* and *Igni_0257* were falsely annotated and are in fact one single gene, encoding for the ACS, which provides the primary acceptor molecule for the cycle (Ramos-Vera *et al.*, 2011, Mayer *et al.*, 2012).

Tab. I.2.: *Specific activities of enzymes/cell extracts of the DC/4-HB cycle in I. hospitalis from Huber* et al., *2008.*

No.	Enzyme	Putative gene in *I. hospitalis*	Specific activity, nmol/min per mg protein	Assay temperature, °C
1	Pyruvate synthase	*Igni_1075-1078* or	115	75
		Igni_1256-1257	145	85
2	Pyruvate:water dikinase	*Igni_1113*	210	85
3	Phosphoenolpyruvate carboxylase	*Igni_0341*	200	85
4	Malate dehydrogenase	*Igni_1263*	1190/745	75
5	Fumarate hydratase	*Igni_0678*	895	75
6	Fumarate reductase	*Igni_0276/ Igni_0445*	840	75
7	Succinate thiokinase	*Igni_0085/ Igni_0086*	195	60
			980	80
8	Succinyl-CoA reductase	*unknown*	94	60
9	Succinate semialdehyd reductase	*unknown*	1430/440	60
	(NADH/NADPH)		3130/2000	80
10	4-Hydroxybutyryl-CoA synthetase	*Igni_0475*	100	60
11	4-Hydroxybutyryl CoA dehydratase	*Igni_0595*	100	40
12	Crotonyl-CoA hydratase	*Igni_1058*	460	40
13	3-Hydroxybutyryl-CoA-dehydrogenase (NADH/NADPH)	*Igni_1058*	225/0	60
14	Acetoacetyl-CoA-β-ketothiolase	*Igni_1401* or	1100	60
		Igni_0377		

2. *Ignicoccus hospitalis* and *Nanoarchaeum equitans*

The genus *Ignicoccus* belongs to the phylum of the Crenarchaeota and was assigned to the order of the *Desulfurococcales* into the family of the *Desulfurococcaceae*. *Ignicoccus hospitalis* was isolated from a hydrothermal area at the Kolbensey Ridge, situated north of Iceland (Huber *et al.*, 2002). Cells of *I. hospitalis* are obligatory anaerobic and follow a chemolithotrophic and hyperthermophilic lifestyle, whereby optimal growth occurs at 90°C. The organism grows by the reduction of elemental sulfur using molecular hydrogen as electron donor. Its autotrophic lifestyle is reflected in its ability to assimilate inorganic carbon via the DC/4-HB cycle (see section 1.1; Jahn *et al.*, 2007, Huber *et al.*, 2008). Regarding biosynthetic pathways, gluconeogenesis proceeds by operation of a reverse Embden-Meyerhof pathway and was suggested to start from PEP. Pentosephosphates are proposed to be synthesized through the ribulose-monophosphate pathway (Jahn *et al.*, 2007). Based on genome analysis and due to its metabolism it is assumed that *I. hospitalis* cannot generate ATP via substrate-level phosphorylation (Huber *et al.*, 2012). Instead, energy is exclusively conserved by an A_1A_OATP synthase, which

uses an ion-gradient across the outer cellular membrane (OCM). The ion-gradient is induced by a primary proton pump, the H_2:sulfur oxidoreductase (Küper *et al.*, 2010, Huber *et al.*, 2012).

Cells of *I. hospitalis* exhibit a slightly irregular coccoid shape with a diameter of 1-4 µm. Their cell appendages, referred to as Iho670 fibers, are 14 nm in width, up to 20 nm long and are mainly composed of the protein Igni_0670 (Müller *et al.*, 2009). The fibers were shown to exhibit a type IV pili-like structure and are embedded in the inner membrane by a unique anchor structure (Yu *et al.*, 2012, Meyer *et al.*, 2014).

Unlike most Archaea, *I. hospitalis* cells do not possess an S-layer as outermost structure (Rachel *et al.*, 2002, Fig. I.2 A and B). In addition to an inner membrane, they feature an OCM, which encases an intermembrane compartment (IMC). Both membranes are different in their composition: The inner membrane consists of archaeol and caldarchaeol, while the OCM only contains archaeol derivates. The most abundant protein in the OCM is Ihomp1, which forms pore-like complexes (Burghardt *et al.*, 2007, Rachel *et al.*, 2002). Based on immuno-EM, the A_1A_O ATP synthase and the H_2:sulfur oxidoreductase were shown to be exclusively located in the OCM of *I. hospitalis*, as well (Küper *et al.*, 2010).

The IMC contains a highly dynamic endogenous membrane system, primarily consisting of membrane-surrounded vesicular structures and tubes derived from the cytoplasm (Huber *et al.*, 2000, Paper *et al.*, 2007, Huber *et al.*, 2012). Latest studies showed that these structures are mainly cytoplasmic protrusions (only few putative vesicles; Heimerl, 2014). Recently, interaction of the inner membrane system with the OCM was demonstrated to be mediated by circular structures (Fig. I.2 D, Heimerl, 2014). In addition, the presence of a filamentous matrix in the IMC was revealed, which is likely to represent a cytoskeleton (Fig. I.2 C, Heimerl, 2014). Altogether, the ultrastructure is reminding of a primitive eukaryotic endogenous membrane system, as shown for *Giardia lamblia* (Heimerl, 2014). Due to the exclusive location of the ATP synthase and the H_2:sulfur oxidoreductase in the OCM of *I. hospitalis*, it is assumed that large quantities of ATP are available in the IMC (Küper *et al.*, 2010, Mayer *et al.*, 2012). The acetyl-CoA synthetase (ACS), which consumes ATP was the first enzyme that was shown to be located in the IMC (Mayer *et al.*, 2012).

The cytoplasm was described to contain DNA and ribosomes. Given those facts, a spatial and a functional compartmentalization of the *I. hospitalis* cell becomes evident: DNA replication and protein biosynthesis take place in the cytoplasm separated from energy conservation in the IMC (Fig. I.3 A, Küper *et al.*, 2010).

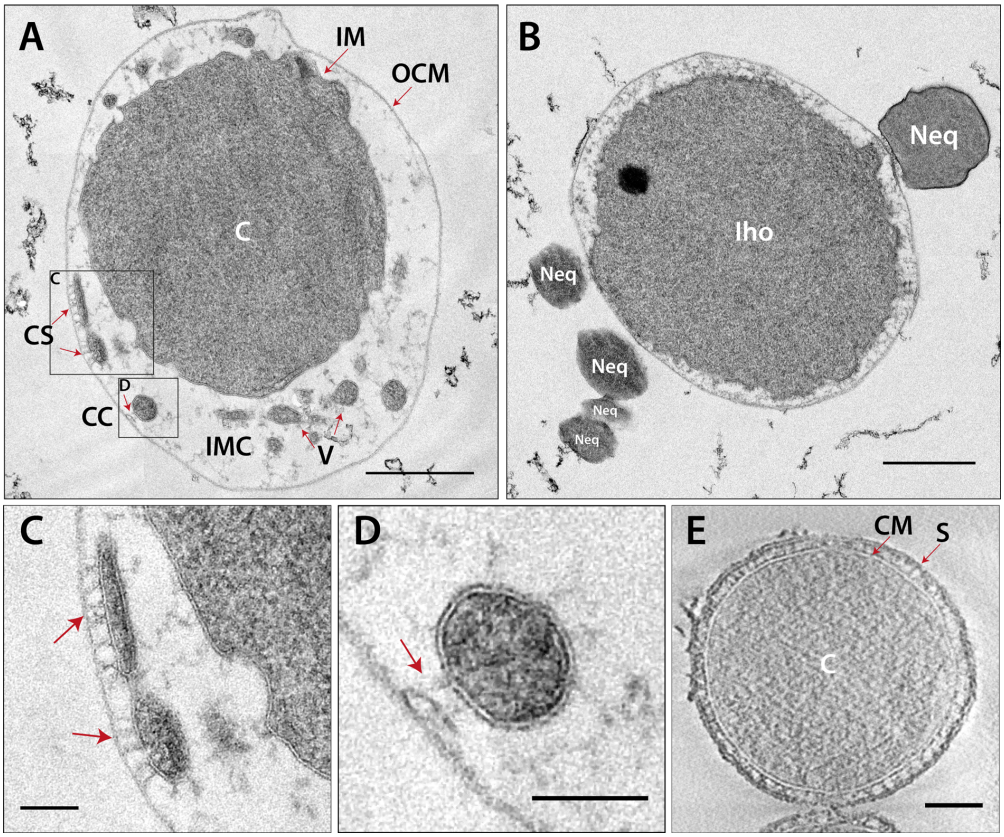

Fig. I.2.: ***Ultrastructure of I. hospitalis and N. equitans.*** *Ultrathin sections of Epon-embedded cells of the co-culture KIN4M.* ***A*** *and* ***B****: Ultrastructure of I. hospitalis and N. equitans; C= cytoplasm, IMC= intermembrane compartiment, IM= inner membrane, OCM= outer cellular membrane, V= cytoplasmic protrusions, CC= circular complexes, CS= filaments in the IMC, Iho= I. hospitalis, Neq= N. equitans, size bars: 500nm. Note the attached N. equitans cells on the I. hospitalis surface in picture B.* ***C*** *and* ***D****: Enlargements of picture A. Filaments in the IMC (C, elements of a putative cytoskeleton) and circular complexes (D), size bar: 100 nm.* ***E****: Ultrastructure of N. equitans (layer of a tomogram; from Heimerl, 2014); C= cytoplasm, CM= cytoplasmic membrane, S= S-layer, size bar: 100 nm.*

This raises a number of questions, which are highly relevant for understanding the physiology of this unusual Prokaryote, including the specific functions and the interactions of both membranes with each other and the IMC (Küper *et al.*, 2010, Moissl-Eichinger and Huber, 2011). Recombinant expression of membrane- and transport proteins are currently an active field of research (Stefanie Daxer and Pia Wiegmann).

The genus *Ignicoccus* comprises three additional members: *I. pacificus* (Huber et al., 2000), *I. islandicus* (Huber *et al.*, 2000) and the recently isolated strain MEX13A (Fig. I.3 B, Lange, 2009). All *Ignicoccus* species share a quite similar morphology

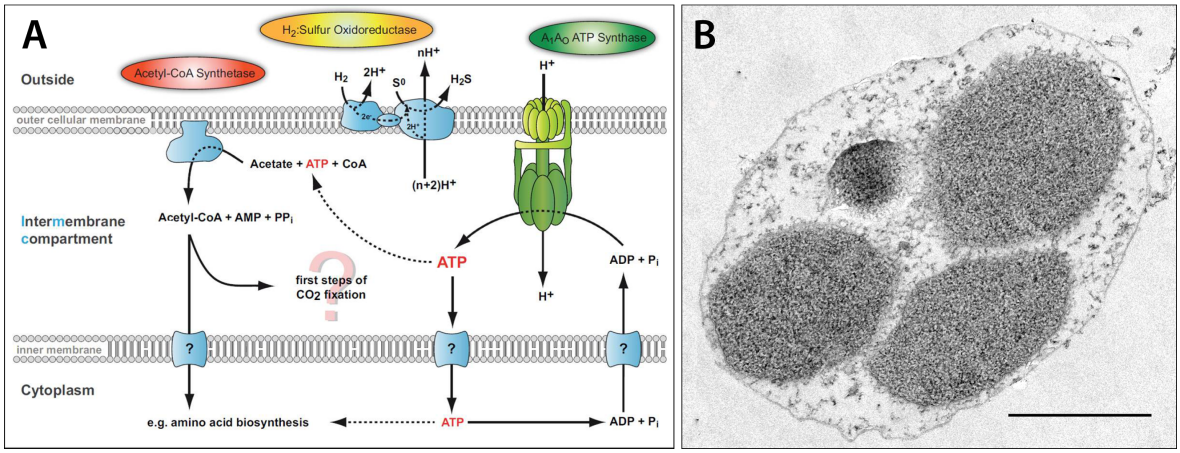

Fig. I.3.: ***A****: Scheme for energy conservation in the IMC of I. hospitalis from Küper* et al.*, 2010 and Huber* et al.*, 2012; The H_2:sulfur oxidoreductase pumps protons from the IMC out of the cell, which are used by the ATP synthase to generate ATP. Structure model of the ATP synthase according to Vonck* et al.*, 2009. ATP is consumed by the ACS, located in the IMC associated with the OCM.* ***B****: ultrastructure of the isolate MEX13A; Note the presence of four cytoplasms, size bar: 1 µm.*

and metabolism. However, the exclusive localization of the ATP synthase and the H_2:sulfur oxidoreductase cannot reasonably be estimated for the other species as shown for *I. hospitalis*, since data obtained from fluorescence microscopy do not coincide with data from TEM analysis (Flechsler, 2010). The formation of 'giant' cells of up to 20 µm and the existence of several cytoplasms in one cell is regarded as characteristic for the isolate MEX13A. Yet, a small percentage of extraordinary larger cells of 5-6 µm has also been observed for the other species. These cells are particularly suitable for studying the dynamic processes in the IMC as the dynamics can be followed in a light- or in a thermomicroscope (Fig. I.3 B, Lange, 2009, Heimerl, 2014).

Besides its striking ultrastructure and the unusual localization of some proteins, *I. hospitalis* is able to serve as host for *N. equitans* (Fig. I.2 B and E). *N. equitans* was found to be directly attached to the surface of *I. hospitalis* and exhibits cell sizes of 350 nm - 500 nm (Huber et al., 2002). *N. equitans* is strictly dependent on *I. hospitalis* and was the first representative of the 'Nanoarchaeota' to be detected and to be grown in the laboratory. Meanwhile, quite a number of Nanoarchaea from diverse ecological habitats have been isolated and one of them can even be cultivated (personal communication Mircea Podar). The ultrastructure of *N. equitans* reveals an electron dense cytoplasm surrounded by a cytoplasmic membrane, a quasi-periplasmic space and an S-layer. With a size of 490 kbp, the organism has one of the smallest known archaeal genomes

and encodes genes for replication, translation, transcription, DNA repair and cell cycle. However, the genome lacks genes for the biosynthesis of nucleotides, amino acids, lipids and cofactors (Waters *et al.*, 2003). In addition, the *N. equitans* genome only encodes subunits of an incomplete ATP-synthase, presumably consisting of five subunits. ATP-production by this incomplete ATP-synthase has not been shown yet (Waters *et al.*, 2003). For this, there has been much speculation about a possible transport of required subunits or of ATP from *I. hospitalis* into *N. equitans* (Küper *et al.*, 2010). On the basis of recent investigations the enzyme was suggested to generate an ion-gradient in free *N. equitans* cells (Kreuter, 2014). In accordance with its minimalistic genome, the organism is not able to grow in pure culture and it is assumed that it even receives the required lipids and amino acids from its host *I. hospitalis* (Jahn *et al.*, 2007, Hamerly *et al.*, 2014). Proteome analysis of a time course of the *N. equitans*/*I. hospitalis* co-culture revealed only low impact of *N. equitans* on its host (Giannone *et al.*, 2011, Giannone *et al.*, 2014). The main effects of *N. equitans* on *I. hospitalis* became apparent in upregulation of genes involved in energy generation, carbon fixation, cellular membrane stabilization and genes for several transporters. *I. hospitalis* genes for transcription factors, replication and cell cycle control proteins were found to be downregulated (Giannone *et al.*, 2011, Giannone *et al.*, 2014).

The contact site between both organisms covers only 40-170 nm (Junglas *et al.*, 2008). Based on tomography, a direct contact of both cells via the cytoplasms was revealed with the S-layer of *N. equitans* being partially disintegrated at the contact site (Heimerl, 2014).

The facts available indicate a parasitic relationship between both Archaea. Nevertheless, the connection of those two organisms was termed "intimate association", since *I. hospitalis* and *N. equitans* form a stable co-culture. (Jahn *et al.*, 2007, Moissl-Eichinger and Huber, 2011).

3. Objectives

The compartmentalized cell structure of *I. hospitalis*, the unique location of its ATP synthase in the OCM and the recent localization of the ACS in the IMC raise questions about the subcellular distribution of the different steps of the CO_2 fixation pathway in this organism (Küper *et al.*, 2010, Mayer *et al.*, 2012). This study mainly aimed to locate certain enzymes (Phosphoenolpyruvate carboxylase (PEP carboxylase), malate dehydrogenase (MDH), succinic semialdehyde reductase (SSR), 4-hydroxybutyryl-CoA

synthetase, crotonyl-CoA hydratase/3-hydroxybutyryl-CoA dehydrogenase) involved in the carbon assimilation cycle to track down its route and to get a deeper understanding in the physiology of these highly unusual cells. In addition, proteins were investigated bioinformatically and enzyme assays were performed with recombinant versions of those proteins to confirm the so far only putative *I. hospitalis* genes of the carbon fixation cycle. In this context, it was attempted to identify and to further characterize the succinic semialdehyde reductase in the genome of *I. hospitalis*, a 'missing gene' of the pathway. Studies of localization were based on immunogold labeling of ultrathin sections for electron microscopy. So as to ensure significance of localization experiments and to optimize sample preparation of *I. hospitalis* for electron microscopy, initially several methods had to be tested and compared and protocols had to be optimized. This included a comparison of immunogold labeling on ultrathin-sectioned *I. hospitalis* cells embedded in different resins (Epon vs Lowicryl) and on cryo-sections, adaptation of antibody incubation times in various protocols and 3D immuno-EM.

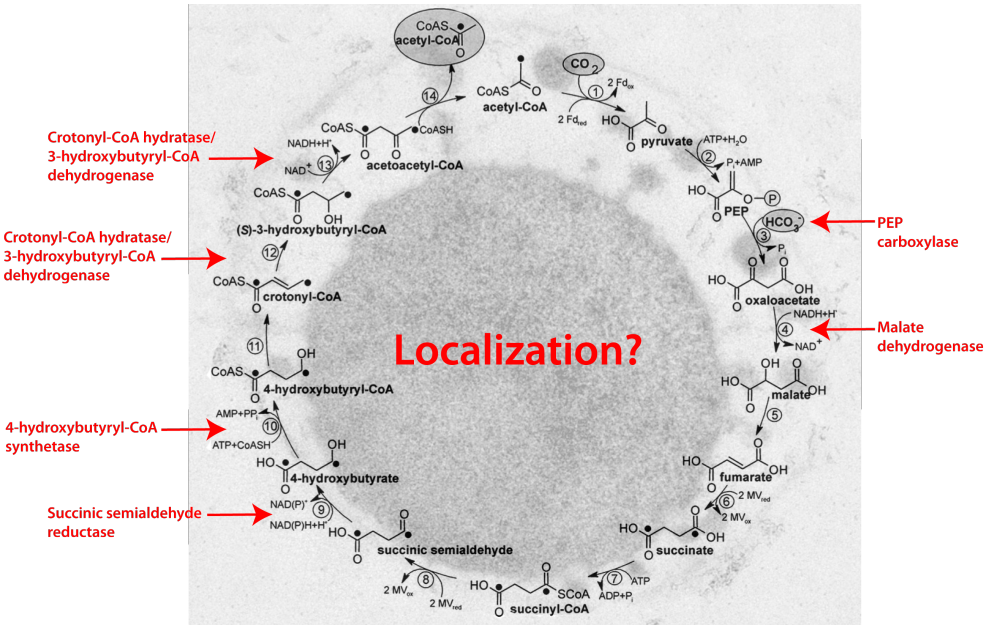

Fig. I.4.: *Dicarboxylate/4-hydroxybutyrate cycle for autotrophic carbon fixation in I. hospitalis. Enzymes: 1, pyruvate synthase; 2, pyruvate:water dikinase; 3, PEP carboxylase; 4, malate dehydrogenase; 5, fumarate hydratase; 6, fumarate reductase; 7, succinate thiokinase; 8, succinyl-CoA reductase; 9, succinate semialdehyde reductase; 10, 4-hydroxybutyryl-CoA synthetase; 11, 4-hydroxybutyryl-CoA dehydratase; 12, crotonyl-CoA hydratase; 13, 3-hydroxybutyryl-CoA dehydrogenase; 14, acetoacetyl-CoA β-ketothiolase, enzymes highlighted in red were examined in the course of this work, from Huber* et al., *2008*

II. Material and Methods

1. Material

1.1. Chemicals

Chemicals not listed here were purchased from Merck, Darmstadt. Gases used for cultivation of microorganisms were provided by Linde, Nürnberg.

Tab. II.1.: *List of (bio-)chemicals*

Product	**Supplier**
Acrylamide/Bis Solution (37.5:1)	Serva, Heidelberg
Agar	Roth, Karlsruhe
Agarose	Roth, Karlsruhe
APS	Serva, Heidelberg
Ampicillin, Na-salt	Roth, Karlsruhe
AMPSO, Na-salt	Sigma-Aldrich, Taufkirchen
ATP, di-Na-salt	Gerbu, Gaiberg
Bromphenol blue, Na-salt	Serva, Heidelberg
BSA, Fraktion V	Roth, Karlsruhe
Chloramphenicol	Roth, Karlsruhe
Citric acid	Sigma-Aldrich, Taufkirchen
Coomassie Brilliant Blue G 250	Serva, Heidelberg
Coomassie Brilliant Blue R 250	Serva, Heidelberg
DTNB	Sigma-Aldrich, Taufkirchen
DTT	Sigma-Aldrich, Taufkirchen
EDTA, di-Na-salt	Serva, Heidelberg
Ethidum bromide	Roth, Karlsruhe
Glutardialdehyde	Fluka Chemie AG, Buchs, CH
Glycerol	Roth, Karlsruhe
Gold, colloidal 15 nm	BBI Solutions, Cardiff, UK

Tab. II.1.: *List of (bio-)chemicals* (continued)

Product	**Supplier**
Gum arabic	Sigma-Aldrich, Taufkirchen
HEPES	Roth, Karlsruhe
Hydrochinone	Riedel de Haën AG, Seelze-Hannover
IPTG	Life Technologies, Darmstadt
Kanamycin sulfate	AppliChem, Darmstadt
MOPS	Sigma-Aldrich, Taufkirchen
NAD, Na-salt	Sigma-Aldrich, Taufkirchen
NADH, reduced Na-salt	Boehringer, Ingelheim
NADP, Na-salt	Sigma-Aldrich, Taufkirchen
NADPH, reduced di-Na-salt	AppliChem, Darmstadt
Oxalacetate, Na-salt	Sigma-Aldrich, Taufkirchen
Pioloform	Plano, Wetzlar
Pyruvate, Na-salt	Fluka Chemie AG, Buchs, CH
Resazurin, Na-salt	Serva, Heidelberg
Sulfur	Riedel de Haën AG, Seelze-Hannover
SDS, Na-salt	Serva, Heidelberg
Silver lactate	Fluka Chemie AG, Buchs, CH
Silver nitrate	Roth, Karlsruhe
Skimmed milk powder	Fluka, Chemie AG, Buchs, CH
Sodium chloride	VWR Int., Leuven, BE
Sodium sulfide	VWR, Darmstadt
TEMED	Sigma-Aldrich, Taufkirchen
Tricine	Roth, Karlsruhe
Tris	Affimetrix, Cleveland, USA
Triton X-100	Roth, Karlsruhe
Tryptone	BD, Heidelberg
Tween 20	Roth, Karlsruhe
Uranyl acetate	Fluka Chemie AG, Buchs, CH
Yeast extract	Roth, Karlsruhe

CoA-esters were synthesized and kindly provided by Dr. Ivan Berg's group (Institute for Microbiology, University of Freiburg). Crotonyl-CoA was synthesized of the appropriate acid anhydride and free CoA according to Simon and Shemin, 1953. (S)- and (R)-3-hydroxybutyryl-CoA were prepared according to Stadtman, 1957.

1.2. Molecular weight markers and DNA size markers

Tab. II.2.: *List of molecular weight markers*

Molecular weight marker	Supplier
PageRuler^{TM} Unstained Protein Ladder; SM0661	Fermentas, St. Leon-Rot
PageRuler^{TM} Prestained Protein Ladder; SM0671	Fermentas, St. Leon-Rot

Tab. II.3.: *List of DNA size markers*

DNA size marker	Supplier
1kb DNA Ladder; N3232	New England Biolabs, Frankfurt am Main
100bp DNA Ladder; N3231	New England Biolabs, Frankfurt am Main

1.3. Enzymes and kits

Tab. II.4.: *List of enzymes and kits*

Product	Supplier
α-Chymotrypsin	Sigma-Aldrich, Taufkirchen
AURION Blocking Solution	Aurion, Wageningen, NL
AURION BSA-c™	Aurion, Wageningen, NL
Champion™ pET Directional TOPO Expression Kit	Life Technologies, Darmstadt
DNAse I	Roche Diagnostics GmbH, Mannheim
dNTP-Mix; NTPMX100	Qbiogene, Heidelberg
Dynabeads® Protein A Immunprecipitation Kit	Life Technologies, Darmstadt
Epon® 812 Mix	Fluka Chemie AG, Buchs, CH
E.Z.N.A.™ Gel Extraction Kit	Omega Bio-Tek, Norcross, USA
LB-Agar	Roth, Karlsruhe
LB-Medium	Roth, Karlsruhe
Lowicryl HM20	Polysciences Inc., Warrington, USA

Tab. II.4.: *List of enzymes and kits* (continued)

Product	**Supplier**
Lysozyme	AppliChem, Darmstadt
Phusion® High-Fidelity DNA Polymerase (2U/µl)	New England Biolabs, Frankfurt am Main
Phusion HF® Buffer (5x)	New England Biolabs, Frankfurt am Main
Protease Inhibitor - Cocktail Tablets	Roche Diagnostics GmbH, Mannheim
Protino® Ni-TED Resin	Macherey-Nagel, Düren
R-Gent SE-EM Silver Enhancement Reagents	Aurion, Wageningen, NL
Qiagen Plasmid Plus Midi Kit	Qiagen, Hilden
Restriction enzymes (and associated buffers)	New England Biolabs, Frankfurt am Main
RNAse A®	Serva, Heidelberg
RNase AWAY®	Roth, Karlsruhe
Roti®-Quant	Roth, Karlsruhe
Trypsin Sequencing Grade	Roche Diagnostics GmbH, Mannheim
Western Lightning® ECL	Perkin Elmer, Rodgau

1.4. Constructs

Gene constructs, produced in the course of this project, were codon-optimized for *E. coli* and cloned into the expression vector pRSETa by Life Technologies, Regensburg (Tab. II.5). Complete sequences of optimized genes and vectors as well as optimized codon quality distribution plots can be viewed on the enclosed DVD (see supplementary). After transformation into an *E. coli* expression strain, constructs were used for production of recombinant proteins.

Tab. II.5.: *List of constructs*

Constructs	**Supplier**
pRSETa_Igni_0341	Life Technolgies, Regensburg
pRSETa_Igni_1263	Life Technolgies, Regensburg
pRSETa_Igni_0132	Life Technolgies, Regensburg
pRSETa_Igni_0475	Life Technolgies, Regensburg
pRSETa_Igni_0379	Life Technolgies, Regensburg
pRSETa_Igni_1058	Life Technolgies, Regensburg

1.5. Antibodies

The anti-A_1 antibody was provided by Ulf Küper (Küper *et al.*, 2010). For generation of the anti-A_1 antibody purified native A_1 subcomplexes of the A_1A_O ATP synthase were injected into a rabbit. For generation of antibodies against the proteins Igni_0341, Igni_1263, Igni_0132, Igni_0379 and Igni_1058, the respective genes were cloned and heterologously expressed in *E.coli*. The obtained proteins were purified and provided to Davids, Burgweinting for injection into rabbits. Antibodies directed against the polyhistidine tag and against double stranded DNA were commercially acquired. Antibodies directed against Igni_1359 and Igni_0955 (from rabbit) were kindly provided by Dr. Arnulf Kletzin, TU Darmstadt. The proteins Igni_1359 and Igni_0955 were purified from *I. hospitalis* cells (KIN4/I). All primary antibodies used in this study were polyclonal except for the anti-polyhistidine antibody and the anti-ds DNA antibody.

Tab. II.6.: *List of primary antibodies*

Primary antibodies	**Protein/Target**	**from**	**generated in**	**Supplier**
Anti-A_1	A_1 subcomplex of the ATP synthase	*Ignicoccus hospitalis*	rabbit	Davids Biotechnologie, Burgweinting
Anti-ACS	Acetyl-CoA synthetase	*Ignicoccus hospitalis*	rabbit	Davids Biotechnologie, Burgweinting
Anti-Igni_0341	PEP carboxylase	*Ignicoccus hospitalis*	rabbit	Davids Biotechnologie, Burgweinting
Anti-Igni_1263	Malate dehydrogenase	*Ignicoccus hospitalis*	rabbit	Davids Biotechnologie, Burgweinting
Anti-Igni_0132	Succinic semialdehyde reductase	*Ignicoccus hospitalis*	rabbit	Davids Biotechnologie, Burgweinting
Anti-Igni_0475	4-hydroxy-butyrate-CoA synthetase	*Ignicoccus hospitalis*	rabbit	Stephen Bell, Bloomington (US)
Anti-Igni_0379	4-hydroxy-butyrate-CoA synthetase	*Ignicoccus hospitalis*	rabbit	Davids Biotechnologie, Burgweinting
Anti-Igni_1058	Crotonyl-CoA hydratase/3-hydroxybutyryl-CoA dehydrogenase	*Ignicoccus hospitalis*	rabbit	Davids Biotechnologie, Burgweinting
Anti-polyhistidine	Polyhistidine tag	-	mouse	Sigma-Aldrich, Taufkirchen
Anti-ds DNA	DNA	-	mouse	Abcam, Cambridge (UK)
Anti-Igni_0955	Multihaem cytochrome c	*Ignicoccus hospitalis*	rabbit	Davids Biotechnologie, Burgweinting
Anti-Igni_1359	Multihaem cytochrome c	*Ignicoccus hospitalis*	rabbit	Davids Biotechnologie, Burgweinting

Tab. II.7.: *List of secondary antibodies and protein A conjugates*

Secondary antibodies and protein A conjugates	**Supplier**
Anti-rabbit IgG + HRP	Sigma-Aldrich, Taufkirchen
Anti-mouse IgG + HRP	Sigma-Aldrich, Taufkirchen
Goat anti rabbit (ultrasmall gold)	Aurion, Wageningen, NL
Mouse anti rabbit (ultrasmall gold)	Aurion, Wageningen, NL
Goat anti rabbit (6 nm gold)	Aurion, Wageningen, NL
Mouse anti rabbit (6 nm gold)	Aurion, Wageningen, NL
Dynabeads Protein A	Life Technologies, Darmstadt

1.6. Organisms

Tab. II.8.: *List of microorganisms*

Archaea	**Strain**	**Source of supply**	**Reference**
Ignicoccus hospitalis and Nanoarchaeum equitans	KIN4/M	BBR 17/10/4	Huber *et al.*, 2002
Ignicoccus hospitalis	KIN4/I	BBR 17/12/4	Paper *et al.*, 2007
Ignicoccus islandicus	Kol8	BBR 17/10/1	Huber *et al.*, 2000
Ignicoccus pacificus	LPC33	BBR 17/10/2	Huber *et al.*, 2000
"Ignicoccus morulus"	MEX13A	BBR 29/08/4	Lange, 2009
Escherichia coli	TOP 10	Life Technologies, Darmstadt	
Escherichia coli	BL21 Star™ (DE3)	Life Technologies, Darmstadt	
Escherichia coli	Rosetta 2 (DE3)	Novagen, Merck KGaA, Darmstadt	

1.7. Buffers and solutions

Tab. II.9.: *List of buffers and solutions*

Buffer/solution	Chemical agent	Amount	Concentration
Antibiotics			
Ampicillin stock	Ampicillin, Na-salt		100 mg/ml
	Filter sterilize and store at −20°C		
Chloramphenicol stock	Chloramphenicol in ethanol		34 mg/ml
	Filter sterilize and store at −20°C		
Kanamycin stock	Kanamycin sulfate		30 mg/ml
	Filter sterilize and store at −20°C		
Isolation of gDNA (according to Ramakrishnan and Adams, 1995)			
Salt-out mixture	NaCl		5 M
Cell suspension solution	Tris/HCl pH = 8.0		0.5 M
	EDTA		0.2 M
	NaOH		0.46 M
RNase mixture	RNase A		1 mg/ml in 50% glyerol
	NaCl		0.02 M
	EDTA		0.001 M
	Tris/HCl pH = 7.5 - 7.6		0.05 M
Cell lysis denaturing solution	SDS		15%
	Adjust pH to 6.6		
Protease mixture	Proteinase K		20 mg/ml
	Tris/HCl pH = 8.0		0.05 M
	$CaCl_2$		0.005 M
TE Buffer	Tris/HCl pH = 8.0		0.01 M
	EDTA		0.001 M
Electrophoresis of DNA (according to Sambrook *et al.*, 1989)			
10 x Loading dye (pH = 8.0)	Bromphenol Blue		0.25 % (w/v)
	Xylene cyanol		0.25 % (w/v)
	Glycerol		50 % (v/v)
	EDTA		20 mM

Tab. II.9.: *List of buffers and solutions* (continued)

Buffer/solution	Chemical agent	Amount	Concentration
10 x TAE Buffer	Tris/Acetate (pH = 8.0)		40 mM
	EDTA		1 mM
Ethidium bromide stock	Ethidium bromide		10 mg/ml
	Store in the dark at 4°C		

Plasmid Preparation (according to Birnboim and Doly, 1979, modified)

Acetate solution	Glacial acetic acid	5M
	KAc (until pH = 4.8)	5M
	Store at 4°C	
Alkaline SDS solution	SDS	1 % (w/v)
	NaOH	200 mM
GTE buffer	Glucose	50 mM
	Tris/HCl pH = 8.0	25 mM
	EDTA pH = 8.0	10 mM

Preparation of competent *E. coli* cells (according to Hanahan, 1983)

TFB	MES/KOH (1 M, pH = 6.3)	10 mM
	$MnCl_2$ x 4 H_2O	45 mM
	$CaCl_2$ x 2 H_2O	10 mM
	KCl	100 mM
	Hexaminecobalt chloride	3 mM
FSB	Potassium acetate (pH = 7.5)	10 mM
	$MnCl_2$ x 4 H_2O	45 mM
	$CaCl_2$ x 2 H_2O	10 mM
	KCl	10 mM
	Hexaminecobalt chloride	100 mM
	Glycerol	10 % (v/v)
DnD	DTT	1 M
	DMSO	90 % (v/v)
	Potassium acetate (pH = 7.5)	10 mM

Tab. II.9.: *List of buffers and solutions* (continued)

Buffer/solution	**Chemical agent**	**Amount**	**Concentration**
Expression and Purification			
IPTG	IPTG	1,19 g	500 mM
	$H_2O_{Millipore}$	ad 10 ml	-
	Filter sterilize		
Lysozyme	Lysozyme	100 mg	100 mg/ml
	$H_2O_{Millipore}$	ad 1 ml	-
	Store at 4°C		
DNase	DNase	2 mg	2 mg/ml
	$H_2O_{Millipore}$	ad 1 ml	-
	Store at 4°C		
1 x LEW	NaH_2PO_4 x 2 $H_2O_{Millipore}$	7.8 g	50 mM
	NaCl	17.5 g	300 mM
	$H_2O_{Millipore}$	ad 1000 ml	-
	Adjust pH to 8.0		
Denaturing Solubilization Buffer	NaH_2PO_4 x 2 $H_2O_{Millipore}$	7.8 g	50 mM
	NaCl	17.5 g	300 mM
	Urea	480.5 g	8 M
	$H_2O_{Millipore}$	ad 1000 ml	-
	Adjust pH to 8.0		
(Denaturing) Elution Buffer	NaH_2PO_4 x 2 $H_2O_{Millipore}$	7.8 g	50 mM
	NaCl	17.5 g	300 mM
	(Urea	480.5 g	8 M)
	Imidazole	17.0 g	250 mM
	$H_2O_{Millipore}$	ad 1000 ml	-
	Adjust pH to 8.0		
Electrophoresis of proteins (according to Laemmli, 1970, Schägger and Von Jagow, 1987)			
2 x Loading dye	Glyerol		10 % (v/v)
	SDS		5 % (w/v)
	Tris/HCl, pH = 7.5		50 mM
	Na_2EDTA		10 mM
	Bromphenol Blue		0.01 % (w/v)

Tab. II.9.: *List of buffers and solutions* (continued)

Buffer/solution	Chemical agent	Amount	Concentration
	DTT		5 mM
	$H_2O_{Millipore}$	ad 10 ml	-
Anode buffer	Tris/HCl, pH = 8.8	24.22 g	200 mM
	$H_2O_{Millipore}$	ad 1000 ml	-
Cathode buffer	Tris/HCl, pH = 8.3	12.11 g	100 mM
	Tricine	17.92 g	100 mM
	SDS	1.00 g	0.1 % (w/v)
	$H_2O_{Millipore}$	ad 1000 ml	-
Stacking gel buffer	Tris/HCl	3.03 g	0.5 M
(pH = 6.8)	SDS	0.20 g	0.4 % (w/v)
	$H_2O_{Millipore}$	ad 50 ml	-
Separating gel buffer	Tris/HCl	9.10 g	1.5 M
(pH = 8.8)	SDS	0.20 g	0.4 % (w/v)
	$H_2O_{Millipore}$	ad 50 ml	-
Western blotting			
Semidry blotting	Tris	3.03 g	25.0 mM
buffer (Towbin	Glycine	14.41 g	192.0 mM
et al., 1979)	Methanol p.A.	200 ml	20.0 %
	$H_2O_{Millipore}$	ad 1000 ml	-
TBS	Tris/HCl pH = 7.6	2.42 g	20 mM
	NaCl	8.0 g	137 mM
	$H_2O_{Millipore}$	ad 1000 ml	-
TBS-T	for TBS-T, add 0.1 % (v/v) Tween 20 to TBS		
Staining (according to Neuhoff *et al.*, 1988, Blum *et al.*, 1987)			
Fixation	Methanol	500.00 ml	50.0 % (w/v)
	Acetic acid	100.00 ml	10.0 % (w/v)
Coomassie staining	Coomassie Brilliant Blue G250	2.50 g	0.25 % (w/v)
	Methanol	300.0 ml	30.0 % (v/v)
	Acetic Acid	100.0 ml	10.0 % (v/v)

Tab. II.9.: *List of buffers and solutions* (continued)

Buffer/solution	Chemical agent	Amount	Concentration
Coomassie destaining	Methanol	300.0 ml	30.0 % (v/v)
	Acetic Acid	100.0 ml	10.0 % (v/v)
Coomassie fixation/de-staining for immunization	Ethanol	300.0 ml	30.0 % (v/v)
	Acetic Acid	100. 0 ml	10.0 % (v/v)
Coomassie staining for immunization	Coomassie Brilliant Blue G250	2.50 g	0.25 % (w/v)
	Ethanol	300.0 ml	30.0 % (v/v)
	Acetic Acid	100. 0 ml	10.0 % (v/v)
Silver washing I	Ethanol	500.00 ml	50 % (v/v)
Silver washing II	Ethanol	100.00 ml	10 % (v/v)
Silver blocking	$Na_2S_2O_3$	100 mg	0.02 % (w/v)
	$H_2O_{Millipore}$	ad 450 ml	-
Silver staining	$AgNO_3$	100 mg	0.1 % (w/v)
	$H_2O_{Millipore}$	ad 100 ml	
	Prepare immediately prior to use and add 75 µl 37 % (v/v) Formaldehyde		
Silver developing	Na_2CO_3	30 g	6 % (w/v)
	$H_2O_{Millipore}$	ad 500 ml	-
	Prepare immediately prior to use and add 250 µl 37 % (v/v) Formaldehyde		
Silver stopping	Acetic acid	100 ml	10 % (v/v)
Uranyl acetate solution	Uranyl acetate		2 % (w/v)
Oxalic acid solution	Oxalic acid	1.9 g	0.3 M
	$H_2O_{Millipore}$	ad 50 ml	-
Neutral uranyl acetate solution	Uranyl acetate (4 % (w/v))	5 ml	2 % (w/v)
	Oxalic acid solution (0.3 M)	5 ml	0.15 M
	Mix in a ratio of 1:1 and carefully add 25 % ammonium-hydroxyde until pH of 7		
Gel drying solution	Ethanol		22% (w/v)
	Glycerol		2% (w/v)
	2-Propanol		1% (w/v)

Tab. II.9.: *List of buffers and solutions* (continued)

Buffer/solution	Chemical agent	Amount	Concentration
Immuno labeling			
PBS-BSA	BSA	0.2 g	1%
	1 x PBS	ad 20 ml	-
	Store in aliquots at −20°C		
PBS-Glycine	Glycine	0.10 g	0.1 %
	1 x PBS	ad 100 ml	-
PBS-GA	Glutardialdehyde (25 %)	0.10 ml	2%
	1 x PBS	1.15 ml	-
Silver enhancement solutions (according to Danscher, 1981)			
Solution 1			
Silver lactate solution	Silver lactate	0.11 g	
	$H_2O_{Millipore}$	ad 15 ml	
	Store in aliquots of 150 µl at −20°C		
Solution 2			
Gum arabic solution	Gum arabic	4.95 g	
	$H_2O_{Millipore}$	ad 15 ml	
Hydroquinone solution	Hydroquinone	0.85 g	
	$H_2O_{Millipore}$	ad 15 ml	
Citrate buffer pH=3.8	Citrate	2.55 g	
	Tri-sodium citrate dihydrate	2.35 g	
	$H_2O_{Millipore}$	ad 10 ml	
	Mix 600 µl of gum arabic solution, 150 µl of Hydroquinone solution and 100 µl of citrate buffer; store aliquots at −20°C		
Other Buffers			
PBS	NaCl	8.00 g	137.0 mM
(Sambrook *et al.*, 1989)	KCl	0.20 g	2.7 mM
	Na_2HPO_4	1.40 g	10.0 mM
	KH_2PO_4	0.24 g	1.76 mM
	$H_2O_{Millipore}$	ad 1000 ml	-
	Adjust pH to 7.2 with NaOH		

Tab. II.9.: *List of buffers and solutions* (continued)

Buffer/solution	Chemical agent	Amount	Concentration
HEPES	HEPES	238.3 g	1 M
	$H_2O_{Millipore}$	ad 1000 ml	-
MES	MES	97.6 g	0.5 M
	$H_2O_{Millipore}$	ad 1000 ml	-
MOPS	MOPS	209.3 g	1 M
	$H_2O_{Millipore}$	ad 1000 ml	-
Tris	Tris	121.1 g	1 M
	$H_2O_{Millipore}$	ad 1000 ml	-

1.8. Media

Tab. II.10.: *List of media*

Medium	Chemical agent	Amount	Concentration
SME	NaCl	27.7 g	473.99 mM
(Huber *et al.*, 2000	$MgSO_4$ x 7 H_2O	7.00 g	28.4 mM
Paper *et al.*, 2007)	$MgCl_2$ x 6 H_2O	5.50 g	27.1 mM
	$CaCl_2$ x 2 H_2O	0.75 g	5.1 mM
	KCl	0.65 g	8.7 mM
	NaBr	0.10 g	0.97 mM
	H_3BO_3	0.03 g	0.49 mM
	$SrCl_2$ x 6 H_2O	15 mg	56.3 µM
	KI solution 0.1%	0.10 g	0.30 µM
	$H_2O_{Millipore}$	ad 1000 ml	-
1/2 SME	SME	500.00 ml	2.9 mM
(Huber *et al.*, 2000	KH_2PO_4	0.50 g	9.4 mM
Paper *et al.*, 2007)	$(NH_4)_2SO_4$	0.25 g	-
	$NaHCO_3$	0.16 g	-
	Resazurin, 0.1% (w/v)	1.0 ml	-
	Na_2S x 2 H_2O	0.25 g	-
	$H_2O_{Millipore}$	ad 1000 ml	-

Tab. II.10.: *List of media* (continued)

Medium	Chemical agent	Amount	Concentration
LB (Miller, 1972)	Tryptone	10 g	1%
	NaCl	10 g	1%
	Yeast Extract	5 g	0,50%
	(Agar)	(15 g)	(1.5%)
	$H_2O_{Millipore}$	ad 1000 ml	-
SOC/(SOB) (based on Hanahan, 1983)	Tryptone	20 g	2%
	Yeast Extract	5 g	0,50%
	NaCl	0,58 g	10 mM
	KCl	0,19 g	2,5 mM
	$MgSO_4$	4,92 g	20 mM
	(Glucose)	(3,6 g)	(20 mM)
	$H_2O_{Millipore}$	ad 1000 ml	-
Autoinduction Medium (Studier, 2005, modified)	Na_2HPO_4	6 g	
	KH_2PO_4	3 g	
	Tryptone	20 g	
	Yeast Extract	5 g	
	NaCl	5 g	
	$H_2O_{Millipore}$	ad 1000 ml	
	60 % Glycerol	10 ml	
	10 % Glucose	5 ml	
	8 % Lactose	25 ml	

2. Cultivation

2.1. Cultivation of *Ignicoccus* and *Nanoarchaeum*

2.1.1. Preparation of media

All chemicals, expect sodium sulfide, were dissolved in water and gassed with N_2/CO_2 (80:20 v/v) at 0.5 bar gauge pressure for 30 minutes. Sodium sulfide was dissolved in

1 ml water separately and incubated at 37°C until it was completely dissolved. Sodium sulfide was added to the medium after gassing to reduce residual oxygen. After the pH was adjusted to 6.0 by adding 50 % sulfuric acid, the medium was portioned into 100 ml serum bottles containing a spatula tip of sulfur (20 ml aliquots) in the anaerobic chamber. Serum bottles were then capped with rubber stoppers and additionally sealed with aluminum rings. Subsequently, serum bottles were evacuated and gassed (H_2/CO_2 (80:20 v/v); 1.5 bar gauge pressure) three times at the gassing station. In a last step, serum bottles were sterilized at 110°C for 1 h. 10 % (w/v) stock solutions of yeast extract were autoclaved separately and added if required.

2.1.2. Cultivation

Ignicoccus species were cultivated anaerobically in modified $\frac{1}{2}$ SME (synthetic sea water) medium (Tab. II.10). Serum bottles were inoculated with 0.2 ml of a logarithmically grown preparatory culture and incubated at 90°C while shaking (50 rpm). Additionally, 0.05 % - 0.1 % of yeast extract were added if required.

2.2. Cultivation of *Escherichia coli*

2.2.1. Cultivation

E. coli was cultivated under aerobic conditions in either liquid LB-medium (Tab. II.10) or on solid medium plates (LB-medium containing 1.5 % agar). Cells were incubated in 5 ml - 500 ml batch cultures in reaction tubes or Erlenmeyer flasks. Reaction tubes or flasks were filled to a maximum of 25 % and antibiotics were added if necessary. For inoculation, a single colony was picked, cells were scraped from a glycerol stock or 1 % of a well-grown overnight culture was taken. Incubation was carried out at 37°C while shaking (liquid medium) or in an incubator (solid medium plates).

2.2.2. Long-term storage

E. coli host strains and positive clones were stored as glycerol stocks at −80°C. For this, glycerol was aliquoted in portions à 300 µl in cryovials and autoclaved. 600 µl of an overnight culture were added to a cryovial containing the glycerol and thoroughly mixed.

3. Sterilization

Media, buffers and solutions not sensitive to heat were sterilized by autoclaving for 20 min at 121°C and 1.1 bar gauge pressure. Plastic- and glassware was autoclaved under the same conditions for 40 min. Media containing elemental sulfur was sterilized for 1 h at 110°C. Heat sensitive solutions (e.g. antibiotic stock solutions) were filter-sterilized via 0.2 µm filters.

4. Molecular genetic methods

4.1. Isolation of genomic DNA

Isolation of genomic DNA of *Ignicoccus* was performed according to a protocol developed for sulfur-dependent hyperthermophilic Archaea by Ramakrishnan and Adams, 1995 (Tab. II.9). 0.2 g of frozen cells were resuspended in 1.85 ml of cell suspension solution, after which 50 µl of RNase solution and 100 µl of 15 % SDS solution (pH 6.6) were added. The mixture was incubated for 15 min at 55°C, and after adding 25 µl of proteinase K solution, for one additional hour at 55°C. Proteins and carbohydrates were removed by adding 500 µl of NaCl solution (5 M). After mixing thoroughly, the lysate was incubated on ice for 10 min. Precipitated proteins and other cell components were centrifuged at maximum speed in a tabletop centrifuge. The supernatant was then transferred to a clean tube and 2 ml TE buffer as well as 8 ml of 95 % ethanol were added. After 2 min incubation time, the tube was gently inverted several times. Visible DNA filaments were then scooped into a clean tube and the remaining lysate was centrifuged again. Finally, the supernatant was discarded and the resulting pellet and the DNA filaments were air dried and then dissolved in $H_2O_{Millipore}$.

4.2. Agarose gel electrophoresis of DNA and gel extraction

Agarose gels (0.8 - 1.5 % (w/v)) in 1 x TAE with ethidium bromide (Sambrook *et al.*, 1989, Tab. II.9; final concentration 1 µg/ml) were used for electrophoresis. For this purpose, an appropriate amount of agarose was dissolved in 20 ml 1 x TAE buffer and heated in a microwave. Before casting the dissolved agarose in a gel slide, ethidium bromide was added. After the gel had cooled down, elecrophoresis was performed with 1 x TAE as running buffer. Samples were separated at 120 V for 25 min (Biometra Standard Power Pack P25; Biometra, Göttingen). The DNA samples were mixed with

10 x loading dye depending on their volume and applied into the sample wells. Additionally, 5 µl of a DNA-marker, containing a mixture of DNA fragments of known size and known amount, were applied on the gel (Tab. II.3). Afterwards, DNA was visualized by using a UV-screen. For DNA extraction from agarose gels, the corresponding DNA bands were cut from the gel using a scalpel while being exposed to UV-light. DNA was extracted using a gel extraction kit (E.Z.N.A.™ Gel Extraction Kit).

4.3. Quantitative and qualitative analysis of DNA

The concentration of DNA preparations was determined using NanoDrop UV spectrometry (NanoDrop ND-1000, Peqlab, Erlangen) at a wavelength of 260 nm. To assess the purity of DNA samples, the absorbance was additionally measured at 230 and 280 nm. An OD_{260}/OD_{280} ratio of 1.8 is considered as pure. For OD_{260}/OD_{230} values are supposed to be within the range of 1.8 - 2.2 (NanoDrop 1000 Spectrophotometer, User's Manual).

4.4. Polymerase chain reaction (PCR)

The PCR for the gene *Igni_1113* was carried out according to the instructions of the Champion™ pET Directional TOPO® Expression Kit as shown in tables II.11, II.12 and II.13. For colony PCR, initial denaturation time was extended to 6 min at 95°C (Mullis and Faloona, 1987, Saiki *et al.*, 1988).

Tab. II.11.: *PCR primer for the gene Igni_1113*

Primer	**Sequence**
Igni_1113 F	CACCATGAGCGAGGACAAGGTCAACAA
Igni_1113 R	TCACTGGCGGAGCCTCTCC

4.5. Preparation of plasmids

Plasmid DNA of *E. coli* cultures up to 5 ml was isolated according to a protocol by Karin Barbinger (Tab. II.9, Birnboim and Doly, 1979). 5 ml of a freshly grown overnight-culture (grown in LB-medium with appropriate antibiotics) were centrifuged in a tabletop centrifuge (5417C; Eppendorf AG, Hamburg) at 13000 rpm for 1 min. The supernatant was discarded and cells were dissolved in 100 µl GTE-buffer. Additionally,

Tab. II.12.: *PCR amplification conditions*

PCR step	Temperature [°C]	Time	Cycle number
Initial denaturation	95	1 min	1
Denaturation	95	30 s	34
Annealing	70	30 s	
Elongation	72	165 s	
Final elongation	72	5 min	1
End	8	forever	

Tab. II.13.: *Reaction mixture for PCR*

Reagent	Amount
5 x Phusion HF buffer	4 µl
dNTP mix (each 10 mM)	0.4 µl
Forward Primer (10 mM)	2 µl
Reverse Primer (10 mM)	2 µl
Template	50 - 100 ng
Phusion DNA Polymerase (5 U/µl)	0.2 µl
$H_2O_{Millipore}$	ad 20 µl

1 µl of a RNase A solution (concentration 1 µg/µl) was added and the mixture was then incubated for 5 min at room temperature. Accordingly, 200 µl of alkaline SDS solution were added and the tube was then incubated on ice for 5 min. Immediately after, 150 µl of 5 M potassium acetate were added and thoroughly mixed by inverting the tube several times. After having centrifuged the 'Mini prep' sample in a tabletop centrifuge for 3 min at 13000 rpm the supernatant was transferred to a clean tube. This step was repeated once more before precipitating DNA with 900 µl ethanol (100 %) on ice for a minimum of 5 min. Precipitated DNA was centrifuged (Himac CT15RE; Hitachi, Tokyo, JP) for 30 min at 4°C and 14000 rpm. The supernatant was discarded and DNA was washed one more time with 70 % ethanol on ice. Following this, DNA was centrifuged under the same conditions as in the previous step for 5 min and the supernatant was discarded. Finally, pellets were air dried and dissolved in 35 µl $H_2O_{Millipore}$. For cultures of maximum 50 ml, plasmid DNA was isolated with the QIAGEN Plasmid Plus Midi Kit (Tab. II.4). 'Midi' preparations were used whenever a higher grade of purity was necessary and were performed as stated by the manufacturer.

4.6. Ligation

Ligation was performed according to instructions of the Champion™ pET Directional TOPO® Expression Kit manual (Tab. II.4). A 2:1 ratio of PCR product:TOPO® vector was used. After the ligation process, the reaction mixture was transformed in chemically competent *E. coli* cells (section 4.8).

4.7. Preparation of competent *E. coli* cells

Competent cells of *E. coli* were chemically prepared according to Hanahan, 1983 as described in "The Hanahan Method for Preparation and Transformation of Competent *E. coli*: High-efficiency Transformation" (Tab. II.9).

Cells of the desired *E. coli* strain were transferred from a glycerol stock into 100 ml SOB medium (Tab. II.10) containing 20 mM $MgSO_4$, by using an inoculating loop. Cells were grown at 37°C in a rotary shaker until OD_{600} of 0.4 was reached. The culture was then transferred into 50 ml reaction tubes and chilled on ice for 10 min. Subsequently, cells were centrifuged (2700 g, 10 min, 4°C; Ch. 2454-Rotor, Heraeus Multifuge 3L-R, Buckinghamshire, U.K.) and the supernatant was discarded. Cells were prepared for immediate use or for storage at −80°C. The cell pellet was resuspended in either 20 ml (per 50 ml tube) of ice-cold TFB (Transformation Buffer) or FSB (Frozen Stock Buffer) transformation buffer and incubated for 10 min on ice. Then, cells were centrifuged under the same conditions and resuspended in 4 ml TFB or FSB. Accordingly, 140 µl of DnD (cells resuspended in TFB) or 140 µl of DMSO (cells resuspended in FSB) were added to cells and then reaction tubes were incubated for 15 min on ice. After adding addional 140 µl of DnD or 140 µl of DMSO to cell suspensions, cells resuspended in TFB were incubated for another 15 min on ice before being aliquoted. Cells resuspended in FSB were also incubated on ice, but immediately aliquoted and snap-frozen in liquid nitrogen.

4.8. Transformation

Plasmids were transformed in *E. coli* cells by heat shock using chemical transformation (Sambrook *et al.*, 1989). 1 - 5 ng plasmid DNA in a volume of 1 - 5 µl were gently mixed with 200 µl *E. coli* cells and incubated on ice for 30 min. Afterwards, cells were heat-shocked for 30 s at 42°C and then immediately transferred to ice for 1 min. After adding 250 µl of room temperature SOC medium (Tab. II.10), cells were incubated

at 37°C for 30 min while shaking (200 rpm). Subsequently, the entire incubation reaction was either added to liquid LB-medium containing the appropriate antibiotics (Tab. II.10) and grown overnight at 37°C while shaking (200 rpm; for expression of proteins) or plated on prewarmed selective plates and incubated overnight at 37°C (for analyzing transformants after ligation). For analysis of transformants, colonies were screened for positive clones using colony PCR (section 4.4).

4.9. DNA sequencing and analysis of sequencing data

DNA sequencing for the construct Igni_1113_pET200 was performed by GeneArt (Regensburg, Germany). The bioinformatic tools CHROMAS (visualization of sequence chromatograms) was used for analysis of sequences.

5. Protein-biochemical methods

5.1. Heterologous expression of proteins in *E. coli*

5.1.1. Induction of protein expression with IPTG

In a first step pilot expressions were performed for each construct to determine optimal IPTG concentrations, growth temperatures and incubation times. For this, 100 ml of selective LB medium (Tab. II.10) were inoculated with 1 ml of an *E. coli* overnight culture and incubated at 37°C while shaking. After having reached an OD_{600} of 0.5-0.8, the culture was split into two separate 50 ml cultures and IPTG was added to a final concentration of 0.5-1 mM to one of the cultures. Further incubation was carried out at temperatures between 18°C-37°C while shaking. Hourly, 1 ml of each culture was transferred into a reaction tube, centrifuged and the resulting pellet was stored at −20°C. Pilot expressions induced with IPTG were performed for 6 h (Sambrook *et al.*, 1989).

Cell disruption and purification of recombinant proteins was carried out as stated by the manufacturer under native and denaturing conditions (Purification of His-tag proteins, user manual, Machery Nagel). For analysis of samples, the frozen cell pellets were thawed on ice and resuspended in 500 µl LEW Buffer. Lysozyme was added to a final concentration of 1 mg/ml and then the cell suspension was incubated on ice for 30 min under stirring. Afterwards, cells were carefully sonicated (HD 2070, Bandelin) on ice. For further processing, 5 µg/ml DNase I was added and the cell suspension was

incubated on ice for additional 15 min under stirring. Finally, samples were centrifuged (Himac CT15RE; Hitachi, Tokyo, JP) at 10000 g for 30 min at 4°C. Supernatant and pellet were then separated into different tubes and prepared for SDS PAGE (section 5.3, Tab. II.9).

Different fractions were checked for recombinant proteins by SDS PAGE (section 5.3) and Western Blot analysis (section 7.2). If recombinant proteins were found in the pellet, cell disruption, disruption of inclusion bodies and purification were performed under denaturing conditions in LEW buffer containing 8 M urea (Tab. II.9). Additionally, light microscopy provided first hints for the localization of proteins in *E. coli*. Inclusion bodies, consisting almost exclusively of recombinant protein, can be recognized as strongly refractive structures in cells of *E. coli* and belong to the insoluble fraction of the cytosol and must therefore be purified under denaturing conditions. After having found optimal conditions for expression of proteins, *E. coli* cultures were upscaled (up to 6 l of culture in parallel). Cells were harvested by centrifugation (Rotor: JA-10, Avanti J-26 XP, Beckman Coulter, Fullertom, USA) after termination of the expression and recombinant proteins were purified according to sections 5.1.3 - 5.1.5.

5.1.2. Autoinduction

Autoinduction (AI) is reported to result in higher amounts of protein than conventional IPTG induction (Studier, 2005). Moreover, AI enables the cell metabolism to gently adapt to the new conditions and cultures can be grown to saturation without checking OD_{600} (Studier, 2005). The AI medium contains glucose and lactose, while initially glucose is preferably metabolized. The lower the concentration of glucose, the more lactose is metabolized, resulting in gentle induction of protein expression. Additionally, expression of proteins in inclusion bodies is supposed to be reduced (Studier, 2005). For AI, *E. coli* strains containing the desired plasmid were inoculated in AI-medium (Tab. II.10) and grown until saturation. After harvesting the cells, expression analysis was carried out as described (section 5.1.1).

5.1.3. Heat precipitation

Several proteins of *E. coli* can be removed by heat precipitation. Since proteins of *Ignicoccus* are supposed to be more heat resistant than *E. coli* proteins, heat precipitation was performed as initial purification step. For this, recombinant proteins of the

soluble fraction were incubated at 60°C - 90°C in a water bath incubator for 15 min. Thereafter, the crude extract was incubated for 15 min on ice and then centrifuged at maximum speed for 15 min at 4°C (Himac CT15RE; Hitachi, Tokyo, JP). Recombinant proteins remained in the supernatant and were transferred into a clean tube.

5.1.4. Affinity purification of his-tagged recombinant enzymes

Since all recombinantly expressed proteins were equipped with a polyhistidine tag (6 x histidine), purification by his-tag specific affinity chromatography was carried out after heat precipitation using Protino® Ni-TED 2000 Packed Columns or Protino® Ni-TED Resin (Tab. II.4, Tab. II.9). Due to the high affinity between histidine and immobilized Ni^{2+} ions, his-tagged proteins can first be enriched in the resin and can then be purified after several washing steps (Bornhorst and Falke, 2000). Elution of proteins was performed by adding imidazole, which acts as a histidine analogon. Protein purification was carried out as stated by the manufacturer under native or denaturing conditions. Eluted protein was sampled in different fractions and analyzed by SDS Page and Western Blotting. When purification was performed under denaturing conditions, the purified protein was directly dialyzed (section 5.1.5). Purified protein was either stored at 4°C or in glycerol stocks (1:1) at −20°C.

5.1.5. Dialysis

For dialysis, Slide-A-Lyzer Dialysis Cassettes (10K, MWCO, Thermo Scientific, Bonn) were used as stated by the supplier. If purified enzymes were sensitive to imidazole the buffer was replaced by 5 mM HEPES (pH = 7.5). Proteins purified under denaturing conditions (with a buffer containing 8 M urea) were dialyzed stepwise with a buffer (LEW buffer or 5 mM HEPES; pH = 7.5) at first containing 2 M urea, then 1 M urea and in a final step in a buffer without urea. This procedure was necessary to prevent precipitation of the protein while refolding. Buffers were exchanged at least three times and each step was performed for 2 h or overnight, respectively. Finally, dialyzed proteins were analyzed by SDS PAGE and protein concentration was determined (section 5.2, section 5.3, Tab. II.9).

5.2. Quantification of proteins

Determination of protein concentration was performed colorimetrically using Coomassie Brilliant Blue-G250 (Roti®-Quant, Karlsruhe) based on the Bradford protein

quantification method (Bradford, 1976). BSA of different concentrations (1-20 µg/ml) was used as standard. Quantification was carried out following the instructions of the supplier.

5.3. SDS-polyacrylamide gel electrophoresis

For separation and analysis of proteins vertical, discontinuous SDS polyacrylamide gel electrophoresis (Tris-Tricine running buffers, Tab. II.9) was carried out according to Laemmli, 1970, modified by Schägger and Von Jagow, 1987. Gels were composed of a separating gel (in general 10 % (v/v) acrylamide, however depending on the molecular weight of the desired protein) with a stacking gel on top (4 % (v/v) acrylamide; Tab. II.14). Ingredients for the separating gel were mixed and then casted between two glass plates (10.5 x 10 x 0.3 cm) separated by two plastic spacers and sealed by a rubber gasket. The glass plates were additionally fixed by special clamps. The separating gel was then covered with isopropyl alcohol. After 30 min of polymerization, isopropyl alcohol was removed and the stacking gel solution was cast on top. Additionally, a 10-sample well comb was added to the gel. After polymerization, gels were either directly used for electrophoresis or wrapped in wet towels and plastic bags stored at 4°C. Before loading the gel, protein samples were mixed with 2 x loading dye 1:1 and incubated for 15 min at 95°C in a water bath. DTT (0.1 M (w/v), stored in aliquots at −20°C) was added to the loading dye before use. Gel runs were performed in self-made electrophoresis chambers (Werkstatt Biologie, University of Regensburg) at 10 mA for 15 min and further at 30 mA per gel for approximately 1 h until desired separation of the molecular weight markers or until the visible blue band reached the bottom of the gel. Unstained protein markers (for Coomassie and silver staining) and prestained protein markers (for Western Blotting) were used as molecular weight markers (Tab. II.2).

Tab. II.14.: *SDS-polyacrylamide gels*

Chemical	**separating gel (10 %)**	**stacking gel (4 %)**
Acrylamid Bis solution (37.5:1)	2 ml	0.3 ml
Tris/HCl, 0.5 M, pH = 6.8		0.5 ml
Tris/HCl, 1.5 M, pH = 8.8	1.5 ml	-
$H_2O_{Millipore}$	2.5 ml	1.2 ml
APS, 10 % (w/v)	30 µl	15 µl
TEMED	5 µl	3 µl

5.4. Staining and drying

Detection of proteins was carried out either by Coomassie staining or silver staining according to the following protocols (Tab. II.15, according to Neuhoff *et al.*, 1988, Blum *et al.*, 1987, modified).

Tab. II.15.: *Staining of SDS-polyacrylamide gels*

Coomassie staining	
Solution	Time
Fixation	30 min
Staining	30 min
Destaining	Change destaining solution until backround is completely destained

Silver staining	
Solution	Time
Fixation	30 min
Washing I	10 min
Washing II	10 min
Blocking	1 min
$H_2O_{millipore}$	3 x 20 sec
Staining	20 min
Developing	Until desired intensity
Stopping	-

For documentation and storage, gels were dried between two cellophane foils and mounted in a plastic frame. Before drying, gels and foils were incubated in gel drying buffer for 30 min (Tab. II.9).

5.5. 'Matrix-assisted laser desorption/ionization'-'Time Of Flight Mass Spectrometry' (MALDI-TOF MS/MS)

For tryptic digestion of in-gel proteins, samples were first separated by gel electrophoresis and Coomassie staining. Bands of interest were cut from the gel, cleaved into small pieces of 1 mm^3 and transferred into 1.5 ml reaction tubes. Gel pieces were then incubated (each step 30 min) in 200 µl of the following solutions with shaking:

1. NH_4HCO_3 (50 mM)
2. NH_4HCO_3 (50 mM), Acetonitril (25 %)
3. Acetonitrile (25 %)
4. Acetonitrile (50 %)

Subsequently, samples were lyophilized in a small freeze-drying device (Univapo 150H und Unijet II, Uniequip Laborgerätebau, Martinsried) for at least 1 h and were then transferred in 0.5 ml Safe-Lock tubes. Proteolytic digestion was performed with 0.2 µg of trypsin (sequencing grade) per 10 µl of the gel volume. Trypsin was prepared as stated by the supplier and diluted in 50 mM of NH_4HCO_3 for digestion. The trypsin solution was added to the samples in two steps and it had to be ensured that the trypsin containing buffer was 1.5 fold of the amount of the gel volume. In a first step half the volume of the buffer containing the total amount of trypsin was added and incubated for 5 min at room temperature. As a second step, the remaining volume was added (50 mM NH_4HCO_3) and the reaction mixture was incubated overnight at 37°C. The next day, the supernatant was discarded and peptides were extracted with 30 µl of the following solutions (each step for 1.5 h):

1. NH_4HCO_3 (100 mM)
2. NH_4HCO_3 (100 mM)
3. NH_4HCO_3 (100 mM), Acetonitrile (50 %)

After each step the supernatant was collected and finally supernatants were united in a 0.5 ml Safe-Lock reaction tube. Further processing of the samples was performed by Eduard Hochmuth at the institute of Prof. Deutzmann (University of Regensburg). MALDI-analysis was carried out with a 4700 Proteomics Analyzer; evaluation was accomplished with the software tool Mascot (Matrix Science LTD., Cottrell and London, 1999).

6. Enzyme assays

Enzyme assays were performed in cooperation with Dr. Ivan Berg at the University of Freiburg. Recombinant 'helping enzymes' were provided by the working group of Dr. Ivan Berg. Enzyme activities were determined using either crude extract of *E.coli* or *Ignicoccus* cells, or using purified recombinant proteins.

6.1. Preparation of cell extracts

Cell extracts for enzyme assays were prepared using a Mixer Mill MM 200 (Retsch GmbH, Haan). Depending on the enzyme assay, 50 mg - 100 mg of pelleted and frozen

cells were resuspended in a suitable buffer in a 1.5 ml reaction tube (e.g. 50 mM Tris buffer pH = 8 or 20 mM MOPS buffer pH = 7). Additionally, the resuspended cell mixture contained a few milligrams of DTT and DNAse, and 1.1 g of glass beads (0.1 - 0.25 mm in diameter). Cells were disrupted at 30 Hz for 10 min in a cell mill. Finally, the cell suspension was centrifuged at 14000 rpm for 10 min in a tabletop centrifuge. Cell extracts were found in the supernatant and available for enzyme assays.

6.2. Enzyme assays linked with the reduction/oxidation of NAD(P)$^+$/NAD(P)H

Enzyme activities involving the reduction/oxidation of NAD(P)$^+$/NAD(P)H were determined and monitored photometrically at 365 nm (ϵ_{NADH} = 3.4 x 10^3 M^{-1} cm^{-1}; ϵ_{NADPH} = 3.5 x 10^3 M^{-1} cm^{-1}) at appropriate temperatures. Reaction mixtures had a volume of 0.5 ml and measurements were carried out in 0.5 ml glass cuvettes (Hellma, Muellheim; diameter = 1 cm) under aerobic conditions in a heatable photospectrometer (Ultraspec 1100 pro; Amersham, Sweden) equipped with an external graph recorder. PH-values of buffers were adjusted to the indicated values at 20°C and were controlled after each reaction using pH strips (MColorHost^{TM}, Merck Millipore, Darmstadt). Assays were started with substrate unless indicated otherwise and were performed with crude extract of induced *E. coli* cultures, crude extract of *I. hospitalis* or recombinant protein. For calculation of K_M-values and v_{max} the software tool GraphPad Prism 6 (Statcon, Witzenhausen) was used.

6.2.1. Characterization of malate dehydrogenase

Malate dehydrogenase assay was performed according to Ramos-Vera *et al.*, 2009 and optimized for the recombinantly expressed protein Igni_1263 (Tab. II.16). MDH activity was monitored by the oxaloacetate-dependent oxidation of NADPH to NADP$^+$ and malate. Assays were performed at 45°C.

Kinetic parameters (K_M and v_{max}). For determination of kinetic parameters, substrates or cosubstrates were added to the reaction mixture in different concentrations (oxaloacetate: 2 mM - 0.01 mM; NADH/NADPH: 0.5 mM -0.01 mM). For oxaloacetate, K_M and v_{max} were determined in a reaction mixture as described in Tab. II.16 at constant concentrations of NADPH. Kinetic parameters for NAD(P)H were determined in a reaction mixture as described in Tab. II.16 at constant concentrations of oxaloacetate.

Tab. II.16.: *Reaction mixture for MDH assay*

Chemical agent	Concentration	Stock	Volume
H_2O	-	-	ad 500 µl
MOPS pH = 7.0	100 mM	1 M	50 µl
$MgCl_2$	5 mM	1 M	2.5 µl
NADPH	0.3 mM	5 mM	30 µl
Enzyme/crude extract	x mM	x mM	x µl
Oxaloacetate	4 mM	50 mM	40 µl

Metal dependencies and substrate specificity. Further characterization of the enzyme including determination of metal dependencies and substrate specificity were performed at 45°C, as well. To test the effect of divalent metal ions on enzyme activity, all components of the assay except oxaloacetate and $MgCl_2$ were mixed and EDTA (0.5 mM or 1 mM) was added. The mixture was incubated for 15 min. The reaction was monitored in a spectrophotometer and was started by addition of substrate. If appropriate, reactivation of the enzyme was tested by adding $MgCl_2$ (5 mM). In addition, the effect of $CaCl_2$ and $MnCl_2$ on MDH activity was tested. At the same time control assays were performed without EDTA and either with or without $MgCl_2$.

To estimate substrate specificity of MDH, oxaloacetate was substituted by pyruvate, acetaldehyde, propionic aldehyde and butyric aldehyde in different reaction mixtures.

6.2.2. Characterization of succinic semialdehyde reductase

Succinic semialdehyde reductase assay. Enzyme activity of SSR was determined based on Ramos-Vera *et al.*, 2011 and optimized for the recombinantly expressed protein Igni_0132 (Tab. II.17). Here, the conversion of succinic semialdehyde to 4-hydroxybutyrate under oxidation of NADH to NAD^+ was measured. Assays were performed at 65°C.

Kinetic parameters (K_M and v_{max}). For determination of K_M-values, substrates or cosubstrates were added to the reaction mixture in different concentrations (SSA: 0.5 mM - 0.005 mM; NADH/NADPH: 0.5 mM - 0.005 mM; section 6.2.1).

Metal dependencies and substrate specificity. Effects of divalent metal ions on SSR activity and substrate specificity were determined according to the reaction scheme in Tab. II.17 and as described in section 6.2.1.

Tab. II.17.: *Reaction mixture for SSR assay*

Chemical agent	Concentration	Stock	Volume
H_2O	-	-	ad 500 µl
Tris/HCl pH = 7.8	100 mM	1 M	50 µl
DTT	5 mM	50 mM	50 µl
$MgCl_2$	5 mM	1 M	2.5 µl
NADH	0.5 mM	5 mM	30 µl
Enzyme/crude extract	x mM	x mM	x µl
Succinic semialdehyde	0.2 mM	50 mM	2 µl

For determination of substrate specificity, malonic semialdehyde, acetaldehyde, propionic aldehyde and butyric aldehyde were added to the reaction mixture instead of succinic semialdehyde. Malonic semialdehyde was synthesized from malonyl-CoA and recombinant malonyl-CoA reductase (MCR) from *Sulfolobus tokodaii* (Alber *et al.*, 2006). Compounds were mixed according to Tab. II.18 (Kockelkorn and Fuchs, 2009). After complete transformation of malonyl-CoA to malonic semialdehyde (visual control with photometer), the assay was started by adding recombinant SSR. The assay was performed at 50°C.

Tab. II.18.: *Substrate specificity: Malonic semialdehyde assay*

Chemical agent	Concentration	Stock	Volume
H_2O	-	-	ad 500 µl
Tris/HCl pH = 7.8	100 mM	1 M	50 µl
DTT	5 mM	50 mM	50 µl
$MgCl_2$	5 mM	1 M	2.5 µl
NADPH	0.5 mM	5 mM	30 µl
MCR	0.5 mM	5 mM	50 µl
Malonyl-CoA	5 mM	100 mM	25 µl
Enzyme/crude extract	x mM	x mM	x µl

Reverse reactions. Activity of the SSR in the direction of NAD^+ was measured using the following assay mixture in a Tris/HCl buffer (pH = 8.5) at 65°C (Tab. II.19). The assay was started with either 4-hydroxybutyrate or 3-hydroxypropionate.

Tab. II.19.: *Reaction mixture for SSR assay: Reverse reaction*

Chemical agent	Concentration	Stock	Volume
H_2O	-	-	ad 500 µl
Tris/HCl pH = 8.5	100 mM	1 M	50 µl
DTT	5 mM	50 mM	50 µl
$MgCl_2$	5 mM	1 M	2.5 µl
NAD^+	5 mM	50 mM	50 µl
Enzyme/crude extract	x mM	x mM	x µl
4-hydroxybutyrate/ 3-hydroxypropionate	10 mM	100 mM	50 µl

6.2.3. Characterization of crotonyl-CoA hydratase/(S)-3-hydroxybutyryl-CoA dehydrogenase

Crotonyl-CoA hydratase/(S)-3-hydroxybutyryl-CoA dehydrogenase assay. Activity of crotonyl-CoA hydratase/3-hydroxybutyryl-CoA dehydrogenase was measured according to Ramos-Vera *et al.*, 2011 and optimized for the recombinantly expressed protein Igni_1058 (Tab. II.20). The conversion of crotonyl-CoA and (S)-3-hydroxybutyryl-CoA to acetoacetyl-CoA under the reduction of NAD^+ to NADH was determined and the reaction was started adding either crotonyl-CoA or (S)-3-hydroxybutyryl-CoA. The assay was performed at 50°C.

Tab. II.20.: *Reaction mixture for crotonyl-CoA hydratase/(S)-3-hydroxybutyryl-CoA dehydrogenase assay*

Chemical agent	Concentration	Stock	Volume
H_2O	-	-	ad 500 µl
Tris/HCl pH = 8.0	100 mM	1 M	50 µl
DTT	5 mM	50 mM	50 µl
NAD^+	5 mM	50 mM	50 µl
Enzyme/crude extract	x mM	x mM	x µl
Crotonyl-CoA/(S)-3-hydroxybutyryl-CoA	3 mM	100 mM	15 µl

Kinetic parameters (K_M and v_{max}). K_M and v_{max} were determined as described in sections 6.2.1. The concentration of one substrate or cosubstrate was varied, while the concentration of other substrates was kept at the same level (crotonyl-CoA: 1 mM - 0.05 mM; (S)3-hydroxybutyryl-CoA: 1 mM - 0.05 mM; NAD^+: 5 mM - 0.01 mM).

Substrate specificity. For determination of substrate specificity, (R)-3-hydroxybutyryl-CoA and 3-hydroxypropionyl-CoA were added to the reaction mixture instead of (S)-3-hydroxybutyryl-CoA. In another experiment NAD^+ was substituted by $NADP^+$. For determination of enzyme activity on 3-hydroxypropionyl-CoA, a coupled assay according to Tab. II.21 was performed. In an initial step, 3-hydroxypropionyl-CoA was synthesized by mixing the different components of Tab. II.21 and adding recombinant propionate-CoA transferase (PCT) from *Clostridium propionicum* (Selmer *et al.*, 2002). The reaction mixture was incubated for 10 min at 37°C, allowing the formation of 3-hydroxypropionyl-CoA. Thereafter, the recombinant enzyme Igni_1058 and the recombinant crotonyl-CoA carboxylase/reductase (CCR) from *Rhodobacter sphaeroides* were added (Erb *et al.*, 2009). CCR from *Rhodobacter sphaeroides* catalyzes an NADPH dependent reaction from acryloyl-CoA to methylmalonyl-CoA, and does not convert 3-hydroxypropionyl-CoA. Due to utilization of helping enzymes, the assay was performed at 42°C. In addition, a control assay of the conversion of crotonyl-CoA to acetoacetyl-CoA was carried out at 42°C.

Tab. II.21.: *Reaction mixture for substrate specificity: 3-hydroxypropionyl-CoA assay*

Chemical agent	Concentration	Stock	Volume
H_2O	-	-	ad 500 µl
Tris/HCl pH = 7.8	200 mM	1 M	100 µl
DTT	5 mM	50 mM	50 µl
NADPH	0.5 mM	5 mM	50 µl
$NaHCO_3$	40 mM	1 M	20 µl
Acetyl-CoA	0.2 mM	20 mM	5 µl
3-hydroxpropionate	5 mM	100 mM	25 µl
PCT	5 % (v/v)	1.6 mg/ml	25 µl
Incubation at 37°C for 10 min			
CCR	4 % (v/v)	7.4 mg/ml	20 µl
Enzyme/crude extract	x mM	x mM	x µl
Assay was performed at 42°C			

Reverse reactions. To track the conversion of 3-hydroxybutyryl-CoA to crotonyl-CoA, the use of recombinant CCR from *Rhodobacter sphaeroides* was necessary, as well (Tab. II.22). CCR reductively carboxylates crotonyl-CoA to ethylmalonyl-CoA (primary substrate) by oxidizing NADPH to $NADP^+$ (Erb *et al.*, 2009). This reaction can be monitored by a photometer. The assay was performed at 42°C and (S)- and (R)- 3-hydroxybutyryl-CoA were used as substrates.

Tab. II.22.: *Reaction mixture for crotonyl-CoA hydratase/(S)-3-hydroxybutyryl-CoA dehydrogenase assay: Reverse reaction*

Chemical agent	Concentration	Stock	Volume
H_2O	-	-	ad 500 µl
Tris/HCl pH = 7.8	200 mM	1 M	100 µl
DTT	5 mM	50 mM	50 µl
NADPH	0.5 mM	5 mM	50 µl
$NaHCO_3$	40 mM	1 M	20 µl
CCR	4 % (v/v)	7.4 mg/ml	20 µl
Enzyme/crude extract	x mM	x mM	x µl
(S)/(R) 3-hydroxybutyryl-CoA	3 mM	100 mM	15 µl

6.3. Further enzyme assays

6.3.1. Characterization of PEP carboxylase

PEP carboxylase activity was measured at 75°C as the PEP-fixation of [^{14}C]-bicarbonate into an acid-stable product. The assay was performed by Achim Mall (University of Freiburg) and the assay mix contained the following components (Tab. II.23, Hügler, 2003). The reaction mixture additionally contained 250 kBq/ml NaH[^{14}]CO_3 and was startet by addition of PEP.

Tab. II.23.: *Reaction mixture for PEP carboxylase assay*

Chemical agent	Concentration	Stock	Volume
H_2O	-	-	ad 500 µl
Tris/HCl pH = 8.5	100 mM	1 M	50 µl
$MgCl_2$	5 mM	1 M	2.5 µl
DTE	5 mM	50 mM	50 µl
$NaHCO_3$	15 mM	100 mM	75 µl
Enzyme/crude extract	x mM	x mM	x µl
PEP	5 mM	50 mM	50 µl

6.3.2. Characterization of 4-hydroxybutyryl-CoA synthetase

For determination of 4-hydroxybutyryl-CoA synthetase activity, the following components were pipetted in an 1.5 ml reaction tube and incubated in a water bath incubator at 60°C or 80°C (according to Ramos-Vera *et al.*, 2011, Tab. II.24). The reaction was started by adding 4-hydroxybutyrate (10 mM) and was stopped after 0, 5 and 10 min

by pipetting 100 µl of the reaction mixture into a reaction tube containing 10 µl of HCl (1 M) at each time point. Samples were then provided to Dr. Ivan Berg (University of Freiburg) for HPLC analysis. Apart from HPLC analysis it was also possible to determine enzyme activity colorimetrically. To do so, 100 µl reaction mixture of each time point were added to 900 µl detection buffer (100 mM Tris/HCl pH = 7.8, 1 mM EDTA, 1 mM DTNB). This assay was designed for detection of free CoA. DTNB binds free SH-groups, resulting in a disulfide consisting of CoA and thionitrobenzoat, thus resulting in a yellowish coloring. Assays were measured photometrically at 412 nm according to Huber *et al.*, 2008 and Gallenberger, 2007 (ϵ_{DTNB} = 13.6 x 10^3 M^{-1} cm^{-1}). The assay was carried out with enzyme of *I. hospitalis* purified by IP and crude extract of *I. hospitalis* (KIN4 I).

Tab. II.24.: *Reaction mixture for 4-hydroxybutyryl-CoA synthetase assay*

Chemical agent	Concentration	Stock	Volume
H_2O	-	-	ad 500 µl
MOPS pH = 7.2	100 mM	1 M	50 µl
ATP	3 mM	100 mM	15 µl
$MgCl_2$	3 mM	1 M	1.5 µl
CoA	1 mM	50 mM	10 µl
Enzyme/crude extract	x mM	x mM	x µl
4-hydroxybutyrate	10 mM	100 mM	50 µl

7. Immunological methods

7.1. Immunization

For immunization, purified recombinant proteins (section 5.1) were loaded on a polyacrylamide gel (section 5.3) and stained with Coomassie (section 5.4). If proteins were supposed to be used for immunization, Coomassie staining was performed without methanol. In addition, a mix of ethanol (30 % (v/v)) and of acetic acid (10 % (v/v)) in water was used as fixing- and destaining solution (Tab. II.9). After staining with Coomassie, the gel was incubated in acetic acid (5 % (v/v) in water) for 15 min and then the relevant protein bands were cut out with a scalpel. Davids Biotechnologie (Regensburg, Germany) used the gel bands for immunization of rabbits. Pre-immune sera and test sera were requested in advance and were analyzed by Western blotting (section 7.2).

7.2. Western Blotting

7.2.1. Semi-dry protein transfer

Proteins were transferred from the polyacrylamide gel to a PVDF membrane (0.45 µm) by semi-dry transfer for Western Blot analysis (Towbin *et al.*, 1979). After SDS-PAGE, the stacking gel was detached from the separation gel. The separation gel and six Whatman papers were then incubated in transfer buffer for 15 min. In addition, the PVDF membrane (PVDF, 0,45 µm; Immobilion-P; Merck Millipore, Billerica, MA, USA) was soaked in methanol p.a. for at least 1 min. Three Whatman papers, membrane, gel and again three more Whatman papers were then assembled (in this order from bottom to top) in a semi-dry Western Blot apparatus (TransBlot® SD SemiDry Transfer Cell; Biorad, München). To ensure a proper transfer of proteins to the membrane it was essential that the membrane did not dry up and to remove air bubbles. Transfer was carried out at 11 V for 35 min.

7.2.2. Immunoreaction

After protein transfer, the membrane was washed with water and then incubated in different buffers and antibody dilutions according to Tab. II.25. Blocking as well as antibody incubation steps were carried out at 4°C while shaking gently. The remaining steps were performed at room temperature. Primary antibodies were used in dilutions of 1:200 to 1:50000. Secondary antibodies were diluted from 1:10000 to 1:50000.

Tab. II.25.: *Western Blot protocol*

Step	**Solution**	**Time**
Washing	TBS-T	10 min
Blocking	TBS-T; 5 % (w/v) milk powder	1 h; overnight
Washing	TBS-T	10 min
Primary AB	TBS-T; 3 % (w/v) milk powder; prim. AB	1 h; overnight
Washing	TBS-T	10 min
Secondary AB	TBS-T; 1 % (w/v) milk powder; sec. AB	1 h; overnight
Washing	TBS-TT	2 x 10 min
Washing	TBS	3 x 10 min

7.2.3. Detection of proteins

Western Blot analysis was performed using HRP conjugated goat anti-rabbit IgGs as secondary antibodies (Tab. II.7). Detection was carried out with Western Lightning® Chemiluminescent Reagent and the device was used as stated by the manufacturer (Tab.II.4). Visualization of the peroxidase reaction was done with a Fusion FX 7 Imager (Vilber Lourmat, Eberhardzell).

7.3. Immuno labeling of ultrathin sections

Immunogold labeling techniques described below are based on Rachel *et al.*, 2010. For immuno labeling, grids with ultrathin sections were incubated stepwise on drops of different solutions on top of a parafilm (Pechiney Plastic Packaging, Chicago, IL, USA) with the sample side on the drop. Prior to use, each solution was centrifuged in a table top centrifuge for 3 min at 14000 rpm. Antibody dilutions were always prepared freshly. In each experiment a negative control was performed by incubation of the ultrathin section with PBS-BSA 0.1 % (w/v) (without primary antibody). For immuno labeling followed by silver enhancement, sections were mounted on nickel grids. Labeling experiments were always performed in the same air-conditioned room, to keep steady conditions (air humidity and temperature). Furthermore, it was important to perform ultrathin sectioning and immuno labeling within a narrow time frame since labeling intensity decreases by time (Flechsler, 2010).

7.3.1. Immuno labeling of resin sections

Immuno labeling of resin ultrathin sections was performed according to the protocol Tab. II.26 or with reagents from Aurion (Tab. II.4) as stated by the manufacturer. For immuno labeling, ultrathin sections of either Epon-embedded cells or Lowicryl-embedded cells were used. Primary antibodies were diluted from 1:20 to 1:1000 and secondary antibodies (IgG coupled to 6 nm gold or IgG coupled to 'ultrasmall' gold) or protein A linked with 6 nm gold, were used in dilutions of 1:20 to 1:50. For "speed immuno labeling", antibody incubation times were decreased down to 5 min for both antibodies.

Tab. II.26.: *Protocol for immuno labeling of resin ultrathin sections*

Step	Solution	Time
Inactivation of free aldehyde groups	1 x PBS - Glycine 0.1 % (w/v)	5 min
Blocking	1 x PBS - BSA 1 % (w/v)	10 min
Primary AB	1 x PBS - BSA 0.1 % (w/v); prim. AB	5 min - 1h
Washing	1 x PBS - BSA 0.1 % (w/v)	5 x 2 min
Secondary AB	1 x PBS - BSA 0.1 % (w/v); sec. AB	5 min - 1h
Washing	1 x PBS - BSA 0.1 % (w/v)	5 x 2 min
Washing	1 x PBS	2 x 2 min
Cross-linking of epitopes and AB's	1 x PBS - GA 2 % (v/v)	5 min
Washing	1 x PBS	2 x 2 min
Washing	$H_2O_{millipore}$	3 x 2 min

7.3.2. Immuno labeling of cryo-sections

Besides labeling of resin sections, labeling of cryo-sections was performed. Immuno labeling of cryo-sections prepared according to Tokuyasu (Tokuyasu, 1973) was carried out in cooperation with Dr. York-Dieter Stierhof and Rebecca Kühn (ZMBP, University of Tübingen). For this, primary antibodies were diluted from 1:10 to 1:1000 and secondary antibodies (IgG coupled to 6 nm gold or IgG coupled to ultrasmall gold) were used in dilutions of 1:50 to 1:100 (Tab. II.27).

In the last step, cryo-sections were embedded in 0.4 % (w/v) uranyl acetate in 2 % methylcellulose. For this, a fresh, medium-sized drop containing the solution was applied on parafilm. Grids were fished with a loop and then carefully dried from the side with a filter paper. Grids were allowed to further dry in the loop for a minimum of 30 min. Finally, grids were carefully cut from the loop with a syringe or tweezers.

7.3.3. Silver enhancement

Immuno labeling was followed by silver enhancement, if performed with IgGs conjugated with 'ultrasmall' gold. Silver enhancement was carried out according to Danscher, 1981. For this, 150 µl of silver lactate (solution I) and and 850 µl of a solution consisting of gum arabic, hydroquinone and citrate buffer (solution II; Tab. II.9) were mixed and centrifuged for 3 min at 14000 rpm. Grids were incubated on droplets of the silver enhancement solution in the dark for 10 min to 20 min (depending on the batch of the silver enhancer). Thereafter, grids were washed six times in a drop of $H_2O_{Millipore}$ and finally heavy metal stained with uranyl acetate (section 9.2.6). Alternatively, silver enhancement was performed with R-Gent SE-EM Silver Enhancement Reagents from

Tab. II.27.: *Protocol for immuno labeling of cryo ultrathin sections*

Step	Solution	Time
Washing	1 x PBS	3 x 2 min
Inactivation of free aldehyde groups	1 x PBS - Glycine 0.1 % (w/v)	15 min
Blocking	1 x PBS - BSA 1 % (w/v)	30 min
Washing	1 x PBS	3 x 2 min
Primary AB	1 x PBS - BSA 0.1 % (w/v); prim. AB	1h
Washing	1 x PBS - BSA 0.1 % (w/v)	6 x 5 min
Secondary AB	1 x PBS - BSA 0.1 % (w/v); sec. AB	1h
Washing	1 x PBS - BSA 0.1 % (w/v)	6 x 5 min
Washing	1 x PBS	6 x 2 min
Cross-linking of epitopes and AB's	1 x PBS - GA 2 % (v/v)	5 min
Washing	1 x PBS	3 x 2 min
Washing	$H_2O_{Millipore}$	6 x 2 min
Silver enhancement	Silver enhancer	25 - 50 min
Heavy metal contrasting	neutral UAc 4% (w/v)	5 min
Heavy metal contrasting	UAc 0.4 % (w/v) in 2 % methylcellulose	5 min on ice
Embedding	UAc 0.4 % (w/v) in 2 % methylcellulose	on ice

Aurion (Wageningen, NL, Tab. II.4) as stated by the manufacturer.

7.4. Immunoprecipitation

For immunoprecipitation (IP), a Dynabeads® Protein A immuno precipitation Kit (Life Technologies, Darmstadt; Tab. II.4) was used. For cell disruption, 0.5 g cells of *Ignicoccus* were dissolved in buffer (Tab. II.9) and disrupted using glass beads (Disrupter beads, 0.1 mm, Scientific Industires, Bohemia, US) and a vortexer (Vortex Genie 2, Scientific Industires, Bohemia, US). The kit was used as stated by the supplier. Precipitated proteins were used in enzyme assays in combination with various buffers. For enzyme assays, precipitated proteins were used either eluted or linked with magnetic beads.

8. Microscopy

8.1. Phase contrast microscopy

Phase contrast microscopy was carried out with a Zeiss Axiostar plus (Zeiss, Oberkochen) equipped with 10 x ocular lenses and 40 x objective lenses (n = 0.65) or 100 x oil immersion objective lenses (n = 1.25). Light microscopy was used to control cell disruptions and growth of *Ignicoccus* and *Nanoarchaeum*.

8.2. Transmission electron microscopy

Transmission electron microscopy (TEM) was performed with a 120 kV Philips CM12 (FEI, Eindhoven, NL) equipped with a LaB6 cathode and a 1 k x 1 k (pixel) CCD slow-scan camera (TEM-1000, TVIPS, Gauting) or with a JEOL JM-2100F (JEOL Ltd., Tokyo, JP) equipped with a field emission cathode (200 kV) and a 4 k x 4 k (pixel) CMOS camera (TemCam-F416; TVIPS, Gauting). The software EM-Menu 4.0 (TVIPS, Gauting) was used for digital documentation.

9. Microscopic preparation techniques

Methods described in the following sections are based on protocols summarized in Rachel *et al.*, 2010. Protocols were optimized for the organisms used in this study.

9.1. Filtration methods - Enrichment of cells

Since *Ignicoccus* does not generally grow to high cell densities and as *Ignicoccus* is very sensitive to any kind of mechanical treatment, filtration was introduced to gently enrich cells. For this, different filtration methods summarized in this section were used as described in Heimerl, 2014 and developed further.

1. A 50 ml reaction tube was cut open at one end, giving it two openings and a hole was drilled into the lid. The opening on the lid side was covered with a PVDF membrane (pore size 0.2 µm) along with two to three Whatman papers, before the lid was carefully closed. The tube was filled from the other side with medium containing organisms and was then placed on paper tissues with the lid side until the liquid had almost passed through. Usually, the rest of the liquid contained enriched cells and was directly used for further processing.

2. A commercially available filter attachment (25 mm Swinnex Filter Holder; Merck Millipore, Darmstadt) equipped with polycarbonate round filters (0.4 µm and 0.2 µm pore size) was used for concentration of cells. For this, a 50 ml syringe was filled with 40 ml of a liquid culture and was mounted on the filter attachment. After filtration, cells remained in a small amount of liquid. To further enrich cells, organisms were carefully washed with medium from the filter.

Both procedures were carried out under aerobic conditions (in the fume hood) or under anaerobic conditions in the anaerobic chamber. Density of cells was checked using a phase contrast microscope.

To further develop and automate the filtering methods, commercially available filter attachments were used. Medium was either filled into a bottle-top filter with a screw thread and attached to a Schott flask or into a tube top filter attached to a 50 ml reaction tube. Both apparatus were then connected to a water pump jet and the liquid was withdrawn carefully. Filtration was stopped when only a small amount of liquid was left on the filter material. Cells were then washed off the membrane with the rest of the liquid, or if necessary with medium.

9.2. Preparation of ultrathin- and semi-thin sections

9.2.1. High-pressure freezing

High-pressure freezing was performed to maintain the ultrastructure as good as possible and was carried out in a EM PACT2 (Leica, Wetzlar) at approximately 2000 bar. Samples were applied on gold-plated, flat specimen carriers (depth 200 µm, 1.2 mm in diameter, Leica, Wetzlar) fixed in an appropriate holder and were then high-pressure frozen in liquid nitrogen. Samples were stored in liquid nitrogen in the freeze substitution device EM AFS2 (Leica, Wetzlar) until further processing.

9.2.2. Freeze substitution and resin embedding

For freeze substitution, samples were transferred in liquid nitrogen to a EM AFS2 device (Leica, Wetzlar) containing a pre-cooled substitution solution (−140°C). All samples were substituted in HUGA (5 % H_2O, 0.5 % uranyl acetate, 0.5 % glutardialdehyde and 94.5 % acetone) and embedded in either Epon (Tab. II.28) or Lowicryl (Tab. II.29). In the final infiltration/embedding steps freshly prepared resin was used. Epon was

polymerized at 60°C in a warming cabinet and Lowicryl was polymerized at −40°C while exposed to UV-light.

Tab. II.28.: *Protocol for Freeze substitution and Epon embedding*

Temperature	Reagent	Time
−140°C to −90°C	HUGA	1 x 8 h
−90°C	HUGA	1 x 8 h
−90°C to −60°C	HUGA	1 x 6 h
−60°C	HUGA	1 x 8 h
−60°C to −30°C	HUGA	1 x 4 h
−30°C	HUGA	1 x 3 h
−30°C to 0°C	HUGA	1 x 4 h
0°C	acetone	3 x 30 min
0°C to 4°C	acetone	1 x 30 min
4°C to 25°C	acetone / Epon 2+1	1 x 1 h
25°C	acetone / Epon 2+1	1 x 1 h
25°C	acetone / Epon 1+1	1 x 2 h
25°C	acetone / Epon 1+2	1 x 20 h
30°C	Epon (freshly prepared)	1 x 2 h
60°C	Epon	1 x 2 d

9.2.3. Trimming of samples

Epon- or Lowicryl blocks were trimmed before ultramicrotomy. Trimming was especially important when doing serial-sectioning and was carried out either with a razor blade or, for fine tuning, with a specimen trimming device (Leica EM Trim 2; Leica, Wetzlar). Before fine-trimming, resin blocks were pre-screened by checking location and preservation of cells preferably on a large-area-section in the TEM. Then, the cutting area was trimmed to the desired size. To get sections in ribbons it was important that edges of the trimmed block were parallel and for serial-sectioning small cutting surfaces were necessary.

9.2.4. Ultramicrotomy

For ultrathin-sectioning resin blocks were mounted in special holders that were fixed in an ultramicrotome. Ultrathin sections were prepared in a Ultracut E (Leica, Wetzlar) or a Leica EM UC7 (Leica, Wetzlar) using diamond knives (Diatome AG, Biel, CH) with a knife angle of 45° or 35°. Before sectioning, the well at the end of the knife was

Tab. II.29.: *Protocol for Freeze substitution and Lowicryl embedding*

Temperature	Reagent	Time
−140°C	HUGA	1 x 1 h
−140°C to −90°C	HUGA	1 x 1 h
−90°C	HUGA	1 x 6 h
−90°C to −60°C	HUGA	1 x 1 h
−60°C	HUGA	1 x 6 h
−60°C to −40°C	HUGA	1 x 1 h
−40°C	HUGA	7 h
−40°C	acetone	3 x 15 min
−40°C	acetone / Lowicryl 2+1	1 x 2 h
−40°C	acetone / Lowicryl 1+1	1 x 2 h
−40°C	acetone / Lowicryl 1+2	1 x 2 h
−40°C	Lowicryl (freshly prepared)	1 x 16 h
−40°C	Lowicryl / UV light	1 x 2.5 d

filled with sterile filtered $H_2O_{Millipore}$ and further parameters were set including sectioning window, angle between knife and resin block and sectioning speed (0.8 mm/s). For immuno labeling, sections of 50 nm to 100 nm were cut with an 'Ultra knife' (Diatome AG, Biel, CH). Larger areas or thicker sections, as used for tomography (200 nm - 600 nm) were cut with a 'Histo knife' (Diatome AG, Biel, CH). After sectioning, single sections or ribbons were floating on the water surface of the diamond knife and were immediately fished using a fish grid and transferred to a pioloform coated slot grid. Water was carefully removed from the side of the grid with filter paper and both grids were carefully separated using tweezers or an eyelash mounted on a pipette. Until further processing grids was stored in a gridbox.

9.2.5. Preparation of support films for grids

Ultrathin sections were usually placed on either copper slot grids (G2500C 2 mm x 1 mm) or nickel slot grids (G2500N 2 mm x 1 mm) coated with 1.5 % (w/v) pioloform. For this, a dust-free slide was immersed in 1.5 % (w/v) pioloform (1.5 g pioloform in 100 ml chloroform) for 20 to 40 s. To facilitate separation of the film from the slide, the pioloform coated slide was scratched with a razor blade at the edges. After slowly transferring the pioloform film to a water bath filled with $H_2O_{Millipore}$, grids were arranged on the film with the shining side down. The film was then transferred to parafilm and stored in a petri-dish. Before use, the pioloform film arround the grids were perforated with the needle of a syringe.

9.2.6. Uranyl acetate staining

For contrast enhancement of ultrathin sections in TEM analysis, uranyl acetate staining was performed with a 2 % (w/v) uranyl acetate solution. Prior to staining, all solutions were centrifuged for 3 min at 14000 rpm in a table top centrifuge to remove precipitates. One drop of uranyl acetate and four drops of $H_2O_{Millipore}$ were arranged in rows on top of a parafilm. Hereupon, grids were placed with the sample side facing down on top of the uranyl acetate drop and incubated for 15 min in the dark. After incubation, each grid was immediately transferred to the first water drop of each row and incubated for 30 s. This procedure was repeated three times more and then grids were carefully blotted with filter paper from the side.

9.3. Preparation of Tokuyasu cryo-sections

In addition to immunogold labeling of resin sections, immunogold labeling of cryo-sections was performed according to Tokuyasu (Tokuyasu, 1973). This method is considered to be more sensitive for localization of proteins than labeling on resin sections and was therefore suitable for some applications of this research work. Techniques and protocols described in this section are based on "Ultrathin cryo-sectioning and immunogold labeling - A practical introduction" (George Posthuma, Utrecht, NL) and were adapted and optimized for *Ignicoccus* and *Nanoarchaeum*.

9.3.1. Fixation, embedding in gelatine and infiltration in sucrose

After enrichment of cells via filtration (section 9.1; (*I. hospitalis* and *N. equitans* (KIN4/M) and *I. islandicus* (Kol8)), organisms were fixed in 2 % formaldehyde and 0.1 % glutaraldehyde for 30 min at room temperature in a 1.5 ml reaction tube. To remove aldehydes, fixed cells were then centrifuged at 6000 g for 15 min in a table-top centrifuge. Ususally, fixed cells were washed three times with buffer to completely remove aldehydes. Since the ultrastructural preservation could possibly suffer from centrifugation and washing steps, only one centrifugation step was carried out here. The resulting pellets were covered with a droplet of 10 % gelatine, gently mixed and immediately transferred onto ice. After at least 15 min incubation on ice, reaction tubes containing the gelatine-embedded cell pellets were removed using a razor blade and a drop of 2.3 M sucrose to separate the gelatine from the plastic. This step was carried out in a cooling-room, to keep the gelatine in a solid state. Finally, the gelatine blocks were cut into small cubes of 0.5 mm x 0.5 mm and infiltrated in 2.3 M sucrose in

1.5 ml reaction tubes overnight on a rotary incubator. In this context it is important to mention that air bubbles were not supposed to be trapped in the upper part of the tube to ensure proper infiltration of specimens.

9.3.2. Mounting of samples

The following day, infiltrated specimens were removed from the sucrose solution and mounted on an aluminum pin cleaned with acetone. Excess sucrose was removed from the side with a filter paper, however in the end it had to be ensured that sufficient sucrose was left to glue the specimen on the aluminum pin. Mounting gelatine blocks on pins was supposed to be performed quickly to prevent evaporation of water from the samples which could lead to a change of sucrose concentration and formation of sugar crystals. Finally, mounted blocks were frozen and stored in liquid nitrogen until cryomicrotomy.

9.3.3. Trimming and Ultracryomicrotomy

Cryo-sectioning was performed in cooperation with Dr. York Dieter Stierhof and Rebecca Kühn (ZMBP, University of Tübingen) with a Leica UCT/EM FCS (Leica, Wetzlar). Trimming of specimens for ultracryomicrotomy was performed in the cryochamber of the cryomicrotome at −100°C with a trimming knife (Trim 45; Diatome, Biel, CH). For cryo-sectioning, proper trimming is even more important than for room-temperature sectioning. Edges should not have any irregularities and should be perfectly parallel to each other. Additionally, blocks have to be trimmed to a very small size, approximately 0.6 - 0.4 x 0.3 - 0.4 mm in size, and should have rectangular block faces to get good sections. To avoid rapid re-trimming of the sample, specimen blocks are supposed to be about 100 µm in height. Sectioning was performed with a cryo diamond knife (Cryo 35; Diatome Biel, CH) already mounted in the cryochamber at −120°C and sections of 50 - 100 nm were obtained. To get sections in ribbons the tip of the first section has to be carefully touched and drawn in opposite direction of the cutting edge using an eyelash mounted on top of a wooden stick. Sections were transferred from the surface of the knife to a grid using a 'perfect loop' (Diatome AG, Biel, CH). For this, the 'perfect loop' was dipped in a pick-up solution consisting of a 1:1 mixture of 2.3 M sucrose in 0.1 M phosphate buffer and 2 % methyl cellulose in $H_2O_{Millipore}$. The 'perfect loop' was then inserted into the cryochamber and after approximately 4 s (until the drop in the loop started freezing) the sections were care-

fully transferred to the loop without touching the knife with the metal of the loop. Afterwards the loop was removed from the chamber and was allowed to thaw. After thawing, the loop was transferred to the pioloform and carbon coated grids by touching the grid with the loop. Grids were stored on slides in petri-dishes sealed with parafilm or in PBS overnight until immuno labeling (section 7.3.2).

10. Image- and data processing, bioinformatics and databases

Image- and data processing was carried out using the following tools (Tab. II.30). ProtParam was used to calculate general features of amino acid sequences, including molecular masses. TMHMM, SOSUI, Phobius and OCTOPUS were used to detect transmembrane regions. To find signal peptides, Tatfind, Flafind, Phobius, OCTOPUS, Predisi and SignalP were applied on the sequences. Additionally, prediction of subcellular protein localization was carried out with PsortB. Research on conserved domains and motifs was performed using the KEGG and the NCBI databases. In addition, BLAST analyses were carried out using NCBI pBLAST and IMG JGI. T-Coffee was used to produce sequence alignments. To create a 3-dimensional model of a protein, the appropriate protein sequence was submitted to PHYRE2. Putative ligands of a protein were predicted using 3DLigandSite. Generation of images and analysis of the 3-dimensional protein structure were performed with the UCSF Chimera package. Furthermore, image recording was supported by EMMenu 4.0 and image processing was done with ImageJ, Fiji, Photoshop CS5 and Adobe Illustrator CS5. Segmentation and 3D-reconstruction of EM-data were carried out with AMIRA. Analysis and graphic illustration of enzyme data was performed using GraphPadPrism6.

Tab. II.30.: *List of software and bioinformatic tools*

Software/Database	**Reference**
Adobe Illustrator CS5	Adobe, San Jose, CA, US
AMIRA®	FEI, Eindhoven, NL
blastp	Altschul et al., 1990
EMMenu 4.0	TVIPS, Gauting
FIJI	Schneider et al., 2012
FlaFind	Szabo et al., 2007
GraphPad Prism 6	Statcon, Witzenhausen
ImageJ	Abramoff et al., 2004; Schneider et al., 2012
IMG JGI	http://img.jgi.doe.gov/
JabRef	http://jabref.sourceforge.net/
KEGG	http://www.genome.jp/kegg/
LaTex	http://www.dante.de/index.html
Mascot	Matrix Science Ltd.; Perkins et al., 1999
MS Excel 2010	Microsoft, Redmond, WA, US
OCTOPUS	Daley et al., 2005
Phobius	Käll et al., 2007
Photoshop CS5	Adobe, San Jose, CA, US
PHYRE 2	Kelley & Sternberg, 2009
ProtParam	Gasteiger et al., 2005
PsortB	Yu et al, 2010
Predisi	Hiller, 2003
SignalP 4.3	Petersen et al., 2011
SOSUI	Hirokawa et al., 1998
Stitching	Preibisch et al., 2009
Tatfind	Rose et al., 2002
T-Coffee	Mc William et al., 2013
UCSF Chimera	Pettersen et al., 2004
TMHMM 2.0	Krogh et al., 2001
3DLigandSite	Wass et al., 2010

III. Results

Results are divided into two parts, namely in a first methodological part and in a second part mainly dealing with the examination of the carbon fixation pathway in *I. hospitalis*. Since one focus of this study was protein localization via electron microscopy techniques, several methods were tested and compared, protocols were optimized and even transferred from 2D to 3D. Results of these methodological studies are shown from section III.1-III.4. The carbon fixation pathway of *Ignicoccus* and results of further immunocytochemistry experiments are addressed in section III.5-III.12.

1. Immunogold labeling on Tokuyasu-sections, on Lowicryl- and on Epon-sections – a comparison

Basically, our working group used to embed *Ignicoccus* in Epon due to excellent ultrastructural preservation. Immuno-EM revealed, however, that some of the antibodies did not bind on ultrathin sections of Epon-embedded cells. Therefore, in the course of this study, high-pressure-frozen cells of *I. hospitalis*, embedded in two different resins (Epon and Lowicryl) and cryo-sections prepared according to Tokuyasu, were compared regarding structural preservation and labeling intensity after immunocytochemical treatment. Tab. III.1 summarizes antibodies tested on ultrathin sections of *I. hospitalis* and their binding behavior on different resins or cryo-sections, respectively. Interestingly, three of the tested antibodies, did not bind on Epon sections at all, but did, however, on Lowicryl- and on cryo-sections. This was the case for antibodies directed against DNA, against PEP carboxylase and against MDH (Tab. III.1).

In contrast, labeling on Lowicryl- or on Tokuyasu sections revealed a high to very high signal intensity for the same antibodies. A comparison of labeling is shown in Fig. III.1 A-F, which illustrates immunogold labeling on Epon-(A and D), on Lowicryl-(B and E) and on Tokuyasu sections (C and F). Here, *I. hospitalis* cells are labeled with a primary antibody targeted against a protein involved in carbon fixation (crotonyl-CoA

hydratase/3-hydroxybutyryl-CoA dehydrogenase). While in Fig. III.1 A, the OCM is almost exclusively labeled, in Fig. III.1 B and C, gold particles can be additionally discovered in cytoplasmic protrusions and in the cytoplasm itself. Nevertheless, one has to be aware that the number of gold particles on Fig. III.1 B and C is high and primary antibodies should therefore be further diluted for proper immunogold labeling. However, antibodies were used in the same dilution to ensure comparability of experiments. The background signal is low, indicating a reliable and significant labeling. Furthermore, a significant labeling intensity was achieved on Epon sections with all other tested primary antibodies used in dilutions of 1:100 to 1:1000. Comparing density of gold particles, Lowicryl- and cryo-section labeling indeed appeared to be more sensitive. However, considering structural preservation and bearing in mind that cells in Tokuyasu sections were chemically fixed, which may result in delocalization of proteins (Griffiths, 1993), Epon sections (Fig. III.1 G) impress apparently by their excellent preservation of details, which facilitates interpretation of respective subcellular localization. Nevertheless, Lowicryl-embedded cells were also well-preserved and preservation of cryo-sectioned cells partly was a pleasant surprise (Fig. III.1 H). Admittedly, cell-preservation on cryo-sections was very heterogeneous and varied from section to section. In conclusion, all three methods lead to a more or less similar labeling pattern and thus, to the same result. But, due to higher sensitivity of Lowicryl- or Tokuyasu-sections for antibody labeling, higher dilutions of antibodies are recommended. Consequently, labeling on Lowicryl- and Tokuyasu-sections were shown to be a good alternative to localization on Epon-sections, if labeling on those is not sufficient or does not work at all. Similarly, these two alternative ways confirm the results of immunogold localization on Epon and therefore represent an additional control experiment.

Tab. III.1.: *Binding behavior of antibodies on ultrathin sections of I. hospitalis prepared in three different ways. Signal intensity: - no signal; + acceptable signal; ++ strong signal.*

Antibody	**Epon**	**Lowicryl**	**Tokuyasu**
α-DNA	-	+	++
α-A_1-ATP synthase	+	++	++
α-PEP carboxylase	-	+	++
α-malate dehydrogenase	-	+	++
α-succinic semialdehyde reductase	+	no data	++
α-crotonyl-CoA hyratase/ 3-hydroxybutyryl-CoA DHG	+	++	++

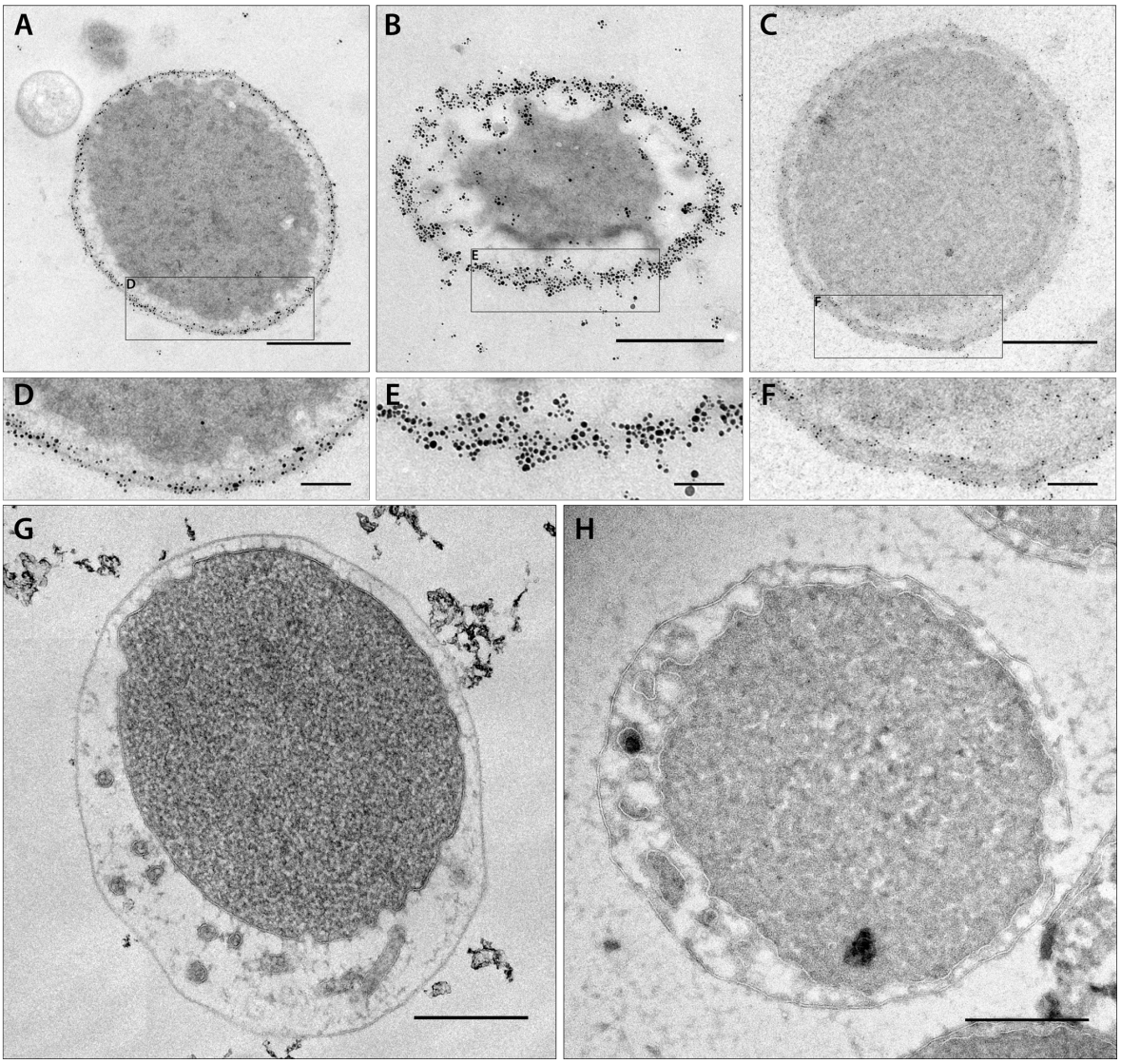

Fig. III.1.: ***Comparison of immuno labeling on Epon-, on Lowicryl- and on cryo-sections***. *Epon-section (**A** and **D**), Lowicryl-section (**B** and **E**), cryo-section (**C** and **F**) of I. hospitalis cells labeled with an antibody directed against crotonyl-CoA hydratase/3-hydroxybutyryl-CoA dehydrogenase in a dilution of 1:100. For detection a secondary antibody was used coupled to an 'ulrasmall' gold particle that was afterwards silver enhanced for 35 min. Note the higher labeling density on the Lowicryl- and on the cryo-section compared to the signal on the Epon-section. **D** and **E**: Unlabeled Epon- (D) and unlabeled cryo-section (E) of I. hospitalis. Note the well-preserved ultrastructure. Size bar A-C, G-H: 500 nm, D-F (zoom-ins on A-C): 100 nm*

2. "Speed immuno labeling"

In commonly used protocols for immunogold labeling on ultrathin sections, antibody incubation steps are usually carried out for one or two hours. After the complete procedure, which generally takes 4 to 5 hours, immuno-labeled cells often appear faded or pale (Fig. III.3). Therefore, an experiment was performed in which both antibody incubation steps were shortened successively. Immuno-labeled cells, incubated with primary and secondary antibodies for 5, 15, 30, 60 and 90 min, respectively were compared regarding labeling density and structural preservation. Fig. III.2 shows a time-course of antibody incubation steps from 5 to 30 min (Fig. III.2 A-C). For this, Epon-embedded and ultrathin-sectioned cells of *I. hospitalis* were labeled with primary antibodies directed against the A_1-part of the archaeal ATP-synthase (diluted 1:200) and IgGs linked with ultrasmall gold (diluted 1:50) that was afterwards silver enhanced. The zoom-ins (Fig. III.2 D-F) on sections labeled for the respective incubation times give a more detailed view on the gold particles distributed along the OCM. According to these results it becomes clear that labeling density increases with time (5 min - 90 min; Fig. III.2 and Fig. III.3), but it reveals as well, that labeling density is absolutely sufficient after 30 min incubation time for each of the tested antibodies. Note, that even after 5 and 15 min of antibody incubation a significant number of gold particles can be detected in the *I. hospitalis* OCM. Considering structural preservation of details, the accelerated protocol scores considerably better. Fig. III.3 shows an immunolocalization of the ACS (primary antibody diluted 1:100) on ultrathin sections of *I. hospitalis* incubated with antibodies for 30 (Fig. III.3 A), 60 (Fig. III.3 B) and 90 min (Fig. III.3 C). Already at the first glance, the cell with the shortest total incubation time (figure III.3 A) reveals the most details. In Fig. III.3 B and C, OCM, IMC and cytoplasm can be distinguished, taking into account that the cytoplasm of the cell in Fig. III.3 C looks faded. However, in Fig. III.3 A, OCM, IMC and cytoplasm can clearly be recognized and additionally tubes or 'vesicles' of the IMC are visible. Thus, it can be concluded that incubation times of 30 min for primary and secondary antibody each are absolutely sufficient and even help to better reveal structural details.

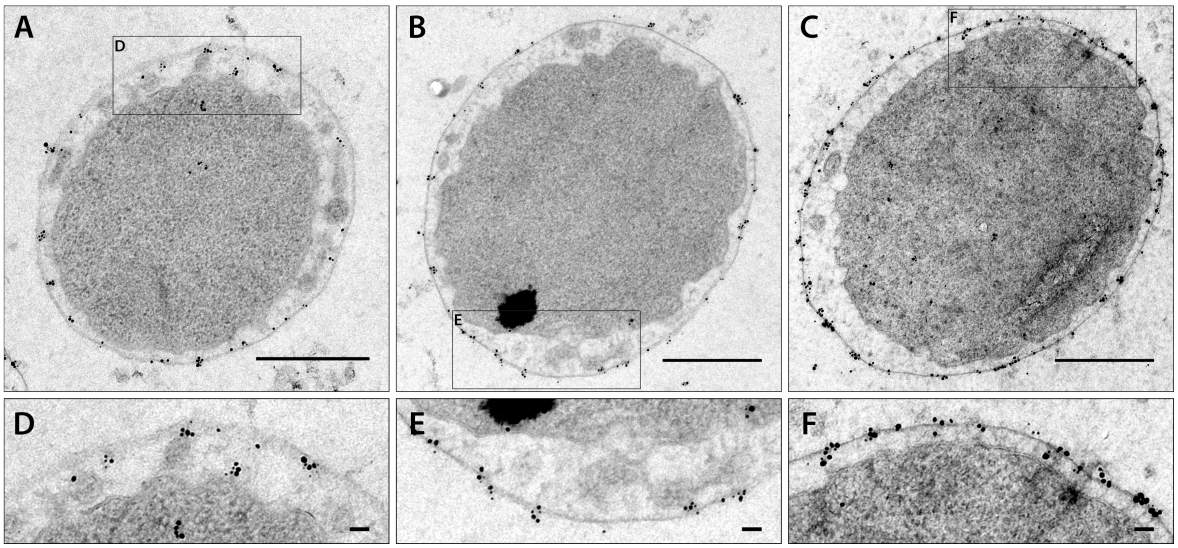

Fig. III.2.: ***Speed immuno-labeling on ultrathin sections of Epon-embedded I. hospitalis cells - signal intensity.*** *1° AB: anti-A_1 diluted 1:200; 2° AB: IgG GAR + 'ultrasmall' gold diluted 1:50; Gold particles were enlarged with a silver-enhancement solution for 25 min;* ***A*** *and* ***D****: Incubation time of 1° and 2° AB 5 min.* ***B*** *and* ***E****: Incubation time of 1° and 2° AB 15 min.* ***C*** *and* ***F****: Incubation time of 1° and 2° AB 30 min.* ***D****,* ***E*** *and* ***F****: Zoom-in on gold particles in the OCM. Note that shorter incubation times are absolutely sufficient; size bar A-C: 500 nm; size bar D-F: 50 nm.*

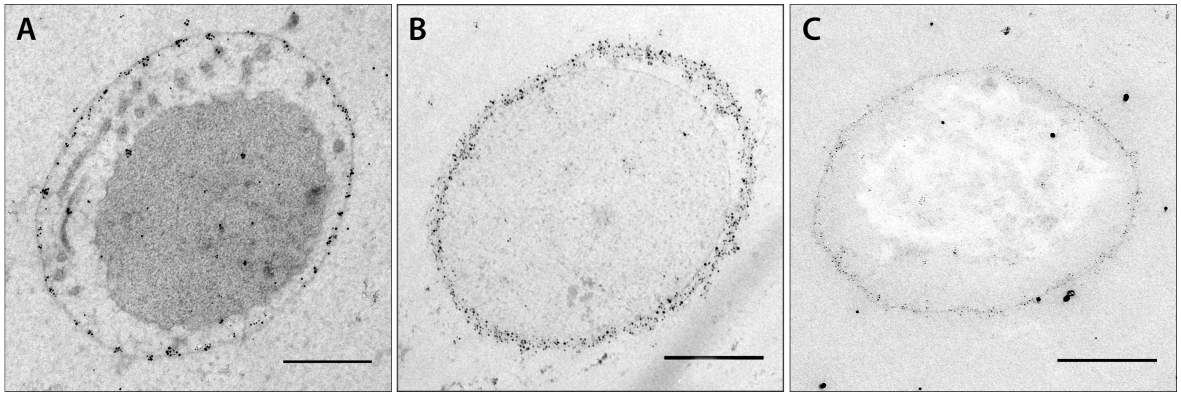

Fig. III.3.: ***Speed immuno-labeling on ultrathin sections of Epon-embedded I. hospitalis cells - structural preservation.*** *1° AB: anti-ACS diluted 1:100; 2° AB: ultrasmall-gold diluted 1:50; Gold particles were enlarged with a silver-enhancement solution for 25 min;* ***A****:Incubation time of 1° and 2° AB 30 min.* ***B****: Incubation time of 1° and 2° AB 60 min.* ***C****: Incubation time of 1° and 2° AB 90 min. Note that shorter incubation times help to better reveal structural details; Size bar: 500 nm.*

3. Three-dimensional immunogold labeling

Beside localization of proteins in 2D, three-dimensional data sets were collected using serial ultrathin sections to investigate the spatial distribution of gold particles and antigens, respectively. 3D-models were generated on the basis of serial sections followed by subsequent immuno-labeling. Data sets were recorded by TEM and visualized using AMIRA®. Video sequences of the 3D reconstruction can be viewed on the enclosed DVD (see supplementary). Fig. III.4 shows 16 selected images of a data set of an *I. hospitalis* cell connected with one cell of *N. equitans*, from a series of 20 images in total. The images were collected from serial sections à 70 nm and cells were immuno-labeled with an antibody directed against the ACS. Detection was carried out with a goat-anti-rabbit IgG coupled to 6 nm gold particles. The overall good ultrastructural preservation is particularly striking in this case. In 2D, the majority of gold particles is evenly distributed following the curvature of the OCM, while only few labels can be detected in the cytoplasm and almost no gold particles can be found in the background. In images B - G, one cell of *N. equitans* can be observed, which appears to be in direct contact with *I. hospitalis*. This becomes obvious the more of both cells is revealed (E and F). In addition, images F - H show a roundish, prominent, black structure which was described recently as putative phosphate storage with a diameter of 80 to 250 nm (Heimerl, 2014). Fig. III.5 A - E shows the 3D reconstruction of the data set (Fig. III.4). Images A and D display the bottom and the top view on the reconstruction including all structures. The cytoplasm is colored in red, whereas OCM and IMC are green. Gold particles are shown as yellow dots and putative vesicles are dark blue. *N. equitans* which is attached to *I. hospitalis* is shown in light blue. Furthermore, the structure labeled in lavender represents a previously unknown structure in the IMC, which has been described recently as putative cytoskeleton (Heimerl, 2014). These filamentous structures in the IMC are suspected to be involved in maintenance of the cell shape (Heimerl, 2014). Due to interpolation processes for 3D-reconstruction, these structures were inflated up to 70 nm and therefore give the impression of being so massive. The blue structures that are referred to as 'putative vesicles' are often misinterpreted as such on single ultrathin sections and on serial ultrathin sections since they appeared as defined structures circumscribed by double-layered membranes (Heimerl, 2014). However, due to poor resolution in z, it is impossible to conclude with certainty that these 'vesicles' or tubes are independent structures. Presumably, the blue structures are connected with the cytoplasm and thus are cytoplasmic extensions

or protrusions that frequently tend to end in bulges (Heimerl, 2014). Picture III.5 B shows *I. hospitalis* without IMC and OCM to focus on the distribution and the amount of gold particles. In image III.5 D, *I. hospitalis* is displayed without cytoplasm, IMC and OCM and therefore a view on the cytoplasmic protrusions in the IMC and the putative phosphate storage is revealed, which is shown as roundish black structure. Picture III.5 E shows the reconstruction from a side view with an original micrograph. In this side view, gold particles appear in rings around the cytoplasm in fixed intervals. The distance is due to serial sections of 70 nm and points out an obvious limitation of serial sectioning or, post-embedding labeling in general. Similarly to the localization in 2D, gold particles in 3D-models can be found preferably in the OCM, underlining the high specificity of immunogold labeling. In almost every section few gold particles were found in the cytoplasm. Especially in these cases, where labeling occurred in lower amounts or just one gold particle was found at a time but regularly, 3D labeling can help to confirm and to identify those gold particles as specific markers.

Fig. III.6 shows the three-dimensional localization of Igni_0475, an enzyme that was hypothesized to be involved in the carbon fixation cycle (see section III.8). The primary antibody was detected with a secondary antibody coupled to 'ultrasmall'-gold particles that were enlarged by silver-enhancement. The reconstruction displays one cell of *I. hospitalis* that is surrounded by five cells of *N. equitans* and consists of four consecutive sections à 70 nm. The model was visualized with AMIRA® VOLTEX, which is a simpler and quicker way of displaying serial sections in 3D than the method shown before. The method is based on threshold and was applied on the data set because gold particles provided good contrast. In this case, the protein appears to be located in the cytoplasm and its protrusions of *I. hospitalis*. Only one small gold cluster was found in association with the OCM. In addition gold particles on structures in the background are revealed, which are likely to be components of lysed cells. These labels in the background might refer to cellular components, since the particles are present on every section and always associated with structures that are regularly observed on ultrathin sections in areas where *Ignicoccus* cells are found. However, most striking here is the strong labeling of *N. equitans*, which can be found on every cell and on every section and therefore underlines specificity of this localization.

To conclude, the 3D-reconstructions support the significance of immunogold labeling in 2D and provide additional information concerning the spatial distribution of gold particles. In addition, specific labeling can be distinguished easier from unspecific gold particles attached to cellular structures on ultrathin sections, if they occur regularly

and on consecutive sections. Furthermore, in circumstances such as those given in the case of cytoplasmic protrusions, localization of proteins might be seen in a completely different light in the overall cellular context.

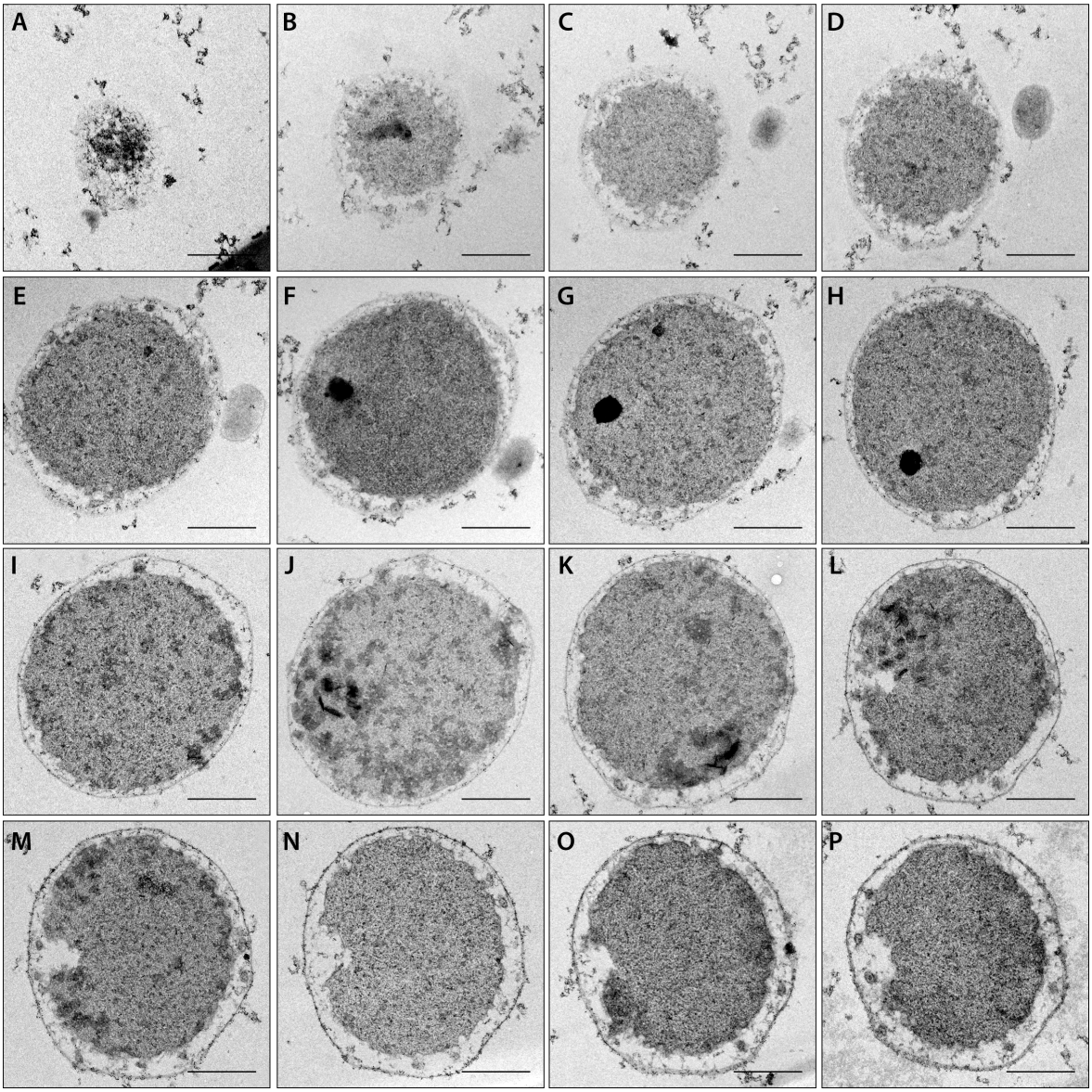

Fig. III.4.: ***Selected images of a data set of an I. hospitalis cell, from a series of 20 sections in total.*** *Images were collected from serial sections (70 nm). Cells were prepared as described (sections 7.3-9) and labeled with a 1° AB directed against the ACS and detected with IgGs GAR + 6 nm gold. Gold particles are associated with the OCM and few gold particles are located in the cytoplasm. Images* ***B-G*** *show one cell of N. equitans linked with I. hospitalis. Images* ***F-H*** *reveal a prominent black roundish structure, representing a putative phosphate storage. Size bar: 500 nm.*

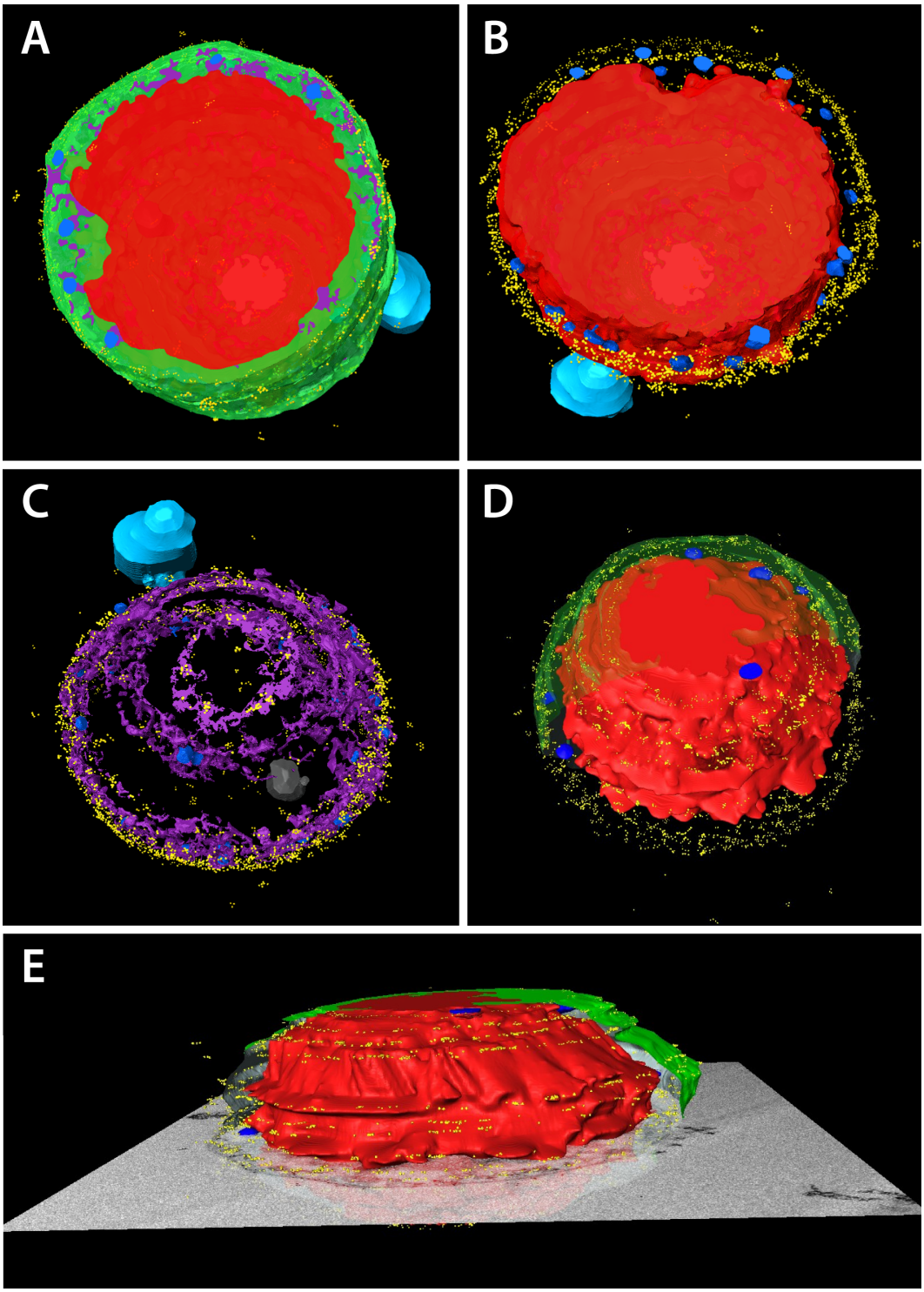

Fig. III.5.: ***3D-reconstruction and visualization of a data set of serial sections from I. hospitalis***. *Cells were prepared as described (sections 7.3-9) and labeled with a 1° AB directed against the ACS and detected with GAR IgG + 6 nm gold. Alignment, segmentation and visualization was done using AMIRA®. Red: Cytoplasm and IM, green: IMC and OCM, yellow: gold particles, dark blue: vesicles, lavender: structures in the IMC, black: putative phosphate storage, light blue: one cell of N. equitans linked with I. hospitalis. Majority of gold particles is located in association with the OCM, only few are located in the cytoplasm.*

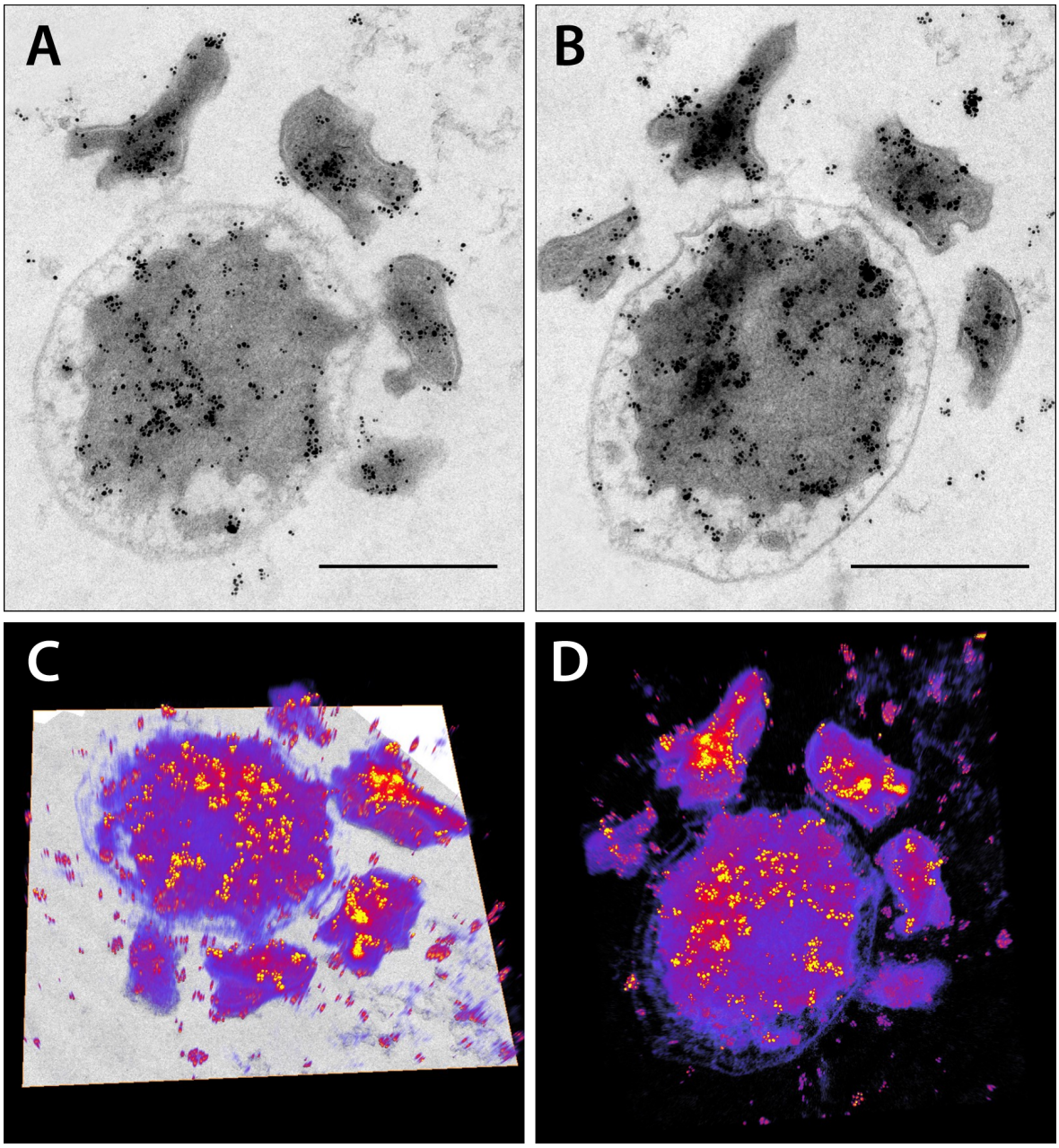

Fig. III.6.: ***Three-dimensional immunogold labeling of Igni_0475.*** *Reconstruction and visualization of a data set of 4 serial sections from I. hospitalis and N. equitans. Cells were prepared as described (sections 7.3-9) and labeled with a 1° AB directed against Igni_0475, a protein that is putatively involved in the carbon fixation cycle. Detection was carried out with a GAR IgG coupled to 'ultrasmall' gold, which was afterwards silver enhanced for 25 min. Alignment, segmentation and visualization were done using AMIRA® VOLTEX.* ***A*** *and* ***B****: Original TEM micrographs showing I. hospitalis surrounded by five N. equitans cells. Size bar 500 nm;* ***C*** *and* ***D****: 3D-reconstruction.*

4. Archaeal gene expression in *E. coli*

Cloning and expression of *Ignicoccus* genes proved to difficult. Initially, three target proteins were chosen for in vitro expression in *E. coli*: Igni_1113 (pyruvate:water:dikinase), Igni_0341 (PEP carboxylase) and Igni_0475 (4-hydroxybutyryl-CoA synthetase). The corresponding genes were amplified via PCR, cloned in an appropriate vector and expressed with and without polyhistidine tag. For expression, these constructs were transformed in various *E. coli* strains: BL21 DE3, BL21 DE3 plys, ER2DE3, Rosetta plys, BL21 Star and Rosetta 2 DE3. Primarily, however, heterologous expression of these *Ignicoccus* genes in *E. coli* was not successful (Igni_1113, Igni_0475) or the expression level was extremely low (Igni_0341). Due to the different codon usage of *E. coli* and *Ignicoccus*, it was suggested that the low expression level could be directly related to this. In that context, 74 and 71 rare codons were identified in sequences of *Igni_0341* and *Igni_0475*, respectively. Within the sequence of *Igni_1113*, even 113 rare codons were found. Given those facts, it was decided to exclusively use codon-optimized gene constructs for expression in *E. coli* (GeneArt, Regensburg). Altogether, constructs for Igni_0341 (PEP carboxylase), Igni_1263 (MDH), Igni_0132 (SSR), Igni_0475 (4-hydroxybutyryl-CoA synthetase), Igni_0379 (4-hydroxybutyryl-CoA synthetase), and Igni_1058 (crotonyl-CoA hydratase/(S)-3-hydroxybutyryl-CoA dehydrogenase) were designed. Results, referring to the expression using codon-optimized gene constructs are presented extensively in the following sections (section 5-9). However, a short summary on that is given in Tab. III.2.

Tab. III.2.: *Heterologous expression of non-codon adapted* and codon-optimized I. hospitalis genes in E. coli. −: no to low expression level; +: weak to sufficient expression level;++: strong to very strong expression level; s: soluble fraction; is: insoluble fraction.*

Gene	No. of rare codons	Expression level
*Igni_1113**	113	−
Igni_0341	74	+; is
Igni_1263	53	++; s
Igni_0132	56	++; s
Igni_0475	71	−
Igni_0379	70	++; s
Igni_1058	77	+; is

5. PEP carboxylase

5.1. Bioinformatical analysis

PEP carboxylases catalyze an irreversible beta-carboxylation of PEP to oxaloacetate and inorganic PO_4^{3-}. Bicarbonate and divalent metal ions are usually used as cosubstrates (Ettema *et al.*, 2004). In Jahn *et al.*, 2007 and Huber *et al.*, 2008, *Igni_0341* was described as PEP carboxylase contributing to the dicarboxylate/4-hydroxybutyrate pathway in *I. hospitalis*. For prediction of properties of Igni_0341, amino acid sequences were analyzed using various public search algorithms. Thus, the molecular mass of the enzyme comprising 488 amino acids was pre-calculated to approximately 56 kDa. This is approximately half of the subunit size of all known bacterial and eukaryotic sequences for PEP carboxylases described so far (Patel *et al.*, 2004) and is in good agreement with molecular masses of archaeal PEP-carboxylases which are in a range of 55-60 kDa (Ettema *et al.*, 2004). Neither signal peptides nor transmembrane domains could be identified within the amino acid sequence using various web-based tools for prediction of signal peptides and of transmembrane helices. The program PSORTb proposes a localization of the enzyme in the cytoplasm (cytoplasm: score 7.5; cytoplasmic membrane: score 1.0; cellwall: score 0.87; extracellular: score 0.63).

When applying NCBI pBLAST on the amino acid sequence, all hits of producing significant alignments were PEP carboxylases of archaeal origin. Top hits were the *P. fumarii* PEP carboxylase with 40 % identity (e-value of $2e^{-117}$) and the PEP carboxylase of *Ignisphaera aggregans* with 34 % identity (e-value of $1e^{-78}$). A domain analysis, searching the NCBI database assigned Igni_0341 to the PEPcase superfamily with best domain hits for a provisional PEP carboxyalse (PRK13655; aa: 1-488; e-value of 0.0) and an archaeal like PEP carboxylase (PEPcase_2; aa: 3-488; e-value of 0.0). These results reflect those described by the KEGG database, where Igni_0341 is described as PEP carboxylase comprising a PEPcase_2 domain (aa: 3-488; e-value of 6 e^{-145}).

Regarding structural elements, a putative Gly-Arg loop (GMGKPPLRGH) at position 238-247 was detected within the amino acid sequence of Igni_0341 as described for *Methanothermobacter thermoautotrophicus* (GMGSAPFRGN; 252-261). The Gly-Arg loop of *E. coli* and maize, consisting of six Gly and two Arg residues, are suggested to form a protective lid for the active site of the enzyme (Patel *et al.*, 2004). The arginine residue present in the Gly-Arg loop might directly be part of the PEP binding site according to Patel *et al.*, 2004. Also important for catalysis might be a His residue that can be found in a conserved element located at position 4-13 near the N-terminus

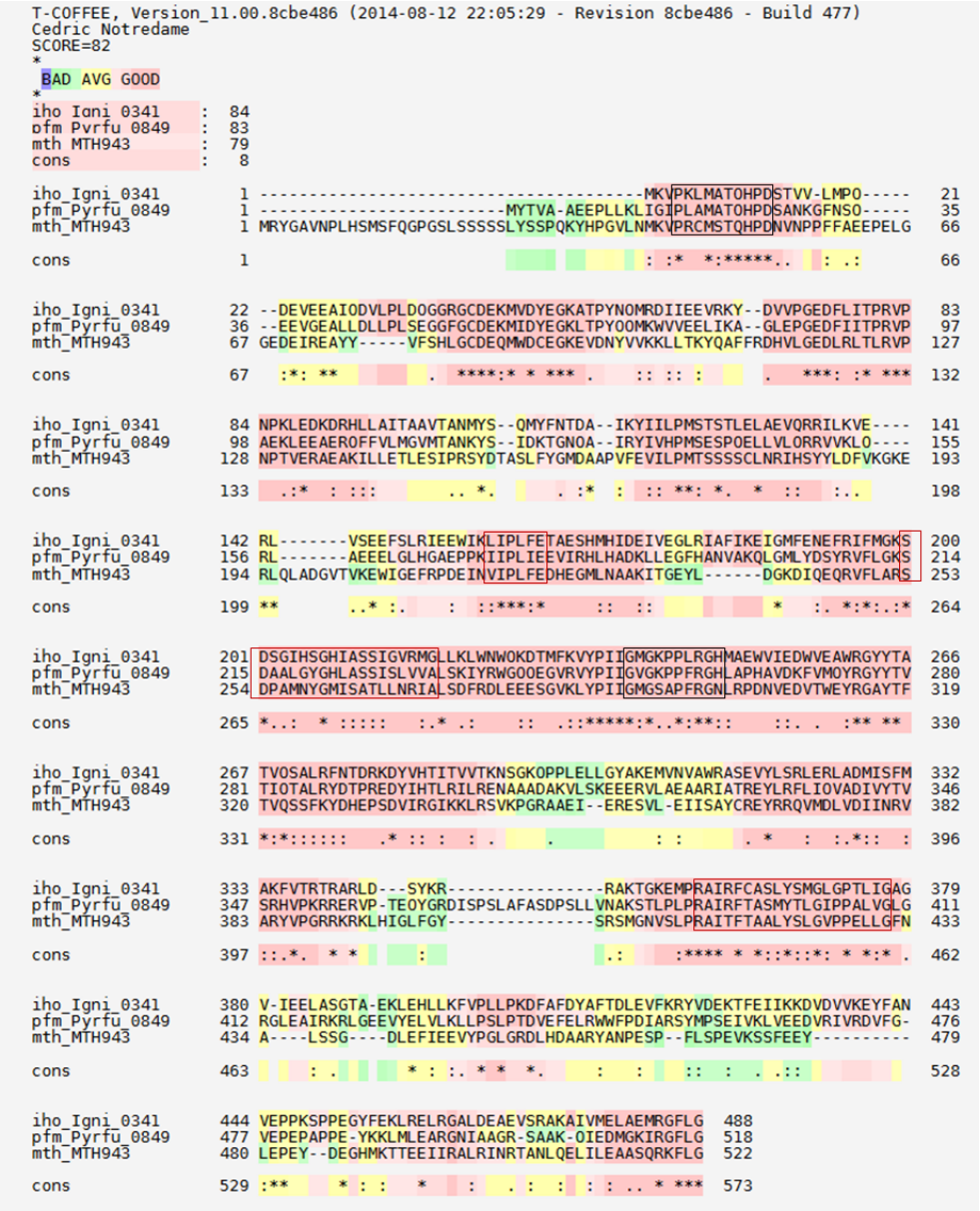

Fig. III.7.: ***Alignment of Igni_0341, Pyrfu_0849 and MTH943***. *Red highlighted sequences represent very similar sequence characters, yellow highlighted sequences stand for average similarity and green highlighted sequences show no similarities. Conserved structures of suggested functional importance are highlighted with boxes. Black boxes: TXHP element (position 4-13) and putative Gly-Arg loop (position 238-247). These elements might be involved in PEP binding and catalysis. Red boxes: position 58-163; position: 200-218; position 358-377. Conserved elements that might be important in fixation of CO_2. Only positions in the I. hospitalis gene are named.*

of the gene (PKLMATQHPD). Further conserved elements could be identified during analysis: At position 58-163: LIPLFE ((V/I/L)(A/I)PL(F/V/I)E), at position 200-218: SDSGIHSGHIASSIGVRMG (SDXAX$_3$GX(S/A)X$_6$A) and at position 358-377: RAIRFCASLYSMGLGPTLIG (RAIX(F/W/Y)X$_{9\text{-}10}$PX$_3$G). These elements might be involved in the fixation of CO_2. To highlight the conservation of these elements that may play a functional role, an alignment of the *I. hospitalis* gene with orthologues of *P. fumarii* and *M. thermoautotrophicus* is shown in figure Fig. III.7.

Additionally, the protein sequence was submitted to the PHYRE database to predict a 3-dimensional model of the protein based on structural homologies since protein folding is considered to be evolutionary more conserved than amino acid sequences (Stryer *et al.*, 2003). To create the 3-dimensional structure one template was selected and 100 % of residues were modeled at $> 90\%$ confidence. Fig. III.8 A displays the structure in rainbow color-coding, computed by PHYRE. The N-terminus of the protein is depicted in blue, whereas the C-terminus is red. When taking a closer look at the secondary structure (Fig.III.8 B) of the modeled protein, it reveals eight parallel β strands arranged in a barrel, linked with seven α helices and therefore reminiscent of a TIM barrel (α8β8). According to Matsumura *et al.*, 2006, the PEP binding site is predicted

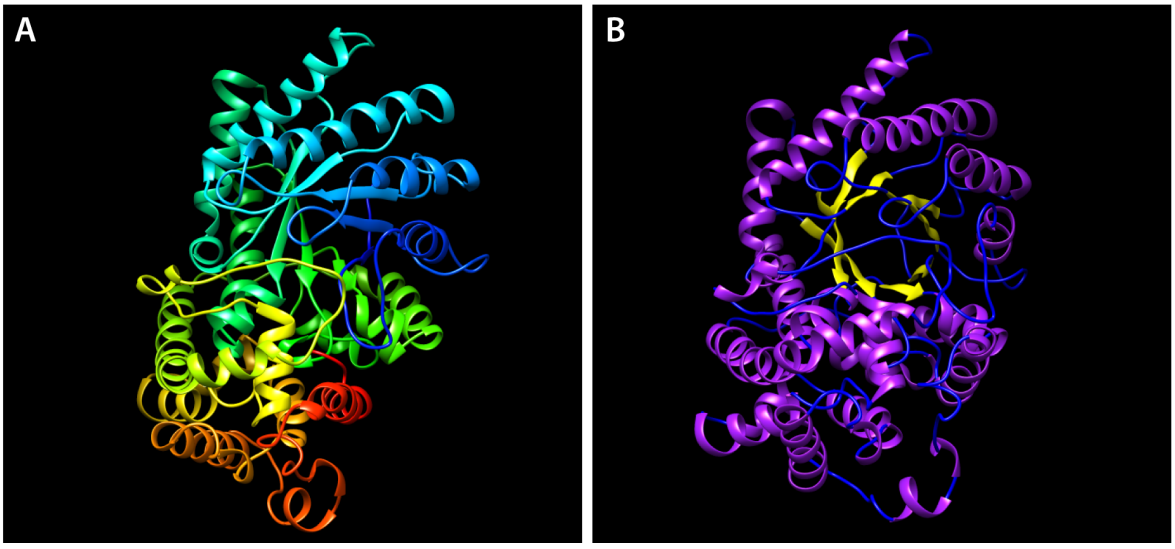

Fig. III.8.: ***Three-dimensional model of Igni_0341.*** *Structure prediction based on structural homologies according to PHYRE. Data were visualized using UCSF Chimera.* ***A****: Structure in rainbow color-code. N-terminus is shown in blue; C-terminus is shown in red.* ***B****: Model with highlighted secondary structure elements. α-helices: purple, β-sheets: yellow; loops: blue. Note eight parallel β-strands arranged in a barrel and surrounded by seven α-helices.*

to be close to the center of the barrel at the C-terminal end of β strands. Furthermore, the structure comprises an all α-helical domain and its quaternary structure is likely to form a homotetramer (Patel *et al.*, 2004).

In addition, PHYRE suggested structural homologies with 100 % confidence and 30 % sequence identity to the archaeal type PEP carboxylase. With 100 % confidence and sequence identities between 16-20 %, the PEP carboxylase from maize and further TIM beta/alpha barrel proteins were listed as homologous structures. Note that for high accuracy of models sequence identities should be above 30-40 %. However, models that are helpful to find homologies can even be achieved for seqeuence identities of 15 %, as long as confidence is at 100 % (Kelley and Sternberg, 2009).

5.2. Cloning and expression of *Igni_0341*

Only extremely low amounts of recombinant protein were expressed despite of using various *E. coli* expression strains, the gene *Igni_0341* was codon-optimized for heterologous expression in *E.coli*. For recombinant expression the codon-optimized construct was cloned into the vector pRSET A, equipped with an N-terminal polyhistidine tag using BamHI and NcoI as restriction sites. The best expression level was reached with *E. coli* strain Rosetta2 (DE3) in auto induction medium (Studier, 2005) for 10 h. Auto induction medium was used to increase the amount of recombinant protein on the one hand and to gently induce protein expression on the other hand. SDS-PAGE followed by Coomassie staining and Western blotting with an anti-polyhistidine antibody revealed a protein band between 55-70 kDa, exclusively in the insoluble fraction of the *E.coli* crude extract (pre-calculated molecular mass: 56 kDa) (Fig. III.9 A and B). The amount of recombinantly expressed protein increased (approximately 10-fold) referring to expression attempts with non-optimized constructs, so that it was now detectable on a Coomassie stained gel. Light microscopy investigation of induced *E. coli* cells revealed strongly refracting inclusions, so called inclusion bodies. Therefore, purification of Igni_0341 was performed from the insoluble fraction using affinity chromatography under denaturing conditions. After purification using buffers containing 8 M urea to solubilize inclusion bodies, a renaturation step was necessary to refold recombinant protein treated with urea. For this, protein was loaded into a Slide-A-Lyzer Dialysis Cassette and dialyzed stepwise as decribed. Despite all efforts to refold the recombinant protein, no active form of the enzyme was obtained. Activity tests for this enzyme were performed by Achim Mall (AG Berg, University of Freiburg). In addition, pro-

tein identity was further controlled with with MALDI-TOF MS/MS analysis, which confirmed the purified protein from *E. coli* as Igni_0341 (score: 569).

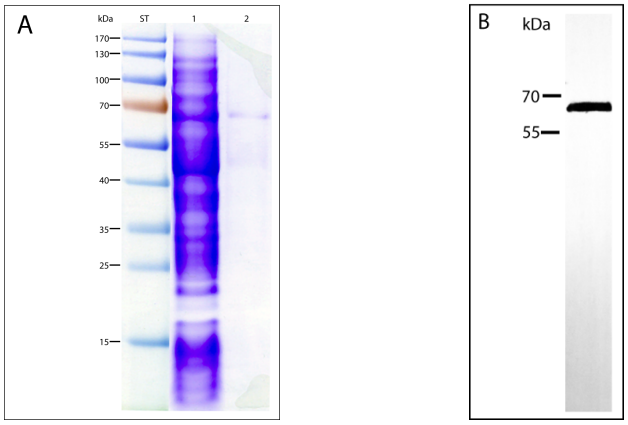

Fig. III.9.: ***Analysis of recombinant protein obtained by expression of Igni_0341.*** ***A****: Purification by affinity chromatography. SDS PAGE (10 % AA; stained with Coomassie), ST: Standard, lane 1: insoluble fraction of E. coli crude extract, lane 2: purified recombinant protein Igni_0341. SDS PAGE analysis shows only one weak protein band after purification between 55-70 kDa.* ***B****: Western Blot analysis of insoluble fraction of E. coli crude extracts after expression of Igni_0341.* 1° *AB: mouse anti-polyhistidine, diluted 1:500;* 2° *AB: GAM igG + HRP, diluted 1:20000. Western Blot shows one band between 55-70 kDa of a his-tagged protein.*

5.3. Antibody specificity and localization of Igni_0341

One focus of this work was the subcellular localization of enzymes involved in carbon fixation in *I. hospitalis*. To ensure significance of results obtained by immunogold labeling on ultrathin sections, it was necessary to check for specificity of antibodies. This was tested using Western Blot analysis with purified protein (data not shown) and freshly prepared crude extract of *I. hospitalis* cells (KIN4/I). The primary antibody (anti-Igni_0341) was diluted 1:5000, while the secondary antibody was used in a dilution of 1:20000. The PEP carboxylase blot, revealed only one band between 55-70 kDa, indicating a specific interaction of antibody and the targeted protein (Fig. III.10). Furthermore, pre-immune sera, which were tested in a Western Blot with crude extract of *I. hospitalis* (KIN4/I), showed no reaction (data not shown).

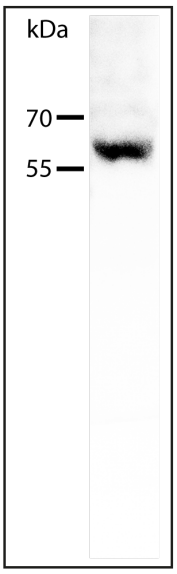

Fig. III.10.: ***Western Blot analysis of specificity of anti-Igni_0341.*** *1 µg of crude extracts of I. hospitalis was applied on 10 % SDS gel. 1° AB: rabbit anti-Igni_0341, diluted 1:5000; 2° AB: GAR IgGs linked with HRP, 1:20000. Western Blot reveals one band between 55-70 kDa.*

5.3.1. Localization on resin-sections

For immunogold labeling of the PEP carboxylase on ultrathin-sections, cells were prepared as described and immuno-labeled with a primary antibody diluted 1:100. The primary antibody was detected with a secondary antibody (dilution 1:50) coupled to 'ultrasmall' gold particles. In accordance with the rather weak Western Blot signal of the PEP carboxylase, no gold particles were observed on Epon-sections. However, on sections of Lowicryl-embedded cells a comparatively weak but significant signal was detected. Gold particles were found almost exclusively in the IMC, associated with the OCM. Only few gold particles were found in the cytoplasm and in cytoplasmic protrusions, which is highlighted with red arrows on the zoom-ins of Fig. III.11. Furthermore, the background signal was very low and no cross-reactions with *N. equitans* were observed. Accordingly, the PEP carboxylase, which is one of the two CO_2 fixing enzymes of the dicarboxylate/4-hydroxybutyrate cycle, is the first enzyme of that pathway that was shown to be localized in the IMC of *I. hospitalis* in association with the OCM.

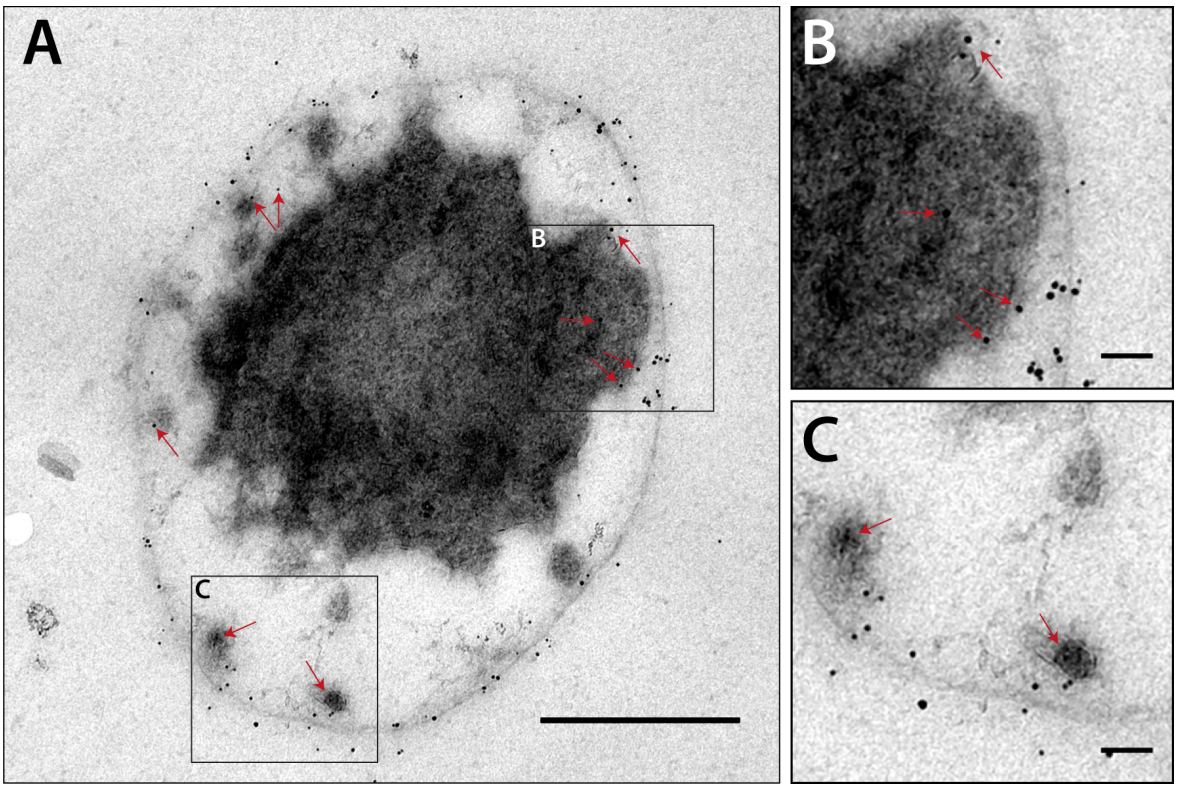

Fig. III.11.: ***A****: Immunogold labeling of PEP carboxylase on an ultrathin section of Lowicryl-embedded I. hospitalis cells. Cells were prepared as described (sections 7.3-9).* 1° *AB: anti-Igni_0341 was diluted 1:100;* 2° *AB: GAR IgG + 'ultrasmall' gold was diluted 1:50; silver enhancement: 30 min; size bar: 500 nm. Note the significant labeling in association with the OCM and the weak background signal.* ***B*** *and* ***C****: Zoom-ins on A; Red arrows highlight additional gold particles in the cytoplasm, cytoplasmic protrusions (B) and on structures in the IMC (C); size bar: 50 nm.*

5.3.2. Localization on cryo-sections

So far, no genetic system for *Ignicoccus* has been developed, which is the reason why it is not possible to simply create knockouts or introduce genetic tags linked with GFP or mCherry to localize proteins. Nevertheless, to provide an additional control experiment for subcellular localization of proteins in *Ignicoccus*, labeling of thawed cryo-sections according to Tokuyasu was performed. Immunogold labeling according to Tokuyasu was carried out with the same antibodies used in same dilutions as for labeling of resin-sections. As described in section III.3.1, preservation of ultrastructure in Tokuyasu sections differed from section to section and overall was by far not as good as that for Epon-embedded cells. However, labeling on cryo-sections provided

a stronger signal compared to labeling on resin-sections. For the PEP carboxylase, gold particles were found in the IMC in association with the OCM. Similar as for resin-sections, some gold particles were detected in the cytoplasm as shown in Fig. III.12. Interestingly, in some cryo-sectioned cells additional labeling occurred at the inner membrane and on structures of the IMC (Fig. III.12). In addition, almost no gold particles were found in the background.

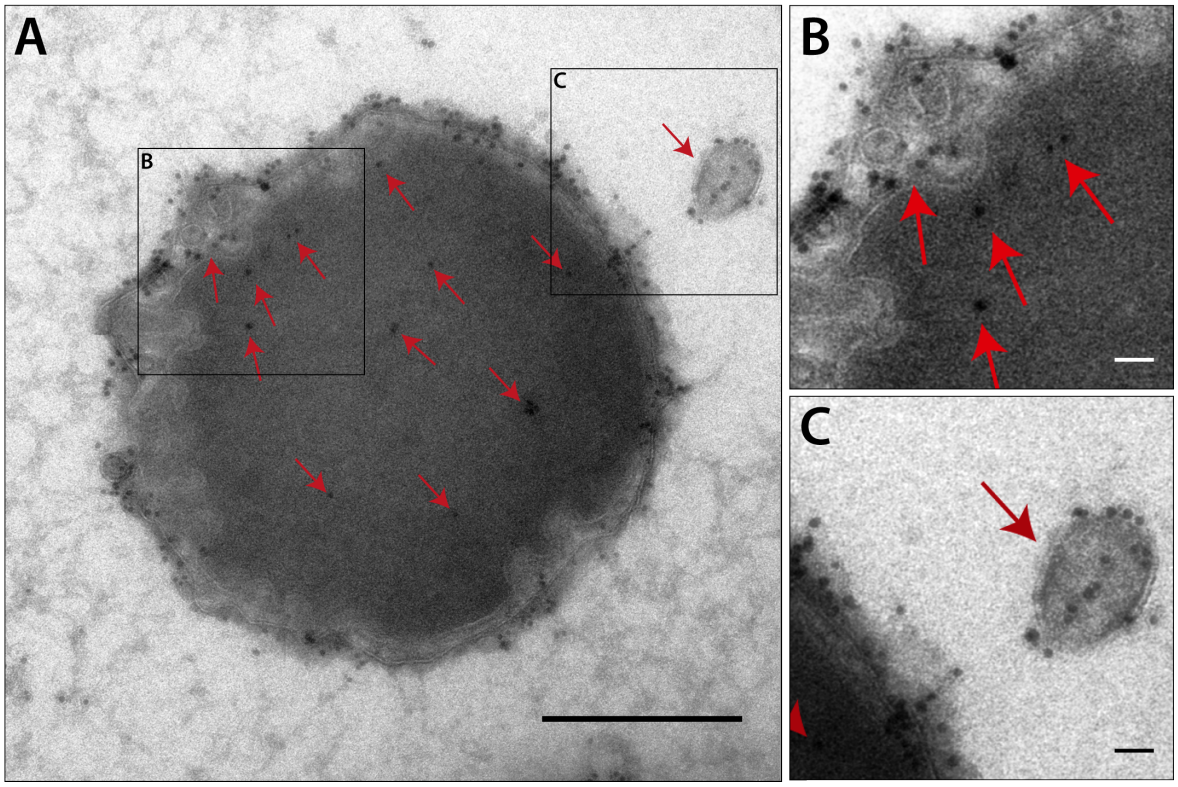

Fig. III.12.: ***A****: Immunogold labeling of PEP carboxylase on a Tokuyasu section of an I. hospitalis cell. Cells were prepared as described (sections 7.3-9). 1° AB: anti-Igni_0341 was diluted 1:100; 2° AB: GAR IgG + 'ultrasmall' gold was diluted 1:50; silver enhancement: 40 min; size bar: 500 nm. Gold particles are located in the IMC along the OCM. Few labels are in the cytoplasm.* ***B*** *and* ***C****: Zoom-ins on A; Red arrows highlight additional gold particles in the cytoplasm, in the IMC (B) and on a vesicular structure outside the cell (C); size bar: 50 nm.*

6. Malate dehydrogenase

6.1. Bioinformatical analysis

In the DC/4-HB pathway of *I. hospitalis* the conversion of oxaloacetate to malate is putatively performed by the protein Igni_1263, which is annotated as a MDH (Jahn *et al.*, 2007, Huber *et al.*, 2008). The genomic sequence of this putative MDH was extensively analyzed using various bioinformatic tools. Hence, the protein consists of 311 amino acids with a pre-calculated molecular mass of approximately 34 kDa. Initially, no significant hits for transmembrane regions were detected when analytical tools were applied on the sequence. However, output data from TMHMM, Phobius and OCTOPUS referred to a possible transmembrane domain within the first 60 amino acids (score of 16.202; TMHMM), which could be a signal peptide, as well. In contrast, Flafind, Tatfind and OCTOPUS did not identify any signal peptides. In addition, Psortb was used to predict subcellular localization of the enzyme. The protein was categorized to be located in the cytoplasm with a score of 9.96 (Cellwall; score: 0.02, Extracellular; score: 0.01).

According to NCBI pBLAST and the KEGG database orthologues of the protein and best hits are LDH/MDH of *P. fumarii* with 41 % identity (e-value of $7e^{-64}$), of *S. islandicus* with 39 % identity (e-value of $1e^{-61}$), of *S. acidocaldarius* with 41 % identity (e-value of $1e^{-59}$) and of *M. cuprina* with 36 % identity (e-value of $7e^{-57}$). Furthermore, a domain analysis using NCBI pBLAST classified Igni_1263 as member of the SDR superfamily (Short-chain dehydrogenases/reductases), which is a functionally diverse family of oxidoreductases that have a single domain including a Rossman fold and a structurally diverse C-terminal region. A motif search using the KEGG database provided similar results, matching with a Ldh_1_N motif (aa: 7-136; e-value of $8e^{-37}$) and a Ldh_1_C motif (aa: 148-310 e-value of $1e^{-19}$) as best hits, as shown in Fig.III.13. Here, the Ldh_1_N motif contains a NAD-binding Rossman fold, whereas the Ldh_1_C motif is described as an unusual α-β fold.

In further analyses using PHYRE, six templates were selected to create a 3D-structure, in which 100 % of residues could be modeled at >90 % confidence. Indeed, the 3-dimensional structure revealed a two-paired Rossmann fold near the N-terminus, consisting of six parallel β-strands linked with four α-helices (Fig. III.14 and B). The Rossmann-fold is a conserved structural element found in many dehydrogenases, which acts as NAD-binding domain. For the C-terminal part of the protein, the model exhibits various α and β elements as displayed in Fig. III.14 A, which shows the structure in

SSDB Motif Search Result

Organism : Ignicoccus hospitalis
Gene : Igni_1263
Definition : malate dehydrogenase (NAD); K00024 malate dehydrogenase [EC:1.1.1.37]

Motif id	From	To	Definition	E value	Score
pf:Ldh_1_N	7	136	lactate/malate dehydrogenase, NAD binding domain	8.1e-32	-
pf:UDPG_MGDP_dh_N	7	112	UDP-glucose/GDP-mannose dehydrogenase family, NAD binding domain	0.0032	-
pf:GFO_IDH_MocA	7	83	Oxidoreductase family, NAD-binding Rossmann fold	0.086	-
pf:ThiF	7	37	ThiF family	0.14	-
pf:Glyco_hydro_4	101	141	Family 4 glycosyl hydrolase	0.19	-
pf:DUF4147	123	158		0.011	-
pf:Ldh_1_C	148	310	lactate/malate dehydrogenase, alpha/beta C-terminal domain	1e-19	-

Search GENES with the same motifs

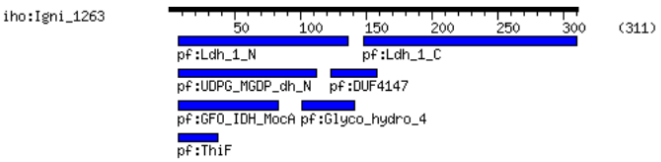

Fig. III.13.: *Conserved domains in Igni_1263 according to the KEGG database. Best hits are a domain of a LDH/MDH, containing a Rossmann fold (aa: 7-136; e-value: $8e^{-37}$ in combination with a C-terminal domain of a LDH/MDH with an unusual α-β fold (aa: 148-310; e-value: $1e^{-19}$).*

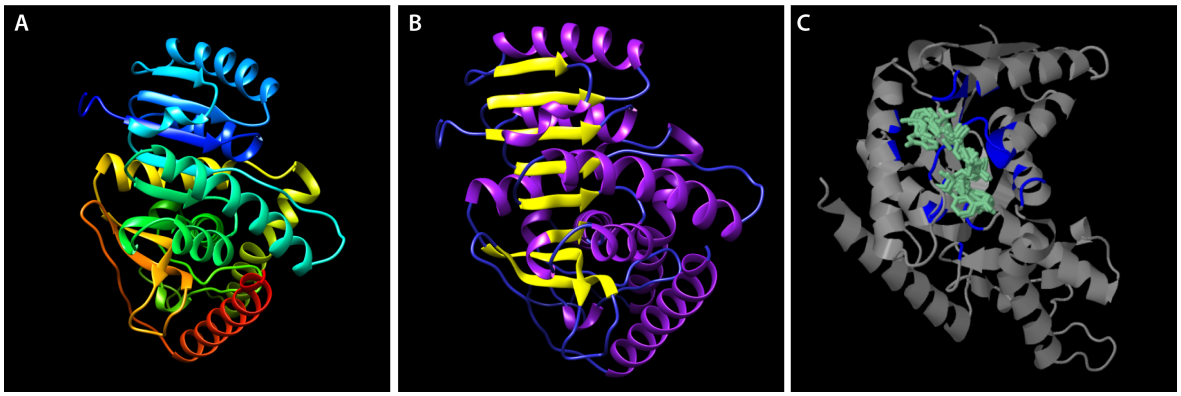

Fig. III.14.: ***Three-dimensional model of Igni_1263****. Structure prediction based on structural homologies according to PHYRE. Data were visualized using UCSF Chimera.* ***A****: Structure in rainbow color-code. N-terminus is shown in blue; C-terminus is shown in red.* ***B****: Model with highlighted secondary structure elements. α-helices: purple, β-sheets: yellow; loops: blue. Note the six parallel β-strands linked with four α-helices, representing the NAD binding domain and the C-terminus consisting of an unusual α/β fold.* ***C****: NAD, NAH and NADP binding site, predicted by 3DLigand.*

rainbow color coding (N-terminus: blue; C-terminus: red). PHYRE also predicted putative NAD(P)-binding site residues, substrate binding residues and LDH/MDH dimer interface residues, as shown in Tab.III.3. In addition, 3DLigandSite suggested 25 ligands in one cluster and provided a structural view on the predicted ligand binding site (Fig. III.14 C). The thus obtained binding site model reached an average lnE of 37.3, indicating a very high confidence for the model. As heterogens for the predicted binding site, 3DLigand lists NAD, NADH and NADP. The model might therefore illustrate the Rossman fold, which is the binding site for NAD.

With 100 % confidence and 36 % template identity, the MDH from *A. fulgidus* is suggested as structure homologue. Further structures proposed as homologues are the dogfish m4 apo-lactate dehydrogenase, the non-allosteric l-LDH from *L. pentosus* and the l-2-hydroxyisocaproate dehydrogenase from *L. confusus* with 100 % confidence and template identities between 25-30 % .

Tab. III.3.: *Binding site residues of Igni_1263. Residues for NAD(P) binding site, for the active binding site and the LDH/MDH dimer interface were predicted by PHYRE.*

NAD(P) binding site	R 14	V 15	G 16	A 37	V 38	A 81	G 82
Active binding site	I 102 P 124	T 122 G 178	N 123	G 146	D 150	A 234	
LDH/MDH dimer interface	T 18 A 52 T 236	T 22 A 53 I 240	S 42 R 153	M 46 R 154	D 48 S 156	I 49 A 157	H 51 N 163

6.2. Cloning and expression of *Igni_1263*

The codon-optimized gene sequence *Igni_1263* was cloned into the vector pRSET A, using NheI and NcoI as cloning sites. After a pilot expression on small scale, optimal conditions for expression were found employing the *E. coli* strain BL21 Star™ (DE3) for 6h at 37°C. Expression of recombinant proteins was induced with 0.8 mM IPTG and was analyzed by SDS PAGE and Western Blot analysis (Fig. III.15). SDS PAGE revealed a strong protein band in the soluble fraction of *E. coli* extracts between 35 and 40 kDa (Fig. III.15 A). With regard to the expected molecular mass of approximately 34 kDa and adding 2.5 kDa for the polyhistidine tag, the strongly induced bands of the soluble fraction match well with the size of the desired recombinant protein. This was confirmed by Western Blot analysis using an anti-polyhistidine antibody that

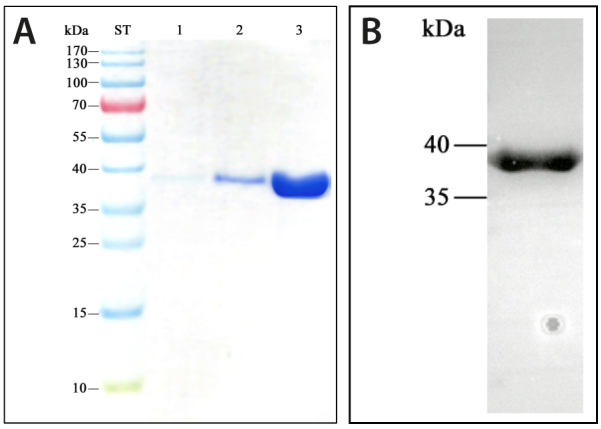

Fig. III.15.: ***Analysis of recombinant protein obtained by expression of Igni_ 1263.*** ***A****: Purification by affinity chromatography and heat precipitation (HP). SDS PAGE (10 % AA; stained with Coomassie), ST: Standard, lane 1: HP at 95°C, lane 2: HP at 90°C, lane 3: HP at 80°C. HP was carried out for 15 min. SDS PAGE analysis shows one protein band per lane between 35-40 kDa.* ***B****: Western Blot analysis of soluble fraction of E. coli extracts after over expression of Igni_ 1263. 1° AB: mouse-anti-polyhistidine, diluted 1:500; 2° AB: GAM IgG + HRP, diluted 1:20000. Western Blot shows one band between 35-40 kDa of a his-tagged protein.*

showed only one strong band at the same mass, indicating that the overexpression was successful. After expression on large scale, recombinant protein was purified from the soluble fraction using Protino® Ni-TED Resin according to manufacturer's instruction (Fig.III.15 **A**). Prior to affinity chromatography with Protino® Ni-TED Resin, heat precipitation was carried out at 85°C to 95°C for 15 min as additional purification step. After heat precipitation followed by affinity chromatography, the recombinant protein Igni_1263 was sufficiently pure. Beside SDS PAGE and Western Blot analysis, protein identity was verified with MALDI-TOF MS/MS analysis (score: 877).

6.3. Characterization of Igni_1263

The recombinant enzyme was successfully tested to catalyze an NADPH dependent reduction of oxaloacetate to malate at a v_{max} of 628 ± 20 U/mg with an apparent K_M of 270 ± 28 µM for oxaloacetate (Fig. III.16 A) and a K_M of 110 ± 26 µM for NADPH (Fig. III.16 B; 45°C, pH 7.0). In addition, the enzyme was active, replacing NADPH by NADH with a v_{max} of 109 ± 6 U/mg and an apparent K_M of 157 ± 21 µM for oxaloacetate (Fig.III.16 C); Tab. III.4).

Besides kinetic properties, substrate specificity was estimated. For this, activity with pyruvate, acetaldehyde, propionic aldehyde and butyric aldehyde was tested using concentrations of 10 mM of each substrate and 0.3 mM of NADPH. The activity of the recombinant protein on these substrates was below 5 % of the activity with oxaloacetate and therefore insignificant, as summarized in Tab. III.5.

Tab. III.4.: *K_M and v_{max} of MDH*

K_M (Oxaloacetate)	269.4 ± 27.0 µM
v_{max} (Oxaloacetate)	628.3 ± 20.0 U/mg
K_M (NADPH)	109.9 ± 25.6 µM
v_{max} (NADPH)	620.6 ± 61.0 U/mg
K_M (NADH)	157.3 ± 21.3 µM
v_{max} (NADH)	108.7 ± 6.0 U/mg

Tab. III.5.: *Substrate specificity of recombinant MDH of I. hospitalis. Substrate concentrations 10 mM; assays were started with substrate.*

Substrate	**Specific activity in U/mg**	**Specific activity in %**
Oxaloacetate	613.4	100.0
Pyruvate	9.9	1.6
Acetaldehyde	12.3	2.0
Propionaldehyde	9.9	1.6
Butyraldehyde	7.4	1.2

Tab. III.6.: *Effect of divalent cations on the activity of recombinant MDH of I. hospitalis*

Metal	**Specific activity U/mg**	**Specific activity in %**
-	534.8	100.0
$MgCl_2$ (5 mM)	613.4	114.7
$CaCl_2$ (5 mM)	570.0	106,6
$MnCl_2$(5 mM)	443.4	82.9
EDTA (0.5 mM)	316.6	59.2
EDTA (1 mM)	365.9	68.4

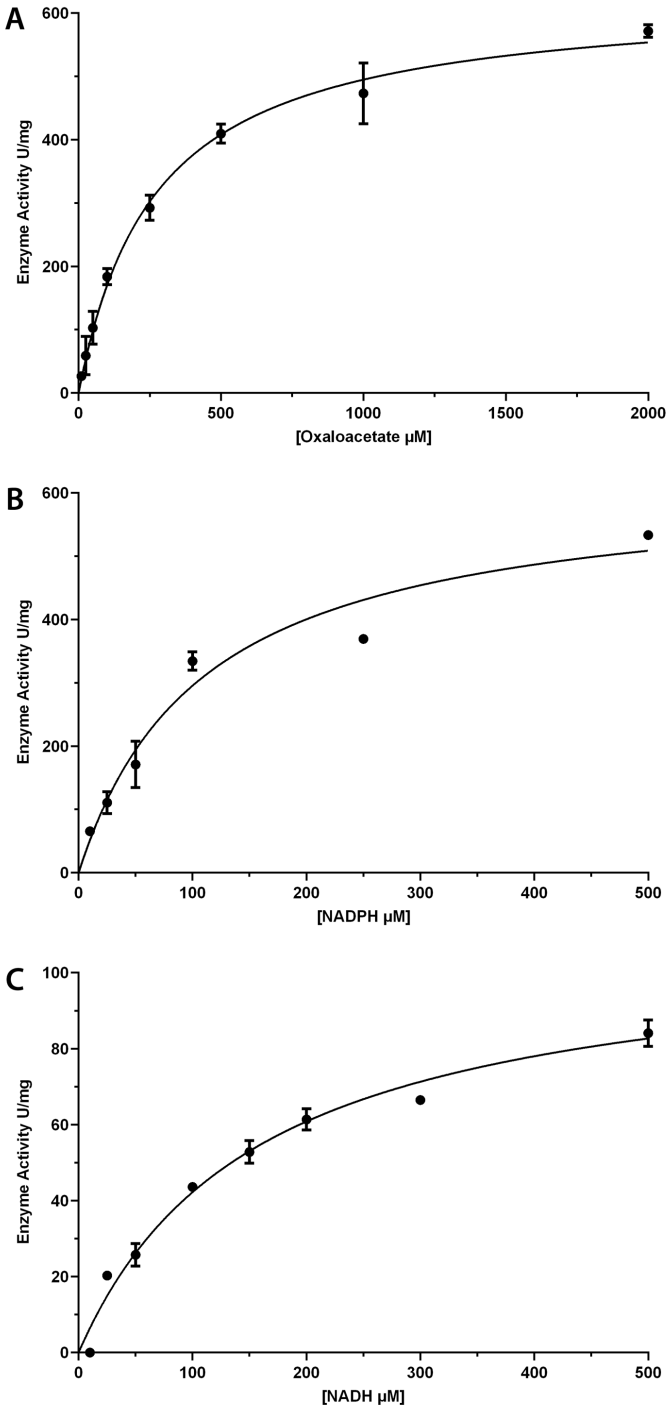

Fig. III.16.: ***[Determination of K_M and v_{max} for oxaloacetate (A), NADPH (B) and NADH (C) of MDH***. *Assays contained 500 µl reaction mixture and were prepared as described (45°C).* ***A**: K_M for oxaloacetate: 270 ± 28 µM , v_{max}: 628 ± 20 U/mg.* ***B**: K_M for NADPH: 110 ± 26 µM , v_{max}: 620.6 ± 61.0 U/mg.* ***C**: K_M for NADH: 157 ± 21 µM , v_{max}: 108.7 ± 6.0 U/mg.*

For determination of metal dependencies of the enzyme, $MgCl_2$, $MnCl_2$ or $CaCl_2$ was added to the reaction assay (Tab. III.6). Although divalent metal ions were not necessary for enzyme activity, addition of $MgCl_2$ and $CaCl_2$ ions slightly stimulated enzyme activity. However, the presence of $MnCl_2$ ions in the assay decreased the activity. When incubating the reaction mixture (without substrate) with 0.5 mM or 1 mM EDTA for 5 min prior to the actual activity test, enzyme activity decreased by approximately 40 % of the original activity. Addition of 5 mM $MgCl_2$ after inhibition with EDTA stimulated enzymatic activity up to approximately 80 %, but complete activity could not be regained after addition of $MgCl_2$ and $CaCl_2$.

6.4. Antibody specificity and localization of Igni_1263

Western Blot analysis and immunogold labeling on ultrathin sections were performed using the polyclonal antibody anti-Igni_1263. Specificity of the antibody was tested by Western Blot analysis using purified recombinant protein (data not shown) and freshly prepared crude extract of *I. hospitalis* cells (KIN4I; Fig.III.17), diluting the primary antibody 1:10000 and the secondary antibody 1:20000. The protein was detected at the expected mass between 35 - 40 kDa on the Western Blot, indicating that the antibody specifically interacted with the *I. hospitalis* version of the recombinant protein Igni_1263. Additionally, a closer look on the Western Blot of the purified protein Igni_1263 detected with an anti-polyhistidine antibody (Fig.III.15 **A**) shows a band with a slightly higher mass compared to the band of *I. hospitalis* crude extract detected with the rabbit anti-Igni_1263 antibody. This effect may probably refer to the his-tagged and non-histagged versions of the protein (2 kDa). Besides, controls using pre-immune serum as primary antibody against *Ignicoccus* crude extract were negative.

6.4.1. Localization on resin-sections

To investigate subcellular localization and distribution of the MDH within cells of *I. hospitalis*, immunogold labeling was performed. Similar to the PEP carboxylase, labeling on Epon-embedded cells was not successful. Thus, immuno-localization was applied to Lowicryl-sections, which is basically assumed to be more promising in answering immuno labeling questions (Kellenberger *et al.*, 1987, McDonald, 2014). When using Lowicryl-sections for immunogold labeling the antigen was detected in the IMC, tightly associated with the OCM as illustrated in Fig. III.18. In addition, sometimes structures in the IMC were labeled. Only occasionally, gold particles were found in

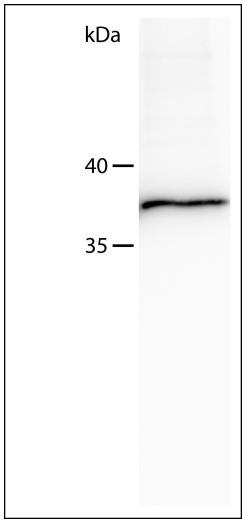

Fig. III.17.: ***Western Blot analysis of specificity of anti-Igni_1263.*** *1 µg of crude extract of I. hospitalis was applied on 10 % SDS gel. 1° AB: rabbit anti-Igni_1263, diluted 1:10000; 2° AB: GAR IgGs + HRP, 1:20000. Western Blot shows one specific band between 35-40 kDa.*

the cytoplasm and at the inner membrane. Here, it was possible to label and to visualize a dividing *Ignicoccus* cell, which in general is only rarely observed. Fig. III.18 B and C display this cell, in which gold particles are particularly found associated with the OCM, as well. In addition, a closer look reveals gold particles following a more or less horizontal line, which might represent the newly-formed OCM (Fig. III.18 C; gold particles along the horizontal line are highlighted in red). Particularly on this ultrathin section, the IMC makes up a large part of the cell and additionally includes many labeled structures. On the left hand side of the cell an accumulation of gold particles can be found. Due to ultrastructural preservation however, for this structure it remains unclear if it is just part of the OCM that is cut tangentially, or if part of the labeled structure at least partially belongs to the IMC.

6.4.2. Localization on cryo-sections

Besides immuno labeling on resin-embedded sections, immuno labeling on cryo-sections was performed according to Tokuyasu (Fig. III.19). Regarding the results, localization of the MDH is in accordance with labeling of resin-sections, in which gold particles mainly occurred evenly distributed in the IMC, associated with the OCM. Nevertheless, in most cases more gold particles than on Lowicryl-sections were identified in the cytoplasm. Especially noteworthy in this context is the ultrastructural preservation of

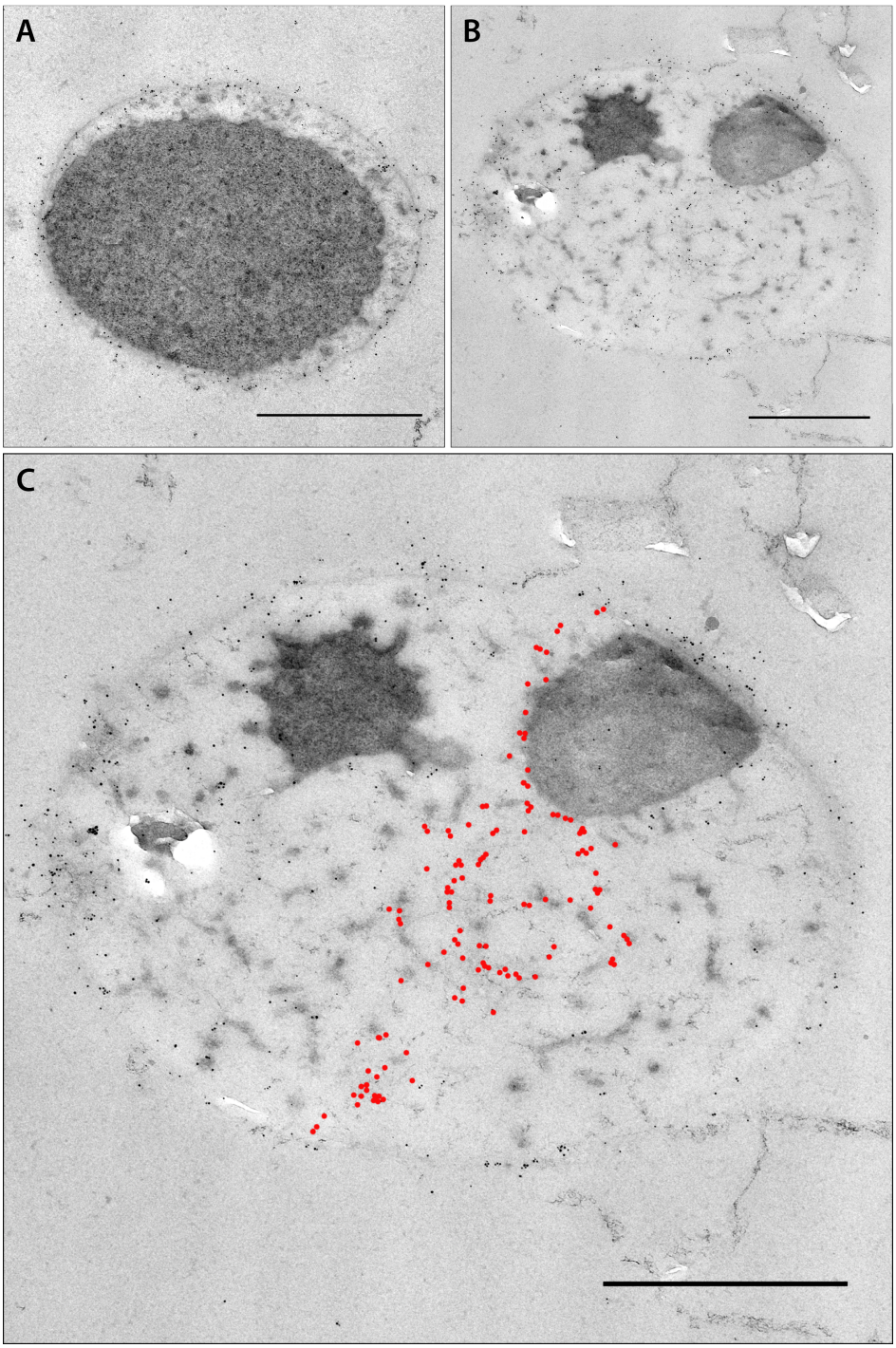

Fig. III.18.: ***Immunogold labeling of MDH on ultrathin sections of Lowicryl-embedded I. hospitalis cells.*** *Cells were prepared as described (sections 7.3-9). 1° AB: anti-Igni_1263 was diluted 1:100; 2° AB: GAR IgG + 'ultrasmall' gold was diluted 1:50; silver enhancement: 40 min; size bar: 1000 nm. Note the significant labeling in the IMC associated with the OCM (**A**). **B**: Dividing cell of I. hospitalis **C**: Enlargement of B; Note the horizontal line of gold particles (highlighted in red) between both cytoplasms. This might represent a newly-formed OCM.*

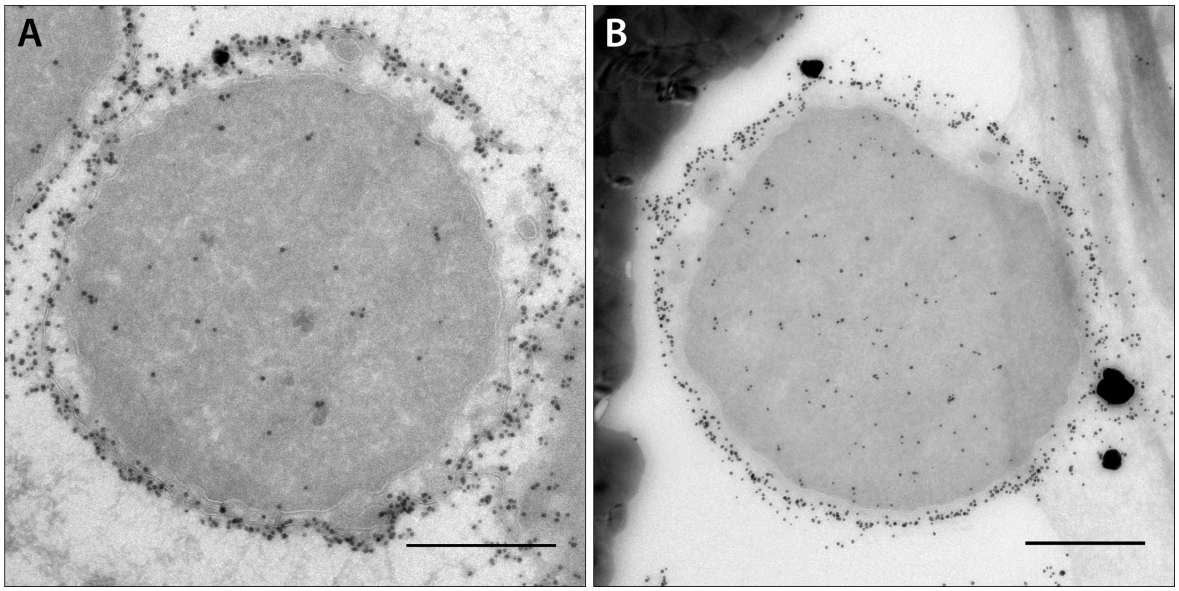

Fig. III.19.: ***Immunogold labeling of MDH on Tokuyasu sections of I. hospitalis cells.*** *Cells were prepared as described (sections 7.3-9).* 1° *AB: anti-Igni_1263 was diluted 1:100;* 2° *AB: GAR IgG + 'ultrasmall' gold was diluted 1:50; silver enhancement: 40 min. Gold particles are located in the IMC along the OCM. Additional labels can be observed in the cytoplasm and its protrusions. Note the well-preserved ultrastructure. Size bar: 500 nm.*

the cryo-sections in this experiment, in particular in Fig. III.19 A, in which different cell compartments are clearly distinguishable from each other. In addition, the bilayer character of the membranes can be recognized clearly and structures in the IMC are visible, as well.

7. Succinic semialdehyde reductase - Identification of a 'missing link'

7.1. Bioinformatical analysis

In the DC/4-HB pathway of *I. hospitalis* the reaction from succinic semialdehyde to 4-hydroxybutyrate is catalyzed by a SSR. Indeed, an enzyme catalyzing this reaction has not been identified in the genome of *I. hospitalis*, so far. To bridge that gap the genome of *I. hospitalis* was intensively searched for suitable candidates using NCBI BLAST. The NCBI database provided three candidates from *I. hospitalis* when searching for aldehyde reductases and alcohol dehydrogenases: Igni_0132, Igni_0628

and Igni_1247. Finally, Igni_0132, which was annotated as iron containing alcohol dehydrogenase, was heterologously expressed in *E. coli* and investigated. Top BLAST hit was an alcohol dehydrogenase from *P. fumarii* with 68 % sequence identity (e-value of 0.0). For *P. fumarii* it is already known that CO_2 is fixed according to the DC/4-HB pathway, as well (Berg *et al.*, 2010b).

Further hits on the BLAST list contained alcohol dehydrogenases of almost exclusive bacterial origin with sequence identities between 40-44% and e-values between $5e^{-91}$ and $4e^{-108}$. The protein Igni_0132 consists of 414 amino acids with a pre-calculated molecular mass of 45 kDa (Protparam). No signal peptides could be identified. In contrast, TMHMM, Phobius and OCTOPUS predicted an internal helix between amino acids 269-289. With only a probability of 11.4%, TMHMM proposes that the N-terminus of the protein is located in the cytoplasm. Nevertheless, Psortb suggests a subcellular localization of the protein in the cytoplasm with a score of 9.96 (Cellwall; score: 0.02, Extracellular; score 0.01). Phobius in contrast, supports a non-cytoplasmic localization. According to NCBI conserved domains, Igni_0132 belongs to the DHQ-Fe-ADH superfamily (Dehydroquinate synthase-like and iron-containing alcohol dehydrogenases). For alcohol dehydrogenases of this family a DHQ synthase like protein fold is described and they are likely to contain iron. Iron-containing dehydrogenases of this family often exhibit a Rossmann fold-like topology, as well (according to Conserved Domains database). In this context, KEGG motif search suggested an iron-containing alcohol dehydrogenase domain (Fe-ADH from aa: 16-403; e-value of 2.10 e^{-120}) and an iron-containing alcohol dehydrogenase-like domain (Fe-ADH_2 from aa: 19-109 and an e-value of 2.20 e^{-8} and from aa: 138-308 and e-value of 0.0001). Furthermore, conserved domains (NCBI) listed an 'ethanol dehydrogenase domain involved in ethanolamine utilization (EutG)' as specific hit, which is described as alcohol dehydrogenase class IV, involved in energy production and conversion (aa: 10-411 ; e-value of $1.61e^{-136}$). Interestingly, as non-specific hit a hydroxyacid-oxoacid transhydrogenase (HOT; e-value of 9.59 e^{-120}) was mentioned. Basically, HOTs catalyze the conversion of γ-hydroxybutyrate to succinic semialdehyde. This reaction is generally coupled to α-ketoglutarate conversion and not to the reduction of NAD^+.

The KEGG database identified two paralogues for Igni_0132 within the genome of *I. hospitalis*: Igni_0617, a FAD-dependent pyridine nucleotide disulfide oxidoreductase and Igni_0659, a pyridine-5-carboxylate reductase. In a 3D structure model prediction using PHYRE, 94 % of the residues could be modeled at > 90 % confidence. Here, six templates were selected to create the model of which 23 residues were modeled *ab initio*.

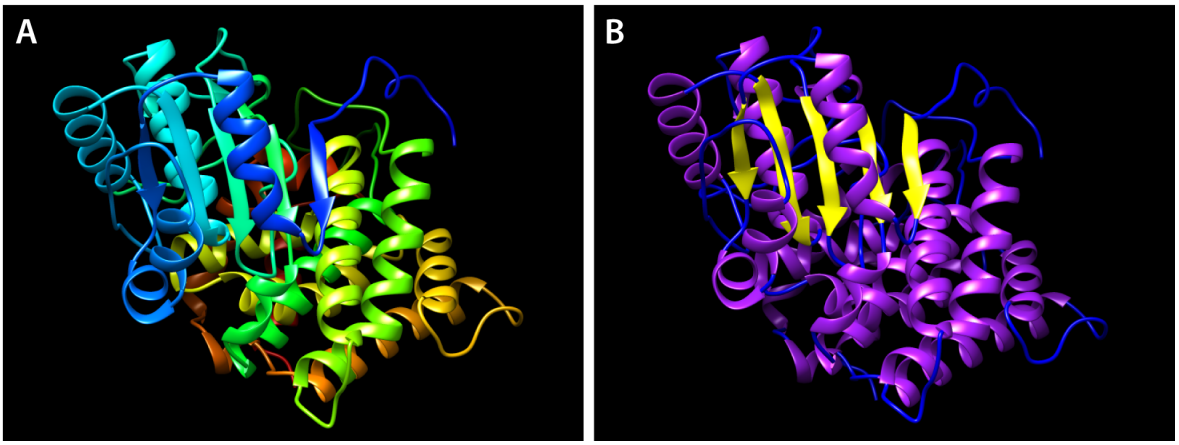

Fig. III.20.: ***Three-dimensional model of Igni_0132.*** *Structure prediction based on structural homologies according to PHYRE. Data were visualized using UCSF Chimera.* ***A****: Structure in rainbow color-code. N-terminus is shown in blue; C-terminus is shown in red.* ***B****: Model with highlighted secondary structure elements. α-helices: purple, β-sheets: yellow; loops: blue. Note the five parallel β-strands, implying a Rossmann-like topology.*

A closer look at the three-dimensional model displays an N-terminal Rossmann-like fold, consisting of five parallel β-strands in combination with four α-helices. The model reveals two more β-strands arranged anti-parallel and an all α-helical domain near the C-terminus (III.20 A and B). Beyond, the Conserved domain database predicted NAD binding site residues, active binding site residues and metal binding site residues according to Tab. III.7.

Apart from that, the sequence was submitted to 3DLigandSite, which proposed four clusters for ligands (Tab. III.8). For all clusters the MAMMOTH score was above 30, which implies a high confidence for the binding site prediction. For cluster 1, $Fe^{2/3+}$ or Zn^{2+} are proposed as ligands, respectively. This prediction goes hand in hand with the domain analysis, since the presence of iron is a feature of dehydrogenases that belong to the DHQ-Fe-ADH superfamily. In cluster 2, a NAD^+ or $NADP^+$ binding site is

Tab. III.7.: *Binding site residues in Igni_0132. Residues for NAD(P) binding site, for the active binding site and for metal binding site were predicted by PHYRE.*

NAD(P) binding site	K 44 T 186	G 99 G 303	S 100	A 101	T 145	A 146	T 148
Active binding site	T 104	I 107	I 167	G 168	T 194	A 205	P 293
Metal binding site	A 201	A 289					

Tab. III.8.: *3DLigandSite prediction. Prediction of potential ligands of Igni_0132. Column 1: Cluster; Column 2: lnE of average MAMMOTH score; Column 3: Ligand likely to be present or associated with the structure.*

Cluster	Average MAMMOTH score	Heterogens
1	32.9	Fe^{3+} (3), Fe^{2+} (2), Zn^{2+} (18)
2	32.8	NAD^{+} (3), $NADP^{+}$ (12)
3	37.2	Ca^{2+} (1)
4	36.7	Ca^{2+} (1)

revealed, which again supports the Rossmann-like fold (Fig. III.20). Furthermore, Ca^{2+} is suggested as ligand in cluster 3 and 4.

Finally some of the homologue structures suggested by PHYRE are summarized: An iron-dependent alcohol dehydrogenase from *Zymomonas mobilis* (100% confidence and 34% template identity), a 1,3-propanediol oxidoreductase (100 % confidence and 39 % template identity) and an iron-containing alcohol dehydrogenase belonging to the DHQ synthase-like superfamily (100 % confidence and 24 % template identity).

7.2. Cloning and expression of *Igni_0132*

For recombinant expression of Igni_0132 the codon-adapted gene construct (containing the restriction sites NheI and NcoI) was transformed in the *E. coli* strain BL21 Star™ (DE3). Optimal conditions for expression were found at 37°C for 6 h using 0.8 mM of IPTG for induction of expression. SDS PAGE and Western Blot analysis with an anti-polyhistidine antibody showed one intense protein band between 40 and 55 kDa, exclusively present in the soluble fraction of *E. coli* crude extracts (Fig.III.21 **A** and **B**). Since the mass of the induced protein (40 - 55 kDa) band correlated with the expected molecular mass of approximately 45 kDa (without his-tag), the protein expression was regarded as successful. According to these results, protein purification from the soluble fraction of *E. coli* extracts was performed using heat precipitation at 85°C for 15 min followed by affinity chromatography. After successful purification, protein bands were further analyzed and confirmed by MALDI-TOF MS/MS analysis (score 698).

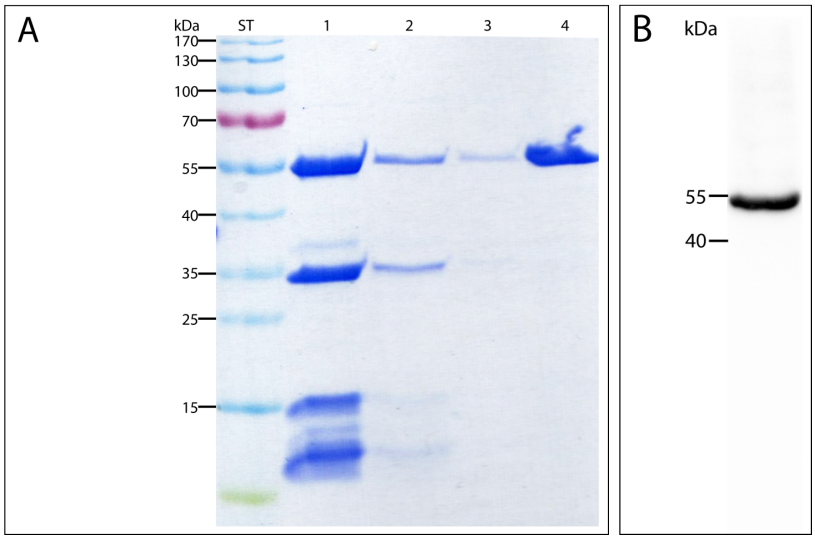

Fig. III.21.: ***Analysis of recombinant protein obtained by expression of Igni_0132.*** ***A****: Purification by affinity chromatography and heat precipitation. SDS PAGE (10 % AA; stained with Coomassie), ST: Standard, lane 1: E. coli crude extract of the soluble fraction after HP at 85°C for 15 min, lane 2: Washing fraction 1-2 of the purification, lane 3: Wash fraction 3-4 of the purification , lane 4: Elution fraction 1 of purified recombinant protein. SDS PAGE analysis shows one protein band at 40 - 55 kDa after purification.* ***B****: Western Blot analysis of soluble fraction of E. coli extracts after expression of Igni_0132. 1° AB: mouse-anti-polyhistidine, dilution 1:500; 2° AB: GAM IgG + HRP, diluted 1:20000. Western Blot shows one band between 40-55 kDa of a his-tagged protein.*

7.3. Characterization of Igni_0132

The recombinant enzyme was successfully tested to act in vitro on succinic semialdehyde and further characterization of the protein revealed an apparent K_M-value of 74.8 ± 7.6 µM for succinate semialdehyde and 245.8 ± 42.7 µM for NADH. The maximum specific activity (v_{max}) was 503.8 ± 20.5 U/mg for succinic semialdehyde. The enzyme was active with NADPH (K_M-value of 149.9 ± 30.67 µM) as well, however v_{max} was no longer reached (v_{max} of 13.0 ± 0.7 U/mg).

Enzyme activity on malonic semialdhyde, acetaldehyde, propionic aldehyde and butyric aldehyde was below 5 % of the activity with succinic semialdehyde. In addition, the enzyme catalyzed the reverse reaction from 4-hydroxybutyrate with a specific activity of 14.1 U/mg, as well. In contrast, 3-hydroxypropionate was not converted by the enzyme. The results referring to substrate specificity are summarized in Tab. III.10.

Tab. III.9.: *K_M and v_{max} of recombinant SSR of I. hospitalis*

K_M (succinic semialdehyde)	74.8 ± 7.6 µM
v_{max} (succinic semialdehyde)	503.8 ± 20.5 U/mg
K_M (NADH)	245.8 ± 42.7 µM
v_{max} (NADH)	497.1 ± 43.5 U/mg
K_M (NADPH)	41.0 ± 9.5 µM
v_{max} (NADPH)	13.9 ± 1.2 U/mg

Tab. III.10.: *Substrate specificity of recombinant SSR of I. hospitalis. Substrate concentrations 10 mM; assays were started with substrate.*

Substrate	**Specific activity in U/mg**	**Specific activity in %**
Succinic semialdehyde	418.0	100.0
Malonic semialdehyde	1.0	0.2
Acetaldehyde	8.0	1.9
Propionaldehyde	10.0	2.4
Butyraldehyde	17.5	4.2
4-hydroxybutyrate	14.0	3.3
3-hydroxypropionate	1.1	0.3

Tab. III.11.: *Effect of divalent cations on the activity of recombinant SSR of I. hospitalis. (* number refers to the addition of 5 mM $MgCl_2$ after inhibition with EDTA)*

Metal	**Specific activity U/mg**	**Specific activity in %**
Without Mg^{2+}	242	100.0
Mg^{2+} (5 mM)	418	172.7
Ca^{2+} (5 mM)	365	150.8
Mn^{2+} (5 mM)	350	144.6
EDTA (0.5 mM)	80.8/158.1 *	33.4/65.3 *
EDTA (1 mM)	99.2/132.3 *	41.0/54.7 *

Different divalent cations (Mg^{2+}, Mn^{2+} and Ca^{2+}) were tested for determination of metal dependencies (Tab. III.11). Addition of these metal ions to the reaction mixture increased enzyme activity approximately 1.5 fold, but was not required. However, incubation of the enzyme with 1 mM EDTA decreased enzyme activity by 70 % and complete activity could not be regained by subsequent addition of Mg^{2+}, Mn^{2+} or Ca^{2+} (Tab. III.11). Due to its high specificity for succinic semialdehyde the enzyme was identified as SSR.

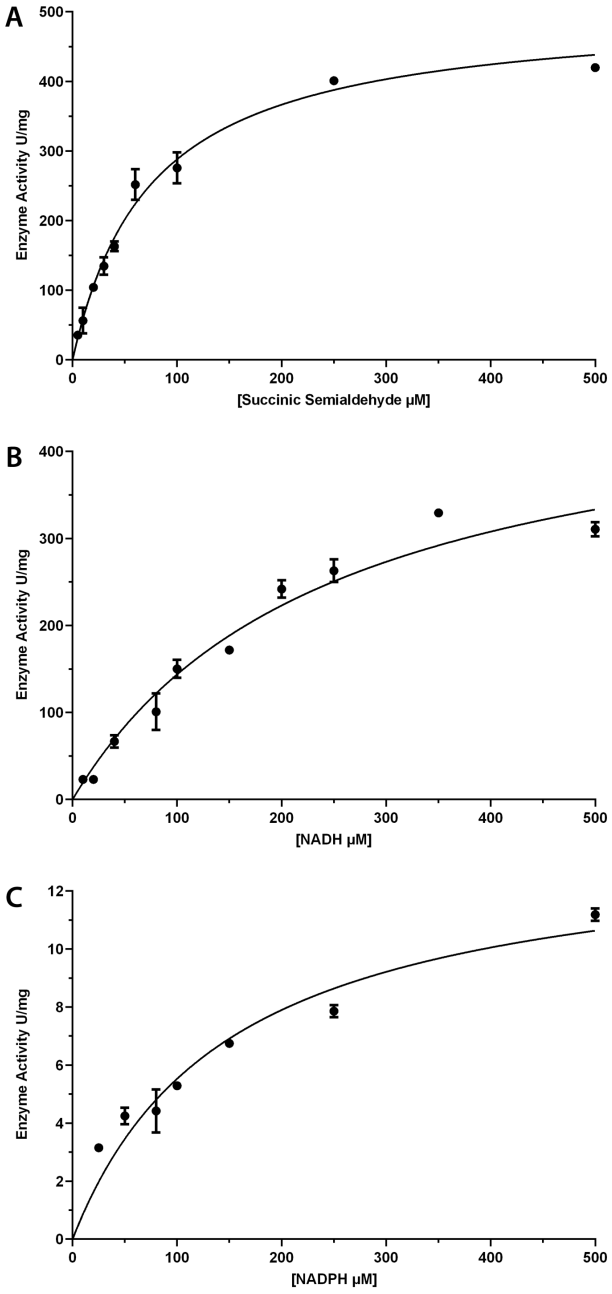

Fig. III.22.: ***Determination of K_M and v_{max} for succinic semialdehyde (A), NADH (B) and NAPDH (C) of SSR***. *Assays contained 500 µl reaction mixture and were prepared as described (65°C).* ***A**: K_M for succinic semialdehyde: 74.8 ± 7.6 µM , v_{max}: 503.8 ± 20.5 U/mg.* ***B**: K_M for NADH: 245.8 ± 42.7 µM , v_{max}: 497.1 ± 43.5 U/mg.* ***C**: K_M for NADPH: 41.0 ± 9.5 µM, v_{max}: 13.9 ± 1.2 U/mg.*

7.4. Antibody specificity and localization of Igni_0132

As described for PEP carboxylase and for MDH, specificity of the polyclonal antibody directed against the SSR of *I. hospitalis* was tested prior to immunogold labeling in a Western blot analysis with purified protein (data not shown) and freshly prepared crude extracts of *I. hospitalis* (KIN4/I). The primary antibody was diluted 1:10000, while the secondary antibody was diluted 1:20000. Here again, only one clear and specific protein band occurred between 40 and 55 kDa, which correlated with a pre-calculated mass of 45 kDa.

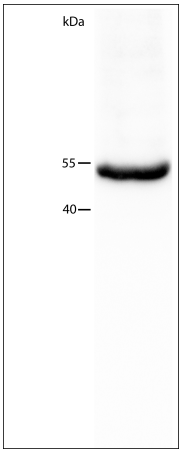

Fig. III.23.: ***Western Blot analysis of specificity of anti-Igni_0132.*** *1 µg of crude extract of I. hospitalis was applied on 10 % SDS gel. 1° AB: rabbit anti-Igni_0132, diluted 1:10000; 2° AB: GAR IgGs + HRP, 1:20000. Western Blot shows one specific band between 40-55 kDa.*

7.4.1. Localization on resin-sections

Determination of the subcellular localization of the SSR was of special interest for its characterization, since the SSR represents an important enzyme for carbon fixation that had not been identified so far. In Fig. III.24 localization of the enzyme is shown on ultrathin sections of Epon-embedded cells of the co-culture *I. hospitalis* and *N. equitans* (primary antibody diluted 1:100; secondary antibody diluted 1:50; silver-enhancement for 40 min). As already shown for the PEP carboxylase and the malate dehydrogenase, the enzyme is almost exclusively located in tight association with the OCM and to a small amount in the cytoplasm and on structures of the IMC. Fig. III.24 B shows again, as in the case of the MDH (Fig. III.18 B), the rare event of a dividing *I. hospitalis* cell, which seems to be connected with or is at least in close proximity

to one cell of *N. equitans*. On this section, the two cytoplasms of the dividing cell represent the dominating structural features and no obvious labeled horizontal line between both cytoplasms was observed. In all four pictures of Fig. III.24 one or more cells of *N. equitans* can be discovered, respectively (D = zoom-in on C). In figures III.24 C and D the cytoplasm of *I. hospitalis* is only weakly stained which indicates a rather desolate condition of the cell and additionally the bulged shape of the inner membrane strengthens the impression of *I. hospitalis* being tapped by *N. equitans*.

In all cases few gold particles can be found on *N. equitans*, which may be coincidence. However, from a statistical point of view, the regular occurrence of gold particles on *N. equitans* points to a specific labeling. Since neither an SSR nor a similar enzyme is annotated for *N. equitans* this might refer to a protein transfer between both organisms. The zoom-in on picture C (Fig. III.24 D), which shows gold particles on the contact site of *N. equitans* and *I. hospitalis*, reinforces the impression of proteins being transferred into *N. equitans*. In addition, this *I.hospitalis* cell is visualized to be surrounded by eight *N. equitans* cells in this ultrathin section. This *I. hospitalis* cell is likely to be surrounded by far more than eight *N. equitans* cells, e.g up to 20 cells, a situation which can frequently be observed by light microscopy in co-cultures of *I. hospitalis* and *N. equitans* after prolonged cultivation (Jahn *et al.*, 2008).

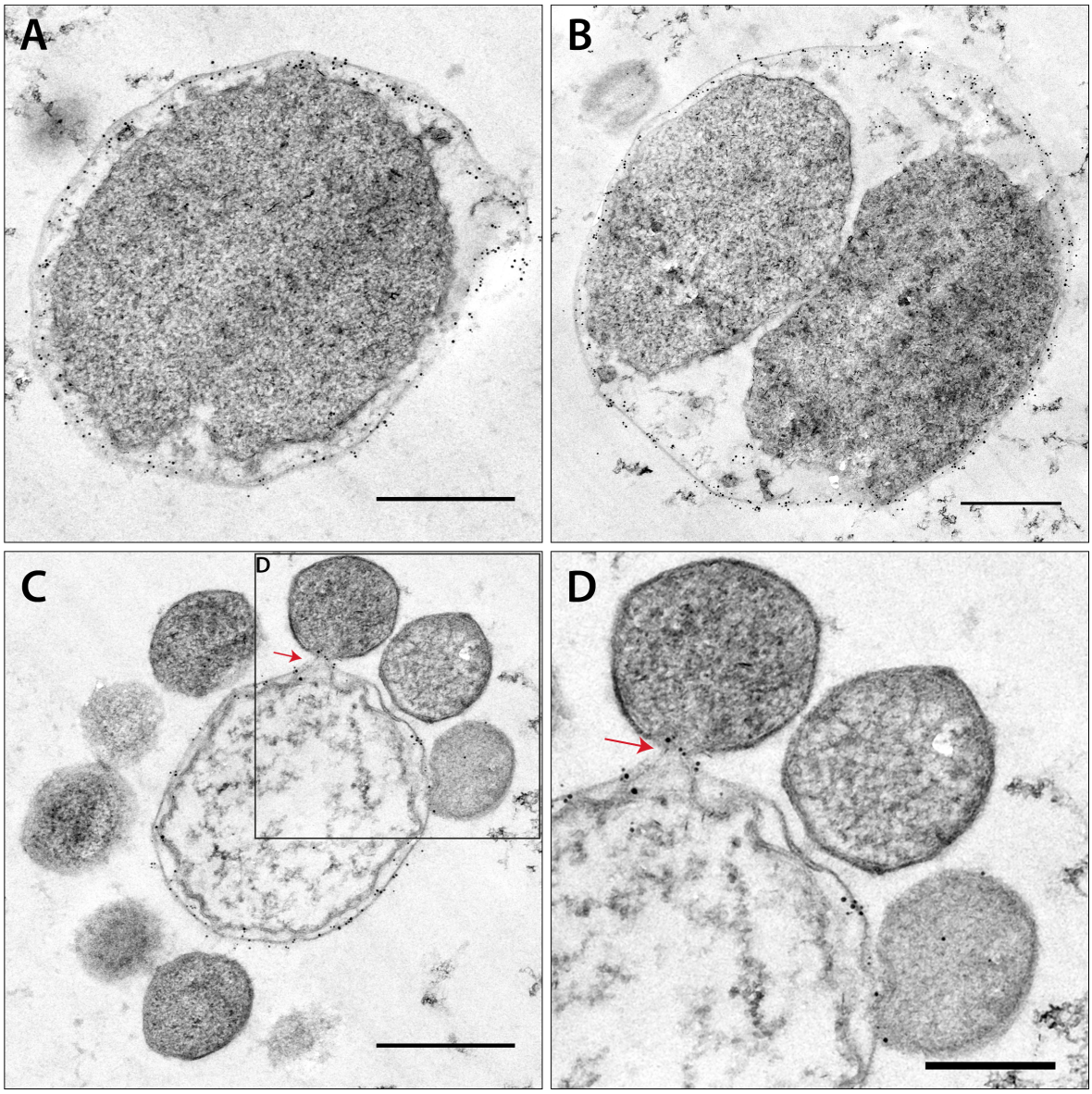

Fig. III.24.: ***Immunogold labeling of SSR on ultrathin sections of Epon-embedded I. hospitalis cells.*** *Cells were prepared as described (sections 7.3-9). 1° AB: anti-Igni_0132 was diluted 1:100; 2° AB: GAR IgG + 'ultrasmall' gold was diluted 1:50; silver enhancement: 40 min; size bars: 500 nm (A-C); 250 nm (D). Note the distribution of gold particles in the IMC, associated with the OCM (A-D).* ***B****: Dividing cell of I. hospitalis in close proximity to one cell of N. equitans.* ***C****: Desolate I. hospitalis cell surrounded by nine cells of N. equitans.* ***D****: Zoom-in on C; Focus on gold particles at the contact site (highlighted with red arrow) between both organisms.*

7.4.2. Localization on cryo-sections

The SSR was labeled on cryo-sections as well, using the same antibody dilutions as for resin-embedded cells. Fig. III.25 shows a very intense labeling of the *I. hospitalis* OCM, and also of structures in the IMC, respectively. Few gold particles can also be found in the cytoplasm. Besides, an increasing number of gold particles was observed linked with structures in the IMC, or the inner membrane. Very often, when cytoplasmic protrusions come close to the OCM, both structures seem to be connected via gold particles, which is particularly striking and could refer to a protein import mechanism via these protrusions, as suggested by Heimerl, 2014.

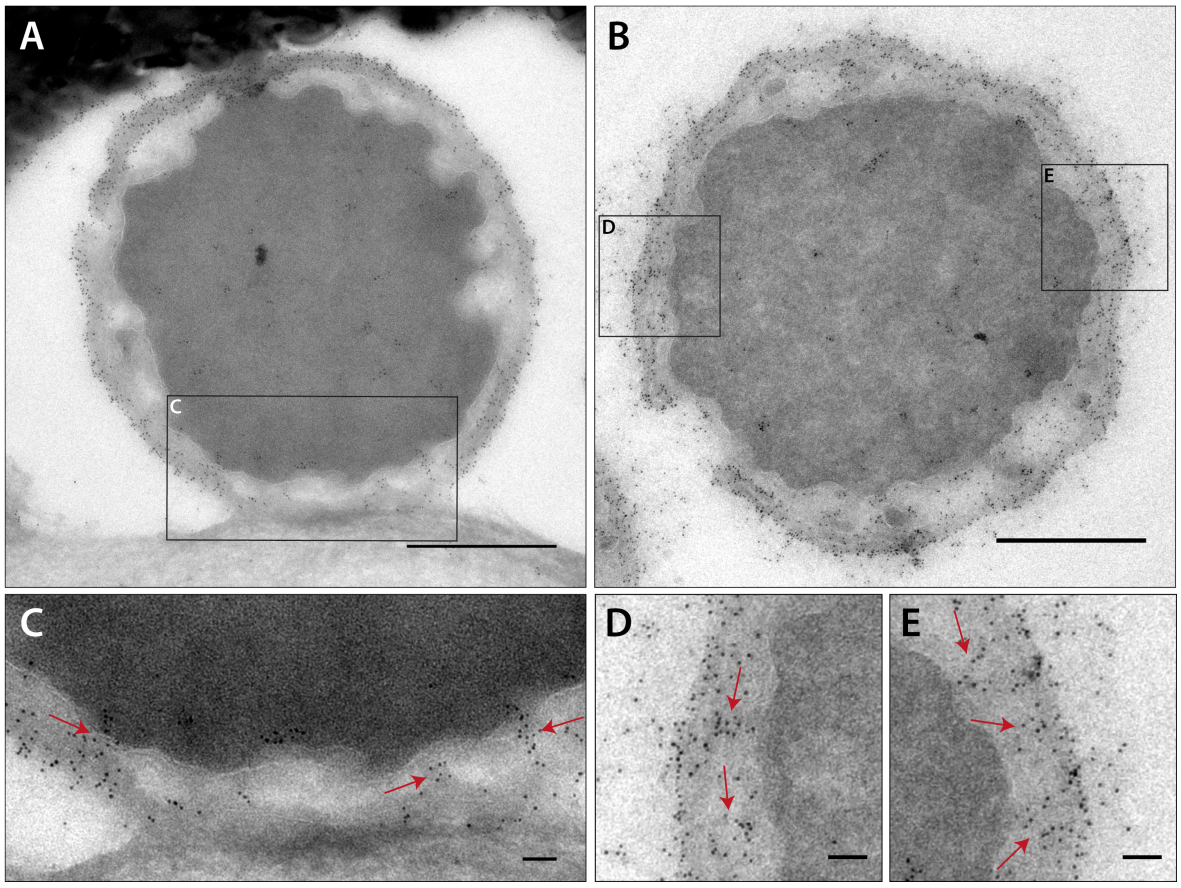

Fig. III.25.: ***Immunogold labeling of SSR on Tokuyasu sections of I. hospitalis cells.*** *Cells were prepared as described (sections 7.3-9). 1° AB: anti-Igni_0132 was diluted 1:100; 2° AB: GAR IgG + 'ultrasmall' gold was diluted 1:50; silver enhancement: 35 min; size bars: 500 nm (A and B); 50 nm (C-E). Gold particles are located in the IMC along the OCM. Additional labels can be observed in the cytoplasm and its protrusions. On zoom-ins of A and B (C-E) areas with close proximity of OCM and cytoplasmic protrusions that seem to be connected via structures labeled with anti-Igni_0132 are emphasized by red arrows.*

8. 4-hydroxybutyryl-CoA synthetase

8.1. Bioinformatical analysis

In Huber *et al.*, 2008 and Gallenberger, 2007 the gene product of *Igni_0475* was suggested to catalyze the reaction from 4-hydroxybutyrate to 4-hydroxybutyryl-CoA under consumption of ATP and CoA. BLAST analysis of the corresponding gene (Berg *et al.*, 2007) from *M. sedula* (*Msed_1422*) computed a significant alignment with *Igni_0475* (69 % sequence identity and an e-value of 0.0).

Nevertheless, in 2011, Ramos-Vera *et al.* reported that a recombinant version of Msed_1422 did neither work on 4-hydroxybutyrate nor on acetate, propionate, 3-hydroxypropionate, 3-hydroxybutyrate, or crotonate, but could possibly act on acylation of proteins and may therefore be involved in covalent modification of proteins. A very recent study published by Hawkins *et al.*, 2013 found two candidates in *M. sedula*, whose recombinant versions were actually ligating CoA to 4-hydroxybutyrate under the consumption of ATP (*Msed_0394* and *Msed_0406*). A BLAST analysis of both genes did not produce significant alignments to corresponding genes of *I. hospitalis*. However, when researching the genome of *I. hospitalis* for CoA synthetases/ligases, five candidates were suggested (*Igni_0086, Igni_0087, Igni_0257, Igni_0386* and *Igni_0379*). Since *Igni_0086* and *Igni_0087* were described as succinyl-CoA synthetase subunit alpha and beta (succinate thiokinase) involved in the carbon fixation and *Igni_0257* and *Igni_0256* together encode for an acetyl-CoA synthetase (Mayer *et al.*, 2012, Ramos-Vera *et al.*, 2011), a BLAST analysis of *Igni_0386* and *Igni_0379* made *Igni_0379* to the most promising candidate.

In the following section *Igni_0475* and *Igni_0379* were analyzed in detail using bioinformatic tools. *Igni_0475* consists of 493 amino acids and has a pre-calculated molecular mass of approximately 57 kDa. Using several prediction tools, neither signal peptides nor transmembrane regions were found. Psortb was not able to state on the localization of the protein (Cytoplasmic membrane score: 2.50; Cytoplasmic score: 2.50; Cellwall score: 2.50; Extracellular score: 2.50). NCBI BLAST hits comprised fatty-acid-CoA ligases of *P. fumarii*, of several *Sulfolobus* species and of *M. sedula* with sequence identities between 94-97 % (e-values of 0.0). Conserved domains inserted the protein into the AFD class I superfamily, a family that includes acyl- and aryl-CoA ligases and an adenylation domain of non-ribosomal peptide synthetases and firefly luciferases. KEGG motif search resulted in several motifs: A Lux E domain (acyl-protein synthetase Lux E, aa: 51-108; e-value of 0.027), an AMP-binding domain

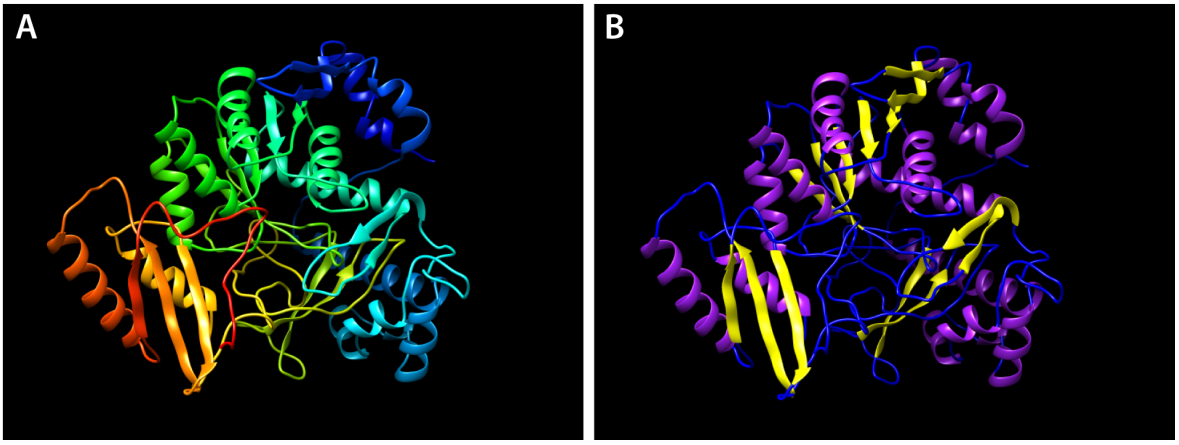

Fig. III.26.: ***Three-dimensional model of Igni_0475.*** *Structure prediction based on structural homologies according to PHYRE. Data were visualized using UCSF Chimera. A: Structure in rainbow color-code. N-terminus is shown in blue; C-terminus is shown in red. B: Model with highlighted secondary structure elements. α-helices: purple, β-sheets: yellow; loops: blue. The structure appears to consist of two subdomains; A larger N-terminal subdomain and a smaller C-terminal subdomain.*

(aa: 131-302, e-value of 0.00029), and an AMP binding_C domain (small domain found C-terminal to AMP binding domain; amino acid: 398-491, e-value of $1e^{-15}$).

In addition, a GH3 motif was found between amino acids 259-379 (GH3 auxin responsive promoter, e-value of 0.079). Moreover, the amino acid sequence was submitted to PHYRE to get a 3-dimensional model and therefore further indications on ligands. PHYRE modeled 100 % of residues at >90+% confidence. Therefore, five templates were selected to model the 3-dimensional structure, whereby only two residues were modeled *ab initio*. The resulting 3-dimensional structure gives the impression of being divided into two subdomains, which could represent the predicted N- and C-terminal AMP binding domains: A smaller C-terminal subdomain consisting of three β-strands surrounded by two α-helices and a larger N-terminal subdomain composed of several β-strands and α-helices, including one larger β-strand area made of seven β-components (III.26 A and B). Active site binding residues and acyl-activating enzyme consensus motif residues (AAE) identified by CDD sites are shown in Tab. III.12. The results of 3DLigandSite are summarized in Tab. III.13. Three clusters were predicted including CoA, Mg^{2+}, AMP, Ca^{2+} and ATP as putative ligands with average MAMMOTH scores around 30.

As structural homologues are suggested: A phenylacetate-CoA ligase from *Bacteroides thetaiotaomicron* with 100 % confidence and 24 % sequence identity, a phenyl-

Tab. III.12.: *Binding site residues of Igni_0475. Residues for an active binding site and for a AAE consesus motif were predicted by PHYRE.*

Active binding site	S 140	N 184	M 185	P 238	I 240	H 241	A 208
AAE	E 269	V 288	W 289	G 290	T 291	T 292	D 293
	Y 361	p 386	V 389	G 397	K 398	L 399	L400
	H 134	G 141	S 142	T 143	G 144	M 145	T 147
	F 148						

Tab. III.13.: *3DLigandSite prediction. Prediction of potential ligands of Igni_0475. Column 1: Cluster; Column 2: lnE of average MAMMOTH score; Column 3: Heterogens that might be present in structure*

Cluster	**Average MAMMOTH score**	**Heterogens**
1	27.7	CoA (6), Mg^{2+} (5), AMP (12), Ca^{2+} (1), ATP (3)
2	28.2	Mg^{2+} (2)
3	27.8	Mg^{2+} (1)

acetate-CoA ligase from *Burkholderia cenocepacia* with 100 % confidence and 23 % sequence identity and an acetyl-CoA synthetase like structure with 100 % confidence and 16-17 % identity. High accuracy of the model is predicted at 30-40 % identity, but even identities of 15 % give useful indications as long as confidence is high.

Igni_0379 is made of 474 amino acids and has a pre-calculated molecular mass of 53 kDa. The web-based program OCTOPUS suggested two transmembrane helices between amino acid 68 and 88 and at amino acid 195-215, while Phobius predicted only one transmembrane region between amino acids 200-221. Furthermore, no signal peptides were detected within the amino acid sequence. Psortb proposed a cytoplasmic localization of the protein with a score of 9.96 (Cellwall, score: 0.02; Extracellular, score: 0.01). Best NCBI BLAST hits were: an AMP-dependent synthetase of *P. fumarii* with 56 % sequence identity (e-value of 1 e^{-177}), an acyl-CoA synthetase of *Pyrobaculum sp. 1860* with 44 % sequence identity (e-value of 1 e^{-103}) and an AMP dependent synthetase of *Vulcanisaeta distributa* with 40 % sequence identity (e-value of 1 e^{-100}). The protein was classified as member of the AFD class I superfamily by Conserved Domains, as well. KEGG motif search suggested an AMP-binding domain (aa: 14-399, e-value of 9.2 e^{-81}) and an AMP binding_C (aa: 409-472, e-value of 5.1 e^{-6}). PHYRE search provided further insights in 3-dimensional structure and putative ligands, as well. 100 % of residues were modeled at >90 % confidence. To create the

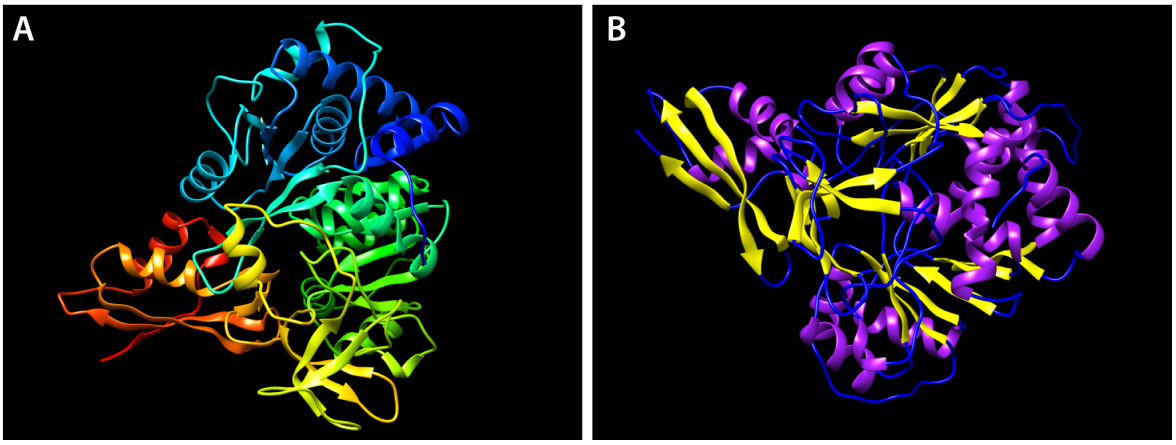

Fig. III.27.: ***Three-dimensional model of Igni_0379.*** *Structure prediction based on structural homologies according to PHYRE. Data were visualized using UCSF Chimera. A: Structure in rainbow color-code. N-terminus is shown in blue; C-terminus is shown in red. B: Model with highlighted secondary structure elements. α-helices: purple, β-sheets: yellow; loops: blue. The structure appears to consist of two subdomains; A larger N-terminal subdomain and a smaller C-terminal subdomain.*

model six templates were used and only one residue was modeled *ab initio*. Similar to the structure for Igni_0475, the structure for Igni_0379 appears to consist of two subdomains; a small C-terminal part and a larger N-terminal part. The smaller part is composed of three β-strands connected with two α-helices and the larger part consists of several β-strands and α-helices with one larger β-strand area made of seven β-strands (Fig. III.27 A and B).

CDD Site identified CoA binding site residues, active binding site residues and acyl-activating enzyme consensus motif residues (AAE) as shown in Tab. III.14. Furthermore, six putative clusters for ligand binding, which include CoA, Mg^{2+}, Ca^{2+}, AMP and ATP as putative heterogens were suggested by 3DLigandSite (Tab. III.15). The

Tab. III.14.: *Binding site residues of Igni_0475. Residues for an active binding site and for an AAE consensus motif were predicted by PHYRE.*

CoA binding site	K 458						
Active binding site	P 196	L 197	P 244	V 246	F 247	L 250	G 272
	A 273	V 294	Y 295	G 296	M 297	T 298	E 299
	I 377	R 389	R 392	G 400	Y 401	P 402	I 403
	K 464						
AAE	F 153	G 157	I 158	A 159	G 160	R 161	M 163

Tab. III.15.: *3DLigandSite prediction. Prediction of potential ligands of Igni_0379. Column 1: Cluster; Column 2: lnE of average MAMMOTH score; Column 3: Heterogens that might be present in structure*

Cluster	Average MAMMOTH score	Heterogens
1	44.0	CoA (1), Mg^{2+} (3), AMP (13), Ca^{2+} (1), ATP (2)
2	50.0	CoA (5)
3	50.1	Mg^{2+} (2)
4	49.8	Mg^{2+} (1)
5	49.8	Mg^{2+} (1)
6	40.8	Mg^{2+} (1)

average MAMMOTH scores, which are in the range of 40-50 are considerably high, implying a high similarity between respective structures and the structure for Igni_0379. According to PHYRE homologous structures could be represented by ACS-like structures with 100 % confidence and identities between 21-24 % and by an AMP-binding protein of *Methanosarcina acetivorans* with 100 % confidence and 24 % identity.

8.2. Cloning and expression of *Igni_0475* and *Igni_0379*

For identification of en enzyme with a 4-hydroxybutyryl-CoA synthetase activity, two putative candidates were cloned and heterologously expressed in *E. coli*: *Igni_0475* and *Igni_0379*. Both codon-optimized genes contained the restriction sites NheI and NcoI and were cloned into the vector pRSETa. Neither the non-codon adapted version of *Igni_0475*, nor the codon-optimized construct could be expressed successfully in *E. coli*. However, expression of only a part of the protein, employing the *E. coli* strain Rosetta2 (DE3), was successful. Expression, purification and immunization of the rabbits were performed by Dr. Steve Bell (Bloomington, Indiana (US), data not shown).

Additionally, a codon-adapted sequence of *Igni_0379* was overexpressed in the *E. coli* strain BL21 Star™ (DE3) at 30°C for 4 h using 0.8 mM of IPTG for induction. In SDS PAGE followed by Coomassie staining and in Western blot analysis using an anti-polyhistidine antibody for detection of his-tagged proteins, a band between 55 - 70 kDa occurred in the soluble and in the insoluble fraction of *E. coli* crude extracts. This correlated with a pre-calculated molecular mass of approximately 53 kDa. Purification from the soluble fraction of *E. coli* crude extract was possible combining heat precipitation 80°C for 15 min and affinity chromatography with Protino® Ni-TED Resin.

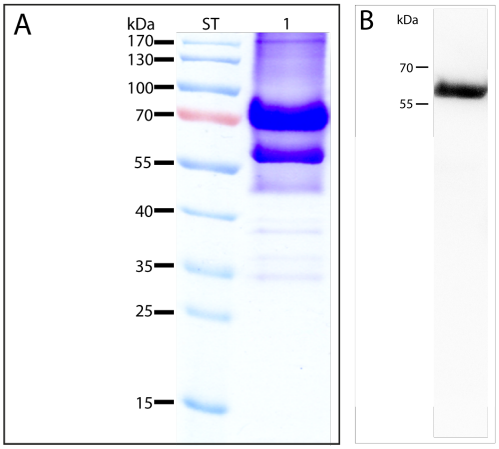

Fig. III.28.: ***Analysis of recombinant protein obtained by expression of Igni_0379.*** ***A****: Purification by affinity chromatography and heat precipitation (HP). SDS PAGE (10 % AA; stained with Coomassie), ST: Standard, lane 1: Fraction that contains purified protein. HP was carried out for 15 min at 80°C. SDS PAGE analysis shows two prominent protein bands at above 55 kDa and at 70 kDa and several weaker bands. Pre-calculated mass of Igni_0379 is 53 kDa, which corresponds to the lower prominent band* ***B****: Western Blot analysis of soluble fraction of E. coli extracts after expression of Igni_0379. 1° AB: mouse-anti-polyhistidine, diluted 1:500; 2° AB: GAM IgG + HRP, diluted 1:20000. Western Blot shows only one band between 55-70 kDa of a his-tagged protein.*

However, an unknown protein of approximately 70 kDa co-purified with the recombinant protein that was not detectable by Western blotting. Therefore, the 53 kDa protein was confirmed to be Igni_0379 using MALDI-TOF MS/MS analysis (score: 1010).

8.3. Activity tests on Igni_0475 and on Igni_0379

Enzyme assays with both, Igni_0475 and Igni_0379 should provide further information if one of the proteins exhibits the requested 4-hydroxybutyryl-CoA synthetase. Since overexpression of the whole protein Igni_0475 failed, an alternative way to measure enzyme activity had to be developed and established. For this, immuno precipitations (IP) with *Igniccocus* cell extract (KIN4/I) were performed using the antibody directed against a part of the protein. The IP was directly followed by enzyme assays at 60°C or 80°C, using either the resulting IP-eluate or the precipitated protein still linked with the beads instead of recombinant protein (sections II.6.3 and II.7.4). However, initially it had to be established whether the antibody binds specifically to its corresponding target antigen. Fig. III.29 A shows a Coomassie stained SDS gel of the respective IP, on which

three prominent bands are visible. The bands at approximately 25 kDa and 50 kDa refer to the light and the heavy chains of IgG. The upper band slightly above 55 kDa was checked using MALDI TOF MS/MS analysis, which confirmed the precipitated protein as Igni_0475 (score 629). Based on these results a colorimetrically test using DTNB for detection of free CoA and analysis with UPLC were performed to provide evidence for enzyme activity. The enzyme assay with cell extract of KIN4/I served as positive control for the colorimetric test system since it had been used successfully in previous works (Gallenberger, 2007, Jahn *et al.*, 2008). As additional control, MDH and SSR were immuno precipitated from KIN4/I cell extract and tested for enzyme activity in a respective assay (Fig. III.30). For MDH an activity of 7.25 µmol/ml cell extract (*I. hospitalis*; Fig. III.30 A) and for SSR an activity of 5.66 µmol/ml cell extract (*I. hospitalis*; Fig. III.30 B) were measured. Using the IP-eluate instead of cell extract, activity for MDH was 5.4 µmol/ml IP eluate (Fig. III.30 C) and activity for SSR was 0.77 µmol/ml IP eluate (III.30 D).

The results from the 4-hydroxybutyryl-CoA assay with cell extract from KIN4/I clearly showed a decrease in color intensity with increasing incubation time (0, 5 and 10 min) as depicted in Fig. III.29 B. Note that after 10 min incubation time, the yellowish coloring has almost completely vanished. In contrast, the assay with IP-eluate (shown in Fig. III.29 C) instead of cell extract does not show a significant decrease in color intensity. Similarly, no significant differences could be detected in the photometer at 412 nm and UPLC analysis did not provide evidence for formation of 4-hydroxybutyryl-CoA in assays with IP-eluate. In addition to 4-hydroxybutyrate, acetate and propionate were tested as substrates, but without detectable binding of CoA. Analogous, the same experiment was performed with Igni_0379 with both recombinant protein and immuno precipitated protein. Again, in this experiment, the control assays were positive whereas no activity was detected either with the recombinant protein or with the immuno-precipitated protein. Thus, it should be noted, that neither Igni_0475 nor Igni_0379 were active on 4-hydroxybutyrate, acetate and propionate in these enzyme assays and it therefore still remains unclear whether one of the corresponding genes encodes for a 4-hydroxybutyryl-CoA synthetase, the enzyme assay as proposed here is inadequate or not physiological (in *I.hospitalis*), or another synthetase is responsible for catalysis of this reaction.

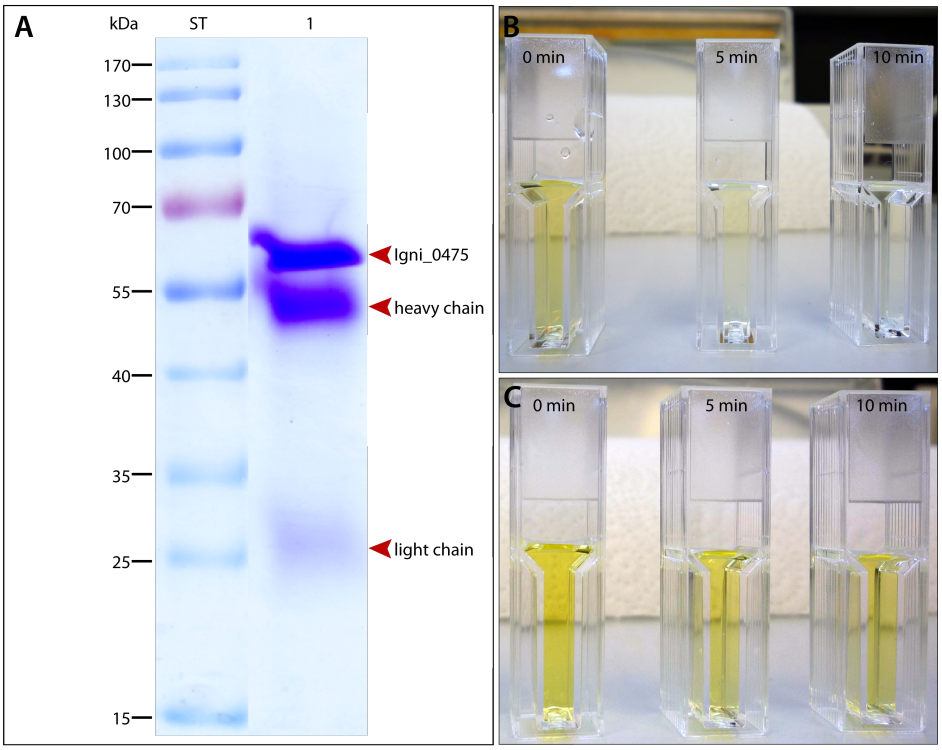

Fig. III.29.: ***IP of and enzyme assay with Igni_0475.*** ***A****: Coomassie stained SDS gel of an IP with cell extract of I. hospitalis (KIN4/I) and an antibody directed against a part of Igni_0475. Note the three bands at ∼ 25, ∼ 50 and between ∼ 55 and ∼70 kDa. The bands at ∼ 25 and ∼ 50 kDa refer to light and heavy chain of the IgG and the band above ∼ 55 kDa was identified as Igni_0475 in MALDI TOF analysis.* ***B*** *and* ***C****: Enzyme assay for detection of 4-hydroxybutyryl-CoA synthetase activity. Free CoA was detected with DTNB.* ***B****: Control assay with cell extract from I. hospitalis (KIN4/I). Note that with increase of time, the yellow color vanishes, indirectly indicating formation of 4-hydroxybutyryl-CoA.* ***C****: Enzyme assay with IP-eluate. Note that the yellow color preserves its intensity almost completely throughout the whole experiment, indicating no formation of 4-hydroxybutyryl-CoA.*

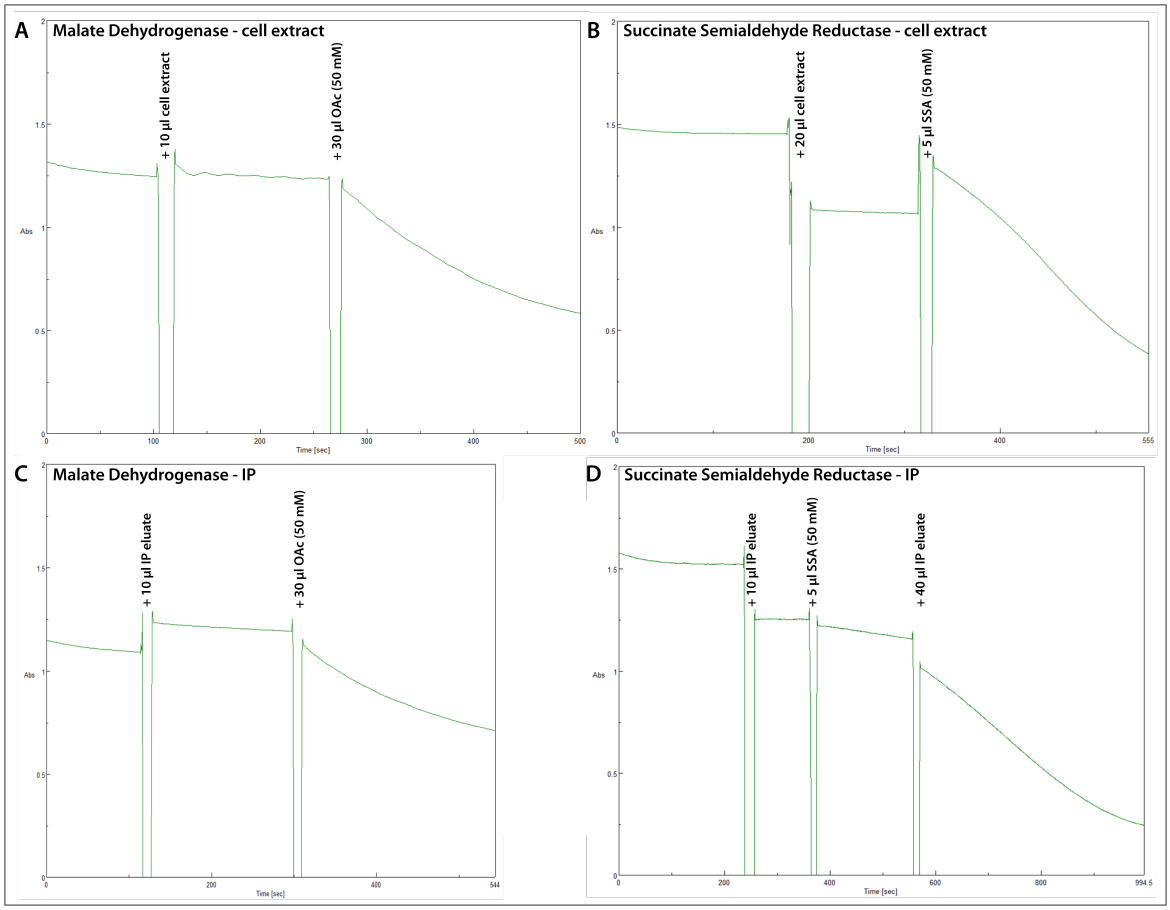

Fig. III.30.: *Control assays for immuno precipitated proteins.* ***A*** *and* ***B****: Activity assays for MDH and SSR in cell extracts of I. hospitalis (KIN4/I).* ***C*** *and* ***D****: Activity assays for MDH (C) and SSR (D) with immuno precipitated proteins from cell extracts of I. hospitalis (KIN4/I) with the respective antibodies. Note that in all cases enzyme activity was detectable, but more remarkable is the fact that immuno precipitated proteins were both active, as well.*

8.4. Antibody specificity and localization of Igni_0475 and Igni_0379

To determine specificity of the antibodies directed against the proteins Igni_0475 (III.31 A) and Igni_0379 (III.31 B), Western Blots were performed with crude extracts of *I. hospitalis* (KIN4/I). Both antibodies were able to detect one prominent band between 55 and 70 kDa, each at the height of the pre-calculated mass of the respective protein. For this, primary antibodies were diluted 1:10000 and secondary antibodies were diluted 1:20000, respectively. However, in the Western Blot for detection of Igni_0475, two additional but significantly weaker bands at 40 and above

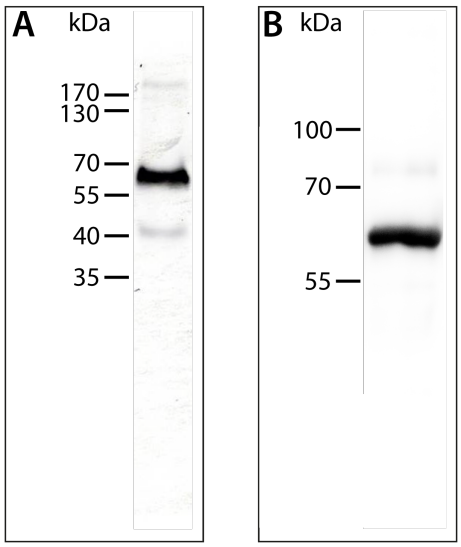

Fig. III.31.: ***Western Blot analysis of specificity of anti-Igni_0475 and anti-Igni_0379.*** *1 µg of crude extract of I. hospitalis was applied on 10 % SDS gel.* ***A:*** 1° *AB: rabbit anti-Igni_0475, diluted 1:10000;* 2° *AB: GAR IgGs linked with HRP, diluted 1:20000. Western Blot shows one prominent band between 55-70 kDa and two additional weaker bands at 40 and above 170 kDa.* ***B:*** 1° *AB: rabbit anti-Igni_0379, diluted 1:10000;* 2° *AB: GAR IgGs linked with HRP, diluted 1:20000. Western Blot shows one prominent band between 55-70 kDa.*

170 kDa were observed, which could refer to degradation products (40 kDa) or an oligomeric version of the protein (170 kDa). After IP no additional bands occurred neither on Coomassie-, nor on silver-stained SDS gels. Given those facts, antibody specificity of both antibodies was confirmed.

8.4.1. Localization on resin-sections

Immunogold labeling on ultrathin sections of Epon-embedded *I. hospitalis* cells with antibodies directed against Igni_0475 revealed a cytoplasmic localization of the protein (Fig. III.32). In contrast to other proteins of the CO_2 fixation cycle examined so far, no labeling was detected in the OCM, but in the cytoplasm and to some extent in cytoplasmic protrusions. Whenever *N. equitans* was attached to *I. hospitalis*, strong labeling of *N. equitans* cells was observed and occasionally, gold particles were found directly at the contact site (Fig. III.32 A and C).

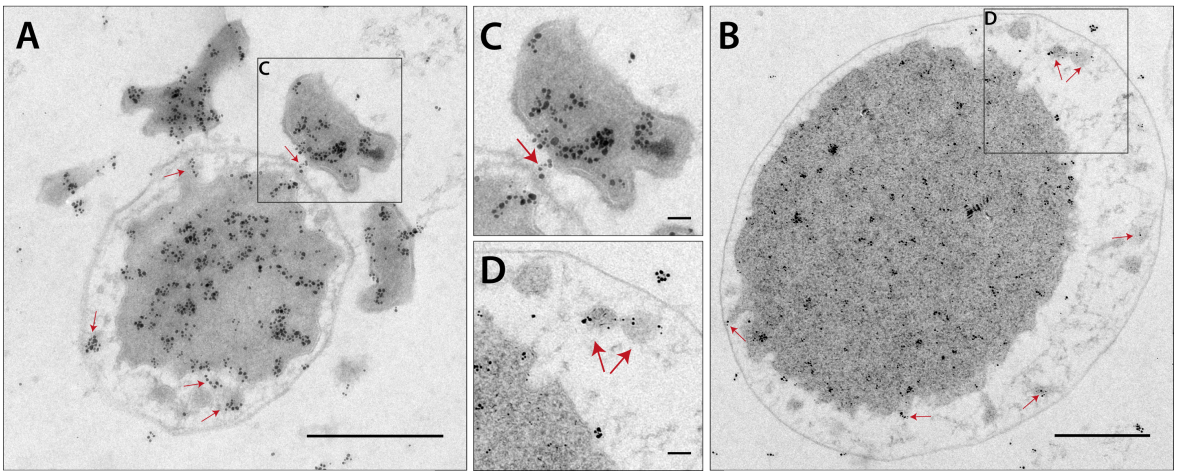

Fig. III.32.: ***Immunogold labeling of Igni_0475 on ultrathin sections of Epon-embedded I. hospitalis cells.*** *Cells were prepared as described (sections 7.3-9).* 1° *AB: anti-Igni_0475 was diluted 1:100;* 2° *AB: GAR IgG + 'ultrasmall' gold was diluted 1:50; silver enhancement: 30 min; size bars: 500 nm (A-B); 50 nm (C-D).* ***A*** *and* ***B****: Protein is located in the cytoplasm of I. hospitalis and N. equitans. Additional gold particles can be observed at the contact site between N. equitans and I. hospitalis (****C****) and in cytoplasmic protrusions (****D****). Red arrows highlight labeling at the contact site and in protrusions.*

In contrast, Igni_0379 was mainly located in association with the OCM on ultrathin sections of *I . hospitalis* (Fig. III.33). Only few gold particles (below 5 %), were detected in the cytoplasm or in the background, respectively. In addition, some gold particles were located on cytoplasmic protrusions, or on structures of the IMC, as illustrated on Fig.III.33 B and its zoom-ins (Fig.III.33 C-F). Labeled structures in the IMC are highlighted by red arrows. Incidentally, no cross reaction with cells of *N. equitans* were observed.

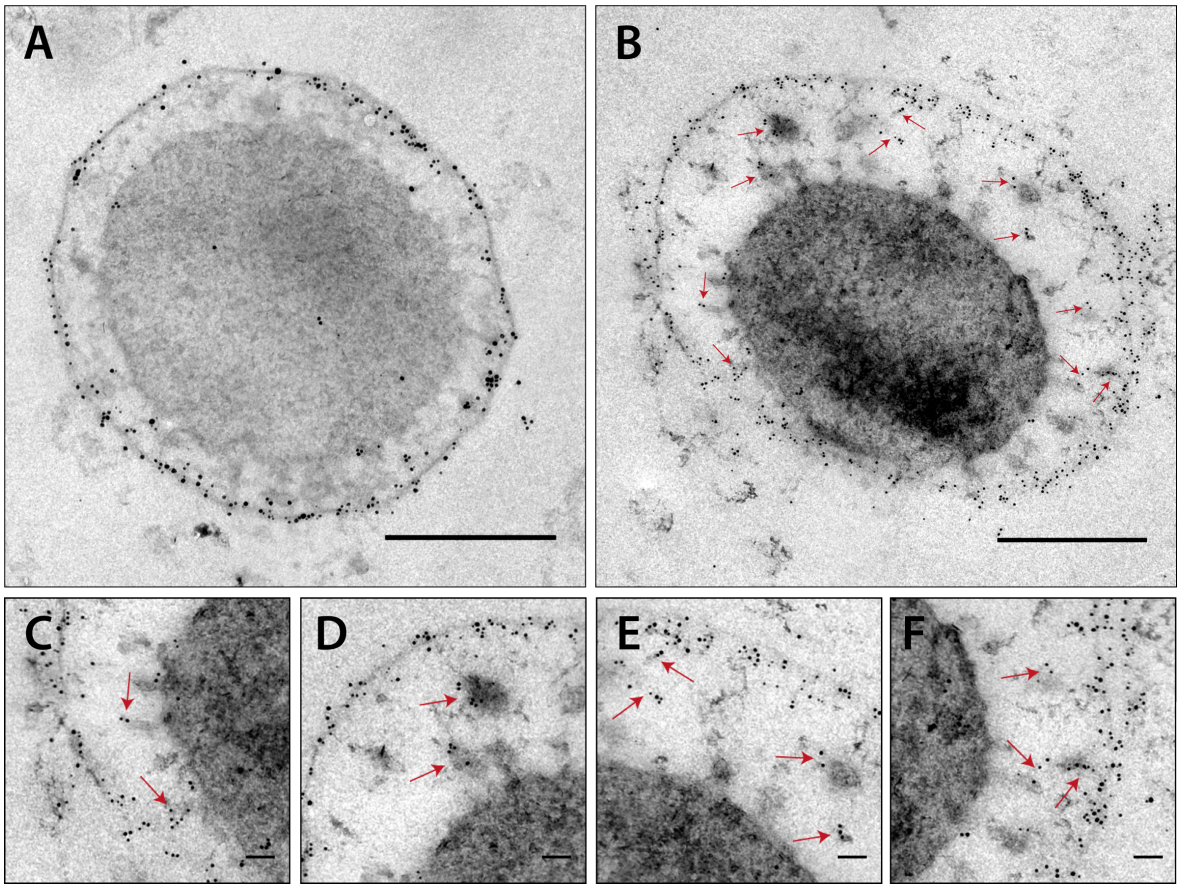

Fig. III.33.: ***Immunogold labeling of Igni_0379 on ultrathin sections of Epon-embedded I. hospitalis cells.*** *Cells were prepared as described (sections 7.3-9). 1° antibody (anti-Igni_0379) was diluted 1:100; 2° antibody (GAR IgG + 'ultrasmall gold') was diluted 1:50; silver enhancement: 35 min; size bars: 500 nm (A-B); 50 nm (C-F). The protein was located almost exclusively in the OCM of I. hospitalis and in cytoplasmic protrusions. C-F: Zoom-ins on B. Labeling of cytoplasmic protrusions is highlighted by red arrows.*

9. Crotonyl-CoA hydratase/3-hydroxybutyryl-CoA dehydrogenase

9.1. Bioinformatical analysis of Igni_1058

Crotonyl-CoA hydratase/3-hydroxybutyryl-CoA dehydrogenase was suggested to be a bifunctional enzyme that catalyzes two steps of the carbon fixation pathway in *I. hospitalis* (Huber *et al.*, 2008). In a first step it converts crotonyl-CoA to (S)-3-hydroxybutyryl-CoA; in a second step this product is dehydrogenated to acetoacetyl-CoA while reducing NAD^+ to NADH. The gene *Igni_1058* is likely to encode for

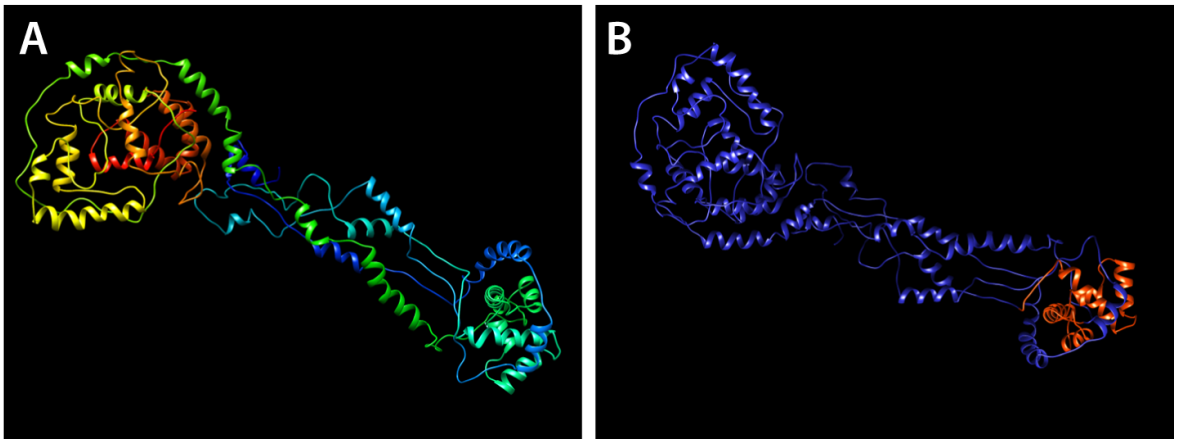

Fig. III.34.: ***Three-dimensional model of Igni_1058.*** *Structure prediction based on structural homologies according to PHYRE. Data were visualized using UCSF Chimera.* ***A****: Structure in rainbow color-code. N-terminus is shown in blue; C-terminus is shown in red. Note that the protein structure is uncommonly long-stretched.* ***B****: Structure color-coded in a confidence key. Red areas indicate high confidence, blue areas indicate low confidence. Note that only 95 residues out of the sequence are colored in red, implying a highly unreliable structure prediction.*

such a fusion protein and was therefore examined in detail using bioinformatic tools. Protparam calculated 683 amino acids and a molecular mass of 74.7 kDa. OCTOPUS suggested two transmembrane helices for the protein. Thus, the first proposed helix is located at position 24-44 and the second helix between amino acids 525 and 545. Furthermore, Phobius suggested a signal peptide from amino acid 1-15 and a non-cytoplasmic localization of the whole protein. In addition, the web-based programs SignalP-4.1 and Predisi identified the transmembrane helix near the N-terminus as signal peptide, as well. In contrast, Psortb predicted a cytoplasmic localization of the protein with a score of 7.50 (Cytoplasmic membrane, score: 1.00; Cellwall, score: 0.87; Extracellular, score: 0.63). Best BLAST hits produced by NCBI pBLAST with an e-value of 0.0 and a sequence identity of >95 % involved various 3-hydroxyacyl-CoA dehydrogenases of *P. fumarii*, of *A. camini*, of *A. pernix* and of different uncultivated *Acidilobus* species. As specific hits for conserved domains were listed: An N-terminal part of a 3-hydroxyacyl-CoA dehydrogenase domain with an NAD binding motif (3HCDH_N, aa: 25-209, e-value of 2.31 e^{-83}), a C-terminal part of a 3-hydroxyacyl-CoA dehydrogenase (3HCDH, aa: 214-308, e-value of 4.48e^{-34}; aa: 337-422, e-value of 1.27e^{-20}), and a crotonase-like domain beloning to the crotonase/enoyl-CoA hydratase superfamily (aa: 432-624, e-value of 2.48e^{-65}). Thus, evaluation of the domain analysis provided

Tab. III.16.: *Predicted binding site residues of Igni_1058. Residues for a substrate binding site, for a trimer interface and for oxyanion hole forming residues were predicted by PHYRE.*

Substrate binding site	N 451	L 453	V 484	G 488	F 489	L 491	T 492
Trimer interface	A 532	G 534	G 535	E 558	I 559		
	A 516	V 524	L 545	R 546	L 547	A 548	N 560
	V 561	G 562	I 563	G 569	Q 571	R 572	L 573
	R 575	L 576	R 581	A 582	Q 584	L 585	L 587
	L 588	P 591	L 602	W 605	V 620	L 623	S 624
OAH forming	D 490	G 536					

considerable indications of Igni_1058 being a fusion protein. Above all, the amino acid sequence was submitted to PHYRE, which was only able to model 14 % of residues at >90 % confidence. For this, two templates were selected to model the protein, of which 587 residues were modeled *ab initio* which is proclaimed to be highly unreliable. The resulting 3-dimensional structure, color-coded in rainbow colors, consists exclusively of α-helices connected by coiled structures and appears to be inconveniently long-stretched (Fig. III.34 A). A look at Fig. III.34 B, from which insufficient confidence of the structure becomes apparent, reveals only one area, consisting of 95 residues, which is colored in red (red indicates high confidence). Nevertheless, the amino acid sequence revealed substrate binding site residues, trimer interface residues and residues indicating the formation of an oxyanion hole. All of these elements are located within the crotonase-like part of the protein (Tab. III.16).

Since there is evidence for a fusion protein, the amino acid sequence was virtually cut into two pieces (after residue 421) and both parts were submitted to PHYRE separately, to gain a deeper understanding of the protein structure. As a result two models were provided by PHYRE in which 100 % (residues 1-421) and 99 % (residues 422-683) of residues were modeled at $>$ 90 % confidence, respectively. Hence, part one of the protein exhibits a Rossmann-fold like topology situated in close proximity to the N-terminus and an all α -helical part for the rest of the protein. Structural homologies were suggested to different oxidoreductases at 100 % confidence and sequence identity of >31 %. This includes homologies for a putative 3-hydroxybutyryl-CoA dehydrogenase from *E. coli* K 12 (39 % sequence identity), a peroxisomal bifunctional enzyme (32 % sequence identity) and a fatty acid β-oxidation multienzyme complex from *Pseudomonas fragi* (35 % sequence identity). According to these results, this first part of the protein, comprising a Rossmann-fold like topology, might catalyze the NAD^+ dependent dehydrogenase reaction from 3-hydroxybutyryl-CoA to acetoacetyl-CoA. The

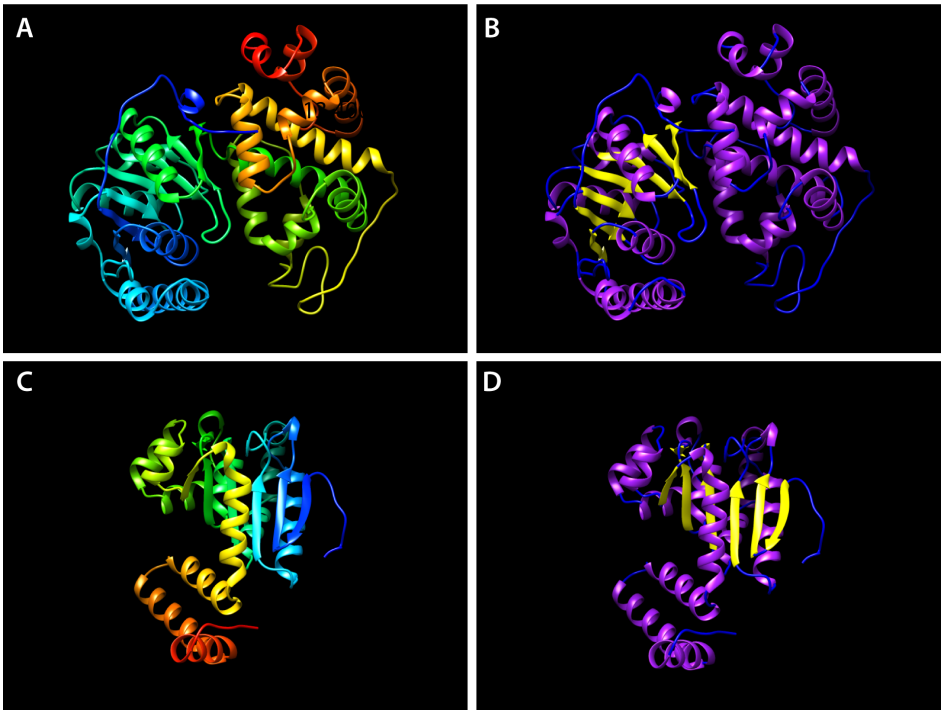

Fig. III.35.: ***Three-dimensional model of Igni_1058 divided into two parts.*** *Structure was divided into two parts before submission to PHYRE (cut after residue 421) Structure prediction based on structural homologies according to PHYRE. Data were visualized using UCSF Chimera.* ***A*** *and* ***C****: Structure of part 1 (A) and 2 (C) in rainbow color-code. N-terminus is shown in blue; C-terminus is shown in red.* ***B*** *and* ***D****: Model with highlighted secondary structure elements of part 1 (B) and 2 (D). Part one comprises a Rossman fold, an might therefore catalyze the NAD^+ dependent dehydrogenase reaction from 3-hydroxybutyryl-CoA to acetoacetyl-CoA. Part two might therefore be the hydratase part, converting crotonyl-CoA to (S)-3-hydroxybutyryl-CoA.*

model for the second part of the protein consists of two β-strand regions arranged in two rows and several α-helices. In general, PHYRE suggested homologue structures at 100 % confidence and sequence identities >30 % from various lyases, or isomerases, respectively. Best structural homology was found for a PaaF-PaaG hydratase-isomerase complex from *E.coli* at 100 % confidence and 40 % template identity. Additionally, homologies for a enoyl CoA hydratase from *Polaromonas sp.* (31 % sequence identity), from *Streptomyces coelicolor* (31 % sequence identity) and from *Myocbacterium tuberculosis* (39 % sequence identity) were proposed. This second part of the enzyme might therefore be the hydratase part, converting crotonyl-CoA to (S)-3-hydroxybutyryl-CoA.

9.2. Cloning and expression of *Igni_1058*

The codon-optimized gene construct pRSETa-Igni_1058 with the restriction sites BamHI and EcoRI was heterologously expressed in the *E. coli* strain BL21 Star™ (DE3). Best expression rates were achieved with an incubation of *E. coli* cells at 30°C for 6 h using 0.8 mM of IPTG for induction. For checking expression efficiency, SDS PAGE followed by Coomassie staining was carried out. This revealed one intense band between 70 - 100 kDa in both the soluble and the insoluble fraction of *E. coli* crude extracts. Further controls, performing a Western Blot with an anti-polyhistidine antibody confirmed that expression was successful. Since relative molecular masses of the recombinant protein (band between 70 - 100 kDa) correlated with the expected pre-calculated molecular mass of approximately 75 kDa, the protein was further purified from the *E. coli* crude extract (Fig.III.36 **B** and **C**). Purification was initially performed from the soluble fraction of *E. coli* extracts with Protino® Ni-TED Resin. However, purification by affinity chromatography and heat precipitation was not successful. Moreover, even when performing heat precipitation only at 60°C the protein disintegrated almost completely (data not shown).

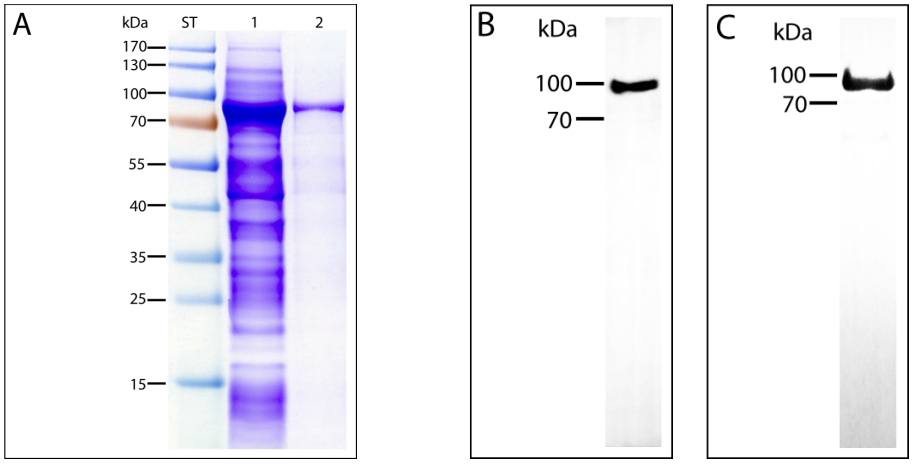

Fig. III.36.: ***Analysis of recombinant protein obtained by expression of Igni_1058.*** ***A****: Purification of the insoluble fraction of E. coli extract by affinity chromatography. SDS PAGE (10 % AA; stained with Coomassie), ST: Standard, lane 1: E. coli crude extract of the insoluble fraction, lane 2: Elution fraction 1 of purified recombinant protein. SDS PAGE analysis shows one protein band at 70 - 100 kDa after purification.* ***B*** *and* ***C****: Western Blot analysis of soluble (****B****) and insoluble fraction (****C****) of E. coli extracts after expression of Igni_1058. 1° AB: mouse-anti-polyhistidine, 1:500; 2° AB: IgG GAM + HRP, 1:20000. Both Western Blots show one band between 70 - 100 kDa of a his-tagged protein.*

Concluding that the his-tag was indeed present (Western Blot with anti-polyhistidine antibody was positive) but folded inwardly and therefore not accessible when performing affinity chromatography, purification was carried out under denaturing conditions from the soluble fraction using 2 M urea and from the insoluble fraction using 8 M urea, respectively. Due to the much higher amount and the increased purity of recombinant protein purified from inclusion bodies, protein from this fraction was used for further processing (Fig.III.36 **A**). Immediately after purification, recombinant protein was dialyzed using a 'Slide-A-Lyzer Dialysis Cassette'. Dialysis was carried out stepwise (2 M urea, 1 M urea, without urea), decreasing the concentration of urea in the buffer (5 mM HEPES, pH=7.5) to avoid precipitation of the protein. Finally, the recombinant purified protein was further analyzed and success of protein expression was confirmed by MALDI-TOF MS/MS analysis (score 863).

9.3. Characterization of Igni_1058

Prior to determination of K_M and v_{max}, the optimal pH for enzyme activity was determined. As it is known that esters hydrolyze under acidic and alkaline conditions, different buffers and mixtures of buffers in a pH range between 6 - 9 (Tris/HCl 9 - 7, MOPS 7, MES 6.5 - 6) were used while taking temperature dependencies of buffers into account. Maximum enzyme activity was measured at a pH of 8 at 50°C in Tris/HCl buffer.

For characterization, K_M and v_{max} for crotonyl-CoA, 3-hydroxybutyryl-CoA and NAD^+ were determined at 50°C. Although purified under denaturing conditions, the enzyme was still active at a v_{max} of 7.3 U/mg and exhibited K_M values for crotonyl-CoA of 71.0 ± 8.1 µM and for (S)-3-hydroxybutyryl-CoA of 86.0 ± 13.1 µM, respectively. Since only small amounts of recombinant purified enzyme had been available, the determined K_M-value for NADH (14.7 ± 1.7 µM) can only be considered as provisional result and determination should therefore be repeated (Tab. III.17). Furthermore, the enzyme acted stereospecific only on (S)-3-hydroxybutyryl-CoA, which differs from (R)-3-hydroxybutyryl-CoA in the orientation of a hydroxyl group at stereo center C3. When replacing NAD^+ by $NADP^+$ as co-substrate for the dehydrogenase reaction, enzyme activity decreased by approximately 86 %, implying that NAD^+ is preferably used as oxidizing agent. Another aspect was to check the crotonyl-CoA hydratase part for activity on 3-hydroxypropionyl-CoA, which was carried out in a coupled enzyme test at 42°C. However, no activity was detected with 3-hydroxypropionyl-CoA. Finally, the

Tab. III.17.: *K_M and v_{max} of crotonyl-CoA hydratase/3-hydroxybutyryl-CoA dehydrogenase*

K_M (Crotonyl-CoA)	71.0 ± 8.1 µM
v_{max} (Crotonyl-CoA)	6.1 ± 0.2 U/mg
K_M (3-Hydroxybutyryl-CoA)	86.0 ± 13.1 µM
v_{max} (3-Hydroxybutyryl-CoA)	7.3 ± 0.3 U/mg
K_M (NAD^+)	14.7 ± 1.7 µM
v_{max} (NAD^+)	5.5 ± 0.1 U/mg

Tab. III.18.: *Substrate specificity of recombinant crotonyl-CoA hydratase/3-hydroxybutyryl-CoA dehydrogenase of I. hospitalis. Substrate concentrations 10 mM; assays were started with substrate.*

Substrate/Co-substrate	**Specific activity in U/mg**	**Specific activity in %**
Crotonyl-CoA	5.0	100
(S)-3-Hydroxybutyryl-CoA	6.8	136
(R)-3-Hydroxybutyryl-CoA	-	0
$NADP^+$	0.7	13.6
3-Hydroxypropionyl-CoA	-	0
Reverse: 3-Hydroxybutyryl-CoA	20.1	402

reverse reaction from 3-hydroxybutyryl-CoA to crotonyl-CoA was tracked, which was performed in a coupled enzyme assay at 42°C, as well. The reverse reaction with (S)-3-hydroxybutyryl-CoA was catalyzed with a specific activity of 20.1 U/mg. Using activity tests, it was successfully demonstrated that Igni_1058 is actually able to catalyze the reactions from crotonyl-CoA and from 3-hydroxybutyryl-CoA to acetoacetyl-CoA. In combination with the results from the bioinformatics, Igni_1058 can be regarded as bifunctional crotonyl-CoA hydratase/3-hydroxybutyryl-CoA dehydrogenase, involved in carbon fixation in *I. hospitalis*.

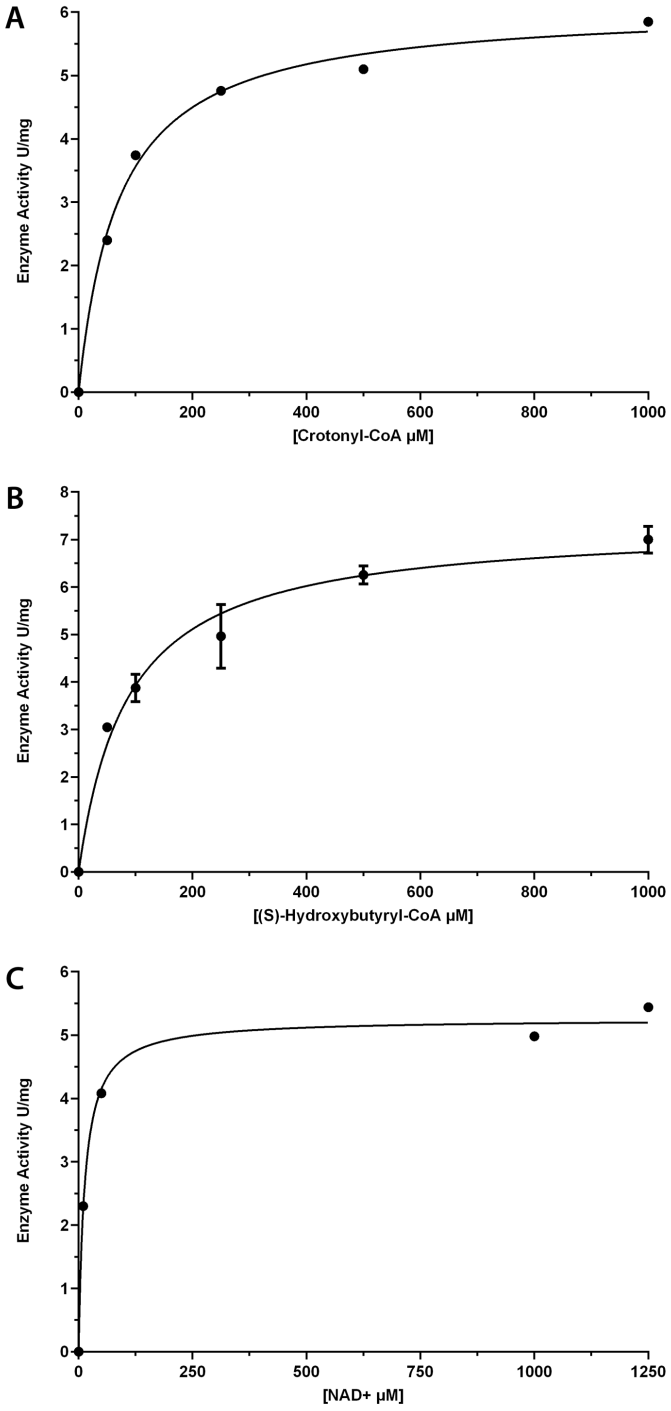

Fig. III.37.: ***Determination of K_M and v_{max} for crotonyl-CoA (A), -3-Hydroxybutyryl-CoA (B) and NAD^+ (C) of crotonyl-CoA hydratase/3-3-Hydroxybutyryl-CoA dehydrogenase (C)***. *Assays contained 500 µl reaction mixture and were prepared as described above (50°C).* ***A**: K_M for crotonyl-CoA: 71.0 ± 8.1 µM, v_{max}: 6.1 ± 0.2 U/mg.* ***B**: K_M for 3-Hydroxybutyryl-CoA: 86.0 ± 13.1 µM , v_{max}: 7.3 ± 0.3 U/mg.* ***C**: K_M: 14.7 ± 1.7 µM, v_{max}: 5.5 ± 0.1 U/mg.*

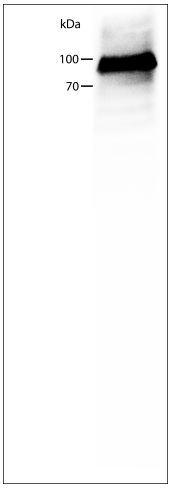

Fig. III.38.: ***Western Blot analysis of crude extracts of I. hospitalis cells.*** *1° AB: rabbit anti-Igni_1058, 1:10000; 2° AB: IgG GAR + HRP, 1:20000. Western Blot shows one band between 70-100 kDa.*

9.4. Antibody specificity and localization of Igni_1058

For testing specificity of the antibody directed against crotonyl-CoA hydratase/3-hydroxybutyryl-CoA dehydrogenase (anti-Igni_1058), Western Blots were performed, as well. For this, purified protein and freshly prepared crude extract of *I. hospitalis* (KIN4/I) were separated in an SDS gel and transferred onto a Western Blot membrane. The primary antibody was diluted 1:10000 and secondary antibody was diluted 1:20000. As a result, one clear band between 70-100 kDa was detected on the Western Blot membrane, which correlated with the pre-calculated mass of approximately 75 kDa (Fig. III.38).

9.4.1. Localization on resin-sections

Finally, Igni_1058 was located on ultrathin sections of Epon-embedded *I. hospitalis* cells. Labeling strongly occurred in the IMC in association with the OCM of *I. hospitalis* (Fig III.39). Just as described for the localization of the other enzymes putatively involved in carbon fixation, gold particles were found on structures of the IMC, as indicated by red arrows, and very few were detected in the cytoplasm. Occasionally, gold particles were observed on *N. equitans* and at the contact site as described before for the succinic semialdehyde reductase and for Igni_0475 (candidate for 4-hydroxybutyryl-CoA synthetase). Immunogold labeling with antibodies directed against *I. hospitalis* proteins were frequently found in cells of *N. equitans* or at the contact site. These observations emphasize the intimate association between those two organisms.

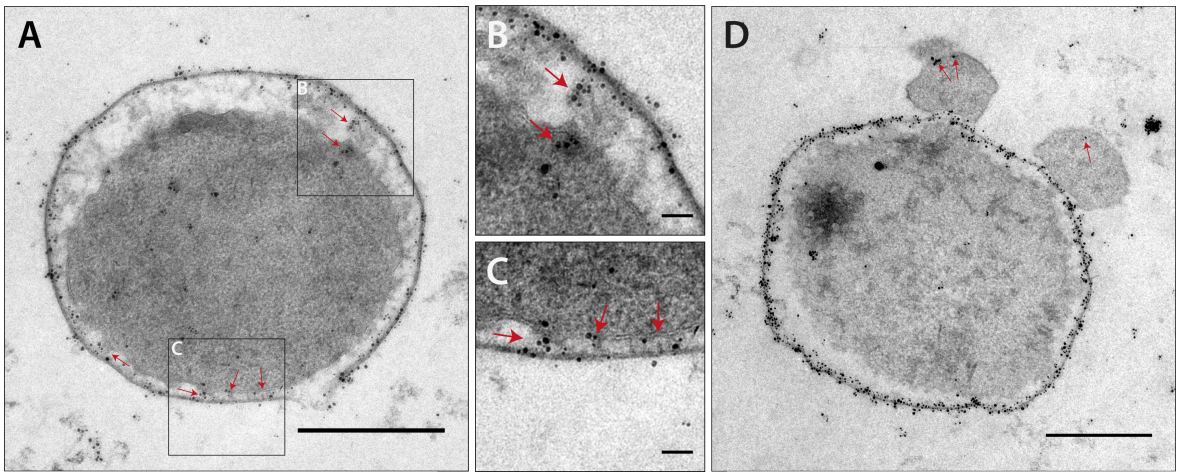

Fig. III.39.: ***Immunogold labeling of crotonyl-CoA hydratase/3-HB-CoA dehydrogenase on ultrathin sections of Epon-embedded I. hospitalis cells***. *Cells were prepared as described (sections 7.3-9). 1° AB: anti-Igni_1058 was diluted 1:100; 2° AB: IgG GAR + 'ultrasmall' gold was diluted 1:50; silver enhancement: 25 min; size bars: 500 nm (A and D); 50 nm (B and C). Note the distribution of gold particles in the IMC, associated with the OCM (A and D). Rarely, gold particles can be observed on N. equitans.* ***B*** *and* ***C****: Zoom-ins on A; Focus on gold particles in cytoplasmic protrusions and on structures of the IMC. Note that inner membrane and OCM are very close at some areas (highlighted with red arrows).*

9.4.2. Localization on cryo-sections

Using immunogold localization according to Tokuyasu with the same antibody dilutions as in resin-section labeling, gold particles were detected in the IMC associated with the OCM as well, but also to some extent in the cytoplasm and at the inner membrane. However, it remains unclear whether labeling occurs at the inner membrane or in the IMC, since both structures cannot clearly be distinguished here (III.40 B). At some spots, both membranes are in close proximity to each other and even appear to be connected. Additionally, Fig. III.40 shows a roundish and very heavily stained structure that is fully covered by gold particles. This might again represent the above mentioned putative phosphate storage. Notably, the structure as visible in this experiment exhibits about the same size range (diameter 200 to 250 nm).

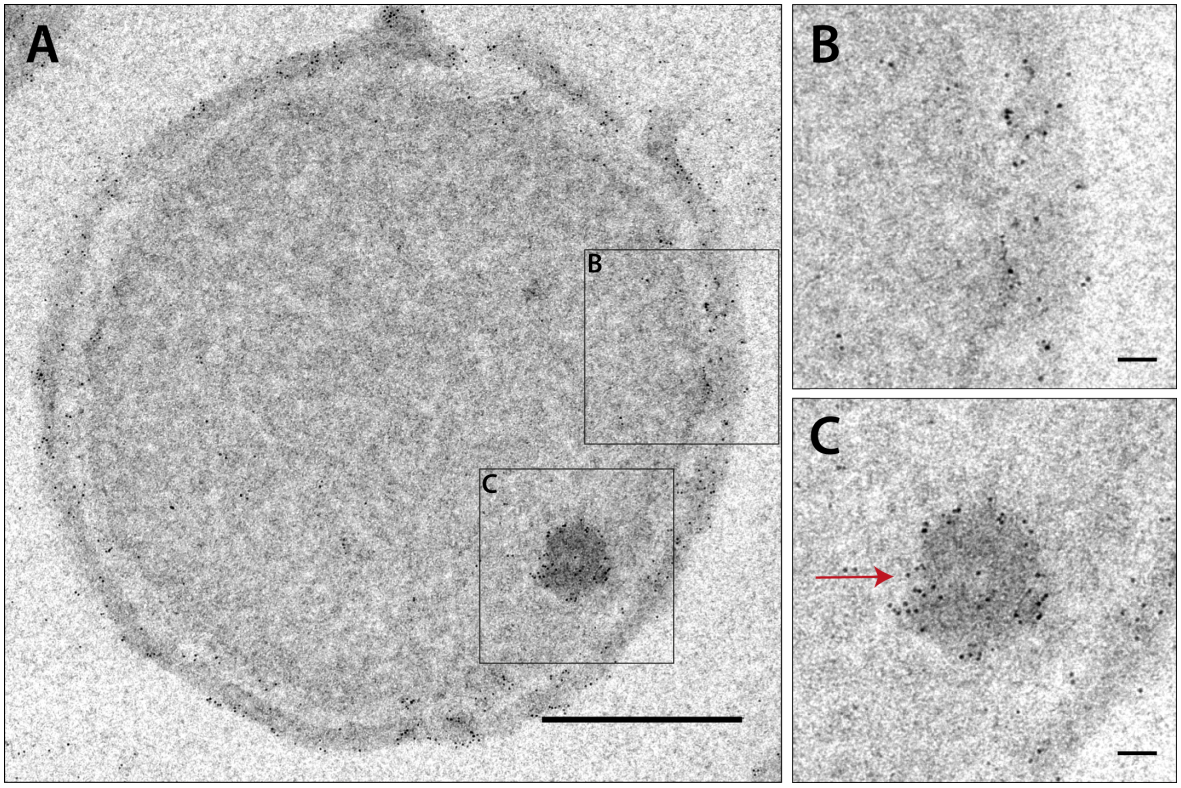

Fig. III.40.: ***Immunogold labeling of crotonyl-CoA hydratase/3-hydroxybutyryl-CoA dehydrogenase on Tokuyasu sections of I. hospitalis cells.*** *Cells were prepared as described (sections 7.3-9). 1° AB: anti-Igni_1058 was diluted 1:100; 2° AB (GAR IgG + 'ultrasmall gold') was diluted 1:100; silver enhancement: 35 min; size bars: 500 nm (A); 50 nm (B and C).* ***A****: Gold particles are located in the IMC along the OCM. Additional labels can be observed in the cytoplasm and its protrusions.* ***B*** *(zoom in on A) illustrates the insufficient ultrastructural preservation of the cell. In* ***C*** *(zoom-in on A), a labeled roundish black structure of unknown function is shown.*

10. Localization of enzymes involved in CO_2 fixation in *I. hospitalis* - a summary

The following section briefly summarizes all known facts on enzymes addressed in this work to provide an overview. During this work six enzymes that are putatively involved in carbon fixation of *I. hospitalis* were examined considering localization and enzyme activities (Tab. III.19). All of these enzymes, including the ACS (Mayer *et al.*, 2012), were mainly located in the IMC, associated with the OCM - with one notable exception: Igni_0475 whose activity as 4-hydroxybutyryl-CoA synthetase is in doubt anyway, was found to be located in the cytoplasm of *I. hospitalis*. Interestingly, a strong labeling signal occurred in cells of *N. equitans*, as well (Fig. III.41).

Tab. III.19.: *Summary - Localization and enzyme activities. Signal intensity: - no signal; + weak signal; ++ strong signal; +++ very strong signal.*

Enzyme	**Location**	**Cross reaction *N. equitans***	**Activity in heterologously expressed proteins**
Acetyl-CoA synthetase	IMC	±	3 U/mg (90°C; Ramos-Vera *et al.*, 2011)
PEP carboxylase	IMC	−	−
Malate dehydrogenase	IMC	−	613 U/mg (45°C)
Succinic semialdehyde reductase	IMC	±	418 U/mg (65°C)
4-hydroxybutyryl-CoA synthetase candidate Igni_0475	Cytoplasm	+++	−
4-hydroxybutyryl-CoA synthetase candidate Igni_0379	IMC	±	−
Crotonyl-CoA hydratase/ 3-hydroxybutyryl-CoA DHG	IMC	±	6 U/mg / 7 U/mg (50°C)

However, in activity tests on both candidate proteins for the 4-hydroxybutyryl-CoA synthetase (*Igni_0475* and *Igni_0379*), neither the recombinant proteins nor the immuno-precipitated proteins from *I. hospitalis* were active on 4-hydroxybutyrate and additional substrates. In contrast, enzyme activities were obtained for the MDH, for the SSR and for the crotonyl-CoA hydratase/3-hydroxybutyryl-CoA dehydrogenase as shown in table III.19. Thereby, the SSR represents a special case, since for the first time an enzyme catalyzing the conversion of succinic semialdehyde to 4-hydroxybutyrate was successfully identified in *I. hospitalis*.

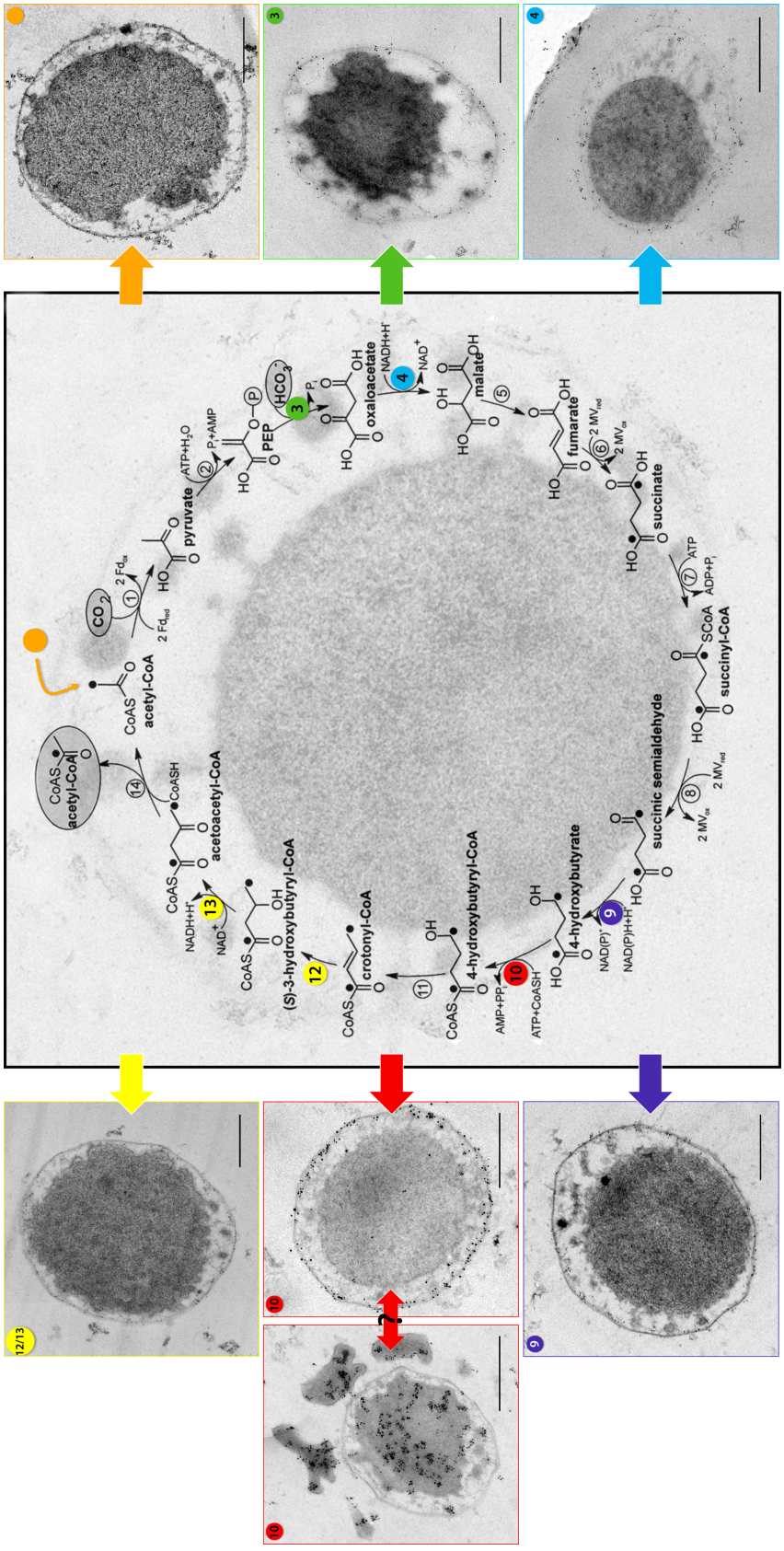

Fig. III.41.: *Summary of the localization of enzymes involved in the DC/4-HB cycle of autotrophic carbon fixation in I. hospitalis. Metabolic pathway according to* Huber et al., *2008. Localization of ACS (orange), PEP carboxylase (3), MDH (4), SSR (9), crotonyl-CoA hydratase (12), 3-hydroxybutyryl-CoA dehydrogenase (13) in the IMC of I. hospitalis, associated with the OCM. For 4-hydroxybutyryl-CoA synthetase (10) two candidates were identified: Igni_0475 was located in the cytoplasm and Igni_0379 was shown to be located in the IMC, associated with the OCM. Size bars: 500 nm.*

11. CO_2-fixation in *Ignicoccus islandicus*

Another point dealt with in this research work was carbon fixation in further *Ignicoccus* strains. To date, only the activity of the CO_2 fixing pyruvate synthase has been proven in cell extracts of *I. islandicus* and *I. pacificus* (Hügler, 2003). Therefore, the presence of further enzymes involved in carbon fixation was attempted to be tested for *I. islandicus*, representing the type strain of the genus *Ignicoccus*. This question was addressed bioinformatically, on the one hand and experimentally using Western Blot analysis and immunogold labeling, on the other hand. The results of the bioinformatic approach are summarized in Tab. III.20, in which the 14 enzymes of the dicarboxylate/4-hydroxybutyrate cycle, the corresponding genes of *I. hospitalis* and the provisional gene numbers of *I. islandicus* are listed. In addition, the corresponding e-values and the number of amino acids for both, the *I. hospitalis* and the *I. islandicus* versions of enzymes, are shown. For all *I. hospitalis* proteins of the cycle and for the ACS, suitable candidates were found in the genome of *I. islandicus*, indicating that *I. islandicus* fixes carbon according to the DC/4-HB cycle. In addition, the *I. islandicus* counterparts to the *I. hopitalis* enzymes investigated in this project, were further analyzed using the PHYRE database. Basically, structure predictions from the *I. islandicus* amino acid sequences were very similar to those obtained for *I. hospitalis*. Thus, the *I. islandicus* sequences for PEP carboxylase, MDH and SSR were predicted to exhibit similar features and to have the same structure homologues as their *I. hospitalis* counterparts. Interestingly, the *I. islandicus* candidates for the 4-hydroxybutyryl-CoA synthetase appeared to have the same homologues indeed, but for both candidates two transmembrane regions were suggested each (IIs_00895: aa 172-196 and aa 222-237; Iis_00941: aa 61-89 and aa 195-218; see supplementary). Moreover, PHYRE succeeded in creating a three-dimensional model for the *I. islandicus* fusion protein crotonyl-CoA hydratase/3-hydroxybutyryl-CoA dehydrogenase, which was not possible for the *I. hospitalis* version of the protein (for additional information see supplementary).

For Western Blots, cell extracts of *I. islandicus* were separated on a SDS gel, blotted onto a membrane and then incubated with antibodies directed against enzymes of the carbon fixation pathway of *I. hospitalis*. Simultaneously to examination of cross-reactivity of antibodies directed against *I. hospitalis* proteins with proteins of *I. islandicus*, Western Blots served the purpose to ensure specificity of antibodies, which was important for the respective immunogold labeling experiments. In fact, assumptions based on bioinformatics could be confirmed experimentally. Basically, the antibodies

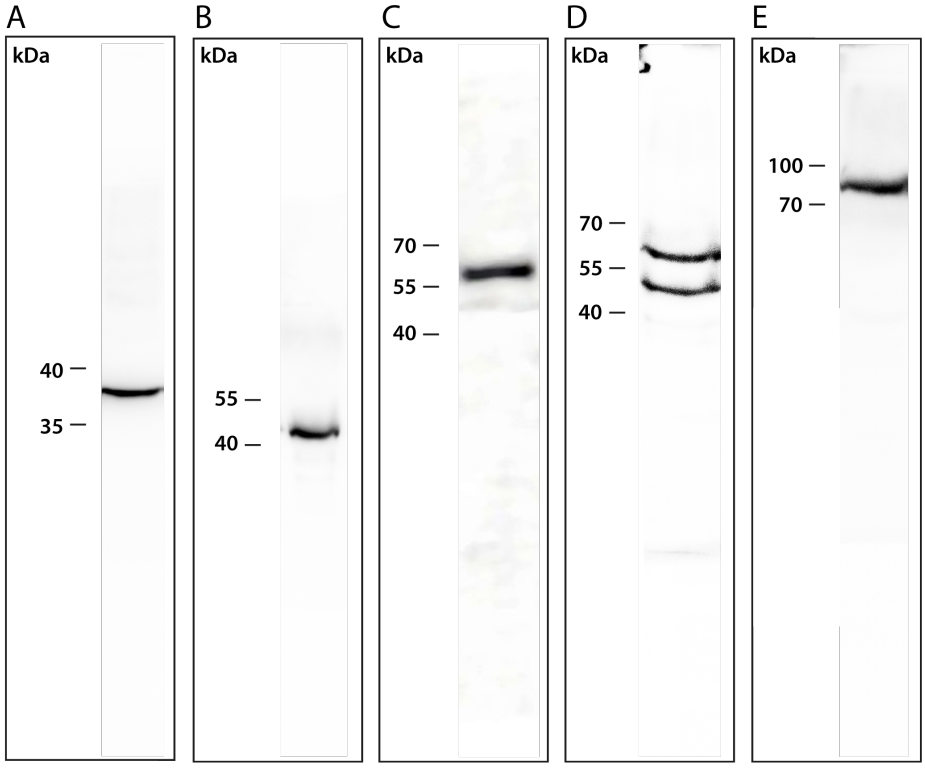

Fig. III.42.: *Western Blot analysis of crude extract of I. islandicus cells.* ***A****: MDH,* ***B****: SSR,* ***C****: Igni_ 0475,* ***D****: Igni_ 0379 and* ***E****: Crotonyl-CoA hydratase/3-HB-CoA dehydrogenase. Dilution 1° ABs: 1:10000; 2° AB: IgG GAR + HRP, diluted 1:20000. The I. islandicus proteins, which are putatively involved in carbon fixation interact specifically with the respective antibodies from I. hospitalis.*

specifically labeled one band in Western Blot analysis with cell extracts of *I. islandicus* as shown in Fig. III.42 A-D. However, for the PEP carboxylase of *I. islandicus* the Western Blot did not show one distinct band, but a smear and in the Western Blot using the antibody directed against Igni_0379, two bands occurred (an upper band between 55-70 kDa and a lower band between 40-55 kDa). Hence, the lower band could be a result of protein degradation.

Based on previous unsuccessful labeling attempts of enzymes on Epon- or Lowicryl-embedded cells of *I. islandicus* and *I. pacificus*, cryo-section labeling became the method of choice for subcellular localization of enzymes in these organisms. Due to these earlier experiments it is also important to mention, that primary antibodies were used in dilutions of 1:50 in this experiment. Since preparation of Tokuyasu sections was comparably labor-extensive (no equipment available in our laboratory and thus, only limited experiences with this method; experiments performed in the laboratory

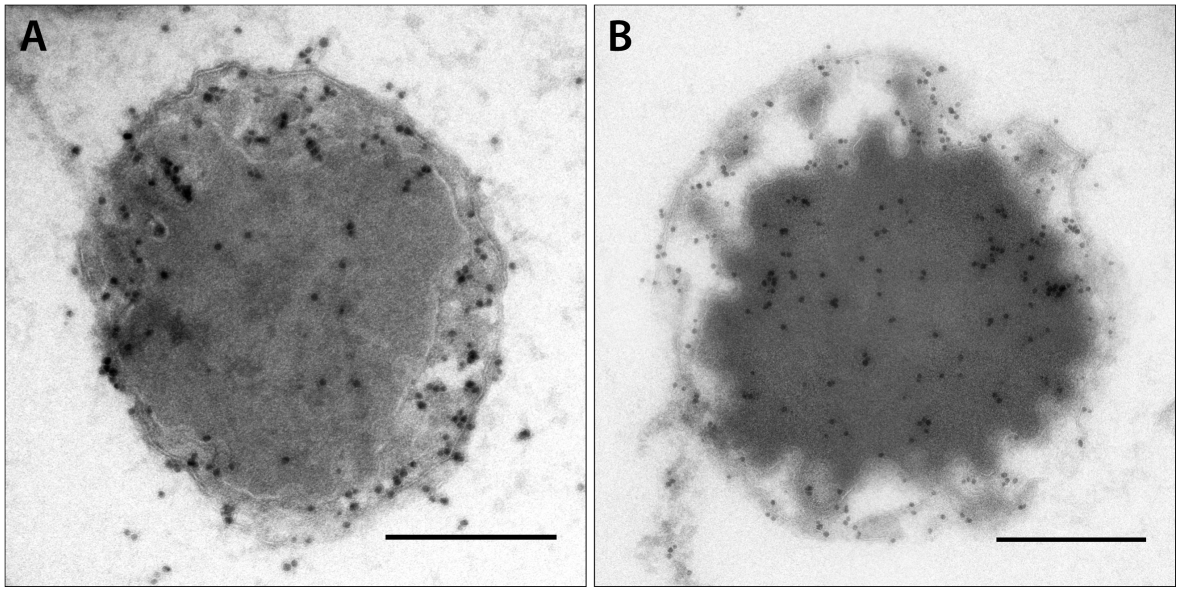

Fig. III.43.: ***Subcellular localization of carbon fixation in I. islandicus. Cryo-ultrathin sections immuno labeled according to Tokuyasu of I. islandicus****. **A**: Localization of MDH. **B**: Localization of SSR; Distribution of gold particles in the OCM, the IMC and the cytoplasm. Dilution of* 1° *AB: 1:50,* 2° *AB: IgG GAR + 'ultrasmall'-gold; diluted 1:50; silver enhancement: 40 min; size bars 500 nm.*

of York-Dieter Stierhof, ZMBP Tübingen), cryo-section immunogold labeling was only performed on *I. hospitalis* (positive control) and *I. islandicus*, representing the type strain of the genus *Ignicoccus*, and optimization of labeling was therefore not feasible, as well. When locating the MDH on *I. islandicus*, gold particles were found in association with the OCM, in the IMC and in the cytoplasm, as shown in Fig. III.43 A. Some gold particles were found in the background, which could refer to lysed cell relicts. Compared to cryo-section labeling of the MDH of *I. hospitalis*, more gold particles were detected in the IMC, not associated with the OCM. In Fig. III.43 B, *I. islandicus* labeled with antibodies directed against the SSR is depicted. In this case, no gold particles were found in the background, but in association with the OCM, the cytoplasm and also to some extent in the IMC. In comparison to the *I. hospitalis* localization, here more gold particles are detected in the cytoplasm, as well, which is probably due to the fact that antibodies were used in higher concentrations than for the respective experiment with *I. hospitalis* to ensure a positive signal on the cells. Nevertheless, labeling occurred in both cases in the IMC, in two states, namely in association with the OCM and in connection with structures in the IMC.

Tab. III.20.: *Genes involved in autotrophic carbon fixation in I. hospitalis and I. islandicus.*

No.	Enzyme	Gene no. in *I. hospitalis*	No. of aa	Provisional gene no. in *I. islandicus*	No. of aa	E-value
1	Pyruvate synthase	*Igni_1075-1078* or	82/175/288/360	Iis_00951-00951	82/176/286/377	$6e^{-53}$/ e^{-88}/ e^{-167}/ e^{-177}
		Igni_1256-1259	189/102/396/322	*Iis_00796-00799*	189/101/396/323	$3e^{-107}$/ $3e^{-55}$/ 0.0/ 0.0
2	Pyruvate:water dikinase	*Igni_1113*	821	*Iis_00939*	821	0.0
3	Phosphoenolpyruvate carboxylase	*Igni_0341*	488	*Iis_00678*	488	0.0
4	Malate dehydrogenase	*Igni_1263*	311	*Iis_00792*	310	0.0
5	Fumarate hydratase	*Igni_0678*	492	*Iis_01549*	512	0.0
6	Fumarate reductase	*Igni_0276*/ *Igni_0445*	561/319	*Iis_01019*/ *Iis_01382*	561/311	0.0/$2e^{-161}$
7	Succinate thiokinase	*Igni_0085*/ *Igni_0086*	296/376	*Iis_00102*/ *Iis_00101*	292/377	$2e^{-156}$/0.0
8	Succinyl-CoA reductase	unknown	-	-	-	-
9	Succinate semialdehyd reductase	*Igni_0132*	414	*Iis_00103*	411	0.0
10	4-Hydroxybutyryl-CoA synthetase	*Igni_0475* or	493	*Iis_00895*	483	0.0
		Igni_0379	474	*Iis_00941*	476	0.0
11	4-Hydroxybutyryl CoA dehydratase	*Igni_0595*	512	*Iis_00092*	507	0.0
12	Crotonyl-CoA hydratase	*Igni_1058*	683	*Iis_00919*	678	0.0
13	3-Hydroxybutyryl-CoA-dehydrogenase	*Igni_1058*	683	*Iis_00919*	678	0.0
14	Acetoacetyl-CoA-β-ketothiolase	*Igni_1401* or	396	*Iis_00087*	401	0.0
		Igni_0377	353	*Iis_00267*	356	$3e^{-142}$
	AcetylCoA synthetase	*Igni_0256-0257*	645	*Iis_01374*	644	0.0

12. Further immuno-localizations

12.1. Localization of DNA in the genus *Ignicoccus*

So far, DNA was proved to be located in the cytoplasm of *I. hospitalis* only on the light microscopy level using DAPI, or Syto9, two fluorescent stains that bind strongly to DNA (Küper *et al.*, 2010, Daxer, 2011). Electron microscopy on immunogold labeled sections has not been employed, so far. For this experiment, cells of *I. hospitalis* were immunogold labeled using a commercially available antibody directed against DNA (the antibody was recommended by Michael Laue and coworkers, RKI, Berlin). The antibody labeled the cytoplasm of *I. hospitalis* and of *I. islandicus* in equal amounts as depicted in Fig. III.44. Likewise, gold particles were detected in the *N. equitans* cytoplasm (Fig. III.44 B). In Fig. III.44 micrographs of DNA localizations on Lowicryl- and on cryo-sections of *I. hospitalis* (A and B) and *I. islandicus* (C and D), are displayed. In every picture an exclusive labeling of cytoplasms is revealed. However, the difference in gold particle density between Lowicryl- and cryo-section labeling is remarkable. Whereas gold particles are equally distributed across the whole cytoplasm on cryo-sections (Fig. III.44 B and D), gold particles on Lowicryl-sections appear to be accumulated in various spots (Fig. III.44 A and C).

Fig. III.45 shows further examples of the localization of DNA on cryo-sections of *I. hospitalis* (Fig. III.45 A) and on a Lowicryl-embedded *I. hospitalis* cell that probably undergoes the process of cell division (Fig. III.45 B). In Fig III.45 A it is clearly recognizable that also cytoplasmic protrusions contain gold particles, or DNA, respectively, which in turn emphasizes a connection between cytoplasm and its protrusions. Micrograph III.45 B shows a dividing cell or at least a cytoplasm that has split in two parts, which are the only labeled structures on this image. In conclusion, by means of immunogold labeling using an anti-DNA antibody, it was possible to clearly depict the localization of DNA in *I. hospitalis* on the EM level. Additionally, by the exclusive labeling of the cytoplasm, which corresponds with results from fluorescent staining of previous works (Küper *et al.*, 2010, Daxer, 2011), reliability of immunogold labeling on ultrathin sections itself was confirmed.

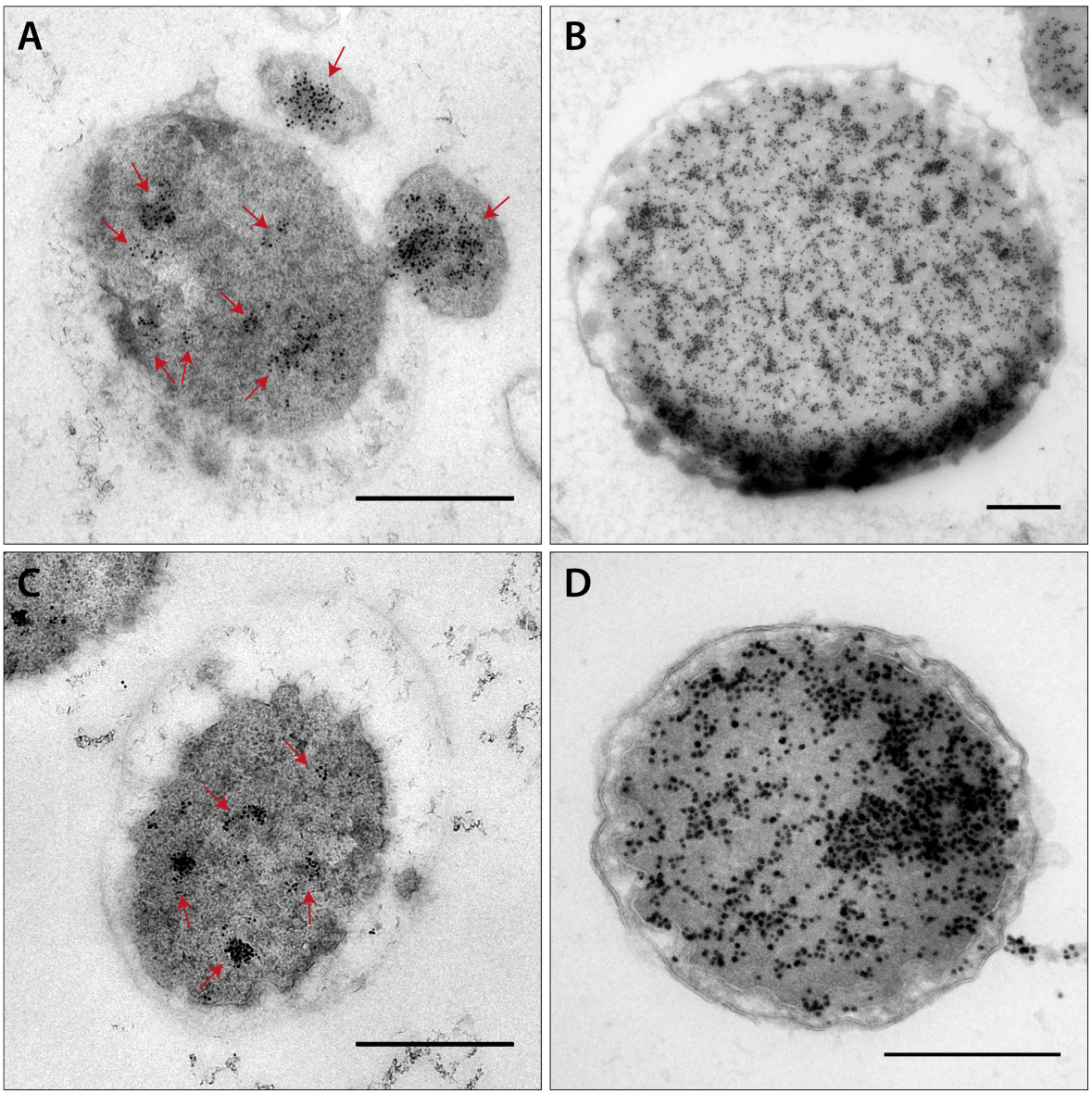

Fig. III.44.: ***Localization of DNA in I. hospitalis and I. islandicus***. ***A****: Ultrathin section (70 nm) of Lowicryl-embedded I. hospitalis and N. equitans cells immuno-labeled with an anti-DNA antibody. Note the gold particles accumulated in spots and on N. equitans (highlighted by red arrows). Note also the connection between the cytoplasms of both organisms.* ***B****: Cryo section of an I. hospitalis cell labeled with an anti-DNA antibody according to Tokuyasu. Note the evenly distributed gold particles across the whole cytoplasm.* ***C****: Ultrathin section (70 nm) of a Lowicryl-embedded I. islandicus cell immuno-labeled with an anti-DNA antibody. Note again the accumulated gold particles.* ***D****: Cryo section of an I. islandicus cell labeled with an anti-DNA antibody according to Tokuyasu. Note the evenly distributed gold particles across the whole cytoplasm. Dilution of 1° AB 1:50; 2°: IgG GAR + 'ultrasmall' gold, diluted 1:50; silver enhancement: 35 min; size bars: 500 nm.*

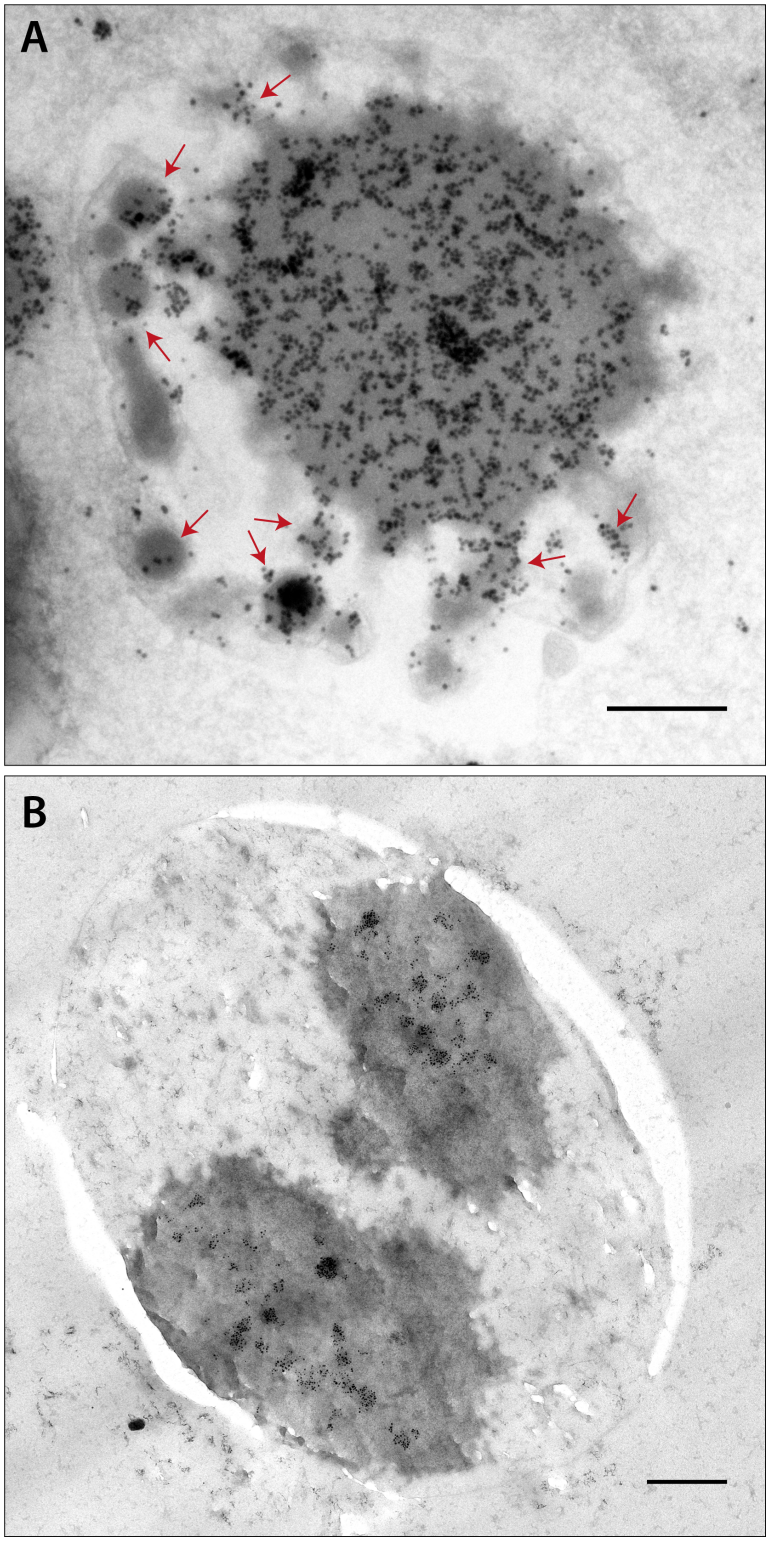

Fig. III.45.: ***Localization of DNA in cytoplasmic protrusions and in dividing cells.*** ***A****: Cryo-section of an I. hospitalis cell, immuno-labeled with an anti-DNA antibody according to Tokuyasu, Note the gold particles in the cytoplasmic protrusions (highlighted by red arrows).* ***B****: Ultrathin section (70 nm) of a Lowicryl-embedded putatively dividing cell of I. hospitalis. Note the distribution of DNA in both cytoplasms. Dilution of 1° AB 1:50; 2° AB IgG GAR + 'ultrasmall' gold, diluted 1:50; silver enhancement: 35 min; size bars: 500 nm.*

12.2. Localization of two octahaem cytochromes in *I. hospitalis*

Additional immuno localizations were performed with antibodies targeting Igni_0955 and Igni_1359. Both proteins were purified by Dr. Arnulf Kletzin's working group (TU Darmstadt) and belong to the HAO family (hydroxylamine dehydrogenase family). However, the proteins were neither active on hydroxyl amine, nor on inorganic sulfur compounds, but Igni_0955 was reduced by the *I. hospitalis* hydrogenase. In immunocytochemistry experiments, proteins were located in both the OCM and in the inner membrane. In addition, many gold particles were observed on structures of the IMC (Fig. III.46). Due to localization and the reductive effect of the hydrogenase on Igni_0955, both proteins are assumed to function as electron carriers between the hydrogenase, which is located in the OCM, and intracellular reductases (Naß *et al.*, 2014). It should be stressed in conclusion, that the localization of Igni_0955 and Igni_1359 is another example for labeling of an additional structure of *I. hospitalis*, namely the inner membrane.

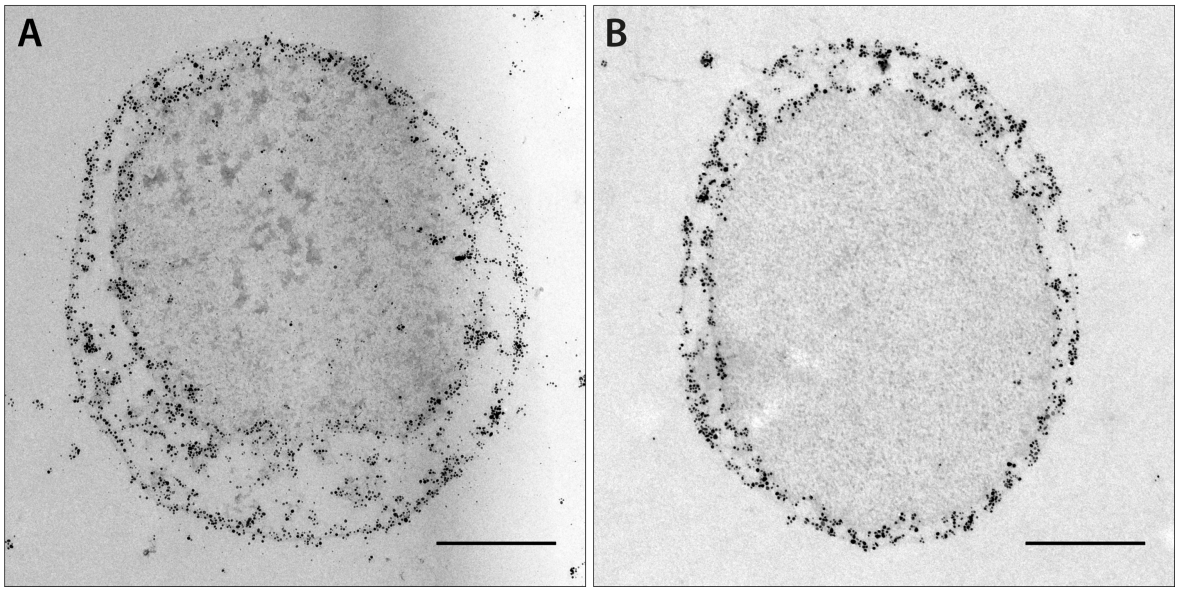

Fig. III.46.: ***Localization of two octahaem cytochromes in I. hospitalis****. Ultrathin sections (70 nm) of Epon-embedded I. hospitalis cells. Dilution of* 1° *AB: 1:1000;* 2° *AB: IgG GAR + 'ultrasmall' gold, diluted 1:50; silver enhancement: 35 min. Proteins are located in the OCM, in the inner membrane and associated with structures of the IMC.* ***A****: Localization of Igni_0955.* ***B****: Localization of Igni_1359. Size bars: 500 nm. Micrographs from Naß* et al., *2014.*

IV. Discussion

1. Methodology

1.1. Resin-section labeling versus Tokuyasu-section labeling

Although more and more alternative ways for protein localization for high resolution microscopy are being developed, which includes genetic tags coupled to fluorescent dyes for correlative microscopy, immunogold labeling on ultrathin sections for electron microscopy is still a frequently used and powerful tool for subcellular localization of proteins. In the last 50 years, various tools and techniques have been developed to optimize structural preservation resulting in improved labeling efficiency of sensitive or even of low copy number antigens. Despite all efforts to optimize preservation of antigenicity of samples, the highest labeling efficiency on sections was estimated to be only 10 % (Griffiths and Hoppeler, 1986). This detection limit is dependent on parameters such as accessibility and sensitivity of antigens for fixatives or organic solvents (Ripper *et al.*, 2008).

In general, there are two main options and several techniques derived from these methods to prepare cells or tissues for post-embedding immunogold localization: Preparation of ultrathin resin sections of chemically fixed or cryo-fixed samples, and preparation of chemically fixed cryo-sections according to Tokuyasu (Tokuyasu, 1973). To combine advantages of labeling efficiency of the Tokuyasu method with excellent ultrastrucutral preservation, the frozen-hydrated method could be tested for *Ignicoccus*. This method represents a hybrid technique that combines high-pressure cryo-fixation and freeze-substitution with the Tokuyasu technique and leads to an improved morphology and to better preservation of antigenicity (van Donselaar *et al.*, 2007, Ripper *et al.*, 2008, van Niftrik *et al.*, 2010). Karreman *et al.*, 2011 suggested another highly promising cryo-method called "VIS2FIX". "VIS2FIX" is short for vitreous sections of cryo-fixed samples that were fixed in two different ways using a freeze-substitution device. The whole procedure lasts for 8 h including HPF, sectioning, AFS and immuno-

gold labeling and results in excellent ultrastructural preservation with high suitability for immunocytochemistry.

The first option (ultrathin resin sections) can be initiated by aldehyde fixation, but this will not further be discussed, because cryo-immobilization, which is commonly referred to as cryo-fixation, followed by freeze-substitution became the method of choice during the last decades (McDonald, 2014). Cryo-fixation keeps the sample in a near native state and leads to improved ultrastructural conservation of samples (Studer *et al.*, 2008). This is usually followed by freeze-substitution and embedding in a resin (epoxy resins or methacrylates).

In this research work, immunogold labeling was compared on Tokuyasu sections and on resin sections (Epon vs. Lowicryl), regarding signal intensity and structural preservation. Prior to fixation, *Ignicoccus* cells were concentrated via filtration (Heimerl, 2014), which was an important step to ensure excellent maintenance of the complex *Ignicoccus* ultrastructure. When prepared according to the Tokuyasu method, cells were chemically fixed, embedded in gelatine, infiltrated in sucrose and frozen in liquid nitrogen. Ultrathin sectioning, which was followed by immunocytochemistry, was performed in a cryomicrotome (section II.9.3).

In contrast, for immunogold labeling on ultrathin resin sections, *Ignicoccus* cells were cryo-immobilized using a HPF, which is considered the most reliable fixation technique for ultrastructural analysis (Murk *et al.*, 2003). This was followed by freeze-substitution in an AFS and embedding in either an epoxy resin (Epon) or a methacrylate resin (Lowicryl HM20). After polymerization of resin, blocks were sectioned prior to immunogold labeling using a room-temperature microtome (section II.9.2).

Tokuyasu labeling is considered the "most efficient procedure for immunogold labeling" (Peters *et al.*, 2006). Earlier theories suggested an increased labeling efficiency of up to 10 - 30-fold, compared to that of resin-section labeling, assuming that all antigens are labeled within a section of 100 nm in depth. However, in reality this value has never been attained, but an actual efficiency increase of 2-3-fold was observed (Kellenberger *et al.*, 1987). Examinations using transverse resin re-embedded and immuno-labeled cryo-sections by Stierhof and Schwarz, 1989 explained why the theoretical increase of 10-30-fold was not achieved. Since antibodies were not able to invade the whole cryo-section due to the use of aldehydes, labeling was almost exclusively restricted to the surface and only in damaged sections gold grains could be observed inside the section. An advantage of the Tokuyasu method is that antigens are kept in an aqueous medium for the whole procedure and therefore, loss of antigenicity is not caused by harsh organic solvents

(freeze-substitution) or during embedding (Schwarz and Hohenberg, 2001, Griffiths, 1993). Aldehyde fixation is a relatively slow (minutes) and selective process, because aldehydes have to diffuse into the cell and because they react with distinct groups only (Schwarz and Hohenberg, 2001, Griffiths, 1993). This leads to changes in local pH, disturbance of ion balances and affects osmolarity in different organelles, resulting in denaturation and collapse of biomolecules (Collins *et al.*, 1977, Lee *et al.*, 1982, Johnson, 1985, Schwarz and Hohenberg, 2001, Griffiths, 1993). Another disadvantage is the increased loss of soluble proteins and small molecules, in particular membrane lipids (Schwarz and Hohenberg, 2001, Griffiths, 1993). In 2003, Murk *et al.*, published a comparison of high-pressure freezing and aldehyde fixation in which they claimed that "aldehyde fixation causes an organelle-specific dehydration". According to their study, endosomes and lysosomes of cryo-fixed cells were larger and revealed smoother membranes, while aldehyde fixed cells were deformed and had a reduced volume without change of membrane length.

For immunocytochemistry on resin-sections, the EM-community in general prefers embedding in methacrylates. This arose from the fact that the surface of epoxy-sections is three times smoother than that of methacrylate-sections, as demonstrated by Kellenberger *et al.*, 1987. This effect is caused by the fact that Epon acts as fixative as well, and thus, covalently reacts with molecules (Matsko and Mueller, 2005). Moreover, Lowicryl resins are polymerized under UV at sub-zero temperatures, which is assumed to be less harmful to dehydrated cells and tissues than polymerization of Epon or Araldite resin at 60°C up to 100°C (McDonald, 2014).

All these facts indicate a decreased antigenicity of biomolecules in Epon-embedded samples, and/or a highly reduced accessibility of the antibodies to the targets. Another disadvantage to be mentioned is the autofluorescence of Epon at 500 - 570 nm, which makes it inconvenient in combination with fluorophores and for correlative microscopy, respectively (Del Castillo *et al.*, 1986). Combined with the fact that colloidal gold tends to stick to hydrophobic surfaces, Epon appears to be and is often quoted as inappropriate as embedding resin for immuno-EM (e.g. "a drawback of the 'HPF-freeze substitution-Epon' embedding method is that most molecules lose their antigenicity during the procedure" in: Zeuschner *et al.*, 2006). In fact, previous studies from our own laboratory have shown that Epon sections are useful for immuno labeling studies, at least when studying archaeal cells (Flechsler, 2010, Meyer, 2010, Küper *et al.*, 2010, Mayer *et al.*, 2012, Heimerl, 2014).

In contrast, Lowicryl exhibits a rougher surface than Epon and does not (or to a lower extent) react covalently with biomolecules. The so called relief may occur "as consequence of sectioning being a cleavage" (Kellenberger *et al.*, 1987), and has a depth of about 2 - 6 nm, depending on the Lowicryl used for the application (Kellenberger *et al.*, 1987). This results in a higher accessibility of the antigenic sites, in fact due to a larger surface area on the section surface compared to Epon sections. This is in contrast to misbeliefs from the past, that claimed antibodies and markers to be able to penetrate into Lowicryl-sections.

Despite the number of disadvantages of the Tokuyasu technique, signal intensity on Tokuyasu sections of *I. hospitalis* was considerably increased compared to that on Epon and was even higher than that on Lowicryl sections. Thus, a strong to very strong signal intensity was attained with all antibodies used in this research work on Tokuyasu-sections of *I. hospitalis*. Even proteins of *I. islandicus* could be detected on ultrathin sections prepared according to Tokuyasu, which had not been achieved using sections of resin-embedded *I. islandicus* cells. Regarding immunogold labeling on Epon sections of *I. hospitalis*, some antigens could not be detected, namely DNA, PEP-carboxylase and MDH. However, on Lowicryl- and on Tokuyasu-sections these antigens could be detected with a strong signal intensity. For all other tested antibodies, a strong signal was present on both, on sections of Epon- and on sections of Lowicryl-embedded *Ignicoccus* cells. In this context, labeling of DNA in cells of *Ignicoccus* should be examined in detail. From light microscopy it was suggested that DNA is not located in cytoplasmic protrusions (Daxer, 2011, Küper *et al.*, 2010). However, data obtained from localization experiments on the EM-level seem to provide controversial results, at the first glance. On Lowicryl-sections, DNA labeling appears in several clusters and is restricted to the "core" cytoplasm of *Ignicoccus*. In contrast, on cryo-sections, gold particles were found evenly distributed in the cytoplasm and its protrusions (Fig. III.45). This finding might be due to enhanced antibody accessibility to target structures on cryo-sections.

Considering ultrastructural preservation, epoxy resins turned out to be the method of choice in this study. For *Ignicoccus*, an excellent cellular ultrastructure was obtained throughout using Epon as embedding resin, provided that it is preceded by gentle cell harvesting, HPF and an appropriate, optimized freeze-substitution protocol. As a result, a clear compartmentalization of cells was visible including an electron dense cytoplasm (see also Heimerl, 2014). Moreover, structural details were revealed, such as double-layered membranes, tubes in the IMC surrounded by membranes and even

structures on top of the protrusions (Fig. I.2 A-C). Preservation of Lowicryl-embedded cells was sufficient but to some degree compromised: the compartmentalized character of the cell was still recognizable, but with fewer details. Occasionally, cells appeared to be totally or half broken out from the resin, which might be due to Lowicryl not reacting covalently with the sample (Griffiths, 1993). A positive surprise was the good preservation of cells in Tokuyasu sections, which admittedly varied from section to section. However, well-preserved cells appeared in good order and condition with an electron dense cytoplasm, and with clearly visible, negatively contrasted membranes (Fig. III.1).

Another point that should be kept in mind is equipment and time requirement. For both methods expensive equipment is needed, whereas cryo-immobilization and freeze-substitution require more expensive tools and time than the Tokuyasu method (in fact, the time requirement for HPF/FSF/Epon embedding was challenged recently, by McDonald, 2014 who provided evidence that a one-day-protocol is viable). In both cases an ultramicrotome is needed, whereas resin-embedded samples have different demands on the microtome than frozen samples. Preparation of cryo-sections requires by far more skill than room-temperature sectioning, which is due to static charges in the cryo-microtome chamber and the low temperature (below −120°C). "Tokuyasu"-samples cannot easily be stored for later control experiments, while resin-embedded samples can be stored almost infinitely. Considering the time factor, Tokuyasu-sectioning is faster. Results of immunogold labeling can be admired by microscopy within one working day, starting from fixation. In contrast, for resin-section labeling it can take one week or more until sections can be examined in the microscope, which is due to cryo-immobilization, freeze substitution and embedding. However, protocols for accelerated freeze-substitution in "3 h and less" have been described, that result in excellent preservation of cell morphology, are suitable for immunocytochemistry and on top make a freeze-substitution device redundant (McDonald and Webb, 2011, McDonald, 2014).

Finally, immunocytochemistry using three different methods lead to similar results, which contributes to the credibility and significance of immuno-EM of this study. Although resulting in lower labeling efficiency, an unbeatable advantage of Epon sections is their excellent structural preservation capability, which enables labeling of structural details and their visualization on an ultrastructural level. Therefore, Tokuyasu- and Lowicryl-sections can be considered as a good alternative especially for sensitive- or low copy-number antigens and are recommended to be used as additional controls.

1.2. "Speed immuno labeling"

In protocols for post-embedding labeling, incubation times for primary antibodies varied from 30 min (Aurion's protocol for immunogold labeling) to 18 h (Miyake and Colquhoun, 2012). Similar referrals, varying from 45 min to 2 h (Richards *et al.*, 2001) were found for secondary antibodies or for marker molecules, respectively. However, according to Griffiths, high affinity binding can be observed more quickly than non-specific binding and incubation of 5 to 30 min might therefore be sufficient (Griffiths, 1993). Additionally, the group of Hyatt claimed that specific labeling can be achieved after 15 min incubation of both, primary and secondary antibody (Hyatt, 1991).

To find out the best parameters for labeling of *Ignicoccus* proteins, different incubation times of primary and secondary antibodies were compared regarding labeling density and structural preservation of cells. In the following, the term 'incubation time' is used in a generalized sense and refers to both, primary and secondary antibody incubation steps. In this experiment, two primary antibodies were used whose binding behavior on cells of *I. hospitalis* have been studied for a while in our lab (anti-A_1 ATP synthetase and anti-ACS). GAR IgGs linked with 'ultrasmall' gold were used as secondary antibodies. Moreover, five different incubation times were tested (5, 15, 30, 60 and 90 min). This resulted in significant labeling of the *Ignicoccus* OCM after having sections incubated for 5 and 15 min using the anti-A_1-ATP-synthetase antibody. After a 30 min incubation step, a sufficient and significant gold particle density was observed. However, there was no substantial difference regarding signal intensity after 60 min and after 90 min incubation time, respectively. These observations are in line with reports by Hyatt who showed that immunogold labeling reaches a saturation level after 60 min incubation at room temperature, or at 37° C, respectively (Hyatt, 1991).

Similar studies to this approach were performed by Griffiths on thawed cryo-sections, using two different antibodies. In this experiment, two different incubation times were tested, namely 30 min and 3 h and in addition concentration of antibodies was varied. The results of this study suggest, that incubation times longer than 30 min have "little effect on either signal or noise" (Griffiths, 1993).

Apparently, preservation of the ultrastructure appeared to be different depending on the incubation times. Long incubation steps (90 min) frequently lead to cells with a faded cytoplasm, as shown in an extreme example of the time course in Fig. III.3. In contrast, cells were well-preserved after a 30 min incubation period, in general. Besides a dark-contrasted cytoplasm, structural details of the IMC, such as tubes and 'vesicles' were clearly visible. The use of an accelerated protocol clearly demonstrated that

shorter incubation times (30 min) are fully sufficient and contribute to better maintenance of ultrastructural details. With respect to *Ignicoccus*, a detailed preservation of ultrastructure is of major importance regarding labeling of fine structures in the IMC. This might be advantageous for other samples exhibiting a complex ultrastructure, as well, such as the eukaryotic primary cilium or planctomycetes. Of course, one should bear in mind that optimal incubation times and additional parameters (e.g. antibody concentration) may be different for distinct epitopes and therefore have to be determined separately for every system.

1.3. Three-dimensional immuno labeling

In recent years, there was huge progress in the field of 3D electron microscopy. The continuous development in sample preparation (from conventional methods to cryo-methods), the development of microscopes themselves and the ongoing progress in computing power and visualization tools (e.g. ImageJ, Fiji, IMOD and AMIRA®), play a decisive role in this context. Current electron microscopy methods that aim to obtain 3D-reconstructions of biological samples comprise serial sectioning, tilt-series based (serial-) electron tomography (ET), "serial block face"-SEM (SBF-SEM) and "focused ion beam"-SEM (FIB-SEM). Serial-sectioning and ET are used in TEM analysis starting from ultrathin sections (40-70 nm), or semithin sections (200-500 nm) that have to be cut by an ultramicrotome. Basically, serial sectioning of resin-embedded samples (Sjorstrand, 1958, Ware and LoPresti, 1975, Stevens *et al.*, 1980) represents the classical way and is limited by its poor resolution in z, which is up to twice the thickness of the section (Nyquist, 1928, Shannon, 1949, McEwen and Marko, 2001). The resolution in x and y was estimated to be between 1-3 nm. In contrast, ET (Hoppe, 1982, Frank, 1992, Baumeister, 2002) features high resolution (xy-resolution: 1-3 nm; z-resolution: 4-8 nm (Donohoe *et al.*, 2006, Hoenger and McIntosh, 2009), thus providing many structural details. SBF-SEM (Denk and Horstmann, 2004) and FIB-SEM (Knott *et al.*, 2008, Wanner *et al.*, 2013, Villinger *et al.*, 2012) are two highly automated SEM-methods in which the surface of the block is imaged instead of the section (Vihinen *et al.*, 2013). New block faces are produced inside the SEM chamber by cutting with a microtome (SBF-SEM) or by milling with a Ga^{2+}-ion beam (FIB-SEM) (Vihinen *et al.*, 2013). Both methods result in lower resolutions compared to TEM ET, but are characterized by their potential to analyze relatively large volumes (Knott *et al.*, 2008). For SBF-SEM, sections of 15-20 nm thickness are usually cut, leading

to a resolution in z of 30-40 nm (xy-resolution below 10 nm). In contrast, isotropic resolutions in x, y and z of 10-20 nm are achieved in FIB-SEM analysis. In previous works, 3D-models for *Ignicoccus* were obtained, using serial-sections (Wasserburger, 2008, Junglas, 2006, Heimerl, 2009), serial-section ET (Heimerl, 2014) and FIB-SEM (Heimerl, 2014).

Basically, all these methods for 3D-EM can be combined with immunocytochemistry, although with some constraints that are inherent to each method. In immuno-EM, immuno labeling helps to locate proteins, whereas EM provides the ultrastructural context (Ladinsky and Howell, 2007). Additionally, 3D immuno labeling offers two major advantages. Firstly, determination of antigen distribution trough a larger volume becomes possible and secondly, discrimination of specific from unspecific labeling might be achieved using quantitative analysis (Müller-Reichert *et al.*, 2003). In general, there are two ways for localization of proteins in cells or tissues, namely pre- and post-embedding labeling. It is feasible to combine pre-embedding labeling with all options for 3D microscopy. In contrast, post-embedding labeling is limited to serial-sectioning and ET, so far, since only the blockfaces are imaged in SBF-SEM- and in FIB-SEM-analysis. Another advantage of the pre-embedding method is that antibodies penetrate into the sample and thus, labeling is distributed in the overall 3-dimensional volume (Stirling, 1990). Regarding post-embedding labeling, gold particles are restricted to the surface of the section (Stierhof *et al.*, 1986). Therefore, production of thinnest possible sections that provide enough contrast (40-50 nm) is desirable, in order to maximize the surface to volume ratio and thus to increase the number of labels (Morphew, 2007). Most critical in pre-embedding labeling are fixation and permeabilization method, two steps that are essential to get antibodies into cells and tissues (Griffiths, 1993). For permeabilization, non-ionic detergents, such as Triton-X-100 are preferably used, since they do not cause conformational changes in proteins (Humbel *et al.*, 1998). More recently, a well-controlled permeabilization by targeted laser perforation was described (Jiménez and Post, 2012). This technique can be used on chemically fixed and on cryo-fixed cells and therefore may lead to good or even excellent ultrastructural preservation according to the authors. Nevertheless, by making cells penetrable for antibodies and markers, membranes become perforated or are removed, which leads to a loss and to a redistribution of an uncontrolled number of soluble proteins, biomolecules, ions, and solutes (Melan and Sluder, 1992). Hence, this might lead to a false labeling pattern. In addition, these effects might be "significant enough to influence the labeling pattern even at the fluorescence microscopy level" (Humbel *et al.*, 1998). Another significant

down-side of pre-embedding labeling is poor preservation of ultrastructure resulting from permeabilization, redistribution, loss of proteins and chemical fixation (Humbel *et al.*, 1998). Although, in post-embedding labeling, distribution of gold particles is limited to the section surface causing a lower-labeling efficiency, this method is preferred for immuno-EM due to its superior quality in terms of ultrastructure (Humbel *et al.*, 1998).

In this work, 3D-EM was combined with immuno-EM using serial sections of *I. hospitalis* and post-embedding labeling of enzymes putatively involved in the carbon fixation pathway of the organism. First approaches for 3D-immuno-EM of *I. hospitalis* were performed by Heimerl, 2009 and Flechsler, 2010, starting from serial sections, as well.

Epon-sections of 70 nm were cut, immuno-labeled and primary antibodies were detected by GAR IgGs coupled to 6 nm gold particles. After data acquisition, images were aligned, manually segmented and visualized using AMIRA®. In the course of this thesis, one 3D-reconstruction consisting of four consecutive sections labeled with an antibody targeted against Igni_0475 was obtained using AMIRA® VOLTEX and two 3D-reconstructions of ACS-labeled *Ignicoccus* cells consisting of 20 consecutive slices were obtained. In the VOLTEX-reconstruction, the cytoplasms of *I. hospitalis* and the attached *N. equitans* cell were exclusively labeled. Structural preservation was less impressive here, but the labeling in the cytoplasm provided a strong contrast due to the use of 'ultrasmall' gold as marker. On the basis of the enhanced contrast of gold particles, it was possible to visualize the reconstruction using AMIRA® VOLTEX, which was less time-consuming, but did not reveal as many details than shown with manual segmentation.

Regarding structure, serial sectioning of the ACS-labeled *Ignicoccus* cell revealed a putative phosphate storage in the cytoplasm of *I. hospitalis* of about 80-250 nm (Heimerl, 2014) and one cell of *N. equitans* directly attached to *I. hospitalis*. In the IMC, several vesicular structures were found referred to as putative vesicles. In reality, these vesicular structures might rather be cytoplasmic protrusions (Heimerl, 2014). However, 50-70 nm sections do not allow discrimination between free vesicles and cross-sectioned tubules (Zeuschner *et al.*, 2006). Hence, ET of semithin sections might be helpful to clearly identify the true form of those putative vesicles as shown by Heimerl, 2014. Besides, another structure was found in the IMC, which could represent a putative cytoskeleton according to Heimerl, 2014. Actually, a supportive and shaping structure in the IMC would be conceivable. Using ET, an extensive filamentous matrix in the IMC was detected that interconnected the endogenous membrane system among

itself and with the OCM (Heimerl, 2014). These rather thin filaments in the 3D model presented here are (for technical reasons) enlarged to the section thickness of 70 nm and thus appear to be more voluminous than they really are. But still, their location and interconnecting properties become evident.

Considering 3D distribution of gold particles, labeling of the ACS is preferably located in the IMC associated with the OCM, as expected from 2D data. These results once again demonstrate the significance of immunogold labeling with the ACS-antibody on cells of *Ignicoccus*. Besides the strong labeling in the IMC, only few gold particles were found in the cytoplasm. As gold particles in the cytoplasm occurred on almost every section, these labels can be considered as significant as well. Additionally, these findings are in line with the fact that DNA and ribosomes are located in the cytoplasm, which might be the compartment where the ACS is generated.

Besides poor resolution in z, 3D reconstructions of post-embedding labeled cells revealed further disadvantages. Physically separated sections can show small angle differences and small deformations because of shrinking by beam damage in the electron microscope (Morphew, 2007). In addition, antibodies can just bind to the surface of ultrathin sections, making gold particles appear as rings around cells (except for the localization of cell surface proteins). This is an obvious limitation of the method. Furthermore, especially manual segmentation was enormously time-consuming. This deficit might be partially eliminated at least, by using 'ultrasmall' gold instead of 6 nm gold as marker molecule. 'Ultrasmall' gold particles are more difficult to handle and are less calculable than 6 nm gold, which is due to the need for silver enhancers. But, the enhanced gold particles provide more contrast, which enables the utilization of automatic segmentation tools for gold particles.

An alternative for serial section labeling of ultrathin sections is labeling of (serial) semithin sections combined with ET analysis, which benefits from higher resolution in z (Donohoe *et al.*, 2006; Zeuschner *et al.*, 2006). A differentiation between true vesicles and cytoplasmic protrusions is possible using ET (Heimerl, 2014). However, the ratio of volume to surface decreases and thus, the number of labels (Morphew, 2007). Nevertheless, this 3D-method is described to be particular useful for antigen localization trough large volumes (Morphew, 2007). In 2006, Zeuschner *et al.*, reported on the successful discrimination between COPI and COPII vesicles, that are morphologically identical, using immunogold localization and ET.

All these microscopy techniques, whether combined with pre- or post-embedding labeling have their pros and cons. Currently, there is no perfect solution for 3D-immuno-

EM, since post-embedding labeling is restricted to the section surface, and since at least conventional pre-embedding labeling causes severe changes in ultrastructure. A solution to this might be provided by clonable tags (Morphew, 2007). However, for *Ignicoccus*, serial section labeling of ultrathin or semithin sections using TEM analysis with or without tilting the sample, currently remain the only options to analyze distribution of proteins in a 3D context. This is mainly attributable to the fact that there is no genetic system and that pre-embedding labeling does not appear to be an adequate solution for *Ignicoccus*.

Nevertheless, post-embedding serial section labeling is manageable with *Ignicoccus*, because in general, it is a small organism with a size from 1-5 µm. Therefore, the production of serial sections to cover a whole cellular volume is accomplishable without unreasonable expense. In addition, at least the enzymes of the carbon fixation pathway seem to be abundant in cells of *Ignicoccus*, which generally leads to sufficient labeling density in post-embedding labeling combined with excellent ultrastructural preservation.

2. CO_2 fixation in *Ignicoccus*

2.1. Bioinformatics and enzyme activities

Genes of *I. hospitalis* for a PEP carboxylase (Igni_0341), a MDH (Igni_1263), a 4-hydroxybutyryl-CoA synthetase (Igni_0475) and a crotonyl-CoA hydratase/3-hydroxybutyryl-CoA dehydrogenase (Igni_1058) were suggested to participate in the DC/4-HB pathway (Huber *et al.*, 2008; Jahn, 2007). A candidate for a SSR had not been detected, so far. In this study, amino acid sequences and enzyme kinetics of recombinantly expressed versions of those enzymes, including a candidate for a SSR, were examined to investigate if the gene products of these genes are actually catalyzing the predicted reactions and are likely to be involved in carbon fixation of *I. hospitalis*.

PEP carboxylase. The molecular mass of the purified recombinant gene product Igni_0341 corresponds to the general size of known archaeal PEP carboxylases (Sako *et al.*, 1997, Sako *et al.*, 1996, Patel *et al.*, 2004, Ettema *et al.*, 2004). A subunit size between 55-60 kDa, which is roughly the half of that from Bacteria and Eukaryotes, is considered a general feature of archaeal PEP carboxylases (Patel *et al.*, 2004, Ettema *et al.*, 2004). PEP carboxylases have been studied for a while in Bacteria and

Eukarya and are present in all photosynthetic organisms and, in addition, in most non-photosynthetic bacteria and protozoa. Until recently, only activities of archaeal PEP carboxylases could be detected in cell extracts, but no homologues have been found in archaeal genomes (Patel *et al.*, 2004, Ettema *et al.*, 2004).

Bioinformatic analysis classified the amino acid sequence of the protein Igni_0341 as member of the archaeal PEP carboxylases. Although different in sequence, a few characteristics of the primary structure of eukaryotic and bacterial PEP carboxylases were partially conserved in the archaeal-type counterparts. These elements are putatively involved in catalytic properties of the enzyme (see section III.5).

The 3D structure of Igni_0341 was predicted to consist of eight β-strands arranged in a barrel, linked with seven α-helices. PHYRE suggested homologies to the structure of the archaeal-type PEP carboxylases (30 %) and to the PEP carboxylases of *E. coli* and maize (16-20 %, see section III.5, Fig.III.8).

Specific activity for PEP carboxylase could only be determined from cell extracts of *I. hospitalis* (200 nmol/min per mg protein; Huber *et al.*, 2008). No active form of recombinantly expressed protein was obtained for Igni_0341 in *E.coli*.

Taking all facts together, the analysis of the primary structure, which contained various conserved elements that might be important for catalysis, the predicted secondary structure that is likely to include an eight stranded β-barrel and the presence of specific enzyme activities for PEP carboxylases in cell extracts of *Ignicoccus* (Huber *et al.*, 2008) strongly indicate that *Igni_0341* encodes for an archaeal PEP carboxylase involved in the DC/4-HB pathway of *I. hospitalis*.

Malate dehydrogenase. MDHs are involved in various metabolic pathways, such as gluconeogenesis, citric acid cycle, exchange of metabolites between cytoplasm and subcellular organelles, and are present in all three domains of life (Musrati *et al.*, 1998). Basically, MDHs exhibit a dinucleotide-binding domain and form dimers or tetramers with a monomeric subunit size of 30-35 kDa (Musrati *et al.*, 1998). This is in agreement with the pre-calculated molecular mass of the protein Igni_1263. Sequence similarities of the primary structure of MDHs are considerably low except for highly conserved elements involved in catalysis. This is also reflected by the *Ignicoccus* gene *Igni_1263*, which shows highest similarity to a LDH/MDH of *P. fumarii*. However, the 3D structure seems to be conserved (Langelandsvik *et al.*, 1997; Musrati *et al.*, 1998. MDHs of numerous Archaea have been characterized in detail, so far and all of these enzymes were assigned to the LDH-like MDH subfamily (Kawakami *et al.*, 2009). The MDH of *A. fulgidus* was suggested as structural homologue for Igni_1263.

According to structural prediction tools, the protein Igni_1263 exhibits a Rossmann fold, which is characteristic for MDHs. The Rossmann fold is responsible for nucleotide binding and typically contains a glycine consensus pattern (Lesk, 1995). The glycine motif of Igni_1263, which is located in a loop between β-strands and α-helices and in an α-helix itself, is $GXGX_2G$ (GTGRVG; aa: 12-17) and corresponds to that found in LDHs and LDH-like MDHs (Rossmann *et al.*, 1974, Charnock *et al.*, 1992).

The recombinant enzyme preferentially used NADPH as cosubstrate. With a few exceptions including MDHs of *Mc. jannashii*, *Aeropyrum pernix* and MDHs found in chloroplasts, NADH is the preferred cosubstrate for MDHs described so far (Kawakami *et al.*, 2009, Lee *et al.*, 2001, Musrati *et al.*, 1998). Interestingly, enzyme assays using cell extract of *I. hospitalis* revealed a higher activity with NADH than with NADPH (Huber *et al.*, 2008). These observations might be due to different properties of the native enzyme and the recombinant enzyme. Furthermore, this might indicate the presence of an additional NADH-dependent MDH in *I. hospitalis*. However, no further candidates have been detected in the genome of *I. hospitalis*. Enzyme activity with other substrates was below 5 % and was therefore considered insignificant. Note that the enzyme was not active on pyruvate. Pyruvate was included in substrate specificity tests, since the sequence of the protein Igni_1263 contained the typical glycine motif of LDHs and LDH-like MDHs.

Due to its predicted topology and its kinetic features, Igni_1263 can be confirmed as MDH involved in the DC/4-HB pathway of *I. hospitalis*.

Succinic semialdehyde reductase. SSR is a specific enzyme for archaeal carbon fixation pathways. In previous studies, no candidate for a SSR had been detected in the genome of *I. hospitalis* (Huber *et al.*, 2008). However, in cell extracts of *I. hospitalis* specific activities of a NADH-dependent enzyme converting succinic semialdehyde to 4-hydroxybutyrate protein could be determined (Huber *et al.*, 2008).

Although lacking homologies to sequences of SSRs of *M. sedula* and *T. neutrophilus*, which were annotated as Zn-dependent alcohol dehydrogenases, an appropriate candidate for a SSR (*Igni_0132*) was found in the genome of *I. hospitalis*.

The protein Igni_0132 was assigned to the DHQ-Fe-ADH superfamily (Dehydroquinate synthase-like and iron-containing alcohol dehydrogenases). For alcohol dehydrogenases of this family a DHQ-synthase-like protein fold is suggested and they are likely to contain iron and a Rossmann-like fold topology. Proteins exhibiting a Rossmann-like structure are often referred to as Rossmannoids and are distinguished

from the classical Rossmann fold by differences in number and arrangement of β-strands and the lack of sequence homology (Kozbial and Mushegian, 2005). Similar to the Rossmann fold, Rossmanoids contain alternating α-helices and β-sheets with the β-sheets arranged in one level (Kozbial and Mushegian, 2005). Actually, the 3D model for Igni_0132 calculated by PHYRE contained five parallel β-strands alternating with α-helices, which represents a Rossmann-like protein fold involved in nucleotide binding.

The measured enzyme activity is consistent with enzyme studies of *I. hospitalis* cell extracts, in which NADH was the preferably used cosubstrate during conversion of succinic semialdehyde. Differences in the ratio of NADH/NADPH conversion of the recombinant enzyme and the activity measured in cell extracts might derive from differences of native and recombinant protein.

The K_M value of 75 µM for succinic semialdehyde is in the same range with the K_M values obtained for the recombinant SSR of *M. sedula* (Msed_1424; 52 µM) and of *T. neutrophilus* (Tneu_0419; 30 µM; Kockelkorn and Fuchs, 2009, Ramos-Vera *et al.*, 2011). In addition, v_{max} of Igni_0132 is very similar to values determined for the recombinant enzymes of *M. sedula* (700 U/mg) and *T. neutrophilus* (580 U/mg; Kockelkorn and Fuchs, 2009, Ramos-Vera *et al.*, 2011).

Divalent cations had a stimulating effect on the activity of the recombinant protein Igni_0132. Whether metal ions are anchored in the protein as annotated for Igni_0132 or whether the protein is activated by metal ions from the surrounding medium, remains unclear.

Furthermore, activity of the recombinant enzyme with acetaldehyde, propionic aldehyde and butyric aldehyde was below 5 % and therefore regarded as insignificant. Additionally, the enzyme did not act on malonic semialdehyde and on 3-hydroxypropionate. Thus, it can be excluded that the enzyme is a malonic semialdehyde reductase such as present in the 3-hydroxypropionate pathway (Berg *et al.*, 2007). In addition, the enzyme catalyzed the reverse reaction starting with 4-hydroxybutyrate.

In conclusion, kinetic constants indicate high affinity of the enzyme for succinic semialdehyde and thus, a strong preference for this substrate. Supporting this, the enzyme acts highly specific on succinic semialdehyde, confirming Igni_0132 as SSR of the carbon fixation cycle in *I. hospitalis*.

4-hydroxybutyryl-CoA synthetase. Two candidate genes from *I. hospitalis* for a 4-hydroxybutyryl-CoA synthetase were analyzed: *Igni_0475* and *Igni_0379*. *Igni_0475* was suggested to act as 4-hydroxybutyryl-CoA synthetase by Huber *et al.*, 2008, since it showed 69 % sequence identity to *Msed_1422*, which was assumed to catalyze the respective reaction in the 3HP/4HB pathway (Berg *et al.*, 2007). Nevertheless, the *M. sedula* enzyme turned out not to act on 4-hydroxybutyrate and instead, it was suggested to be involved in acylation of proteins (Ramos-Vera *et al.*, 2011). Ramos-Vera *et al.*, 2011 suggested two more genes of *M. sedula* putatively encoding for a 4-hydroxybutyryl-CoA synthetase, namely *Msed_1353* and *Msed_1291*. Both genes showed similarities to the 4-hydroxybutyryl-CoA synthetase of *T. neutrophilus*, but however none of those genes exhibited similarities to a corresponding gene in *I. hospitalis*. In addition, the gene products of both *M. sedula* genes did not work specifically on 4-hydoxybutyrate. Moreover, Hawkins *et al.*, 2013 suggested *Msed_0394* and *Msed_0406* as 4-hydroxybutyryl-CoA synthetase, since both enzymes were active on 4-hydroxybutyrate. While Msed_0394 acted promiscuous on propionate and acetate, Msed_0406 was suggested to be the missing 4-hydroxybutyryl-CoA synthetase of the *M. sedula* 3HP/4HB pathway. However, no homologies to the sequences of both *M. sedula* enzymes could be detected within the genome of *I. hospitalis*. In addition, Msed_0406 exhibited a high K_M-value (2000 µM) and a low v_{max} (1.70 U/mg), indicating a weak affinity for the substrate (Hawkins *et al.*, 2013). Taken together, the low K_M-value and the fact that synthetases very often accept various substrates, there is still no proven 4HB-CoA ligase in *M. sedula* (Ramos-Vera *et al.*, 2011, Patel and Walt, 1987). Given those facts, the *I. hospitalis* genome was scanned for CoA synthetases/ligases. Since it was shown that *Igni_0257* and *Igni_0256* together encode for an ACS, Igni_0379 remained the most promising candidate (Mayer *et al.*, 2012, Ramos-Vera *et al.*, 2011).

Both proteins, Igni_0475 and Igni_0379 were assigned to the AFD class I superfamily (adenylate forming domain class I). Proteins of this family include acyl and aryl CoA ligases or proteins with an adenylation domain of non-ribosomal peptide synthetases and firefly luciferases.

Immuno precipitated Igni_0475 was neither active on 4-hydroxybutyrate nor on acetate or propionate. Possibly, IP inactivated the enzyme by interference with the active center and/or elution from the beads could have lead to denaturation of the enzyme. Thus, it still remains unsolved if Igni_0475 in vivo catalyzes the reaction from 4-hydroxybutyrate to 4-hydroxybutyryl-CoA.

Igni_0379 was obtained as soluble recombinant protein after overexpression in *E. coli*. Nevertheless, the enzyme was not active on 4-hydroxybutyrate, acetate or propionate, as well. Possibly, the N-terminal his-tag prevented the enzyme to fold correctly or interfered with the formation of the active site (Ramos-Vera *et al.*, 2011). This option could be checked by overexpression of a non-his-tagged version of the protein (Ramos-Vera *et al.*, 2011). Another reason for inactivity of the enzyme was illustrated in a study by Ramos-Vera *et al.*, 2011, which reported on low activity of the *T. neutrophilus* 4-hydroxybutyryl-CoA ligase being due to putative inactivation by acetylation of a Lys residue. The authors proposed in- and reactivation by acetylation and deacetylation as an artifact of the *E. coli* expression system. Moreover, immuno-precipitated protein (Igni_0379) from *I. hospitalis* cell extracts were analyzed in a respective enzyme assay, as well. Similar as Igni_0475, Igni_0379 was not active at all.

Consequently, it remains unanswered if one of the two proteins is able to catalyze the conversion of 4-hydroxybutyrate to 4-hydroxybutyryl-CoA in vivo or not. Moreover, data from overexpression of candidate genes for a 4-hydroxybutyryl-CoA synthetase from *I. hospitalis*, *M. sedula* and *T. neutrophilus* illustrate that expression of synthetases is not trivial, at least using *E. coli* as host system. Alternatively, it is worth trying another expression system, preferably a crenarchaeotic or a eukaryotic system.

Crotonyl-CoA hydratase/3-hydroxybutyryl-CoA dehydrogenase. Steps 12 - 13 of the carbon fixation cycle were postulated to be catalyzed by the gene product of Igni_1058, a bifunctional enzyme homologous to an enzyme of *M. sedula* involved in the 3-HP/4-HB pathway (Msed_0399, Ramos-Vera *et al.*, 2011). Primarily, the PHYRE database failed to create a 3-dimensional model. However, modeling of a structure became possible when dividing the amino acid sequence into two parts. Thus, two independent structures were created, one of which exhibited a Rossmann-fold-like topology near the N-terminus with a glycine consensus motif GAGVMG ($GXGX_2G$). Therefore this part most likely represents the 3-hydroxybutyryl-CoA dehydrogenase part of the protein (aa: 1-421). The second structure (aa: 422-end) revealed homologies to a hydratase/isomerase complex of *E. coli* and therefore might be the hydrolase part of the protein.

In accordance with activity assays using cell extracts of *I. hospitalis*, NAD^+ was preferably used as cosubstrate (Huber *et al.*, 2008). The enzyme neither converted the (R)-version of 3-hydroxybutyryl-CoA nor 3-hydroxypropionyl-CoA. Similar substrate specificity was observed for the *M. sedula* pendant (Msed_0399) of Igni_1058 (Ramos-Vera *et al.*, 2011).

The generally low values for v_{max} are possibly due to purification of the recombinant protein from the insoluble fraction of *E. coli* extracts linked with only partial activity. Nevertheless, the data correlate with those of the recombinant *M. sedula* enzyme, which exhibited a v_{max} of 13.8 U/mg at 65°C (Ramos-Vera *et al.*, 2011).

Considering structure prediction and enzyme kinetics, Igni_1058 can clearly be confirmed as crotonyl-CoA hydratase/3-hydroxybutyryl-CoA dehydrogenase of the CO_2 fixation pathway in *I. hospitalis*.

2.2. Localization of enzymes of the DC/4-HB cycle

Antibody specificity and significance of immunogold labeling. A particular problem of immunogold labeling in general is the specificity of antibodies. The mere fact that protein localization in *I. hospitalis* repeatedly revealed unusual localizations for some proteins, such as the ATP synthase and the ACS in the OCM, raised questions about significance and credibility of these results (Küper *et al.*, 2010, Mayer *et al.*, 2012). Accordingly, various controls were performed, including Western Blot analysis of primary antibodies and pre-immune sera, and immunogold labeling with secondary antibodies only, to exclude unspecific binding of antibodies. As shown in section III.5-11, the respective antibodies recognized their targeted proteins at the expected sizes in Western Blot analysis using crude cell extracts of *I. hospitalis* and *I. islandicus*, respectively. This indicates high affinity between antibodies and antigen and contributes to the credibility of localization experiments on ultrathin sections. However, the antibody against the protein Igni_0475 revealed a very strong signal at the expected size of approximately 55 kDa and two additional bands. These bands might be traced back to degradation products (40 kDa) and oligomeric versions of the protein (170 kDa). At that point it is worth noting that this Western Blot was carried out with frozen and thawed *I. hospitalis* extract, which might be an explanation for the occurrence of the lower band. Nevertheless, an IP was performed with freshly prepared cell extract to examine the specificity of this antibody. Actually, both the Coomassie- and the silver stained SDS gel of the immuno precipitated cell extracts revealed just one band between 55-70 kDa, which was confirmed to be Igni_0475 (MALDI analysis; section III.8.2). Further Western Blots were performed with freshly prepared cell extracts of *Ignicoccus*.

Additional experiments that support credibility of immunogold labeling were performed with Lowicryl- and with cryo-sections leading to essentially identical labeling

patterns as on Epon sections (sections III.5-11 and IV.1.1). Moreover, localization of DNA in the cytoplasm of *I. hospitalis* and *I. islandicus* was confirmed with immunogold labeling using a commercial antibody directed against double and single stranded DNA (section III.12.1 and IV1.1). This is in line with previous studies using DAPI and Syto9 staining, which showed DNA to be exclusively accommodated in the cytoplasm (Küper *et al.*, 2010, Daxer, 2011). As an example for localization of a protein at multiple sites of the cell, the two cytochromes (Igni_0955 and Igni_1359) were shown to be located at the OCM, at the inner membrane and at structures in the IMC (Fig. III.46). Due to their localization and the reducing effect of the OCM-bound hydrogenase on Igni_0955, the cytochromes are assumed to act as e^--carrier between the hydrogenase in the OCM and intracellular reductases (Naß *et al.*, 2014).

Meanwhile, various proteins and cell components accommodated in all the different compartments of *Ignicoccus* and with a variety of functions have been targeted by immunogold localization. Every single experiment considerably contributed to complete the overall picture of cell structure and organization of this quite astonishing prokaryote (Gürster, 2007, Burghardt *et al.*, 2008, Wasserburger, 2008, Heimerl, 2009, Küper *et al.*, 2010, Meyer, 2010, Flechsler, 2010, Mayer *et al.*, 2012, Naß *et al.*, 2014, Heimerl, 2014). This includes proteins and cell components located in the cytoplasm, such as DNA, Igni_0475, Vps4 (Igni_0994), CdvA (Igni_0996), Snf7-like protein (Igni_0101) and a WD40 protein (Igni_0561) and proteins located in the IMC and in association with the OCM, such as cytochromes (Igni_0955 and Igni_1359), proteins involved in carbon fixation (Igni_0341, Igni_1263, Igni_0132, Igni_0379?, Igni_1058) and the ACS (Igni_0256-0257). Moreover, proteins in the OCM were located, comprising different subunits of the ATP synthetase, the H_2:sulfur oxidoreductase, Ihomp (Igni_1227) and the fiber protein (Igni_0670). Currently, the two cytochromes (Igni_0955 and Igni_1359), the fiber protein Iho670 and the fiber-associated protein Iho668 are the only proteins that were shown to be located in the inner membrane, however not exclusively.

Nevertheless, in a long-term perspective the establishment of a genetic system for *I. hospitalis* might be advantageous or even inevitable. Introduction of fluorescent genetic tags or creation of knockout mutants could help to support significance of current localization experiments. Research on fluorescent proteins compatible with an hyperthermophilic anaerobic lifestyle is still in early stages, but reports on heat stable flavin-based fluorescent molecules which were successfully tested under anaerobic conditions have already been published (Mukherjee and Schroeder, 2015). There is,

however, one point that must be viewed with a critical eye when introducing genetic tags. These tags are considerably large in size (GFP: 27 kDa) and might therefore change native properties of a protein in a way that it is prevented from being exported into its natural destination (Snapp, 2005). This might be critical for *I. hospitalis*, since unusual protein localizations occurred frequently.

Localization. In contrast to what was expected a few years ago (Podar *et al.*, 2008) and different than proposed by various tools for prediction of subcellular localization, all enzymes that have been associated with the carbon fixation pathway in *I. hospitalis* with one exception (Igni_0475) were shown to be mainly located in the IMC, tightly associated with the OCM. For most of the proteins, 5-10 % of labels were detected in the cytoplasm and for some proteins, at least on cryo-sections, structures in the IMC were found to be labeled. Furthermore, no difference was observed in the labeling pattern of autotrophically grown cells and cells that were grown with addition of 0.05 % yeast extract (data not shown).

The fact that protein biosynthesis takes place in the cytoplasm in *I. hospitalis* might provide an explanation for the gold particles found in this compartment (Küper *et al.*, 2010). Compared to gold particle distribution of other enzymes involved in carbon fixation, a slightly increased number of labels in the cytoplasm was found on cryo-sections of cells labeled with the MDH antibody (Fig III.19). Although synthesis of metabolic enzymes is dependent on the cell cycle, this effect might only partially be explained by enhanced biosynthesis of MDH. Most likely, the enzyme is involved in additional metabolic pathways taking place in the cytoplasm, such as biosynthesis of amino acids or gluconeogenesis (Huber *et al.*, 2012). For Eukaryotes, several isoforms of this enzyme have been described, located in the cytoplasm, in mitochondria and in chloroplasts which are distinguished from each other by their specificity for the cofactor $NAD(P)^+$ (Musrati *et al.*, 1998). In Eukaryotes, glucenogenesis starts in the mitochondria, where MDH is involved in the citric acid cycle. Here, gluconeogenesis starts by the formation of oxaloacetate from pyruvate catalyzed by a pyruvate carboxylase. For transport into the cytoplasm, oxaloacetate is converted to malate by a MDH. In the cytoplasm, where gluconeogenesis is continued, malate is re-converted to oxaloacetate by a cytoplasmic MDH (Stryer *et al.*, 2003). However, for *I. hospitalis* the presence of a pyruvate carboxylase was not confirmed. Furthermore, gluconeogenesis in *I. hospitalis* was suggested to start from PEP, since no PEP carboxykinase gene was found in the genome, which would be able to convert oxaloacetate to PEP (Jahn *et al.*, 2007).

Nevertheless, it is at least conceivable that similar as in Eukaryotes, malate formation takes place in the IMC. Then malate is transported into the cytoplasm, where it is converted to oxaloacetate by a cytoplasmic MDH. Hence, oxaloacetate would be available in the cytoplasm as precursor for biosynthesis of amino acids (Podar *et al.*, 2008, Huber *et al.*, 2012).

Another possibility, which might lead to increased appearance of MDH in the cytoplasm is protein moonlighting. The term moonlighting refers to proteins that have multiple, but often unrelated functions in a cell. This is a widespread phenomenon and is often observed for highly conserved enzymes. Astonishingly, it is assumed that seven out of eight proteins of the citric acid cycle are moonlighters. For instance, the enzyme aconitase from yeast is known to be involved in the citric acid cycle. In addition, the enzyme has been shown to be important for mitochondrial DNA stability. This example illustrates that both functions of the enzyme are not related and that the second function is not predictable from the genomic sequence, as well (Huberts and van der Klei, 2010). Under the light of its small genome, it seems reasonable that *Ignicoccus* developed multiple functions for one enzyme. In addition, moonlighting functions are often described for metabolic enzymes, which would be in agreement with the MDH of *I. hospitalis*. Further study is needed to find out if the MDH fulfills another, unrelated task in the cytoplasm of *I. hospitalis*.

Particularly for the SSR, but also for the protein Igni_0379 (candidate for 4-hydroxybutyryl-CoA synthetase), gold particles occurred on structures in the IMC in addition to labels associated with the OCM. Especially the labeling pattern of SSR on cryosections mediated the impression that cytoplasmic protrusions or the inner membrane are connected with the OCM by structures in the IMC. This mediating structure was partially enhanced by the presence of gold particles (Fig. III.25) and might indicate an alternative transport route for proteins across cytoplasmic protrusion in the IMC, as suggested by Heimerl, 2014.

There is still uncertainty regarding enzyme identity of the 4-hydroxybutyryl-CoA synthetase. As discussed in IV.2.1, both enzymes, Igni_0475 and Igni_0379, were not active on 4-hydroxybutyrate and thus it remains unclear if one of both enzymes participates in the DC/4-HB cycle. Concerning localization, one of the proteins was found in the cytoplasm (Igni_0475), while the other enzyme was shown to be located in the IMC in association with the OCM (Igni_0379). However, the 'appropriate localization' regarding the other enzymes involved in the carbon fixation pathway, can only serve as another indication of Igni_0379 being the missing enzyme.

Furthermore, various special ultrastructural features were labeled, which were particularly striking when evaluating EM data. This comprises a darkly-stained inclusion that was fully covered in labels of crotonyl-CoA hydratase/3-hydroxybutyryl-CoA dehydrogenase, similar in shape and size of the putative phosphate storage (Fig. III.40). However, the putative phosphate storage usually appears to be much darker (Fig. III.4) and FIB-SEM analysis revealed several examples for an additional type of inclusions in the cytoplasm of *I. hospitalis* (Heimerl, 2014).

Besides strongly binding to phosphate groups, uranyl ions bind to carboxyl-groups, as well. Thus, simply the accumulation of the enzyme might have lead to the prominent staining. Protein accumulation might refer to the formation of polyhydroxybutyrate (PHB). PHB serves as carbon energy source and its formation is induced under physiological stress. In *Rhodosprillum rubrum* the production of PHB from acetyl-CoA via crotonyl-CoA hydratase and 3-hydroxybutyryl-CoA dehydrogenase has been shown (Anderson and Dawes, 1990). The data obtained from FIB-SEM analysis and the fact that *I. hospitalis* seems to be equipped with at least a part of the required enzymes for the formation of PHB, support the existence of PHB inclusions in *I. hospitalis*.

Finally, Fig. III.24 reveals gold particles at the contact site between *I. hospitalis* and *N. equitans*, when locating the SSR. Moreover, with this antibody cells of *N. equitans* occasionally contained labels, as well. Admittedly, these gold particles never occurred in large numbers, but frequently, indicating a significant labeling. In addition, no SSR and no similar protein is annotated in the genome of *N. equitans*. This indicates another example of possible protein transfer between both organisms in the direction of *N. equitans*. In addition, the desolate appearance of *I. hospitalis* on this micrograph mediates the impression of *I. hospitalis* being tapped by *N. equitans*. Neverthless, on the proteomic and on the transcriptomic level, the co-culture of those two organisms does not reveal typical features of a viral infection process (Giannone *et al.*, 2014). Similar observations with labels at the contact site were also made for crotonyl-CoA hydratase/3-hydroxybutyryl-CoA dehydrogenase and for the ATP synthase (Flechsler, 2010). Whether labeling of *N. equitans* with these antibodies is significant and whether labeling at the contact site is interpreted in the correct way remains unanswered at this point. Conspicuously, the occurrence of gold particles on *N. equitans* and at the contact site is observed more frequently and for various proteins. Labeling of consecutive sections might provide the missing statistical information for gold particles on *N. equitans* and at the contact site and might supply further indications for a putative protein transfer mechanism. From C-tracer labeling studies, transfer of amino

acids and lipids from *I. hospitalis* to *N. equitans* has already been shown. This is in line with the minimalistic genome of *N. equitans*, which lacks genes for amino acid- and lipid synthesis (Waters *et al.*, 2003, Jahn *et al.*, 2008). A more recent study that compared proteomics and transcriptomics of the pure culture (KIN4/I) and of the co-culture (KIN4/M), showed a gradual increase in levels for enzymes involved in carbon fixation in the co-culture. This might be a reaction to an "increased demand of important metabolic products" (Giannone *et al.*, 2014). In addition, Hamerly *et al.*, 2014 demonstrated that *N. equitans* actually exploits metabolites generated by its host *I. hospitalis*. In this context, it is worth mentioning that Igni_0475, which was located in the cytoplasm of *I. hospitalis* was also detected in large amounts in the *N. equitans* cytoplasm. Cross-reactions can be excluded since no similar protein was found in the genome of *N. equitans*. Occurrence of proteins in the cytoplasm of both organisms has already been described for some immuno localization experiments, although proteins were only found to be annotated in the *I. hospitalis* genome. This comprises the proteins Vsp4, CdpA, Snf7(-like) and WD40, for which a transport into *N. equitans* was assumed (Heimerl, 2014). Whether this transport is directed or undirected is still under investigation. Indications for an undirected transport or more precisely a shared protein pool were provided by data obtained from EM, which showed the fusion of both cytoplasms (Heimerl, 2014). It also remains unclear if *N. equitans* uses the function of the acquired proteins or if proteins are simply degraded, thus used as carbon and nitrogen source.

Apart from that, the enzymes of the DC/4-HB pathway were detected in the genome of *I. islandicus*, as well. On cryo-sections, MDH and SSR of *I. islandicus* were located in the IMC, indicating that carbon fixation in the IMC is a general feature of all *Ignicoccus* strains. Localization on resin sections was not successful and therefore antibodies were used in higher concentrations on cryo-sections, which might have lead to an increase of insignificant labeling.

In summary, localization experiments revealed fascinating new insights in organization and function of *I. hospitalis* and in the co-culture of *I. hospitalis* and *N. equitans*. It would be interesting to receive more detailed information on the EM level on the life cycle of both organisms. Analysis in temporal resolution might provide new details referring to protein expression and distribution in different stages of the cell cycle and to colonization and re-colonization of *I. hospitalis* by *N. equitans*.

Carbon fixation in the IMC. Questions that arise from the localization studies concerning the carbon fixation pathway in *I. hospitalis* are related to the sense of the pathway being located in the IMC, in general. Moreover, it would be interesting how proteins are exported from the cytoplasm into the IMC and how metabolic products are imported from the IMC into the cytoplasm.

Previously, the ATP synthetase and the ACS were shown to be integrated into or associated with the OCM of *I. hospitalis*, respectively (Küper *et al.*, 2010, Mayer *et al.*, 2012). Hence, the primary acceptor molecule for carbon fixation (Acetyl-CoA) and a large amount of ATP are available in the IMC. The presence of ATP is essential, since the carbon fixation pathway consumes five ATP equivalents to form one pyruvate molecule (Huber *et al.*, 2008). Thus, availability and a rapid conversion of ATP by the cycle would contribute to enhanced cell growth rates, which might be a crucial factor in competition for nutrients and colonization of new habitats.

During bioinformatic analysis, protein sequences were submitted to web-based programs for localization prognosis. However, most of the sequences were suggested to be cytoplasmic. Regarding the striking ultrastructure of *I. hospitalis* and comparing proposed localizations to experimentally verified localizations, it becomes obvious that prediction tools are not convenient for *I. hospitalis* and other prokaryotes exhibiting a similar, compartmentalized ultrastructure. In addition, protein sequences were analyzed bioinformatically to identify signal peptides or transmembrane domains that could give indications of proteins being transported and located in the IMC attached to the OCM. For the ACS neither signal peptides nor transmembrane domains could be detected within the sequence. A 3D-model of the enzyme revealed a mushroom-like shape with a foot domain that might serve as an anchor for docking onto the OCM (Mayer *et al.*, 2012). Using tools for prediction of secondary structure, one putative transmembrane helix close to the N-terminus for the MDH was detected. For the SSR, a putative internal helix was proposed and for Igni_0379 one or two transmembrane regions were predicted, respectively. In addition, for the crotonyl-CoA hydratase/3-hydroxybutyryl-CoA dehydrogenase two putative transmembrane regions were predicted. Using a eukaryotic prediction algorithm, the first helix was suggested to be a signal peptide (sections III.5-11). In this context, Payne *et al.*, 2012 reported on the diversity of prokaryotic signal peptides, but their analysis included only one archaeal species (*Methanospirillum hungatei*). The archaeal signal peptide motif turned out to be different from prokaryotic motifs, but similar to those found in Eukaryotes. Due to secondary structure predictions it seems likely that the five proteins mentioned

above are located in the IMC, either linked to the OCM via hydrophobic interactions or integrated into the OCM. In contrast, for the PEP carboxylase no transmembrane helices have been detected. Another study by Schmid *et al.*, 2013 compared experimentally verified extracellular proteins from *P. furiosus* to proteins that were predicted to be extracellular. Actually, the analysis revealed that only 15 out of 58 proteins were prognosticated to carry a signal peptide. Accordingly, it is likely that bioinformatic tools failed to predict signal sequences at all in case of *Ignicoccus*. Alternatively, the PEP carboxylase might be associated with the other proteins of the pathway in one or more multienzyme complexes. The possibility of the carbon fixation pathway being arranged in complexes would provide additional benefit for the cell, since efficiency of the cycle could be increased by substrate channeling. Moreover, side reactions of intermediates are reduced in such complexes. Due to shorter distances, substrates could be transformed more rapidly, which enhances efficiency as well (Stryer *et al.*, 2003). Actually, the existence of multienzyme complexes in carbon fixation has already been suggested. For *Euglena gracilis*, a complex was proposed consisting of PEP carboxylase, MDH and acetyl-CoA carboxylase. This association might be involved in a control mechanism for acetyl-CoA carboxylase that lacks allosteric inhibition in *Euglena gracilis* (Wolpert and Ernst-Fonberg, 1975). On the basis of gel chromatography, a study by Queiroz-Claret and Queiroz, 1992 gives indications for a multienzmye complex in a CAM plant containing MDH and PEP carboxylase. An approach to find out more about multienzyme complexes in *I. hospitalis* might start from immuno precipitations with *I. hospitalis* cell extract and with antibodies directed against the enzymes of the carbon fixation combined with MALDI analysis.

Possible transport routes for proteins and metabolites. Having established that the carbon fixation cycle operates in the IMC and that protein biosynthesis takes place in the cytoplasm assumed from the presence of DNA and ribosomes, the transport of proteins involved in carbon fixation in the IMC needs to be discussed. In general, proteins are transported across membranes via the Sec and the Tat pathways, which are present in all domains of life (Natale *et al.*, 2008). While the Sec system translocates unfolded proteins across cytoplasmic membranes, the Tat system transports folded proteins across the membrane. In *I. hospitalis* components of the Sec pathway and the Tat system were identified in the genome (Podar *et al.*, 2008). Usually, a specific signal sequence is required for transport with these systems. For the Sec pathway the signal sequence is an N-terminal extension of the protein exhibiting a tripartite structure (NHC-regions) of 20 amino acids in average. The signal sequence

of the Tat system has a similar appearance, but additionally contains a twin-arginine motif at the interface between N- and H-region (Natale *et al.*, 2008). For enzymes of the CO_2 fixation pathway, no such signal peptides have been identified, except for the crotonyl-CoA hydratase/3-hydroxybutyryl-CoA dehydrogenase. Possibly, tools for signal peptide prediction failed to predict signal sequences in *I. hospitalis* due to an unknown signal peptide pattern in this unusual prokaryote. Alternatively, there might be additional unknown transport routes in *I. hospitalis*. So far, there are at least indications for another way of transportation, based on cytoplasmic protrusions. In previous studies, subunits of the ATP synthase could be located in those protrusions using immunogold labeling (Flechsler, 2010, Küper *et al.*, 2010). More recently, the existence of pore-like structures underneath the OCM was shown on the basis of electron tomography. These structures indirectly connect protrusions or the cytoplasm itself with the OCM. Thus, two potential possibilities for protein transport are provided (Heimerl, 2014). Similar, this route could also contribute to import of metabolic intermediate products of the carbon fixation cycle into the cytoplasm (Heimerl, 2014). Metabolites like oxaloacetate or PEP are precursors for metabolic processes such as biosynthesis of particular amino acids or gluconeogenesis. Furthermore, the proteins Igni_0539 and Igni_0829 could act as transporters for oxaloacetate and additional dicarboxylic acids from the IMC into the cytoplasm. BLAST analysis revealed a CitT domain for both sequences, which are typical for various di- and tri-carboxylic transporters.

Moreover, it would be interesting if the carbon fixation cycle is the only pathway of *I. hospitalis* that takes place in the IMC or if even more pathways, partially or as a whole, are located in this compartment. For instance, localization of the gluconeogenesis or the aspartate pathway would be particularly interesting since PEP and oxaloacetate are synthesized by the carbon fixation cycle and therefore available in the IMC.

In addition, there are more examples of prokaryotes exhibiting an apparently similar ultrastructure as *Ignicoccus*. Like *Ignicoccus*, anammox bacteria have an autotrophic lifestyle in which carbon fixation is suggested to proceed via the acetyl-CoA pathway (van Niftrik, 2013). Although looking very similar at the first glance, only very limited information is available about the recently discovered methanogen, *Methanomassiliicoccus luminyensis* (Dridi *et al.*, 2012). It would be interesting to find out where carbon fixation or other metabolic processes take place in those organisms. Is carbon fixation the only metabolic pathway in *I. hospitalis* that takes place in the IMC and is this spatial separation of a metabolic pathway a unique feature of *Ignicoccus* among Archaea?

2.3. Carbon fixation in the IMC of *I. hospitalis*: A carbon concentrating mechanism?

It is nowadays assumed that oceanic and atmospheric CO_2 concentrations in the Proterozoic (2500-543 Myr years ago) were approximately two orders of magnitude higher than today (Kaufman and Xiao, 2003). About 2.45 billion years ago, oxygen concentrations dramatically increased with the evolution of the oxygenic photosynthesis (Rasmussen *et al.*, 2008). Faced with decreased CO_2 concentrations, living organisms have developed various adaptations to cover their requirement for inorganic carbon (Dobrinski *et al.*, 2005, Raven *et al.*, 2008). These adaptations, referred to as carbon concentrating mechansisms (CCM), evolved polyphyletic and exist in a broad variety of organisms, including cyanobacteria, algae, hornworts, ferns and flowering plants (Raven *et al.*, 2008). More recently, a CCM has been suggested for *Thiomicrospira crunogena*, a chemolithoautotrophic microbe that lives in a hydrothermal vent system (Dobrinski *et al.*, 2005). In simple terms, CCMs usually involve microcompartments that contain the carbon fixing enzyme and that minimize CO_2 leakage, transporters that contribute in intracellular accumulation of HCO_3^- and carbonic anhydrases (CA) that convert HCO_3^- into CO_2 (Meyer and Griffiths, 2013).

Among Bacteria, cyanobacteria and some chemotrophic gammaproteobacteria developed a special, separated microcompartment where carbon fixation takes place, the so called carboxysome (Shively *et al.*, 1973, Price *et al.*, 1993). Carboxysomes harbor tightly packaged RuBisCO and a carbonic anhydrase, are surrounded by a polyhedral protein shell and serve as carbon dioxide concentrating compartments (Cannon *et al.*, 2010). This is advantageous, since RuBisCO is also able to perform an oxygenase reaction in the presence of O_2, leading to decreased CO_2 fixation rates (Moroney and Ynalvez, 2007). The CCM is based on accumulation of HCO_3^- in the cytoplasm, which is supported by multiple uptake systems for inorganic carbon. By means of two thylakoidmembrane-associated proteins, CO_2 entering the cell is additionally converted to HCO_3^-. Accumulated HCO_3^- is transported to the carboxysome, where it is converted to CO_2 by a carbonic anhydrase (CA). CO_2, which is prevented from leaking by the protein shell of the carboxysome is now available and highly concentrated for the RuBisCO (Badger and Price, 2003).

Another very similar CCM has been shown to operate in the unicellular green algae *Chlamydomonas rheinardtii*. Here, concentration of inorganic carbon takes place in the chloroplast and conversion of HCO_3^- to CO_2 is catalyzed by a CA (CAH3) accommo-

dated in the chloroplastic lumen. RuBisCO is found densely packed in the pyrenoid, which is considered a functional analogue of the carboxysomes. In contrast to carboxysomes, the pyrenoid does not contain a protein shell or a membrane. Instead, two proteins inside the chloroplast are assumed to form a barrier to prevent CO_2 leakage (Meyer and Griffiths, 2013).

C4 plants exhibit a slightly different CCM, which involves pre-fixation of CO_2 by a PEP carboxylase in mesophil cells. The product obtained by this reaction is oxaloacetate, which is further converted to malate or aspartate. Malate and aspartate are transported to the bundle sheath cells and they are converted to CO_2 and a C3 product by a C4 decarboxylase.

In conclusion, CCMs are highly diverse and occur in many living organisms. All of these mechanisms contribute to the concentration of CO_2 to enhance carbon fixation. Thus, it would not be surprising, if CCMs are more spread among microorganisms than previously assessed, including chemolithoautotrophs from hydrothermal vent systems. Reasons for the development of such mechanisms by chemolithoautotrophs might have derived from periodical fluctuations of inorganic carbon sources in their natural habitats (Dobrinski *et al.*, 2005). Accordingly, the question arises if the occurrence of the carbon fixation pathway in *Ignicoccus* in the IMC is a CCM , as well. As shown in this study, carbon fixation in *I. hospitalis* takes place in the IMC of the organism, which is separated from the cytoplasm via an inner membrane and shielded from the outside by the OCM. According to recent studies focused on the 3-dimensional cellular ultrastructure of *I. hospitalis* this compartment makes up approximately 40 % of the whole cellular volume, whereas the cytoplasm comprises 60 % of the total cellular volume of an average *I. hospitalis* cell (Heimerl, 2014). Similar as in CCMs of Cyanobacteria and *Chlamydomonas*, enzymes of the *Ignicoccus* carbon fixation pathway are encased in a defined volume with the difference that not only the fixing enzyme but, putatively, the whole pathway is found in a separate compartment. CO_2 can easily cross the membrane by diffusion. Taking into account that the pH in the IMC might be alkaline, intracellular CO_2 would preferably exist as HCO_3^- (Kreuter, 2014). Since HCO_3^- is not able to freely diffuse through membranes, an increase of the HCO_3^- concentration in the IMC occurs. Additionally, HCO_3^- could be transported into the cell by special transport proteins. BLAST analysis of Igni_0454 classified the protein as member of the SLC5 family (e-value of 3.74 e^{-131}). This protein family co-transports Na^+ ions with sugar, amino acids, inorganic ions or vitamins and could therefore represent a Na^+/HCO_3^- symporter that helps to enhance the intracellular HCO_3^- concentration. Furthermore,

there are two carbon fixing enzymes in the DC/4-HB cycle, namely pyruvate synthase fixing CO_2, and PEP carboxylase fixing HCO_3^-. The fact that enzymes of the carbon fixation pathway are mainly located in association with the OCM, might facilitate CO_2 fixation. CO_2 might be directly captured by the pyruvate synthase when crossing the membrane and in this way might be prevented from being converted into HCO_3^- due to the alkaline pH of the IMC. This would be another advantage of enzymes being associated with the OCM, instead of being randomly distributed among the cytoplasm/IMC. Moreover, no gene for a carbonic anhydrase in the genome of *I. hospitalis* was found that could help to interconvert HCO_3^- and CO_2 species and that could contribute in the maintenance of the intracellular CO_2 concentration (Smith and Ferry, 2000).

If carbon fixation in *I. hospitalis* is accompanied by a CCM in the traditional sense remains questionable at present. At least, not all criteria are fulfilled (transport mechanisms for HCO_3^- uptake and CAs), however there are indications for a putative Na^+/HCO_3^- symporter. Nevertheless, enzymes are located in a separate compartment. CO_2 entering the cell can be fixed immediately by the pyruvate synthase due to association of the enzymes with the OCM, or might purely chemically be converted into HCO_3^-, which is the co-substrate for PEP carboxylase. The restricted volume of the IMC (compared to the whole cellular volume) passively contributes in carbon concentrating, since it is the place were CO_2 enters the cell and since inorganic carbon might be trapped in this compartment as HCO_3^-, which is not able to diffuse through membranes. Thus, *I. hospitalis* might exhibit an unconventional, non-traditional way of carbon concentrating that might contribute in an efficiency increase of carbon fixation. Recent studies have shown that enzymes for carbon fixation are up-regulated in the co-culture of *I. hospitalis* and *N. equitans* (Giannone *et al.*, 2014). Under the light of an increased requirement of metabolic intermediates (which might be provided by *I. hospitalis*) of the co-culture, a CCM appears to be particularly beneficial for *I. hospitalis* when *N. equitans* is attached to its surface.

2.4. Conclusions

In conclusion, the IMC of *I. hospitalis* is an important compartment of the cell, since it is the place where energy conservation takes place (ATP synthesis, Küper *et al.*, 2010) and since it is linked to important energy consuming processes, like the activation of acetate to acetyl-CoA via the ACS (Fig. IV.1, Mayer *et al.*, 2012). In addition, acetyl-CoA serves as primary acceptor molecule for the CO_2 fixation pathway and it therefore is reasonable that this pathway is also located in the IMC (Huber *et al.*, 2008). Thus, it can be concluded that the whole CO_2 fixation process takes place in the IMC of *I. hospitalis*, while the necessary enzymes or their precursors are synthesized in the cytoplasm. Moreover, the occurrence of the carbon fixation pathway in the IMC might represent a CCM to enhance the fixation of inorganic carbon in *I. hospitalis*.

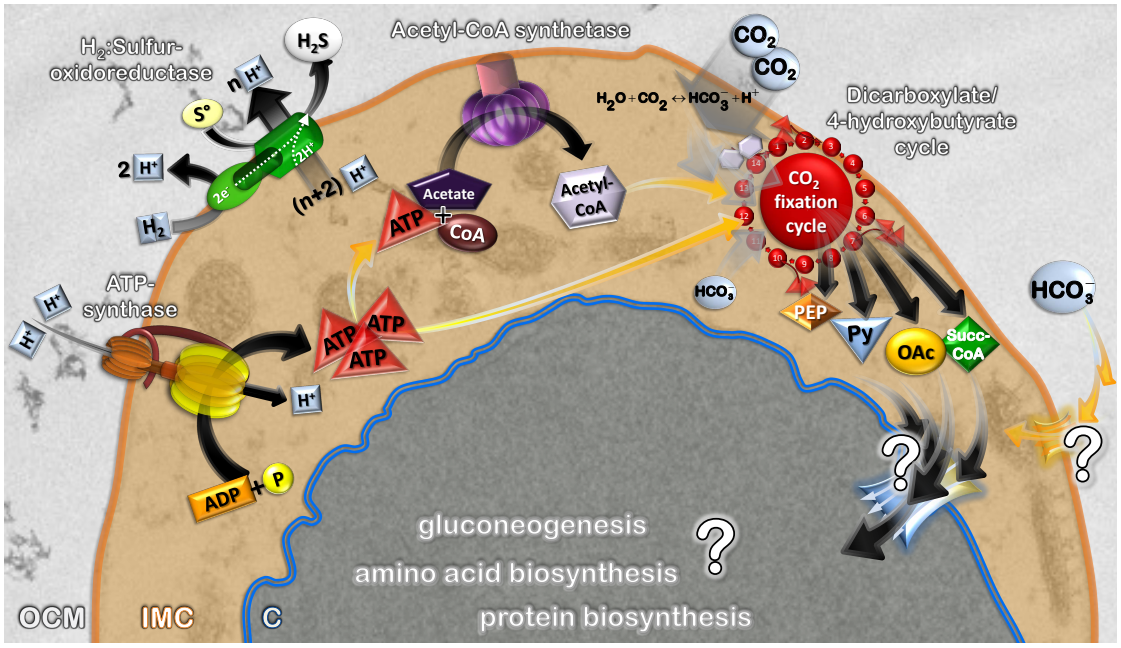

Fig. IV.1.: *The H_2:sulfur oxidoreductase induces a proton gradient across the OCM; protons are used by the ATP synthase to generate ATP in the IMC. ATP is consumed by the ACS (located in the IMC), which catalyzes the formation of acetyl-CoA. Acetyl-CoA, ATP and inorganic carbon are required to operate the carbon fixation cycle, which is also located in the IMC. The required CO_2 enters the IMC by diffusion, while HCO_3^- might enter the cell via transport proteins or might be formed chemically from CO_2 due to alkaline pH values in the IMC. The cycle produces precursors for biosynthesis of amino acids or gluconeogenesis (PEP, pyruvate, oxaloacetate and succinyl-CoA). These intermediates are assumed to be transported into the cytoplasm for further processing. Illustrated by C. Trieb, based on Küper* et al., *2010, enzymes illustrated by V. Heinz.*

V. Summary

This thesis mainly focuses on biochemical investigation and subcellular localization of enzymes involved in the CO_2 fixation pathway of *I. hospitalis*. A further objective was to compare different methods in electron microscopy to optimize immunogold labeling on ultrathin sections of *I. hospitalis*. Comparing immunogold labeling on ultrathin-sectioned *I. hospitalis* cells, embedded in different resins (Epon versus Lowicryl) and on cryo-sections, demonstrated that the three different methods lead to essentially similar labeling patterns. Due to excellent preservation of ultrastructure, immuno-EM on Epon sections proved to be the method of choice for cells of *Ignicoccus*. Utilizing an accelerated protocol for immunogold labeling clearly demonstrated that shorter incubation times for antibodies (30 min) are fully sufficient and contribute to better maintenance of ultrastructural details.

Furthermore, serial sections of the co-culture (*I. hospitalis* and *N. equitans*) were immuno-labeled with an antibody directed against the ACS and visualized in 3D. As expected from 2D immuno-EM, gold particles were mainly detected in the IMC.

To confirm the so far only putative *I. hospitalis* genes of the carbon fixation cycle, candidates for enzymes involved in the pathway were investigated biochemically: Igni_0341 (PEP carboxylase), Igni_1263 (MDH), Igni_0379 and Igni_0475 (4-hydroxybutyryl-CoA synthetase) and Igni_1058 (crotonyl-CoA hydratase/3-hydroxybutyryl-CoA dehydrogenase). Additionally, a candidate gene for a SSR (*Igni_0132*), a 'missing' enzyme of the cycle, was detected in the genome of *I. hospitalis* and heterologously overexpressed in *E. coli*. Based on enzyme assays and bioinformatics, the recombinant 'candidate' enzymes Igni_1263, Igni_0132 and Igni_1058 could clearly be identified as the respective enzymes involved in the carbon fixation pathway of *I. hospitalis*. Recombinant PEP carboxylase was not active in the respective enzyme assay. However, bioinformatical investigations strongly indicate the gene *Igni_0341* to encode for an archaeal PEP carboxylase. Two candidate genes (*Igni_0379* and *Igni_0475*) were investigated to identify a 4-hydroxbutyryl-CoA synthetase involved in the pathway. In fact, non of the enzymes converted 4-hydroxybutyrate to 4-hydroxybutyryl-CoA. Thus,

it remains unclear whether one of those two candidates acts as 4-hydroxybutyryl-CoA synthetase *in vivo*.

Immuno-EM revealed a localization of PEP carboxylase, MDH, SSR and crotonyl-CoA hydratase/3-hydroxybutyryl-CoA dehydrogenase in the IMC of *I. hospitalis*, tightly associated with the OCM. DNA was demonstrated to be exclusively located in the cytoplasm and cytoplasmic protrusions of *Ignicoccus*. From these results it was assumed that the whole CO_2-fixation pathway of *I. hospitalis* takes place in the IMC of the organism, not in the cytoplasm. The occurrence of the carbon fixation pathway in the IMC might represent an unconventional carbon concentrating mechanism of *I. hospitalis*.

Furthermore, genes encoding for enzymes of the DC/4-HB cycle were detected in the genome of *I. islandicus*. MDH and SSR of *I. islandicus* were also shown to be located in the IMC. Similar as demonstrated for *I. hospitalis*, these results strongly indicate that CO_2 fixation of *I. islandicus* takes place in the IMC according to the DC/-4-HB pathway.

VI. Future research

In this project five steps of the DC/4-HB pathway in *I. hospitalis* were shown to be located in the IMC. Therefore, it was assumed that the whole cycle takes place in this compartment. Further approaches could aim to verify enzyme activities and to locate the remaining candidates to ensure the whole cycle being located in the IMC.

New questions arose with respect to the subcellular localization of the pathway: since the cycle operates in the IMC, important precursors for biosynthesis of amino acids or gluconeogenesis (pyruvate, PEP, oxaloacetate and succinyl-CoA) are synthesized within this compartment. One attempt to find out whether gluconeogenesis or another pathway consuming intermediates of the cycle takes place in the IMC or in the cytoplasm, is to target enzymes of these pathway with immuno-EM. Assuming that gluconeogenesis and biosynthesis of amino acids are located in the cytoplasm, it is necessary to investigate how intermediates of the cycle are transported from the IMC into the cytoplasm where they can be introduced into further metabolic pathways. Based on bioinformatics, the genomes of *I. hospitalis* and *I. islandicus* could be searched focusing on transport proteins.

Regarding the 'proteome studies' by Giannone *et al.*, 2014, which demonstrated an up-regulation of enzymes involved in carbon fixation, an interesting field of research would be to find out if there are differences in enzyme distribution and density between pure- (*I. hospitalis*) and co-culture (*I. hospitalis* and *N. equitans*) in distinct growth phases. Additionally, consumption or transfer of *I. hospitalis* proteins into *N. equitans* could be followed in different stages of the cell cycle. These investigations can be implemented by analysis of 'times course' samples. These samples have already been high-pressure-frozen and have been further processed for ultrastructural analysis in temporal resolution.

Some enzymes of the carbon fixation cycle might be organized in protein complexes, which would contribute to enhance carbon fixation. An investigation of this issue can be approached by co-immuno precipitation followed by mass spectroscopy.

The 4-hydroxybutyryl-CoA synthetase of the cycle could not be identified within this thesis. Additionally, studies by Ramos-Vera *et al.*, 2011 supported the fact that heterologous expression of an active form of this enzyme is not trivial. Therefore, other expression systems should be taken into consideration, such as those developed for *Sulfolobales*, yeast or insect cells. Alternatively, one attempt to obtain an active 4-hydroxybutyryl-CoA synthetase is to isolate the enzyme from *I. hospitalis* cell extracts.

Besides a putative phosphate storage, FIB-SEM analysis of *I. hospitalis* revealed a second type of inclusions (Heimerl, 2014). These inclusions might contain PHB, which might represent a further storage substance of *I. hospitalis*. The single steps of PHB formation could be measured biochemically in cell extracts of *I. hospitalis* or in recombinantly expressed versions of these enzymes. Additionally, it could be attempted to detect PHB via light microscopy using lipophilic dyes, such as 'Sudan black'. When one of the approached methods would succeed in identifying PHB inclusions, these inclusions could be isolated from cell extracts via glycerol gradient centrifugation.

This study is only one further step into understanding the physiology of *I. hospitalis*. A main future objective should be the establishment of a genetic system for *I. hospitalis*. This might help to facilitate immuno localization experiments.

Supplementary

Please find attached a DVD containing the following data:

1. **Bioinformatics:** The folder contains additional data concerning enzymes of *I. hospitalis* and *I. islandicus*, including predicted 3D structures (pdb-files), additional data obtained from the Phyre database and cloning information.

2. **EM:** The folder contains video sequences and additional snapshots of a 3D reconstruction of an *I. hospitalis* cell labeled with an antibody directed against the ACS and a video sequence and additional snapshots of a 3D reconstruction of an *I. hospitalis* cell labeled with an antibody directed against the protein Igni_0475 (supporting data section III.3).

Nomenclature

1° AB	Primary antibody
2° AB	Secondary antibody
2D	Two-dimensional
3-HP bicycle	3-hyroxypropionate bicycle
3-HP/4-HB cycle	3-hyroxypropionate/4-hydroxybutyrate cycle
3D	Three-dimensional
A. fulgidus	*Archaeoglobus fulgidus*
C. auranticus	*Chloroflexus auranticus*
C. limicola	*Chlorobium limicola*
E. coli	*Escherichia coli*
H. thermophilus	*Hydrogenobacter thermophilus*
I. hospitalis	*Ignicoccus hospitalis*
M. cuprina	*Metallosphaera cuprina*
M. sedula	*Metallosphaera sedula*
M. thermoautotrophicus	*Methanothermobacter thermoautotrophicus*
N. equitans	*Nanoarchaeaum equitans*
P. fumarii	*Pyrolobus fumarii*
S. acidocaldarius	*Sulfolobus acidocaldarius*
S. islandicus	*Sulfolobus islandicus*
aa	Amino acids
ACS	Acetyl-CoA synthetase
AI	Autoinduction
AMP	Adenosine monophosphate
AMPSO	3-([1,1-Dimethyl-2-hydroxyethyl]amino)-2-hydroxypropanesulfonic acid
APS	Ammonium persulfate
ATP	Adenosine-5'-triphosphate dihydrate
BLAST	Basic Local Alignment Search Tool
BSA	Bovine serum albumin
CA	Carbonic anhydrase
Calvin cycle	Calvin Benson Bassham cycle
CCM	carbon concentrating mechanism

CoA	Coenzyme A
DC/4-HB cycle	Dicarboxylate/4-hydroxybutyrate cycle
DHQ	Dehydroquinate
DNA	Deoxyribonucleic acid
DnD	DMSO and DTT
DTNB	5,5'-Dithiobis-(2-Nitrobenzoic acid)
DTT	1,4-Dithiothreitol
e-value	Expect value
EDTA	Ethylenediaminetetraacetic acid
ET	Electron tomography
FAD	Flavin adenine dinucleotide
FIB	Focused ion beam
FSB	Frozen Stock Buffer
GAM	Goat anti Mouse
GAR	Goat anti Rabbit
GTE	Glucose/Tris/EDTA
h	Hours
HEPES	4-(2-Hydroxyethyl)-1-piperazineethanesulfonic acid
HP	Heat precipitation
HRP	Horse Radish Peroxidase
IgG	Immunoglobulin G
Ihomp	*Ignicoccus hospitalis* outer membrane protein
IMC	Intermembrane compartment
IP	Immuno precipitation
IPTG	Isopropyl β-D-1-thiogalactopyranoside
kDa	Kilodalton
LDH	Lactate dehydrogenase
LEW	Lysis-Equilibration-Wash Buffer
MALDI	Matrix-assisted laser desorption/ionization
MAMMOTH	Matching molecular models obtained from theory
MDH	Malate dehydrogenase
MES	2-(N-morpholino)ethanesulfonic acid
min	Minutes
MOPS	3-(N-morpholino)propanesulfonic acid
MS	Mass Spectrometry
NAD	Nicotinamide adenine dinucleotide hydrate
NADH	Nicotinamide adenine dinucleotide phosphate
NADH	Nicotinamide adenine dinucleotide

NADP ..... Nicotinamide adenine dinucleotide phosphate
OCM ..... outer cellular membrane
PBS ..... Phosphate buffered saline
PCR ..... Polymerase chain reaction
PEP ..... Phosphoenolpyruvate
PHB ..... Polyhydroxybutyrate
S-layer ..... Surface-layer
SBF ..... Serial block face
SDS ..... Sodium dodecyl sulfate
SEM ..... Scanning electron microscopy
SME ..... Synthetic sea water
SSR ..... Succinic semialdehyde reductase
TAE ..... Tris-acetate-EDTA
TBS ..... Tris buffered saline
TBS-T ..... Tris buffered saline and Tween
TE ..... Tris/EDTA
TED ..... Tris-carboxymethyl ethylene diamine
TEM ..... Transmission electron microscopy
TEMED ..... Tetramethylethylenediamine
TFB ..... Transformation Buffer
TOF ..... Time Of Flight
Tris ..... Tris(hydroxymethyl)aminomethane
UAc ..... Uranyl acetate
UV ..... Ultraviolet
VOLTEX ..... Volume texturing

List of Figures

List of Tables

Bibliography

Alber, B., M. Olinger, A. Rieder, D. Kockelkorn, B. Jobst, M. Hügler, and G. Fuchs (2006). "Malonyl-coenzyme A reductase in the modified 3-hydroxypropionate cycle for autotrophic carbon fixation in archaeal *Metallosphaera* and *Sulfolobus spp.*" eng.
In: *J Bacteriol* 188.24, pp. 8551–8559.

Anderson, A. J. and E. A. Dawes (1990). "Occurrence, metabolism, metabolic role, and industrial uses of bacterial polyhydroxyalkanoates." In: *Microbiol Rev* 54.4, pp. 450–472.

Aoshima, M. (2007). "Novel enzyme reactions related to the tricarboxylic acid cycle: phylogenetic/functional implications and biotechnological applications."
In: *Appl Microbiol Biotechnol* 75.2, pp. 249–255.

Badger, M. R. and G. D. Price (2003). "CO2 concentrating mechanisms in cyanobacteria: molecular components, their diversity and evolution." In: *J Exp Bot* 54.383, pp. 609–622.

Bar-Even, A., E. Noor, and R. Milo (2012).
"A survey of carbon fixation pathways through a quantitative lens."
In: *J Exp Bot* 63.6, pp. 2325–2342. URL: ..

Baumeister, W. (2002).
"Electron tomography: towards visualizing the molecular organization of the cytoplasm."
In: *Curr Opin Struct Biol* 12.5, pp. 679–684.

Berg, I. A. (2011).
"Ecological aspects of the distribution of different autotrophic CO_2 fixation pathways."
In: *Appl Environ Microbiol* 77.6, pp. 1925–1936.

Berg, I. A., D. Kockelkorn, W. Buckel, and G. Fuchs (2007).
"A 3-hydroxypropionate/4-hydroxybutyrate autotrophic carbon dioxide assimilation pathway in Archaea." In: *Science* 318.5857, pp. 1782–1786.

Berg, I. A., D. Kockelkorn, W. H. Ramos-Vera, R. F. Say, J. Zarzycki, M. Hügler, B. E. Alber, and G. Fuchs (2010a). "Autotrophic carbon fixation in Archaea."
In: *Nat Rev Microbiol* 8.6, pp. 447–460.

Berg, I. A., W. H. Ramos-Vera, A. Petri, H. Huber, and G. Fuchs (2010b).
"Study of the distribution of autotrophic CO_2 fixation cycles in Crenarchaeota."
In: *Microbiology* 156.Pt 1, pp. 256–269.

Birnboim, H. C. and J. Doly (1979).
"A rapid alkaline extraction procedure for screening recombinant plasmid DNA."
In: *Nucleic Acids Res* 7.6, pp. 1513–1523.

Blum, H., H. Beier, and H. J. Gross (1987).
"Improved silver staining of plant proteins, RNA and DNA in polyacrylamide gels".
In: *electrophoresis* 8.2, pp. 93–99.

Bornhorst, J. A. and J. J. Falke (2000).
"Purification of proteins using polyhistidine affinity tags." eng.
In: *Methods Enzymol* 326, pp. 245–254.

Bradford, M. M. (1976). "A rapid and sensitive method for the quantitation of microgram quantities of protein utilizing the principle of protein-dye binding." In: *Anal Biochem* 72, pp. 248–254.

Burghardt, T., D. J. Näther, B. Junglas, H. Huber, and R. Rachel (2007).
"The dominating outer membrane protein of the hyperthermophilic Archaeum *Ignicoccus hospitalis*: a novel pore-forming complex." In: *Mol Microbiol* 63.1, pp. 166–176.

Burghardt, T., M. Saller, S. Gürster, D. Müller, C. Meyer, U. Jahn, E. Hochmuth, R. Deutzmann, F. Siedler, P. Babinger, R. Wirth, H. Huber, and R. Rachel (2008).
"Insight into the proteome of the hyperthermophilic Crenarchaeon *Ignicoccus hospitalis*: the major cytosolic and membrane proteins." In: *Arch Microbiol* 190.3, pp. 379–394.

Cannon, G. C., S. Heinhorst, and C. A. Kerfeld (2010).
"Carboxysomal carbonic anhydrases: Structure and role in microbial CO_2 fixation."
In: *Biochim Biophys Acta* 1804.2, pp. 382–392.

Charnock, C., U. H. Refseth, and R. Sirevåg (1992).
"Malate dehydrogenase from *Chlorobium vibrioforme*, *Chlorobium tepidum*, and *Heliobacterium gestii*: purification, characterization, and investigation of dinucleotide binding by dehydrogenases by use of empirical methods of protein sequence analysis."
In: *J Bacteriol* 174.4, pp. 1307–1313.

Collins, V. P., B. Arborgh, and U. Brunk (1977).
"A comparison of the effects of three widely used glutaraldehyde fixatives on cellular volume and structure. A TEM, SEM, Volumetric and Cytochemical Study."
In: *Acta Pathol Microbiol Scand A* 85A.2, pp. 157–168.

Cottrell, J. S. and U. London (1999). "Probability-based protein identification by searching sequence databases using mass spectrometry data". In: *electrophoresis* 20.18, pp. 3551–3567.

Danscher, G. (1981). "Localization of gold in biological tissue. A photochemical method for light and electronmicroscopy." In: *Histochemistry* 71.1, pp. 81–88.

Daxer, S. (2011). "Lokalisation stoffwechselrelevanter Enzymkomplexe sowie Anreicherung einer membrangebundenen Pyrophosphatase in Vertretern der archaeellen Gattung *Ignicoccus*". MA thesis. University of Regensburg, Regensburg, Germany.

Del Castillo, P., M. L. Molero, J. M. Ferrer, and J. C. Stockert (1986). "Autofluorescence and induced fluorescence in Epon embedded tissue sections". In: *Histochemistry* 85.5, pp. 439–440.

Denk, W. and H. Horstmann (2004). "Serial block-face scanning electron microscopy to reconstruct three-dimensional tissue nanostructure". In: *PLoS biology* 2.11, e329.

Dobrinski, K. P., D. L. Longo, and K. M. Scott (2005). "The carbon-concentrating mechanism of the hydrothermal vent chemolithoautotroph *Thiomicrospira crunogena*". In: *Journal of bacteriology* 187.16, pp. 5761–5766.

Donohoe, B. S., S. Mogelsvang, and L. A. Staehelin (2006). "Electron tomography of ER, Golgi and related membrane systems." In: *Methods* 39.2, pp. 154–162.

Dridi, B., M. L. Fardeau, B. Ollivier, D. Raoult, and M. Drancourt (2012). "*Methanomassiliicoccus luminyensis gen. nov., sp. nov.*, a methanogenic archaeon isolated from human faeces." In: *Int J Syst Evol Microbiol* 62.Pt 8, pp. 1902–1907.

Erb, T. J., V. Brecht, G. Fuchs, M. Müller, and B. E. Alber (2009). "Carboxylation mechanism and stereochemistry of crotonyl-CoA carboxylase/reductase, a carboxylating enoyl-thioester reductase." In: *Proc Natl Acad Sci U S A* 106.22, pp. 8871–8876.

Ettema, T. J. G., K. S. Makarova, G. L. Jellema, H. J. Gierman, E. V. Koonin, M. A. Huynen, W. M. De Vos, and J. Van Der Oost (2004). "Identification and functional verification of archaeal-type phosphoenolpyruvate carboxylase, a missing link in archaeal central carbohydrate metabolism". In: *Journal of bacteriology* 186.22, pp. 7754–7762.

Evans, M. C., B. B. Buchanan, and D. I. Arnon (1966). "A new ferredoxin-dependent carbon reduction cycle in a photosynthetic bacterium." In: *Proceedings of the National Academy of Sciences of the United States of America* 55.4, p. 928.

Flechsler, J. (2010). "Immunlokalisation von Proteinkomplexen und Enzymen an Isolaten der hyperthermophilen Archaeen der Gattung *Ignicoccus*".
MA thesis. University of Regensburg, Regensburg, Germany.

Frank, J. (1992). "Introduction: Principles in electron tomography". In: *Electron Tomography*.
Ed. by J. Frank. New York, Plenum Press, pp. 1–13.

Fuchs, G. (1986). "CO_2 fixation in acetogenic bacteria: variations on a theme".
In: *FEMS Microbiol. Rev* 39.18, p. 1.

— (2011).
"Alternative pathways of carbon dioxide fixation: insights into the early evolution of life?"
In: *Annu Rev Microbiol* 65, pp. 631–658.

Fuchs, G. and Ivan A. Berg (2014). "Unfamiliar metabolic links in the central carbon metabolism."
In: *J Biotechnol* 192, pp. 314–322.

Gallenberger, M. (2007). "Biochemische Untersuchungen zum Kohlenstoffmetabolismus im Organismensystem *Ignicoccus hospitalis* und *Nanoarchaeum equitans*".
MA thesis. University of Regensburg, Regensburg, Germany.

Giannone, R. J., H. Huber, T. Karpinets, T. Heimerl, U. Küper, R. Rachel, M. Keller, R. L. Hettich, and M. Podar (2011). "Proteomic characterization of cellular and molecular processes that enable the *Nanoarchaeum equitans–Ignicoccus hospitalis* relationship."
In: *PLoS One* 6.8, e22942.

Giannone, R. J., L. L. Wurch, T. Heimerl, S. Martin, Z. Yang, H. Huber, R. Rachel, R. L. Hettich, and M. Podar (2014). "Life on the edge: functional genomic response of *Ignicoccus hospitalis* to the presence of *Nanoarchaeum equitans*." In: *ISME J.*

Griffiths, G. (1993). *Fine Structure Immunocytochemistry*. 1. Aufl.
Springer Verlag, Berlin, Heidelberg.

Griffiths, G. and H. Hoppeler (1986). "Quantitation in immuncytochemistry, correlation of immunogold labelling to absolute numbers of membrane antigens."
In: *J. Histochem. Cytochem* 34, pp. 1389–1398.

Gürster, S. (2007). "*Nanoarchaeum equitans*: Versuche zur Reindarstellung und strukturellen und proteinbiochemischen Charakterisierung".
MA thesis. University of Regensburg, Regensburg, Germany.

Hamerly, T., B. P. Tripet, M. Tigges, R. J. Giannone, L. Wurch, R. L. Hettich,
V. Podar M.and Copié, and B. Bothner (2014).
"Untargeted metabolomics studies employing NMR and LC–MS reveal metabolic coupling

between *Nanoarcheum equitans* and its archaeal host *Ignicoccus hospitalis*".
In: *Metabolomics*, pp. 1–13.

Hanahan, D. (1983). "Studies on transformation of Escherichia coli with plasmids."
In: *J Mol Biol* 166.4, pp. 557–580.

Hawkins, A. S., Y. Han, R. K. Bennett, M. W. W. Adams, and R. M. Kelly (2013). "Role of 4-hydroxybutyrate-CoA synthetase in the CO_2 fixation cycle in thermoacidophilic Archaea."
In: *J Biol Chem* 288.6, pp. 4012–4022.

Heimerl, T. (2009). "Ultrastruktur der Co-Kultur KIN4/M: Serienschnitte, 3D-Modelle und Immunmarkierungs-versuche". MA thesis. University of Regensburg, Regensburg, Germany.

— (2014). "*Ignicoccus* und *Nanoarchaeum*: 3D-Struktur und Proteom".
PhD thesis. University of Regensburg, Regensburg, Germany.

Hoenger, A. and J. R. McIntosh (2009).
"Probing the macromolecular organization of cells by electron tomography".
In: *Current opinion in cell biology* 21.1, pp. 89–96.

Hoppe, W. (1982). "Trace structure analysis, ptychography, phase tomography".
In: *Ultramicroscopy* 10.3, pp. 187–198.

Huber, H., S. Burggraf, T. Mayer, I. Wyschkony, R. Rachel, and K. O. Stetter (2000).
"*Ignicoccus gen. nov.*, a novel genus of hyperthermophilic, chemolithoautotrophic Archaea, represented by two new species, *Ignicoccus islandicus sp. nov.* and *Ignicoccus pacificus sp nov.* and *Ignicoccus pacificus sp. nov.*" In: *Int J Syst Evol Microbiol* 50 Pt 6, pp. 2093–2100.

Huber, H., M. Gallenberger, U. Jahn, E. Eylert, I. A. Berg, D. Kockelkorn, W. Eisenreich, and G. Fuchs (2008). "A dicarboxylate/4-hydroxybutyrate autotrophic carbon assimilation cycle in the hyperthermophilic Archaeum *Ignicoccus hospitalis*."
In: *Proc Natl Acad Sci U S A* 105.22, pp. 7851–7856.

Huber, H., M. J. Hohn, R. Rachel, T. Fuchs, V. C. Wimmer, and Karl O. Stetter (2002).
"A new phylum of Archaea represented by a nanosized hyperthermophilic symbiont."
In: *Nature* 417.6884, pp. 63–67.

Huber, H., U. Küper, S. Daxer, and R. Rachel (2012).
"The unusual cell biology of the hyperthermophilic Crenarchaeon *Ignicoccus hospitalis*."
In: *Antonie Van Leeuwenhoek* 102.2, pp. 203–219.

Huberts, D. H. E. W. and I. J. van der Klei (2010).
"Moonlighting proteins: an intriguing mode of multitasking."
In: *Biochim Biophys Acta* 1803.4, pp. 520–525.

Hügler, M (2003). "Autotrophe CO_2-Fixierung in thermophilen Mikroorganismen". PhD thesis. Alberts-Ludwig-Universität Freiburg, Freiburg i. Br., Germany.

Hügler, M. and S. M. Sievert (2011). "Beyond the Calvin cycle: autotrophic carbon fixation in the ocean." In: *Ann Rev Mar Sci* 3, pp. 261–289.

Humbel, B. M., M. D. de Jong, W. H. Müller, and A. J. Verkleij (1998). "Pre-embedding immunolabeling for electron microscopy: an evaluation of permeabilization methods and markers." In: *Microsc Res Tech* 42.1, pp. 43–58.

Hyatt, A. D. (1991). "Immunogold labelling techniques". In: ed. by Oxford IRL Press. J.R. Harris. Chap. Electron microscopy in Biology: A practical approach, pp. 59–81.

Jahn, U. (2007). "Aspekte der Zellbiologie des archaeellen Wirt-Parasit-Systems *Ignicoccus hospitalis* und *Nanoarchaeum equitans*: Zentrale Stoffwechselwege, Lipide, Histone". PhD thesis. University of Regensburg, Regensburg, Germany.

Jahn, U., M. Gallenberger, W. Paper, B. Junglas, W. Eisenreich, K. O. Stetter, R. Rachel, and H. Huber (2008). "*Nanoarchaeum equitans* and *Ignicoccus hospitalis*: new insights into a unique, intimate association of two Archaea." In: *J Bacteriol* 190.5, pp. 1743–1750.

Jahn, U., H. Huber, W. Eisenreich, M. Hügler, and G. Fuchs (2007). "Insights into the autotrophic CO_2 fixation pathway of the archaeon *Ignicoccus hospitalis*: comprehensive analysis of the central carbon metabolism." In: *J Bacteriol* 189.11, pp. 4108–4119.

Jiménez, N. and J. A. Post (2012). "A novel approach for intracellular 3D immuno-labeling for electron tomography." In: *Traffic* 13.7, pp. 926–933.

Johnson, T. J. A. (1985). "Aldehyde fixatives: Quantification of acid-producing reactions". In: *Journal of electron microscopy technique* 2.2, pp. 129–138.

Junglas, B. (2006). "Die hyperthermophilen Archaeen *Ignicoccus sp.* KIN4/M und *Nanoarchaeum equitans*: Ultrastrukturelle und Immuncytochemische Untersuchungen an Ultradünnschnitten". MA thesis. University of Regensburg, Regensburg, Germany.

Junglas, B., A. Briegel, T. Burghardt, P. Walther, R. Wirth, H. Huber, and R. Rachel (2008). "*Ignicoccus hospitalis* and *Nanoarchaeum equitans*: ultrastructure, cell-cell interaction, and 3D reconstruction from serial sections of freeze-substituted cells and by electron cryotomography." In: *Arch Microbiol* 190.3, pp. 395–408.

Karreman, M. A., E. G. van Donselaar, H. C. Gerritsen, and A. J. Verrips C. T.and Verkleij (2011). "VIS2FIX: a high-speed fixation method for immuno-electron microscopy." In: *Traffic* 12.7, pp. 806–814.

Kaufman, A. J. and S. Xiao (2003). "High CO_2 levels in the Proterozoic atmosphere estimated from analyses of individual microfossils." In: *Nature* 425.6955, pp. 279–282.

Kawakami, R., H. Sakuraba, S. Goda, H. Tsuge, and T. Ohshima (2009). "Refolding, characterization and crystal structure of (S)-malate dehydrogenase from the hyperthermophilic Archaeon *Aeropyrum pernix*." In: *Biochim Biophys Acta* 1794.10, pp. 1496–1504.

Kellenberger, E., M. Dürrenberger, W. Villiger, E. Carlemalm, and M. Wurtz (1987). "The efficiency of immunolabel on Lowicryl sections compared to theoretical predictions." In: *J Histochem Cytochem* 35.9, pp. 959–969.

Kelley, L. A. and M. J. E. Sternberg (2009). "Protein structure prediction on the Web: a case study using the Phyre server." In: *Nat Protoc* 4.3, pp. 363–371.

Knott, G., H. Marchman, D. Wall, and B. Lich (2008). "Serial section scanning electron microscopy of adult brain tissue using focused ion beam milling." In: *J Neurosci* 28.12, pp. 2959–2964.

Kockelkorn, D. and G. Fuchs (2009). "Malonic semialdehyde reductase, succinic semialdehyde reductase, and succinyl-coenzyme A reductase from Metallosphaera sedula: enzymes of the autotrophic 3-hydroxypropionate/4-hydroxybutyrate cycle in *Sulfolobales*." In: *J Bacteriol* 191.20, pp. 6352–6362.

Könneke, M., D. M. Schubert, P. C. Brown, M. Hügler, S. Standfest, T. Schwander, L. Schada von Borzyskowski, T. J. Erb, D. A. Stahl, and I. A. Berg (2014). "Ammonia-oxidizing archaea use the most energy-efficient aerobic pathway for CO_2 fixation." In: *Proc Natl Acad Sci U S A* 111.22, pp. 8239–8244.

Kozbial, P. Z. and A. R. Mushegian (2005). "Natural history of S-adenosylmethionine-binding proteins." In: *BMC Struct Biol* 5, p. 19.

Kreuter, L. (2014). "Isolierung, Charakterisierung und Lokalisierung der ATP-Synthasen der archaeellen Genera *Ignicoccus* und *Nanoarchaeum*". PhD thesis. University of Regensburg, Regensburg, Germany.

Küper, U., C. Meyer, V. Müller, R. Rachel, and H. Huber (2010). "Energized outer membrane and spatial separation of metabolic processes in the hyperthermophilic Archaeon *Ignicoccus hospitalis*." In: *Proc Natl Acad Sci U S A* 107.7, pp. 3152–3156.

Ladinsky, M. S. and K. E. Howell (2007). "Electron tomography of immunolabeled cryosections." In: *Methods Cell Biol* 79, pp. 543–558.

Laemmli, U. K. (1970).
"Cleavage of structural proteins during the assembly of the head of bacteriophage T4."
In: *Nature* 227.5259, pp. 680–685.

Lange, M. (2009). "Neue Hochtemperatur-Organismen von Lesbos und dem Ostpazifischen-Rücken". MA thesis. University of Regensburg, Regensburg, Germany.

Langelandsvik, A. S., I. H. Steen, N. K. Birkeland, and T. Lien (1997). "Properties and primary structure of a thermostable L-malate dehydrogenase from *Archaeoglobus fulgidus*."
In: *Arch Microbiol* 168.1, pp. 59–67.

Lee, B. I., C. Chang, S. J. Cho, S. H. Eom, K. K. Kim, Y. G. Yu, and S. W. Suh (2001).
"Crystal structure of the MJ0490 gene product of the hyperthermophilic archaebacterium *Methanococcus jannaschii*, a novel member of the lactate/malate family of dehydrogenases."
In: *J Mol Biol* 307.5, pp. 1351–1362.

Lee, R. M., R. McKenzie, K. Kobayashi, R. E. Garfield, J. B. Forrest, and E. E. Daniel (1982).
"Effects of glutaraldehyde fixative osmolarities on smooth muscle cell volume, and osmotic reactivity of the cells after fixation." In: *J Microsc* 125.Pt 1, pp. 77–88.

Lesk, A. M. (1995). "NAD-binding domains of dehydrogenases."
In: *Curr Opin Struct Biol* 5.6, pp. 775–783.

Ljungdahl, L. G. (1986). "The autotrophic pathway of acetate synthesis in acetogenic bacteria."
In: *Annu Rev Microbiol* 40, pp. 415–450.

Markert, S., C. Arndt, H. Felbeck, D. Becher, S. M. Sievert, M. Hügler, D. Albrecht, J. Robidart, S. Bench, R. A. Feldman, M. Hecker, and T. Schweder (2007).
"Physiological proteomics of the uncultured endosymbiont of *Riftia pachyptila*."
In: *Science* 315.5809, pp. 247–250.

Martin, W., J. Baross, D. Kelley, and M. J. Russell (2008).
"Hydrothermal vents and the origin of life". In: *Nature Reviews Microbiology* 6.11, pp. 805–814.

Matsko, N. and M. Mueller (2005). "Epoxy resin as fixative during freeze-substitution".
In: *Journal of structural biology* 152.2, pp. 92–103.

Matsumura, H., K. Izui, and K. Mizuguchi (2006).
"A novel mechanism of allosteric regulation of archaeal phosphoenolpyruvate carboxylase: a combined approach to structure-based alignment and model assessment".
In: *Protein Engineering Design and Selection* 19.9, pp. 409–419.

Mayer, F., U. Küper, C. Meyer, S. Daxer, V. Müller, R. Rachel, and H. Huber (2012). "AMP-forming acetyl coenzyme A synthetase in the outermost membrane of the hyperthermophilic crenarchaeon *Ignicoccus hospitalis*." In: *J Bacteriol* 194.6, pp. 1572–1581.

McCollom, T. M. and J. P. Amend (2005). "A thermodynamic assessment of energy requirements for biomass synthesis by chemolithoautotrophic micro-organisms in oxic and anoxic environments". In: *Geobiology* 3.2, pp. 135–144.

McDonald, K. L. (2014). "Out with the old and in with the new: rapid specimen preparation procedures for electron microscopy of sectioned biological material." In: *Protoplasma* 251.2, pp. 429–448.

McDonald, K. L. and R. I. Webb (2011). "Freeze substitution in 3 hours or less." In: *J Microsc* 243.3, pp. 227–233.

McEwen, B. F. and M. Marko (2001). "The emergence of electron tomography as an important tool for investigating cellular ultrastructure". In: *Journal of Histochemistry & Cytochemistry* 49.5, pp. 553–563.

Melan, M. A. and G. Sluder (1992). "Redistribution and differential extraction of soluble proteins in permeabilized cultured cells. Implications for immunofluorescence microscopy." In: *J Cell Sci* 101 (Pt 4), pp. 731–743.

Meyer, C. (2010). "Die Fibers von *Ignicoccus hospitalis*: Ultrastruktur, Verankerung und molekularbiologische Untersuchungen". PhD thesis. University of Regensburg, Regensburg, Germany.

Meyer, C., T. Heimerl, R. Wirth, A. Klingl, and Reinhard Rachel (2014). "The Iho670 fibers of *Ignicoccus hospitalis* are anchored in the cell by a spherical structure located beneath the inner membrane." In: *J Bacteriol* 196.21, pp. 3807–3815.

Meyer, M. and H. Griffiths (2013). "Origins and diversity of eukaryotic CO_2-concentrating mechanisms: lessons for the future". In: *Journal of experimental botany* 64.3, pp. 769–786.

Miller, J. H (1972). *Experiments in Molecular Genetics*. New York, Cold Spring Harbor Laboratory.

Miyake, J. A. and A. Colquhoun (2012). "Electron microscopy and immunogold labelling of proteins involved in brain tumour growth and invasion". In:

Moissl-Eichinger, C. and H. Huber (2011). "Archaeal symbionts and parasites." In: *Curr Opin Microbiol* 14.3, pp. 364–370.

Moroney, J. V. and R. A. Ynalvez (2007).
"Proposed carbon dioxide concentrating mechanism in *Chlamydomonas reinhardtii*."
In: *Eukaryot Cell* 6.8, pp. 1251–1259.

Morphew, M. K. (2007). "3D immunolocalization with plastic sections."
In: *Methods Cell Biol* 79, pp. 493–513.

Mukherjee, A. and C. M. Schroeder (2015).
"Flavin-based fluorescent proteins: emerging paradigms in biological imaging."
In: *Curr Opin Biotechnol* 31, pp. 16–23.

Müller, D. W., C. Meyer, S. Gürster, U. Küper, H. Huber, R. Rachel, G. Wanner, R. Wirth, and A. Bellack (2009).
"The Iho670 fibers of *Ignicoccus hospitalis*: a new type of archaeal cell surface appendage."
In: *J Bacteriol* 191.20, pp. 6465–6468.

Müller-Reichert, T., I. Sassoon, E. O'Toole, M. Romao, A. J. Ashford, A. A. Hyman, and C. Antony (2003). "Analysis of the distribution of the kinetochore protein Ndc10p in Saccharomyces cerevisiae using 3-D modeling of mitotic spindles." In: *Chromosoma* 111.7, pp. 417–428.

Mullis, K. B. and F. A. Faloona (1987).
"Specific synthesis of DNA in vitro via a polymerase-catalyzed chain reaction."
In: *Methods Enzymol* 155, pp. 335–350.

Murk, J L A N., G. Posthuma, A. J. Koster, H. J. Geuze, A. J. Verkleij, M. J. Kleijmeer, and B. M. Humbel (2003). "Influence of aldehyde fixation on the morphology of endosomes and lysosomes: quantitative analysis and electron tomography." In: *J Microsc* 212.Pt 1, pp. 81–90.

Musrati, R. A., M. Kollárová, N. Mernik, and D. Mikulásová (1998).
"Malate dehydrogenase: distribution, function and properties."
In: *Gen Physiol Biophys* 17.3, pp. 193–210.

Naß, B., U. Pöll, J. D. Langer, L. Kreuter, U. Küper, J. Flechsler, T. Heimerl, R. Rachel, H. Huber, and A. Kletzin (2014). "Three multihaem cytochromes c from the hyperthermophilic archaeon *Ignicoccus hospitalis*: purification, properties and localization."
In: *Microbiology* 160.Pt 6, pp. 1278–1289.

Natale, P., T. Brüser, and A. J. M. Driessen (2008). "Sec- and Tat-mediated protein secretion across the bacterial cytoplasmic membrane–distinct translocases and mechanisms."
In: *Biochim Biophys Acta* 1778.9, pp. 1735–1756.

Neuhoff, V., N. Arold, D. Taube, and W. Ehrhardt (1988).
"Improved staining of proteins in polyacrylamide gels including isoelectric focusing gels with

clear background at nanogram sensitivity using Coomassie Brilliant Blue G-250 and R-250". In: *Electrophoresis* 9.6, pp. 255–262.

Nyquist, H. (1928). "Certain topics in telegraph transmission theory". In: *American Institute of Electrical Engineers, Transactions of the* 47.2, pp. 617–644.

Paper, W., U. Jahn, M. J. Hohn, M. Kronner, D. J. Näther, T. Burghardt, R. Rachel, K. O. Stetter, and H. Huber (2007). "*Ignicoccus hospitalis sp. nov.*, the host of 'Nanoarchaeum equitans'." In: *Int J Syst Evol Microbiol* 57.Pt 4, pp. 803–808.

Patel, H. M., J. L. Kraszewski, and B. Mukhopadhyay (2004). "The phosphoenolpyruvate carboxylase from *Methanothermobacter thermautotrophicus* has a novel structure". In: *Journal of bacteriology* 186.15, pp. 5129–5137.

Patel, S. S. and D. R. Walt (1987). "Substrate specificity of acetyl coenzyme A synthetase." In: *Journal of Biological Chemistry* 262.15, pp. 7132–7134.

Payne, S. H, S. Bonissone, S. Wu, R. N. Brown, D. N. Ivankov, D. Frishman, L. Paša-Tolić, R. D. Smith, and P. A. Pevzner (2012). "Unexpected diversity of signal peptides in prokaryotes". In: *MBio* 3.6, e00339–12.

Peters, P. J., E. Bos, and A. Griekspoor (2006). "Cryo-immunogold electron microscopy." In: *Curr Protoc Cell Biol* Chapter 4, Unit 4.7.

Pezacka, E. and H. G. Wood (1984). "Role of carbon monoxide dehydrogenase in the autotrophic pathway used by acetogenic bacteria." In: *Proc Natl Acad Sci U S A* 81.20, pp. 6261–6265.

Pieulle, L., V. Magro, and E. C. Hatchikian (1997). "Isolation and analysis of the gene encoding the pyruvate-ferredoxin oxidoreductase of Desulfovibrio africanus, production of the recombinant enzyme in *Escherichia coli*, and effect of carboxy-terminal deletions on its stability." In: *J Bacteriol* 179.18, pp. 5684–5692.

Podar, M., I. Anderson, K. S. Makarova, J. G. Elkins, N. Ivanova, M. A. Wall, A. Lykidis, K. Mavromatis, H. Sun, M. E. Hudson, W. Chen, C. Deciu, D. Hutchison, J. R. Eads, A. Anderson, F. Fernandes, E. Szeto, A. Lapidus, N. C. Kyrpides, M. H Saier Jr., P. M. Richardson, R. Rachel, H. Huber, J. A. Eisen, E. V. Koonin, M. Keller, and K. O. Stetter (2008). "A genomic analysis of the archaeal system *Ignicoccus hospitalis-Nanoarchaeum equitans*." In: *Genome Biol* 9.11, R158.

Price, G. D., S. M. Howitt, K. Harrison, and M. R. Badger (1993). "Analysis of a genomic DNA region from the cyanobacterium *Synechococcus sp.* strain PCC7942 involved in carboxysome assembly and function." In: *J Bacteriol* 175.10, pp. 2871–2879.

Queiroz-Claret, C. and O. Queiroz (1992). "Malate dehydrogenase forms a complex with and activates phosphoenolpyruvate carboxylase from crassulacean acid metabolism plants". In: *Journal of plant physiology* 139.4, pp. 385–389.

Rachel, R., C. Meyer, A. Klingl, S. Gürster, T. Heimerl, N. Wasserburger, T. Burghardt, U. Küper, A. Bellack, S. Schopf, R. Wirth, H. Huber, and G. Wanner (2010). "Analysis of the ultrastructure of archaea by electron microscopy." In: *Methods Cell Biol* 96, pp. 47–69.

Rachel, R., I. Wyschkony, S. Riehl, and H. Huber (2002). "The ultrastructure of *Ignicoccus*: evidence for a novel outer membrane and for intracellular vesicle budding in an archaeon." In: *Archaea* 1.1, pp. 9–18.

Ramakrishnan, V. and M. W. W. Adams (1995). "Preparation of genomic DNA from sulfur-dependent hyperthermophilic Archaea". In: *Archaea, A Laboratory Manual: Thermophiles*, pp. 95–96.

Ramos-Vera, W. H., I. A. Berg, and G. Fuchs (2009). "Autotrophic carbon dioxide assimilation in *Thermoproteales* revisited." In: *J Bacteriol* 191.13, pp. 4286–4297.

Ramos-Vera, W. H., M. Weiss, E. Strittmatter, D. Kockelkorn, and G. Fuchs (2011). "Identification of missing genes and enzymes for autotrophic carbon fixation in Crenarchaeota." In: *J Bacteriol* 193.5, pp. 1201–1211.

Rasmussen, B., I. R. Fletcher, J. J. Brocks, and M. R. Kilburn (2008). "Reassessing the first appearance of eukaryotes and Cyanobacteria." In: *Nature* 455.7216, pp. 1101–1104.

Raven, John A., Charles S. Cockell, and Christina L. De La Rocha (2008). "The evolution of inorganic carbon concentrating mechanisms in photosynthesis." In: *Philos Trans R Soc Lond B Biol Sci* 363.1504, pp. 2641–2650.

Richards, R. G., G. R. Owen, M. Riehle, A. Gwynn, and A. S. G. Curtis (2001). "Immunogold labelling of fibroblast focal adhesion sites visualised in fixed material using scanning electron microscopy, and living, using internal reflection microscopy". In: *Cell biology international* 25.12, pp. 1237–1249.

Ripper, D., H. Schwarz, and Y. D. Stierhof (2008). "Cryo-section immunolabelling of difficult to preserve specimens: advantages of cryofixation, freeze-substitution and rehydration." In: *Biol Cell* 100.2, pp. 109–123.

Rossmann, M. G., D. Moras, and K. W. Olsen (1974).
"Chemical and biological evolution of nucleotide-binding protein."
In: *Nature* 250.463, pp. 194–199.

Saiki, R. K., D. H. Gelfand, S. Stoffel, S. J. Scharf, R. Higuchi, G. T. Horn, K. B. Mullis, and H. A. Erlich (1988).
"Primer-directed enzymatic amplification of DNA with a thermostable DNA polymerase".
In: *Science* 239.4839, pp. 487–491.

Sako, Y., K. Takai, T. Nishizaka, and Y. Ishida (1997). "Biochemical relationship of phosphoenolpyruvate carboxylases (PEPCs) from thermophilic Archaea".
In: *FEMS microbiology letters* 153.1, pp. 159–165.

Sako, Y., K. Takai, A. Uchida, and Y. Ishida (1996).
"Purification and characterization of phosphoenolpyruvate carboxylase from the hyperthermophilic Archaeon *Methanothermus sociabilis*". In: *FEBS letters* 392.2, pp. 148–152.

Sambrook, J., E. F. Fritsch, and T. Maniatis (1989). *Molecular cloning : a laboratory manual*.
2nd ed. New York : Cold Spring Harbor Laboratory Press.

Schägger, H. and G. Von Jagow (1987). "Tricine-sodium dodecyl sulfate-polyacrylamide gel electrophoresis for the separation of proteins in the range from 1 to 100 kDa".
In: *Analytical biochemistry* 166.2, pp. 368–379.

Schmid, G., G. Mathiesen, M. O. Arntzen, V G H. Eijsink, and M. Thomm (2013).
"Experimental and computational analysis of the secretome of the hyperthermophilic Archaeon *Pyrococcus furiosus*." In: *Extremophiles* 17.6, pp. 921–930.

Schuchmann, K. and V. Müller (2014). "Autotrophy at the thermodynamic limit of life: a model for energy conservation in acetogenic bacteria." In: *Nat Rev Microbiol* 12.12, pp. 809–821.

Schwarz, H. and H. Hohenberg (2001). "Immuno-electron Microscopy". In: *eLS*.

Selmer, T., A. Willanzheimer, and M. Hetzel (2002). "Propionate CoA-transferase from Clostridium propionicum. Cloning of gene and identification of glutamate 324 at the active site."
In: *Eur J Biochem* 269.1, pp. 372–380.

Shannon, C. E. (1949). "Communication in the presence of noise".
In: *Proceedings of the IRE* 37.1, pp. 10–21.

Shively, J. M., F. Ball, D. H. Brown, and R. E. Saunders (1973). "Functional organelles in prokaryotes: polyhedral inclusions (carboxysomes) of *Thiobacillus neapolitanus*".
In: *Science* 182.4112, pp. 584–586.

Simon, E. J. and D. Shemin (1953). "The preparation of S-succinyl coenzyme A".
In: *Journal of the American Chemical Society* 75.10, pp. 2520–2520.

Sjorstrand, F. S. (1958). "Ultrastructure of retinal rod synapses of the guinea pig eye as revealed by three-dimensional reconstructions from serial sections." eng.
In: *J Ultrastruct Res* 2.1, pp. 122–170.

Smith, K. S. and J. G. Ferry (2000). "Prokaryotic carbonic anhydrases."
In: *FEMS Microbiol Rev* 24.4, pp. 335–366.

Snapp, E. (2005). "Design and use of fluorescent fusion proteins in cell biology."
In: *Curr Protoc Cell Biol* Chapter 21, Unit 21.4.

Stadtman, E. R. (1957).
"Preparation and assay of acyl coenzyme A and other thiol esters; use of hydroxylamine".
In: *Methods in enzymology* 3, pp. 931–941.

Stevens, J. K., T. L. Davis, N. Friedman, and P. Sterling (1980). "A systematic approach to reconstructing microcircuitry by electron microscopy of serial sections".
In: *Brain Research Reviews* 2.1, pp. 265–293.

Stierhof, Y. D. and H. Schwarz (1989). "Labeling properties of sucrose-infiltrated cryosections."
In: *Scanning Microsc Suppl* 3, pp. 35–46.

Stierhof, Y. D., H. Schwarz, and H. Frank (1986).
"Transverse sectioning of plastic-embedded immunolabeled cryosections: morphology and permeability to protein A-colloidal gold complexes."
In: *J Ultrastruct Mol Struct Res* 97.1-3, pp. 187–196.

Stirling, J. W. (1990). "Immuno- and affinity probes for electron microscopy: a review of labeling and preparation techniques." In: *J Histochem Cytochem* 38.2, pp. 145–157.

Strauss, G. and G. Fuchs (1993). "Enzymes of a novel autotrophic CO2 fixation pathway in the phototrophic bacterium *Chloroflexus aurantiacus*, the 3-hydroxypropionate cycle."
In: *Eur J Biochem* 215.3, pp. 633–643.

Stryer, L., J. M. Berg, and J. L. Tymoczko (2003). *Biochemie*. 5. Aufl.
Spektrum Akademischer Verlag GmbH Heidelberg, Berlin.

Studer, D., B. M. Humbel, and M. Chiquet (2008). "Electron microscopy of high pressure frozen samples: bridging the gap between cellular ultrastructure and atomic resolution."
In: *Histochem Cell Biol* 130.5, pp. 877–889.

Studier, F. W. (2005). "Protein production by auto-induction in high density shaking cultures."
In: *Protein Expr Purif* 41.1, pp. 207–234.

Tokuyasu, K. T. (1973). "A technique for ultracryotomy of cell suspensions and tissues." In: *J Cell Biol* 57.2, pp. 551–565.

Towbin, H., T. Staehelin, and J. Gordon (1979). "Electrophoretic transfer of proteins from polyacrylamide gels to nitrocellulose sheets: procedure and some applications". In: *Proceedings of the National Academy of Sciences* 76.9, pp. 4350–4354.

van Donselaar, E., G. Posthuma, D. Zeuschner, B. M. Humbel, and J. W. Slot (2007). "Immunogold labeling of cryosections from high-pressure frozen cells." In: *Traffic* 8.5, pp. 471–485.

van Niftrik, L. (2013). "Cell biology of unique anammox bacteria that contain an energy conserving prokaryotic organelle." In: *Antonie Van Leeuwenhoek* 104.4, pp. 489–497.

van Niftrik, L., M. van Helden, S. Kirchen, E. G. van Donselaar, H. R. Harhangi, R. I. Webb, J. A. Fuerst, H. J. M. Op den Camp, M. S. M. Jetten, and M. Strous (2010). "Intracellular localization of membrane-bound ATPases in the compartmentalized anammox bacterium 'Candidatus Kuenenia stuttgartiensis'." In: *Mol Microbiol* 77.3, pp. 701–715.

Vihinen, H., I. Belevich, and E. Jokitalo (2013). "Three dimensional electron microscopy of cellular organelles by serial block face SEM and ET". In: *Microsc. Anal* 27, pp. 7–10.

Villinger, C., H. Gregorius, C. Kranz, K. Höhn, C. Münzberg, G. von Wichert, B. Mizaikoff, G. Wanner, and P. Walther (2012). "FIB/SEM tomography with TEM-like resolution for 3D imaging of high-pressure frozen cells." In: *Histochem Cell Biol* 138.4, pp. 549–556.

Vonck, J., K. Y. Pisa, N. Morgner, B. Brutschy, and V. Müller (2009). "Three-dimensional structure of A_1A_0 ATP synthase from the hyperthermophilic archaeon *Pyrococcus furiosus* by electron microscopy." In: *J Biol Chem* 284.15, pp. 10110–10119.

Wanner, G., T. Schäfer, and U. Lütz-Meindl (2013). "3-D analysis of dictyosomes and multivesicular bodies in the green alga Micrasterias denticulata by FIB/SEM tomography". In: *Journal of structural biology* 184.2, pp. 203–211.

Ware, R. W. and V. LoPresti (1975). "Three-dimensional reconstruction from serial sections". In: *International review of cytology* 40, pp. 325–440.

Wasserburger, N. (2008). "Anzucht, elektronenmikroskopische Präparation und Darstellung der archaeellen Cokultur von *Ignicoccus hospitalis* und *Nanoarchaeum equitans*". MA thesis. University of Regensburg, Regensburg, Germany.

Waters, E., M. J. Hohn, I. Ahel, D. E. Graham, M. D. Adams, M. Barnstead, K. Y. Beeson, L. Bibbs, R. Bolanos, M. Keller, K. Kretz, X. Lin, E. Mathur, J. Ni, M. Podar, T. Richardson, G. G. Sutton, M. Simon, D. Soll, K. O. Stetter, J. M. Short, and M. Noordewier (2003). "The genome of *Nanoarchaeum equitans*: insights into early archaeal evolution and derived parasitism." In: *Proc Natl Acad Sci U S A* 100.22, pp. 12984–12988.

Wolpert, J. S. and M. L. Ernst-Fonberg (1975). "A multienzyme complex for CO_2 fixation." In: *Biochemistry* 14.6, pp. 1095–1102.

Wood, H. G. (1991). "Life with CO or CO_2 and H_2 as a source of carbon and energy." In: *The FASEB journal* 5.2, pp. 156–163.

Yu, X., C. Goforth, C. Meyer, R. Rachel, R. Wirth, G. F. Schröder, and E. H. Egelman (2012). "Filaments from *Ignicoccus hospitalis* show diversity of packing in proteins containing N-terminal type IV pilin helices." In: *J Mol Biol* 422.2, pp. 274–281.

Zeuschner, D., W. J C. Geerts, E. van Donselaar, B. M. Humbel, J. W. Slot, A. J. Koster, and J. Klumperman (2006). "Immuno-electron tomography of ER exit sites reveals the existence of free COPII-coated transport carriers." In: *Nat Cell Biol* 8.4, pp. 377–383.

Acknowledgments

Zum Schluss möchte ich Allen danken, die durch ihre tatkräftige Hilfe zum Gelingen dieser Arbeit beigetragen haben! Mein besonderer Dank gilt:

...meinem Doktorvater **Prof. Dr. Reinhard Rachel**, der mir die Möglichkeit gegeben hat dieses vielversprechende Thema zu bearbeiten. Danke für die hilfreichen Diskussionen, alle Freiheiten, das Vertrauen in meine Arbeit und die stetige Begeisterungsfähigkeit.

...**Prof. Dr. Ralph Witzgall** und **Prof. Dr. Michael Thomm**, für die freundliche Aufnahme und die Mölichkeit meine Doktorarbeit an ihren Lehrstühlen durchführen zu können.

...**Prof. Dr. Reinhard Wirth**, für die Übernahme des RIGeL Mentorats, die Unterstützung und die wertvollen Denkanstösse.

...**PD Dr. Ivan Berg** für die Unterstützung beim Thema CO_2 Fixierung. Vielen Dank für die freundliche Aufnahme in seiner Arbeitsgruppe, die gute Betreuung und die vielen hilfreichen Diskussionen und Gedankenanstösse. Vielen Dank auch an seine Mitarbeiter **Achim Mall**, **Philip Brown** und **Julia Otte** für die Durchführung zahlreicher Enzymtests und die geduldige Unterstützung während meines Laboraufenthaltes.

...**Dr. Harald Huber** für die vielen Tipps und Hinweise zur CO_2 Fixierung innerhalb des 'Igni-Nano' Seminars.

...**Dr. York-Dieter Stierhof** und **Rebecca Kühn** für die Anfertigung der 'Tokuyasu' Schnitte sowie die freundliche Aufnahme in seinem Labor. Das war mir eine grosse Hilfe.

...**Prof. Dr. Wolfgang Liebl**, für die Bereitschaft zur Übernahme des RIGeL Mentorats.

...**Thomas Heimerl**, **Benjamin Salecker** und **Vroni Heinz** für die schöne Zeit im und auÃŸerhalb vom Labor, für zahlreiche Diskussionen, motivierende Gespräche und für viele Ü-Ei-Himbie-Kaffee-Quizpausen. Danke auch an meine SHK **Johanna-Katharina Niethammer** für die zahlreichen Stunden am PC und im Labor sowie sämtlichen Studenten für ihre Mitarbeit **Bianca Aichinger**, **Teresa Meyer**, und **Alex Foith**.

...dem Checker Büro: Danke **Dr. Karin Barbinger**, **Dr. Melanie Zaparty** und **Dr. Tillmann Burghardt** für Tipps und Tricks bei *Igni*-Klonierungen. Ausserdem Danke an **Dr. Patrick Barbinger** für die Organisation eines beheizbaren Photometers und die Unterstützung bei Enzymtests.

...allen Mitgliedern des Lehrstuhls für Anatomie und Mikrobiologie für die gute Zusammenarbeit, insbesondere **Christine Meese** für ihre Hilfe beim Hochdruckgefrieren und Substituieren unzählbarer *Ignicoccus* Proben. Vielen Dank auch an **Conny Niemann** für ihr sonniges Gemüt und die Hilfe an der HPF zu später Stunde.

...Danke an **Lydia Kreuter** für die gute Versorgung mit Ignizellen.

... allen Korrekturlesern dieser Arbeit.

... meinem Freund **Christoph Trieb** der mich mit voller Kraft unterstützt und immer wieder aufgemuntert hat. Danke für den Rückhalt, die Ausdauer und die Geduld.

...meinen Eltern **Anton und Sieglinde Flechsler** und meiner Schwester **Jasmin Omer**, die mich während dieser Arbeit immer unterstützt und motiviert haben.